PERFORMANCE BASED GROUPING AND FRAGILITY ANALYSIS OF BOX-GIRDER BRIDGES IN CALIFORNIA

A Dissertation
Presented to
The Academic Faculty

by

Sujith Mangalathu

In Partial Fulfillment
of the Requirements for the Degree
Doctor of Philosophy in the
School of Civil and Environmental Engineering

Georgia Institute of Technology
May 2017

PERFORMANCE BASED GROUPING AND FRAGILITY ANALYSIS OF BOX-GIRDER BRIDGES IN CALIFORNIA

Approved by:

Dr. Reginald DesRoches, Advisor
School of Civil and Environmental Engineering
Georgia Institute of Technology

Dr. Jamie E. Padgett, Co-advisor
Department of Civil and Environmental Engineering
Rice University

Dr. Brani Vidakovic
School of Industrial and Systems Engineering
Georgia Institute of Technology

Dr. Lauren Stewart
School of Civil and Environmental Engineering
Georgia Institute of Technology

Dr. Iris Tien
School of Civil and Environmental Engineering
Georgia Institute of Technology

Date Approved: March 13, 2017

Dedication

To those who welcomed me with a warm smile during my journey

&

To those who are working hard to make the world a better place

ACKNOWLEDGEMENTS

This dissertation has been made with the help of many individuals and I am grateful for their contribution and support. I thank my primary advisor Prof. Reginald DesRoches, who granted me the privilege to work in his research group. I am grateful to him for the discussions and advice that helped me sort out the technical details of my work. I also thank my co-advisor Prof. Jamie Padgett for her comments and suggestions.

I would like to thank the support I have received from the California Department of Transportation to pursue my doctoral studies. I would like to express my sincere gratitude to Cliff Roblee, for his time and patience in providing insight regarding the bridge inventory in California

I would like to thank my thesis committee Dr. Brani Vidakovic, Dr. Lauren Stewart and Dr. Iris Tien. My special thanks to Dr. Vidakovic considering the many hours I spent in his office and his lectures discussing probability theory and statistics. With his enthusiasm, his inspiration, and his great efforts to explain things clearly and simply, he helped to make statistics fun for me. I also thank Prof. Leonardo Osario (Rice University) for his professional guidance. He provided encouragement, sound advice, good company, and lots of good ideas.

My stay at Georgia Tech was a journey of learning and inspiration. The technical discussion I had with fellow students Farahnaz Soleimani, Parsa Banihashemi, Edwin Lim, Stephen Hsu, and Liu Xi helped me in the dissemination of knowledge in the subject and I thank them for sharing their time. I will always remember the great conversations we had over lunch, and I know that we will break bread together many more times. I also wish to acknowledge Ellen Cormack for her motherly care and advice. Her door is always open for me, and she always has time for my concerns.

I would like to thank the former research members of Prof. DesRoches group – Dr. Karthik Ramanathan and Dr. Jong-Su Jeon. I admire the patience of Dr. Jeon in teaching me the OpenSees and bridge design philosophies. I appreciate his help in writing research papers, sharing his knowledge, and his active interest in my research. I also thank my friend Jiqing

Jiang for her support and discussions. I also thank her for helping me to not to lose confidence and pointing the need for hard work.

I thank my friends Brian Terranova, Ni Pengpeng, Adris Ayala, Yasin Ogras, Jenni Tipler, Yesudas, Gokulnath, Ramanandan, Ashkan, Anver Hisham, Jayakrishnan, Andrea, Dharanidharan, Kiran, Anoob, Yesudas, Prabhash, Nikhil, Gayathri for all the encouragement and support. I believe that I am tremendously fortunate to establish the friendship with these outstanding people. I appreciate Brian, Ni, and Gokulnath for helping me get through the difficult times, and for all the emotional support, entertainment, and caring they provided. I am not sure I would be at Georgia Tech without their encouragement.

I also thank my friends and mentors Dr. Vipin Unnithan, Dr. Robin Davis and Shinto Paul for their inspiration and guidance. The conversations, advice, friendships, and fun helped shape my development as a researcher and a good human being.

I thank my non-Georgia tech friends at Atlanta, Karthika, Arun, Vinod, Indu, Gireesh, Kutty, Mahesh and Subin for the countless fun and activities. They helped me in numerous ways which are impossible to describe. It’s not easy to forget the hiking trips and poker games we had over weekends.

I am thankful to my mother Valsala Kumari, my father Sivasubramanian Pillai and my sister Suchithra MS for their unconditional love, encouragement, and support. No words to explain their sacrifices and admiration. Their support has been unconditional all these years; they have given up many things for me to be at Georgia Tech. I also extend the thanks to my entire family for providing a loving environment for me.

I would be remiss if I didn’t acknowledge the contribution and support I have received from Surya. Over the years she has expressed confidence in my abilities and supported me unconditionally. My love and appreciation is extended to her.

I am deeply indebted towards the movies for providing me a recreational and artistic mind during my Ph.D, particularly the movies of Christopher Nolan, Martin Scorsese, Giuseppe Tornatore, Majid Majidi, Ki-Duk Kim, Asghar Farhadi, Ang Lee and Clint Eastwood. The

movies - The Lives of Others, Life is Beautiful, Cinema Paradiso, Hotel Rwanda, The Prestige - has always a special place in my heart.

I also acknowledge the legendary soccer players Pele, Maradona and Messi for entertaining and motivating me since childhood. I also acknowledge my soccer colleagues at Georgia Tech.

I also extend my thanks to the dedicated and silent service of many at Georgia Tech (Georgia Tech Police, CRC Staff, administrative staff, etc.). Their service helps my stay at Georgia Tech a nice and pleasant one.

I also appreciate the dedicated and patient service of people around the globe to make the world a better place.

As the adage goes - like any journey, it's not what you carry but what you leave behind.

Disclaimer

The current study has been supported by the California Department of Transportation (Caltrans), USA through Project P266, Task 1780: Production development of generation-2 fragility models for California bridges. Any opinions, findings, and conclusions or recommendations expressed in this thesis are those of the author and do not necessarily reflect the views of the Caltrans.

TABLE OF CONTENTS

LIST OF TABLES

LIST OF FIGURES

LIST OF SYMBOLS AND ABBREVIATIONS

ABS	absolute error
ABA	active abutment displacement
ABP	passive abutment displacement
ABT	transverse abutment displacement
ANOVA	analysis of variance
ANCOVA	analysis of covariance
ATC	applied technology council
A_{sp}	area of transverse reinforcement bar
A_{sx}	area of transverse reinforcement bar in x direction
A_{sx}	area of transverse reinforcement bar in y direction
a	regression coefficient - intercept
a_s	acceleration for shear key capacity
B_c	breadth of rectangular/oblong cross-section
B_d	deck width
BRD	bearing displacement
BSST	bridge system damage state
b	regression coefficient - slope
C	circular cross-section
C	structural capacity
CF	confinement factor
COL	curvature ductility
CSP	bridge sub-class with a circular single-column bent and two abutments on piles
CDF	cumulative distribution function
CDT	component damage threshold
CSM	capacity spectrum method
CSUS	central and southeastern United States
Caltrans	California department of transportation
D	Diaphragm abutment bridge
D	structural demand
DEC	deck displacement
DV	decision variable
DM	damage measure
d_s	diameter of spiral bar centers
ED	earthquake direction
EDP	engineering demand parameter
Era 11/E1	bridges constructed before 1970
Era 22/E2	bridges constructed between 1970 to 1990
Era 33/E3	bridges constructed after 1970
FNT	foundation translation
FNR	foundation rotation
f_c	unconfined strength of concrete

f_{cc}	maximum concrete stress
f_{yh}	yield strength of the transverse reinforcement
G(EDP|IM)	CDF of EDP conditioned on *IM*
G(DM|EDP)	CDF of *DM* conditioned on *EDP*
G(DV|DM)	CDF of *DV* conditioned on *DM*
g	acceleration due to gravity
H	column height
H_0	null hypothesis
H_1	alternate hypothesis
H_a	abutment height
H_{al}	alternate hypothesis
JPSDM	joint probabilistic seismic demand model
IDA	incremental dynamic analysis
IM	ground motion intensity
KW	Kruskal-Wallis test
K_{pa}	stiffness of abutment piles
K_b	stiffness of bearing
K_{fr}	rotational stiffness of foundation piles
K_{ft}	translational stiffness of foundation piles
k_e	effective confinement factor
L	span length
L_c	width of rectangular/oblong cross-section
LN	log-normal distribution
M	multi column bent
MSE	mean square estimate
m	mass factor
N	total sample size/number of simulations
NLTHA	nonlinear time history analysis
NSP	nonlinear static procedures
O	oblong cross-section
PC	pre-stressed concrete
PGA	peak ground acceleration
PSDM	probabilistic seismic demand model
R	rectangular cross-section
RC	reinforced concrete
S	single column bent
S11	single span bridge
S22	two span bridge
S34	three and four span bridge
S5x	bridges with more than five spans
$S_{a\text{-}1.0s}$	spectral acceleration at a period of 1.0 s
S_d	median estimate of the demand as a function of the *IM*
S_c	median estimate of the capacity
s	center to center spacing or pitch of spiral or circular hoop
SDOF	single-degree of freedom
SST	total sum of squares

T	two column bent
UST	superstructure unseating displacement
$\Phi(\bullet)$	standard normal cumulative distribution function
Δ	displacement
Δ_t	gap between the deck and shear key
β	regression coefficients
$\beta_{d\|IM}$	dispersion of the demand conditioned on the *IM*
δ_a	abutment displacement in active direction
δ_b	bearing displacement
δ_d	deck displacement
δ_{fnd}	foundation displacement
δ_p	abutment displacement in passive direction
δ_{seat}	seat displacement
δ_t	abutment displacement in transverse direction
δ_u	unseating displacement
δ_{key}	shear key displacement
δ_y	yield displacement
ε_{cc}	maximum concrete strain
λ	penalty factor
λ	mean of fragility curves
μ	mean value
μ_{as}	coefficient of friction for abutments on spread footing
μ_b	coefficient of friction of bearing pad
μ_ϕ	column curvature ductility
ν_{DV}	mean annual frequency of a decision variable
ρ	longitudinal reinforcement ratio
ρ_{cc}	ratio of area of longitudinal reinforcement to the area of core of section
θ_f	foundation rotation
σ	standard deviation
ξ	damping ratio
ζ	dispersion of fragility curves
2SSC	two span seat-abutment bridge with circular cross section and single-column bent
2SSR	two span seat-abutment bridge with rectangular cross section and single-column bent
2SSS	two span seat-abutment bridge with abutments resting on spread footing
2SSS	two span seat-abutment bridge with abutments resting on piles
2SDPS	two span diaphragm-abutment single-column bent bridge with pre-stressed concrete superstructure
2SDRS	two span diaphragm-abutment single-column bent bridge with reinforced concrete superstructure

3SDC	three span seat-abutment bridge with circular cross section and single-column bent
3SDR	three span seat-abutment bridge with rectangular cross section and single-column bent
3SCMCB	three span seat-abutment bridge with rectangular cross section and multi-column bent
3SRMCB	three span seat-abutment bridge with circular cross section multi-column bent bridge

SUMMARY

Fragility curves play a critical role in regional seismic risk assessment and are a key component of tools used to support emergency response and preparedness in California following an earthquake. To have an accurate assessment of regional damage, it is critical to provide fragility curves that best represent the bridge inventory. However, it is impractical to develop unique fragility curves for each structure across a regional portfolio. One strategy that has been adopted to address this challenge is to group bridges into classes with similar design or structural performance. Traditionally, this grouping has been performed based on a relatively subjective identification of sub-classes. However, such an identification leads to a number of bridge classes and unwarranted grouping. This work suggests a performance based grouping methodology to group the box-girder bridges in California, and is the first systematic approach in sub-binning bridge classes for the regional risk assessment. The proposed grouping and analytical fragility methodology is used to derive fragility relationships for single frame box girder bridges in California. This work concludes with the application of machine learning techniques for the generation of bridge-specific fragility curves.

CHAPTER 1 INTRODUCTION

1.1 Problem Description and Motivation

Highway bridges constitute the key components of transportation networks, yet recent earthquakes have demonstrated that these bridges are one of the most vulnerable components of transportation networks. Damage to bridges from an earthquake can pose a serious threat to immediate recovery efforts and cause communities to incur large economic losses. Recovery efforts and loss estimation can typically be calculated via damage functions of structures called fragility functions (Kircher et al., 2006). A fragility curve is defined as a conditional probability that gives the likelihood that a structure or component of that structure will meet or exceed a certain level of damage for a given ground motion intensity (IM). This enables the realistic estimation of economic losses, as well as planning for emergency responses and ascertaining the need for retrofitting.

Fragility curves can be generated by empirical (Shinozuka et al., 2000) or analytical approaches (Basöz and Mander, 1999; Banerjee and Shinozuka, 2007; Gardoni et al., 2003; Zhong et al., 2008; Nielson 2005; Mangalathu et al. 2015a). Empirical methods have been used to develop fragility curves in regions where extensive earthquake records are available. Empirical curves are based on observed damage from previous earthquakes. These types of fragility curves tend to be the most realistic, but are very specific to a particular earthquake and structure and thus have limited application (Jeong and Elnashai, 2007). The limitations of the empirical approach motivate the generation of fragility curves using analytical approaches. Analytical fragility curves are generated using numerical simulations that account for material, geometric, and ground motion uncertainties.

California is a state with a high seismic hazard and a history of damaging earthquakes. Various researchers (Mackie and Stojadinovic, 2001; Mackie and Stojadinović, 2006; Zhang and Huo, 2009) have developed fragility curves for bridges in California that have proved to be valuable in understanding the behavior and seismic vulnerability of bridges. However, the developed fragility curves are structure-specific, and therefore are only beneficial for the risk assessment of a specific bridge (Ramanathan et al., 2015). Fragility curves proposed by Basöz and Mander (1999) are remotely applicable to bridge classes in California and are used in HAZUS (HAZUS-MH, 2003). However, the HAZUS fragility relationships were developed based on simplified two-dimensional analysis, a limited number of bridge parameters, and damage states based on a limited set of field observations. The effects of interior supports, framing systems, and design standards were not addressed in HAZUS fragilities.

This issue was partially addressed in the work of Ramanathan et al. (2015) by generating fragility curves that are applicable to a portfolio of bridges in California. These curves considered uncertainties in attributes such as span length, column height, number of spans, superstructure type, and material properties. However, a detailed review of bridge plans from in-house databases obtained from the California Department of Transportation (Caltrans) shows that their study addresses only a specific class of bridges with a specific column shape (circular), bearing type (elastomeric), and abutment type (abutment on piles). To approximately cover the entire range of the California bridge inventory, their study should be extended to various configurations of bridge components and classes. Such an extension supports regional risk assessment for transportation networks and helps agencies such as Caltrans plan their emergency management response.

The proposed research strives for the generation of fragility curves for various classes of box-girder concrete bridges in California. Each class of bridge systems relies on a combination of configurations of components such as the number of spans, column cross-section, abutment type, type of interior support (number of columns per bent), and design era. Such a classification leads to numerous subclasses for a particular bridge type, which makes it cumbersome to compute the seismic fragility for each subclass. It is also not clear whether all such combinations can yield distinct bridge performance classes, or which parameters need to be most critical to the establishment of the distinct subclasses. Additionally, it is not yet clear whether such a detailed classification would result in a better refinement of the vulnerability assessment. The initial study is directed towards the sensitivity of bridge attributes and the configurations on their fragility curves.

Various studies (Saiidi et al., 1996; Jangid, 2004; Nielson and DesRoches, 2006; Padgett and DesRoches, 2007) have been conducted to evaluate the sensitivity of fragility curves to various input parameters. However, there is a lack of understanding of the effects of various bridge attributes on the fragility curves and the necessity of this understanding to creating groups of bridge classes. Mangalathu et al. (2015b) addressed this issue through the application of a statistical technique called Analysis of Covariance (ANCOVA) on the Probabilistic Seismic Demand Model (PSDM). The research carried out underscored the necessity to create distinct bridge subclasses, as well as the importance of structural attributes on fragility curves. However, their study is limited to two- and three-span single frame bridge configurations constructed before 1970. The effects of span, design era, number of frames, and other attributes have not been addressed in their study. The grouping methodology suggested by them requires extensive numerical simulations. The limitation

of their work is addressed in this study through a simple method based on Analysis of Variance (ANOVA). ANOVA is a statistical technique to compare the population and means, and a grouping methodology based on ANOVA is suggested in this current study. The methodology also helps to identify which bridge attributes significantly impact the seismic bridge response and hence fragility curves. The proposed approach and the methodology are relevant and applicable to other bridge systems too.

The proposed grouping methodology classifies California box-girder bridge inventory Representative bridge systems (called RBS- hereafter) so that it can fairly represent fairly the entire bridge inventory. Real bridges in the California inventory are designed to meet site-specific requirements. While most, in a broad engineering sense, conform well to one of the proposed RBS classes, many real bridges have unique design features and/or combinations that do not 'fit' neatly within the proposed RBS class definitions. To improve fit (or modeling fidelity), one could add a new RBS class to directly capture the unique features but only at the cost of increasing the number of RBS classes requiring analysis. At the extreme, this strategy would lead to the development of bridge-specific models, which is not warranted and is beyond the scope of this work. The current study generates fragility curves for the single frame box-girder bridge classes using the multi-phase analytical approach developed by researchers (Nielson, 2005; Padgett and DesRoches, 2008b; Ramanathan et al., 2015; Jeon et al., 2015).

The proposed grouping and analytical fragility methodology is used to derive fragility relationships for single frame box-girder bridges in California. The study is limited to straight bridges and the effects of skew, curvature, and unbalanced frame will not be addressed.

1.2 Research Objectives

The limitation in the HAZUS grouping of bridge classes and the corresponding fragilities are identified in the subsequent sections. This research aims to improve the grouping of bridge classes in California by suggesting a performance-based grouping methodology. Another objective of the study is to make substantial improvements in the fragility relationships of box-girder bridges in California based on advanced modeling techniques and the available experimental data.

Specifically, this research will attempt to:

- Identify whether it is rational to go beyond the existing HAZUS grouping and fragility relationships.
- Suggest a performance based grouping strategy (instead of more traditional subjective grouping) to group bridge classes with statistically similar performance and damage measures. The proposed methodology will account for the effects of design eras, cross-sections, number of spans, number of frames, abutment types, span continuity, and pier types in grouping the bridge classes.
- Perform a detailed plan review of various bridge classes in Californian through review of the in-house database of bridge plans (hereafter, BIRIS) assembled by Caltrans engineers.
- Use an advanced numerical modeling procedure to capture the seismic response of various bridge components.
- Generate statistically significant yet nominally identical bridge models accounting for the various geometric, material, system and ground motion uncertainties.

- Generate a refined set of fragility curves at system and component level for various box-girder bridge classes in California. These improved fragility curves will help determine the relative vulnerability of various bridge classes. They will also assist the bridge owners such as Caltrans in spending their resources judiciously in their development of retrofitting strategies.
- Extend traditional single-parameter fragility curves to multi-parameter fragility curves using advanced statistical and machine learning techniques such as Lasso, Ridge, and elastic net. Such study will provide insight in quantifying whether the variation of uncertain parameters should be explicitly treated or remain neglected; it eliminates those parameters which have minimal influence on the seismic demand and reduces unnecessary and exhaustive efforts in statistical sampling.

1.3 Dissertation outline

The research is organized into seven subsequent chapters with the following contents:

Chapter 2 presents an overview of existing literature on the grouping of bridge classes and the seismic fragility assessment of bridges.

Chapter 3 provides extensive details about the modeling strategies of various bridge components: superstructure, columns, abutments, foundations, bearings, and shear keys. The chapter also presents the integration of various component models to generate global analytical model of the bridge for fragility analysis

Chapter 4 investigates the application of various performance based grouping strategies such as analysis of variance (ANOVA), Analysis of Covariance (ANCOVA) and Kruskal–

Wallis (KW) towards the grouping of structures of similar performance. The chapter also outlines the grouping of box-girder bridges in California.

Chapter 5 presents an in-depth study of the California bridge inventory using the in-house database called BIRIS, assembled by Caltrans engineers. The chapter also presents statistical distributions of various bridge attributes in California.

Chapter 6 discusses the multi-phase framework adopted in the generation of analytical fragility curves for box girder bridges in California. The chapter also describes the system and component fragility curves for single frame multi-span box girder bridges in California. Insights are provided on the relative performance of various bridge classes and the importance of various design attributes.

Chapter 7 explores the application of regression and machine learning techniques for the generation of multi-parameter seismic demand models and fragility curves.

Chapter 8 presents the conclusions from the present research, key contributions and the suggestions for future research.

CHAPTER 2 EXISTING RESEARCH ON GROUPING OF BRIDGE CLASSES AND BRIDGE FRAGILITY

Probabilistic Performance-based Earthquake Engineering (PBEE) framework (Cornell and Krawinkler, 2000; Moehle and Deierlein, 2004) has evolved to be the next-generation framework in risk mitigation decision making for structure and infrastructure systems. The framework presented by the Pacific Earthquake Engineering Research Center (PEER) is the widely accepted robust methodology for PBEE. The PEER framework calculates the performance of a structure in a probabilistic manner by the rigorous treatment of uncertainties. The underlying approach is shown in Figure 2.1, and the framework assumes that the performance assessment of components as discrete Markov process, where the conditional probabilities between parameters are independent (Moehle and Deierlein, 2004).

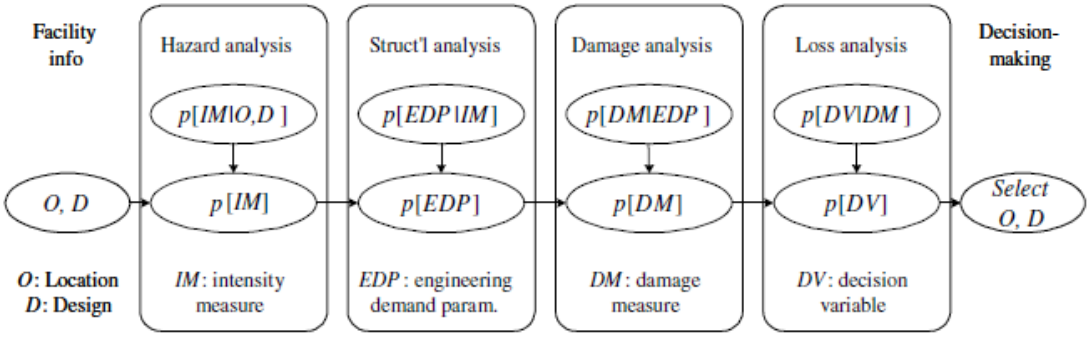

Figure 2.1 – PEER framework for PBEE (Porter, 2003).

The methodology expressed in Figure 2.1 can be expressed in a mathematical form as expressed in Equation 2.1.

$$\nu_{DV}(DV) = \iiint G(DV \mid DM) \cdot \left|dG(DM \mid EDP)\right| \cdot \left|dG(EDP \mid IM)\right| \cdot \left|d\lambda(IM)\right| \qquad (2.1)$$

where ν_{DV} is the mean annual frequency of a decision variable (*DV*, e.g., repair cost, downtime, loss), *G(DV|DM)* is the cumulative distribution function (CDF) of *DV* conditioned on damage measure (*DM*, e.g., damage to structural or non-structural components), *G(DM|EDP)* is the CDF of *DM* conditioned on engineering demand parameter *(EDP*, e.g., curvature ductility, bearing displacement), *G(EDP|IM)* is the demand model describing the CDF of *EDP* conditioned on ground motion intensity measure (*IM*, e.g., peak ground acceleration), and $\lambda(IM)$ is the seismic hazard model describing the mean annual frequency of exceeding an *IM*. The convolution of *G(DM|EDP)* and *G(EDP|IM)* yields fragility curves. A fragility curve can thus be defined as a conditional probability that gives the likelihood that a structure or component will meet or exceed a certain level of damage for a given ground motion intensity (*IM*). The fragility curves intended for regional risk assessment require grouping of bridge classes with similar performance during earthquakes.

2.1 Grouping of bridge classes

Any existing bridge has its own structural characteristics due to its location, soil conditions, geometric and material properties, and construction technique. However, bridges with similar structural properties are expected to show statistically similar performance under a given earthquake loading, and so the bridges with similar performance can be grouped together. The existing literature on the grouping of bridge classes is given in this section.

HAZUS (HAZUS-MH, 2003) is, by far, the most comprehensive document in grouping the bridge classes and seismic vulnerability estimation. HAZUS grouped the bridge classes with similar damage/loss characteristics and suggested fragility relationships to the grouped bridge classes. HAZUS classified the bridge classes based on seismic design, number of spans, span length, bent type, span continuity, and span discontinuity,

and is shown in Figure 2.2. The HAZUS grouping was based on engineering judgment, past experience, and expert opinion. The effects of evolution in seismic design philosophy, column cross-section, and number of frames are not addressed in HAZUS. The limitations of HAZUS grouping are discussed later in this chapter.

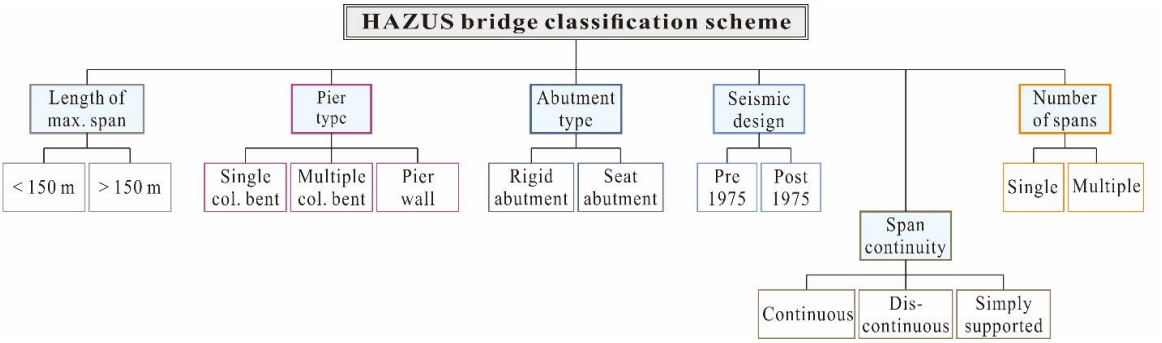

Figure 2.2 – HAZUS grouping of California box-girder bridge inventory.

Moschonas et al. (2008) classified bridges in Greece according to piers (single column circular, single column rectangular, multi-column, or wall-type), deck type (slab, box-girder, or simply supported precast-prestressed beams connected through continuous RC slab) and pier-to-deck connections (monolithic bearings or combination). Although 36 combinations are possible, the authors further reduced the bridge classes to 11 classes (those with five or more bridges). Based on past earthquake data and the previous research, Avsar et al. (2011) classified the highway bridges in Turkey that were constructed after 1990. The important structural attributes identified by the authors are span number (single or multiple), bent (single or multiple), and skew angle (negligible or significant, chosen to be >30°).

Ramanathan et al. (2015) grouped the bridge classes in California based on limited parameters such as abutment type (diaphragm abutment or seat abutment), number of columns per bent (single or multiple), superstructure type (box girder, I-girder, T-girder,

or slab bridges) and design era (pre-1971, 1971-1990, or post-1990). However, the grouping was based on engineering judgment and doesn't consider the effects of number of spans, span discontinuity, span length, or cross-section. Thus, the grouping covers only a limited portion of California bridge inventory.

Mangalathu et al. (2016) suggested a performance-based grouping approach using a statistical technique called Analysis of Covariance (ANCOVA). This technique compares the probabilistic seismic demand models (PSDMs) of different bridge classes. A PSDM is defined as the probability distribution of structural demands (D) conditioned on the ground motion intensity measure (IM). This works presents the first systematic and reliable methodology for grouping bridge classes for performing regional risk assessments. The authors demonstrated their grouping methodology through case studies of two-span and three-span box-girder bridges in California with various design attributes. Their research showed the importance of binning of bridge classes through the comparison of fragility curves for bridge classes with different design attributes as identified by the ANCOVA. However, the focus of the grouping was only on two-span and three-span box-girder bridges and doesn't consider the effect of number of spans, foundation type, design era, or span discontinuity.

Mehr and Zaghi (2016) used analysis of variance (ANOVA) to compare the response of single-frame and multi-frame bridges and group them accordingly. The authors investigated the effects of number of frames, soil type, substructure system, valley shape, intensity of ground motion, and design capacity-to-demand ratio on single and multi-frame bridges. Using the ANOVA results, the authors concluded that a multi-frame system is more robust than a single frame system from a seismic perspective. The authors also noted that the application of ANOVA is yet to be advanced in civil engineering.

The existing bridge groupings suffer some limitations and cannot be used to group the California bridge inventory. Also the structural attributes chosen to classify the bridges vary depending on the type of bridge, bridge location, and research intention. California has close to 29,000 bridges, which vary in age. In order to obtain a reliable estimate of the risk associated with the California bridge inventory, it is crucial to group the entire bridge class that yields similar performance or suffers similar damage following a seismic event.

2.2 Fragility curves

Past decades have witnessed the development of several fragility curve generation methodologies; a brief summary of their evolution is given in this section.

2.2.1 Expert opinion

The earliest attempt to develop a fragility curve was based on expert opinion (ATC, 1985). A panel of 42 earthquake engineering experts was asked to provide probability estimates and the results were presented in the form of damage probability matrices, later converted to vulnerability functions and restoration curves. However, the technique was wholly subjective and depended on the number of experts queried. The limitations of expert-opinion fragility curves, coupled with actual damage data from earthquakes, motivated the generation of empirical fragility curves (Basoz and Kiremidjian, 1998; Shinozuka et al. 2000).

2.2.2 Empirical methods

Basoz and Kiremidjian (1998) assembled data regarding damage to bridges from the 1989 Loma Preita and the 1995 Northridge earthquakes in California and analyzed them to obtain the relationships between bridge damage and ground motion. The authors generated the fragility curves afterwards thorough logistic regression techniques.

Shinozuka et al. (2000) used bridge damage data from the 1995 Kobe earthquake and used Maximum Likelihood Method to estimate the parameters of a lognormal probability distribution describing the fragility curves. These types of fragility curves tend to be the most realistic, but are very specific to a particular earthquake and structure and thus have limited application (Jeong and Elnashai, 2007). The limitations of the empirical approach motivated the generation of fragility curves by analytical approaches.

2.2.3 Analytical methods

Analytical methods can be used to generate fragility curves where earthquake data is not available. Various researchers have employed analysis techniques, with varying levels of sophistication: Yu et al. (1991) generated analytical fragility curves of bridges through Elastic Response Spectrum Analysis of single-degree of freedom (SDOF) models, and Hwang et al. (2000) extended this approach by quantifying the uncertainties in capacity and demand assessments. With this advancement in the modeling capabilities, researchers moved to nonlinear static procedures (NSP). Capacity spectrum method (CSM) and N2 method are the different types of NSP. Developed by Fajfar (2000), N2 method combines the pushover analysis of a multi-degree of freedom (MDOF) system with the response spectrum analysis of an equivalent SDOF system. HAZUS uses the fragility relationships suggested by Mander and Basöz (1999), which are based on CSM. Further details on the fundamental assumptions and limitation of HAZUS fragilities are given in the next section.

Other researchers resorted to the more reliable but computationally expensive nonlinear time history analysis (NLTHA) (Banerjee and Shinozuka, 2007; Choi, 2002; Gardoni et al., 2003; Kim and Shinozuka, 2004; Mackie and Stojadinovic, 2001; Mackie and Stojadinović, 2005; Mangalathu et al., 2016a; Mangalathu et al., 2015; Padgett, 2007; Ramanathan et al., 2015). Recalling the fragility curve as the probability that the seismic demand (D) placed on a component exceeds the capacity (C), the probability can be

computed using Equation 2.1, assuming lognormal distribution for the *D* and *C* (Cornell et al., 2002)

$$P[D > C \mid IM] = \Phi\left[\frac{\ln(S_d / S_c)}{\sqrt{\beta_{d/IM}^2 + \beta_c^2}}\right] \tag{2.1}$$

where S_d is the median estimate of the demand as a function of the *IM*, S_c is the median estimate of the capacity, $\beta_{d|IM}$ is the dispersion of the demand conditioned on the *IM*, β_c is the dispersion of the capacity, and $\Phi(\bullet)$ is the standard normal cumulative distribution function. S_d and $\beta_{d|IM}$ can be estimated from the PSDMs. As previously mentioned, PSDM is defined as the probability distribution of structural demands (*D*) conditioned on the ground motion intensity measure (*IM*). NLTHA employs analysis of bridges with different ground motion intensities to obtain the PSDMs. PSDMs can be generated by a cloud approach (Figure 2.3) or an incremental dynamic analysis approach (Figure 2.4). The cloud approach consists of selecting ground motions that represent the hazard at a region and carrying out NLTHA on the bridge samples. This technique is limited because it makes a prior assumption about the PSDM.

In the IDA approach, ground motions are scaled successively until significant reduction (collapse) of the primary load-bearing elements in the structural system. Hence, IDA can offer the transition of the structural response from elastic to inelastic behavior, finally leading to global dynamic instability, and the accurate and reliable estimates of the global collapse capacity of the structure. The overall formulation of IDA was proposed by (Vamvatsikos and Cornell, 2002). A significant drawback with this approach is that the process involves scaling of ground motions without altering the frequency content of the ground motions. These scaling approaches could lead to unrealistic time histories that might not be representative of the seismic hazard of the site.

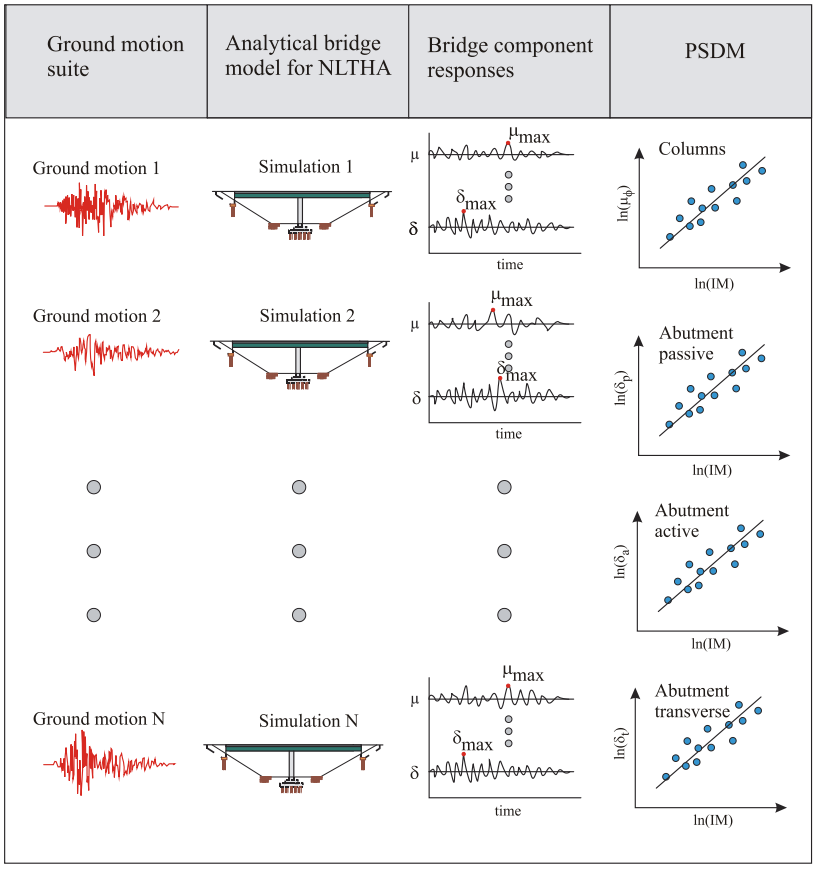

Figure 2.3 – Generation of PSDMs through cloud approach (Ramanathan, 2012).

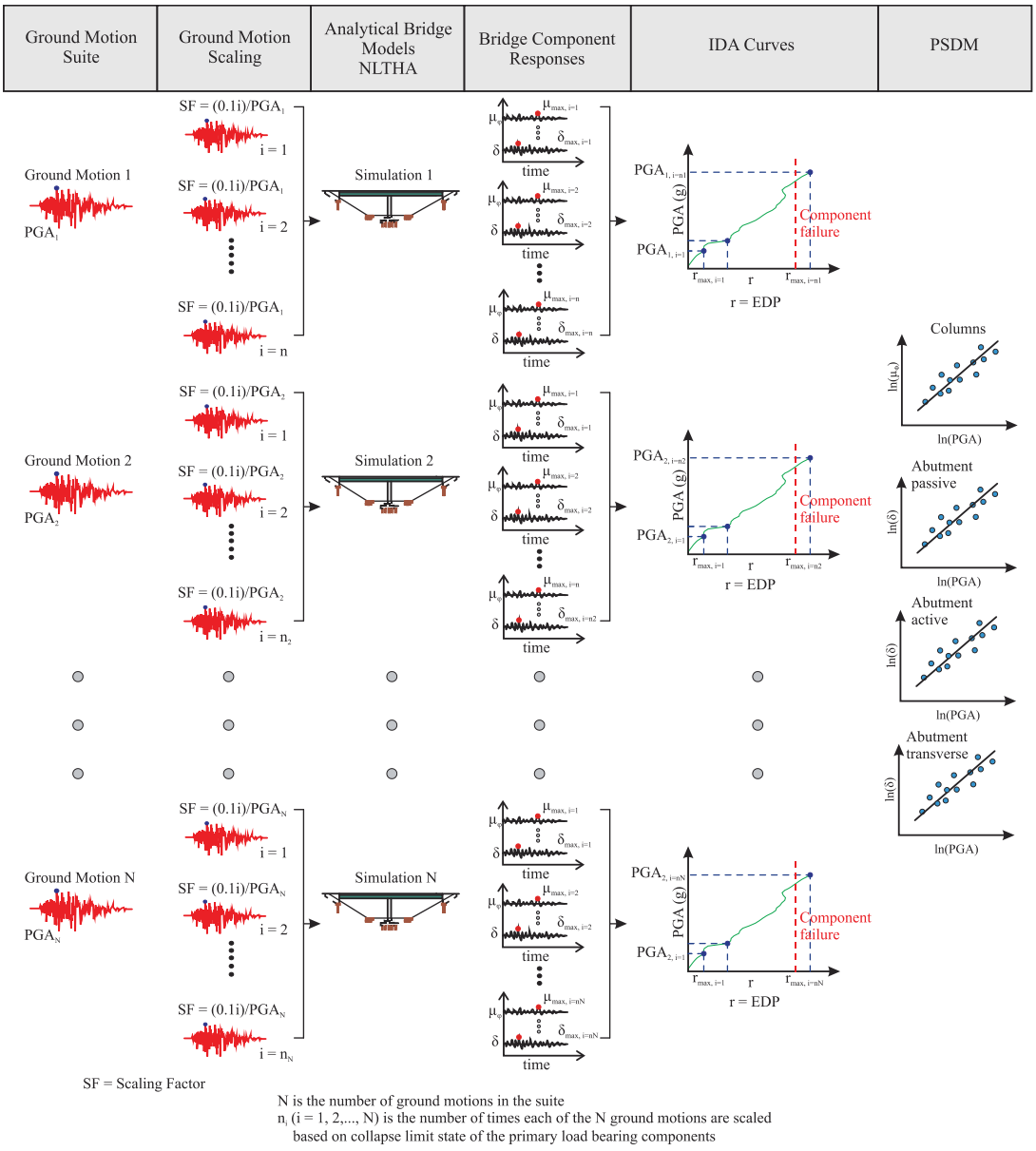

Figure 2.4 – Generation of PSDMs through IDA approach (Ramanathan, 2012).

2.2.4 Parameterized fragility curves

As stated in Ghosh et al. (2013), single-parameter demand models and fragility curves have some limitations: (1) the inability to account for the influence of uncertainty

(modeling) parameters on structural performance during earthquakes without extensive re-simulations for each new set of parameter combinations; (2) the inability to explicitly address the effect of uncertainty parameters on fragility curves; and (3) the inability to incorporate field instrumentation data resulting from monitoring of highway bridges to enable updating of fragility estimates. To alleviate the limitations of single-parameter fragility curves, recent research has been focused on multi-parameter parameterized fragility curves that can account for the variation in the design details or geometric parameters of bridges (Seo and Linzell, 2012; Dukes, 2013; Ghosh et al., 2013; Kameshwar and Padgett, 2014; Park and Towashiraporn 2014; Jeon et al., 2015; Mangalathu et al., 2015; Mangalathu et al. 2017c). Assuming that the input variables are statistically independent, a multi-parameter demand model of each bridge component (demand parameter) is constructed. Samples obtained from this demand model are compared with those of the associated limit state model to obtain the binary survival-failure vector. This vector is used to perform a logistic regression analysis to determine the regression coefficients and thus develop the multi-parameter fragility curve in the component.

Seo and Linzell (2013) used response surface models to generate parameterized fragility curves for curved steel bridges. The authors identified the critical range of the important bridge components using a statistical screening approach.

Dukes (2013) developed multi-parameter demand models of bridge components for two example bridges using the response surface method and then derived parameterized fragility curves for the bridges using logistic regression. The parameterized fragility curves were used to produce bridge-specific fragilities by substituting a specific value for each of six design parameters: longitudinal reinforcement ratio; volumetric transverse ratio; aspect ratio; span length-to-column height ratio; deck depth-to-column diameter ratio; and deck width. This framework was developed for use in the seismic design process in the design

of new bridges. It produces fragility curves without the need to create the curves deterministically with new simulations for each new bridge design.

Ghosh et al. (2013) used a multi-parameter demand model to account for the effect of all uncertain parameters in the generation of fragility curves. The authors used four surrogate modeling techniques (polynomial response surface models, multivariate adaptive regression splines, radial basis function networks, and support vector machines) to determine the best-fitting parameterized demand models involving the uncertain input parameters. To achieve this goal, these authors selected for their case study multi-span simply supported concrete bridges that were not seismically designed, which are typical in the central and southeastern United States (CSUS). They then used ten parameters associated with material and geometric uncertainties, along with an IM (eleven predictor variables), to develop demand models. This work concluded that the MARS model provided the most accurate estimates of component responses with the fewest predictive errors. Using the MARS model and logistic regression, parameterized fragility curves were developed for the component and system level.

Kameshwar and Padgett (2014) suggested a parameterized fragility based multi-hazard risk assessment for highway bridges subjected to earthquake and hurricane events. The authors used stepwise logistic regression with a non-linear logit function to generate the parameterized fragility curves. The significant parameters were identified by the authors using a sequential forward selection scheme. The authors demonstrated the proposed approach with the case studies on multi-span simply supported concrete bridges in South Carolina.

Park and Towashiraporn (2014) estimated the probabilistic seismic damage to track-on steel-plate-girder (TOSPG) bridges in Korea, accounting for variations in the number of spans, pier height, and earthquake magnitude. The authors used response surface

modeling to create second-degree polynomials for the estimation of seismic damage. The study revealed that span length does not significantly affect seismic damage to bridges.

Jeon et al. (2016) employed a Bayesian framework to generate multi-parameter fragility estimates. The framework includes the selection of a bridge class, characterization of bridge attributes such as material and geometric uncertainties, creation of numerical component models, construction of multi-parameter demand models using a Bayesian parameter estimation method, and development of bridge-specific fragility models using logistic regression and one-dimensional fragility curves using a Monte Carlo integration. Additionally, the Bayesian approach used in the suggested framework enables the identification of significant uncertainty parameters affecting seismic demands without performing numerous structural analyses required for design of experiments. The authors demonstrated their approach through a study of two classes of curved bridges commonly found in California: two-frame and three-frame reinforced concrete box-girder bridges with single column bents, diaphragm abutments, and in-span hinge(s).

Stefanidou and Kappos (2016) suggested a methodology for the generation of bridge-specific fragility curves in which the limit state of the bridges is explicitly defined, accounting for the effects of varying geometry, material properties, reinforcement, and loading patterns. The methodology can account for the uncertainty in capacity, demand, and damage state definition. The authors used nonlinear static analysis and IDA to estimate the demand and capacity, and reduced sampling techniques for the uncertainty treatment.

2.3 Fragility curves for concrete bridge classes in California

California is a state with a high seismic hazard and a history of damaging earthquakes. Various researchers have generated fragility curves for bridges in California, using either an empirical (Başöz and Kiremidjian, 1996; Shinozuka et al., 2000) or

analytical approach. This section details the existing analytically based research on the generation of fragility curves of various concrete bridge classes in California.

HAZUS (2003) generated fragility curves of various bridge configurations based on seismic design, span length, bent type, and span discontinuity. However, HAZUS fragility relationships were developed on the basis of a limited number of parameters and simplified two-dimensional analysis, and did not account for the uncertainties in geometric attributes for bridge classes such as the number of spans, span length, deck width, and column height. A critical review of HAZUS fragilities follows this section.

Mackie and Stojadinović (2005) improved HAZUS fragility relationships by reflecting the variation in bridge design parameters, including the skewness, span length, span to column height ratio, and column to superstructure dimension ratio. However, their models are applicable to a smaller subset of bridges, such as single-frame multi-span continuous box-girder bridges with a single column bent.

Ramanathan (2012) generated fragility curves that are applicable to a portfolio for various classes of bridges by accounting for uncertainties in attributes such as span length, column height, number of spans, superstructure type, and material properties. They addressed the evolution in seismic design philosophy by grouping the bridge classes into three eras: pre-1971 bridges (Era 11, hereafter), 1971-1990 bridges (Era 22, hereafter), and post-1990 bridges (Era 33, hereafter). Although the study provides valuable insight regarding the bridge fragilities, it has some limitations, which are noted below:

- The grouping of bridge classes in the study was carried out based on a traditional subjective approach that relies on engineering judgment. Such subjective grouping has been criticized by more recent research which favors performance-based grouping (Mangalathu et al., 2016a; Mangalathu et al., 2016b).

- The study considers that only one type of abutment footing (abutment on piles) is possible in California. However, the plan review of California bridges revealed various abutment footings such as abutment on spread footing, abutment on piles, and tall cantilever footing. Recent studies (Mangalathu et al., 2015; Mangalathu et al., 2016a) have noted that bridge fragilities are significantly influenced by the abutment footing type.

- The study was limited to specific bridge classes in the California bridge inventory. For example, the study on box-girder bridges was limited to two-span bridges, yet bridges with more than two spans are common in California.

- The study only addressed a specific class of bridges with circular column shape. It has been noted from the plan review that various cross-sections such as circular, rectangular, and oblong (interlocking spirals) are present in the California bridge inventory.

- The study assumed that the bearings in seat abutments are elastomeric. However, rocker-type bearings are common in Era 11 bridges (Mangalathu et al., 2016a).

- The study considers only flexural mode of failure for columns in bridges constructed during Era 11, although the lap-splice mode of failure is common in bridges from that era.

- The study was limited to straight (non-flared) columns. It is common in post-1970 bridges (Era 22 and Era 33) to flare the columns in the upper region to provide support to the cap beam under eccentric live load for architectural reasons. The response of the bridge columns to seismic loading is significantly affected by the flares (Sanchez et al., 1997).

- The study didn't consider the effects of frames, pier-type columns, and spread-type footing for foundations in the fragility analysis.

- The capacity estimates or limit state models in Ramanathan (2012) were preliminary estimates (Mangalathu et al., 2016a) and need improvement.

2.4 The need to go beyond HAZUS-based grouping and fragility curves

HAZUS is the most comprehensive document for grouping bridge classes and estimating seismic vulnerability. HAZUS groups bridge classes with similar damage/loss characteristics and suggested fragility relationships to the grouped bridge classes. This section summarizes the HAZUS grouping and fragility relations, and discusses their merits and faults. Figure 2.2 shows the HAZUS-based grouping for the selected California box-girder bridge inventory; Table 2.1 shows the grouping and fragility relationships suggested by HAZUS.

Table 2.1 HAZUS grouping and fragility relationships for bridge classes in California.

Class	Year built	Description (acronym in HAZUS)	Fragility values in terms of $S_{a\text{-}1.0\,s}$				
			Slight	Moderate	Extensive	Complete	Dispersion
HWB1	< 1975	Major bridge Length > 150 m	0.40	0.50	0.70	0.90	0.6
HWB2	≥ 1975	Major bridge Length > 150 m	0.60	0.90	1.10	1.70	0.6
HWB3	< 1975	Single span	0.80	1.00	1.20	1.70	0.6
HWB4	≥ 1975	Single span	0.80	1.00	1.20	1.70	0.6
HWB6	< 1975	Multi-column bent, Simple support, Concrete	0.30	0.50	0.60	0.90	0.6
HWB7	≥ 1975	Multi-column bent, Simple support, Concrete	0.50	0.80	1.10	1.70	0.6
HWB8	< 1975	Single column, Box-girder, Continuous concrete	035	0.45	0.55	0.80	0.6
HWB9	≥ 1975	Single column, Box-girder, Continuous concrete	0.60	0.90	1.30	1.60	0.6
HWB10	< 1975	Continuous concrete (not HWB8/ HWB9)	0.60	0.90	1.10	1.50	0.6
HWB11	≥ 1975	Continuous concrete (not HWB8/HWB9)	0.90	0.90	1.10	1.50	0.6
HWB18	< 1975	Multi-column bent, Simple support, Prestressed concrete	0.30	0.50	0.60	0.90	0.6
HWB19	≥ 1975	Multi-column bent, Simple support, Prestressed concrete	0.50	0.80	1.10	1.70	0.6
HWB20	< 1975	Single-column, Box-girder, Prestressed concrete continuous	0.35	0.45	0.55	0.80	0.6
HWB21	≥ 1975	Single-column, Box-girder, Prestressed concrete continuous	0.60	0.90	1.30	1.60	0.6
HWB22	< 1975	Continuous concrete (not HWB20/HWB21)	0.60	0.90	1.10	1.50	0.6
HWB23	≥ 1975	Continuous concrete (not HWB20/HWB21)	0.90	0.90	1.10	1.50	0.6
HWB28	All other bridges that are not classified		0.80	1.00	1.20	1.70	0.6

The salient features noted from the critical review of HAZUS grouping and fragility relationships for bridges in California are noted below:

- HAZUS classifies bridges in two design eras, pre-1975 and post-1975. However, bridge design philosophies in California were significantly influenced by the historic 1971 San Fernando and the 1989 Loma Prieta earthquakes. The extensive damage from the 1989 Loma Prieta earthquake forced Caltrans to solicit the Applied Technology

Council (ATC) to conduct a detailed study and provide recommendations for design standards, performance criteria, and practices. The recommendations from ATC described in ATC-32 were incorporated in Caltrans design manuals (Caltrans, 2010). A study by Ramanathan et al. (2015) showed that fragility curves are highly influenced by these design philosophies; seismic vulnerability decreases with the evolution in column design philosophy. Therefore, it is necessary to separate the post-1975 bridge class based on the evolution in seismic design philosophy.

- HAZUS classifies the bridge classes that are not addressed in the main classification as *the bridge group*. The *other bridge group* represents the high-risk bridge inventory. This classification leads to a situation where multi-frame bridges that are not addressed explicitly in the main group are in the non-classified group, although the seismic vulnerability of slab bridges is much lower than the vulnerability of continuous box-girder bridges (Mehr and Zaghi, 2016). Therefore, HAZUS classifications significantly overestimate the seismic vulnerability and loss assessment for multi-frame bridges.

- Although HAZUS classifies bridges based on abutment type (monolithic versus non-monolithic, which is inferred as diaphragm versus seat abutments based on recent seismic notions), HAZUS does not suggest explicit fragility relationships based on abutment type. Previous studies (Mangalathu et al., 2016a; Ramanathan et al., 2015) have noted that the demand models and fragilities for various components and bridge systems differ drastically depending on the abutment style. Further, Ramanathan et al. (2015) indicated that diaphragm abutments are less vulnerable than seat abutments in pre-1990 bridges, but that the trend is reversed in post-1990 bridges.

- HAZUS fragility relationships were developed using a limited number of parameters and simplified two dimensional analyses, and did not account for uncertainties in geometric and material attributes for bridge classes such as the number of spans, span

length, deck width, and column height. Also, other researchers (Porter, 2010; Ramanathan, 2012) have criticized the capacity spectrum method (CSM) of structural analysis used in HAZUS. The capacity spectrum method estimates the capacity of bridge in the form of a pushover curve of the column and the demand in the form of a response spectrum. The inability to account the higher-mode contributions and vulnerability of other components leads to a non-reliable estimation of fragility curves.

- HAZUS considers the vulnerability of bridges to be governed by columns alone. As pointed out by Ramanathan (2012), columns are not always the critical components; neglecting the damage to bearings, abutments, and shear keys underestimates the bridge vulnerability.

- HAZUS suggests the same fragility relationships for bridge classes HWB10 and HWB22, and for HWB11 and HWB23. It can be inferred from these grouped fragility relationships that the type of superstructure (reinforced versus pre-stressed concrete) is not a significant parameter for the bridge fragilities. This is consistent with similar conclusions noted in recent studies (Mangalathu et al., 2015a; Mangalathu et al., 2016a). However, slab bridges, T-girder, and box-girder bridges are classified in the same group and Ramanathan (2012) showed that these bridge classes do not have similar fragility curves.

- A comparison of fragility relationships of bridge classes HWB8 and HWB10, HWB9 and HWB11, HWB18 and HWB20, and HWB19 and HWB21 shows that single-column bents (SCBs) are more vulnerable than multi-column bents (MCBs). Ramanathan et al. (2012) and Mangalathu et al. (2016a) showed that SCBs are less vulnerable than MCBs for two- and three-span box-girder bridges.

- While comparing the fragility relationships of bridge classes HWB22 and HWB23, and HWB10 and HWB11 for moderate, extensive, and complete damage states, the effect

of design eras does not have an influence on the fragility relations. Such a conclusion contradicts the research explicitly focusing on the effect of design eras (Mangalathu et al. 2015a; Ramanathan, 2012).

- HAZUS suggests the same fragility relationships for single-span bridges irrespective of the design eras (HWB3 and HWB4). Although it might hold for bridges with diaphragm abutments, it is clearly not the case for bridges with seat abutments as there is an increase in the seat-width provision for newer era bridges. Since span-unseating or bearing displacement is the critical component for single-span seat abutment bridges, new era single-span seat abutment bridges are less vulnerable than their counterparts from previous eras, because of increased seat width.

- HAZUS fragility relationships suggest that simply-supported bridges are more vulnerable than continuous bridges. The study by Ranf et al. (2007) utilized damage data collected from the Nisqually Earthquake in 2011 to reveal that this is not true for lower damage states. As there is not enough data for higher damage states, it is not certain whether the HAZUS fragility relationships (that is, that simply-supported bridges are more vulnerable than continuous bridges) hold for higher damage states. The study also indicated that HAZUS fragility relationships overestimate the damage for simply-supported bridges.

- Although HAZUS classifies bridges without considering the number of frames, Mehr and Zaghi (2016) used three-dimensional nonlinear time history analysis to show that single frame bridges do not have similar fragility curves to multi-frame bridges.

- An extensive plan review of the California bridge inventory revealed various column cross-sections such as rectangular, circular, and oblong. These cross-sections occupy a major portion of concrete bridges in California and recent studies (Mangalathu et al.,

2016a; 2016b) have shown that bridges with circular and rectangular column cross-sections have different seismic demands and fragilities.

- Although HAZUS classifies the bridges based on length (length > 150 m and length < 150 m), it is not clear whether the length is per frame or the total length of the bridge.

- As pointed out by Ramanathan (2012), there is a mismatch between overall bridge functionality in HAZUS and the damage state definitions used in the fragility analysis. Such a discrepancy could cause problems for Departments of Transportation officials in emergency response decisions.

- HAZUS classified California bridges as either single-span or multi-span. The effect of number of spans is accounted in HAZUS by a modification factor. Per HAZUS modification factor, three-span bridges are less vulnerable than their counterparts. A study is needed to verify the HAZUS modification factor.

- The effect of pier shaft foundation type is not addressed in HAZUS.

Given the key points noted from the critical review of HAZUS bridge classification, it is clear that HAZUS groupings and fragility relationships need significant improvement. Also, it is rational to advance the grouping of bridge classes from a traditional perspective relying on the judgment of engineers to one that is performance-based.

2.5 Uncertainty treatment in fragility analysis

As stated previously, the prevalent approach for the generation of fragility curves is the convolution of demand models with capacity models. Demand models are usually obtained by conducting non-linear time history analysis (NLTHA) on bridge models (Choi, 2002; Gardoni et al., 2003; Kim and Shinozuka, 2004; Mackie and Stojadinovic, 2001; Mackie and Stojadinović, 2005; Banerjee and Shinozuka, 2007; Padgett, 2007;

Mangalathu et al., 2015; Ramanathan et al., 2015; Mangalathu et al., 2016a). In the probabilistic seismic performance assessment, bridge models are generated by conducting sampling across the uncertain input parameters (Padgett, 2007; Ramanathan et al., 2015, Mangalathu et al., 2016a; Mangalathu et al., 2015a). It is highly likely that various uncertainties such as geometric, material, or component response parameters exist due to structure-to-structure variation in the generation of fragility curves, especially if the fragility curves are intended for the regional risk assessment of bridges (Mangalathu et al., 2016a). The source of uncertainties can either be due to lack of knowledge (epistemic) or due to inherent randomness (aleatoric). As it is impossible to eliminate uncertainties, the risks due to uncertainty must be properly evaluated and limited.

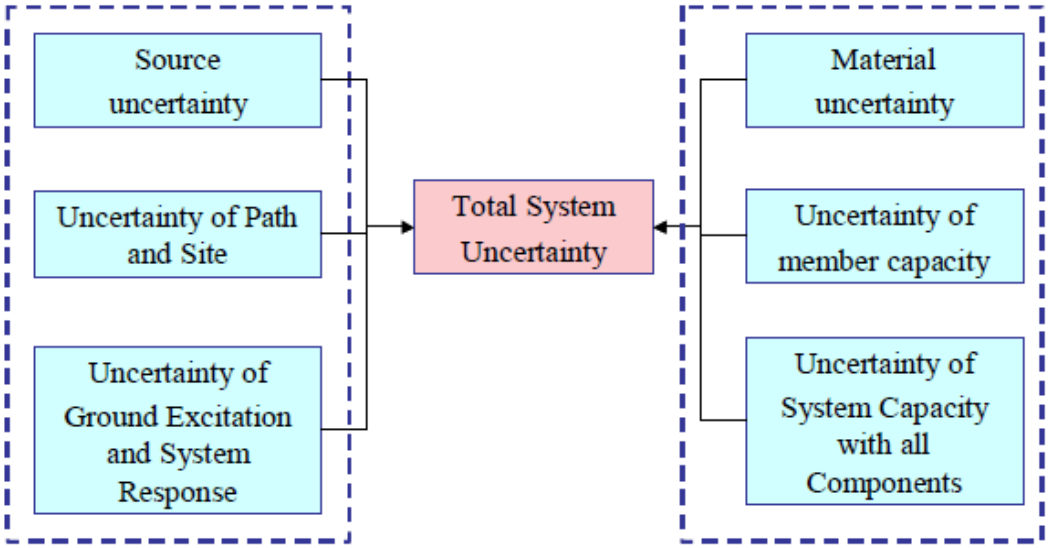

Figure 2.5– Uncertainty sources for system demand and capacity (Ji et al., 2007).

Uncertainties can present both in seismic demand and capacity (Ji et al., 2007, Figure 2.5). Capacity is a property of the system to withstand maximum force or displacement without failure. Researchers have attempted to determine the extent to which uncertainties affect the seismic demand, capacity, and fragilities. The uncertainties in ground motions can be accounted for by including many records of ground motions to cover as many frequencies and seismic energies as possible (Ji et al., 2007). However, the

number of records needed to have a reliable estimate of the fragility is not well defined (Haselton et al., 2012). Celik and Ellingwood (2010) noted that uncertainties in ground motion dominated overall uncertainty in structural response in the case of gravity load designed reinforced concrete frames. Their study concluded that other sensitive parameters affecting the seismic response of reinforced concrete frames are damping, concrete strength, and joint cracking strain. The uncertainty in the capacity is usually accounted for by modeling the capacity or limit state as a random variable (Ji. et al. 2007). For example, HAZUS suggests a dispersion measure to account for variability in the damage state. In the case of bridges, researchers have attempted to assess the sensitivity of seismic demand or have evaluated fragility to the parameter uncertainty (Dicleli and Bruneau, 1995; Nielson and DesRoches, 2006; Padgett, and DesRoches, 2007; Padgett et al., 2010; Ghosh et al. 2013, Jeon et al., 2015).

Dicleli and Bruneau (1995) investigated the response of single-span simply supported and continuous slab-on-girder steel bridges using linear elastic and nonlinear inelastic analysis. Based on elastic spectral analysis, they noted that bearing forces, both in longitudinal and transverse direction, were proportional to span length. The authors concluded from the inelastic time history analysis of bridges that 3-lane bridges are less vulnerable than 2-lane bridges. Another conclusion from their study is that the bridge response was significantly influenced by the stiffness with which the steel bearings are modeled. However, this conclusion was contradicted by the research on simply supported steel-girder bridges conducted by Ala Saadeghvaziri and Rashidi (1998), in which the bridge response was dependent on the stiffness of the bearings only in the transverse direction, but was inconsequential in the longitudinal direction.

Nielson and DesRoches (2006) carried out an experimental design to ascertain the significance of geometric, material, and structural uncertainties of multi-span simply supported steel girder bridges in the central and southeastern United States (CSUS).

Nonlinearities in the abutments, bearings, columns, and bent caps were explicitly considered in their study using detailed 3-D nonlinear models. The authors used a statistical analysis called ANOVA to identify the significant parameters for bridge samples subjected to seismic loading. The study revealed that damping ratio and loading direction are the most important parameters affecting the seismic response of bridges. The study also noted that column ductility and bearings deformations are sensitive to the type and stiffness of bearings.

Padgett and DesRoches (2007) extended the procedure used by Nielson and DesRoches (2006) to retrofitted bridges in CSUS and concluded that fragility curves developed with sensitive parameters are nearly identical to those developed with all potential sources treated as variables. Their study illustrated that preliminary screening of parameters could reduce the simulation and computational efforts for the generation of fragility curves. It has been noted from their study that the uncertainty in ground motion and gross geometry overshadows the contributions of other sources of uncertainty attributed to the bridge modeling. The sensitivity study was further extended by Padgett et al. (2010) to identify the effect of liquefiable soil and modeling parameters on the seismic reliability of critical components of steel bridges in CSUS. Although such studies are valuable for providing critical insights, most of them are rooted in rigorous statistical analysis based on experimental design and demand exhaustive computational efforts. Also, Mangalathu et al. (2017a) demonstrated that underlying assumptions in statistical methods have a significant influence on the identification of critical parameters. Kunnath et al. (2006) investigated the effect of foundation flexibility and soil-structure interaction on the seismic demands. However, the demand model is conditioned only on one parameter (IM) and hence it is difficult to estimate the sensitivity of other parameters on seismic demand. Ghosh et al. (2013) used a multi-parameter demand model to account for the effect of all uncertain parameters in the generation of fragility curves. The authors used four surrogate

modeling techniques, including polynomial response surface models, multivariate adaptive regression splines, radial basis function networks, and support vector machines to determine the best-fitting parameterized demand models involving the uncertain input parameters. However, as noted by a previous study (Padgett, 2007), it is highly unlikely that all of the uncertain parameters have a significant influence on the seismic demand model.

Kameshwar and Padgett (2014) identified the significant parameters that can affect the performance of bridges exposed to earthquake and hurricane hazards through a sequential forward selection scheme. The authors discussed the earthquake and hurricane risks to multiple-span simply supported (MSSS) concrete girder bridges in South Carolina based on variations in column diameter, column slenderness, and length of spans.

Jeon et al. (2016) employed a Bayesian framework to screen the parameters that have a significant influence on the seismic fragility estimate of curved bridges in California. The authors identified that parameters such as damping ratio, mass factor, longitudinal gap, backfill type, pile stiffness, column longitudinal reinforcement ratio, rotational and transverse stiffness of footing, bridge angle, main span length, side span-to-main span length ratio, and column height have a significant influence on the seismic demand of bridges. The study concluded that seven parameters (the earthquake direction factor, concrete strength, rebar yield strength, coefficient of friction, and shear modulus of elastomeric bearing pads, transverse gap, and abutment height) have little impact on all demand models. However, the framework suggested by authors is computationally expensive because they performed a set of stepwise regressions until the reduced model satisfied an acceptable value.

The random nature of earthquakes, and differences in geometric, material and structural attributes of bridges cause significant uncertainties in the estimation of seismic

demand and fragilities of bridge classes. The literature review on the uncertainty treatment of input parameters in bridge fragilities suggests the sensitivity parameters vary depending on the type of bridge and its location. Although these studies have been invaluable in acquiring an understanding of the effects of significant variables on the seismic demand and fragilities of bridges, there is still a need for identifying the relative impact of each uncertain input variable and the level of treatment needed for these variables in the estimation of seismic demand models and fragility curves. As the current study focuses on the box-girder bridges in California, a sensitivity study is needed for the box-girder bridges in California that can (1) identify the variables that exhibit strongest influences on seismic demand and seismic fragilities; (2) provide insight in quantifying whether the variation of uncertain parameters should be treated explicitly or be neglected; 3) eliminate the parameters which have a minimal influence on seismic demand and reduce unnecessary and exhaustive efforts in statistical sampling; (4) identify parameters which could reduce the uncertainty in demand models and fragility curves by more explicit evaluation of the uncertainty distribution (e.g., by developing an extensive database); and (5) help bridge owners (such as California Department of Transportation) spend their resources judiciously (e.g. data collection, field investigations, censoring) on parameters that have significant influences on bridge fragilities.

2.6 Closure

California is a state with a high seismic hazard and a history of damaging earthquakes. It has close to 29,000 bridges with varying ages and design parameters based on the year of their construction. However, it is cumbersome and time-consuming to develop unique fragility curves for each structure across a regional portfolio. One strategy that has been used to address this challenge is to group bridges into classes based on similar design or structural performance. Traditionally, this grouping has been conducted based on a relatively subjective identification of sub-classes. It is not known whether the subjective

classification yields distinct seismic performances (or seismic demand) between the grouped bridge classes. The literature review suggests the need for a performance-based grouping that can cover the entire California bridge inventory.

Fragility curves, which are probabilistic tools used to assess seismic damage to highway bridges, can be generated based on expert opinion, empirical approach, and through numeric methods. A review of the current methods for generating fragility curves is given in this chapter. Caltrans' current deployment of ShakeCast uses HAZUS-based bridge fragility models developed in the 1990s to support loss estimation by the Federal Emergency Management Agency. By necessity, these early models were derived with simplified analysis methods, compared to a limited set of damage observations, and use a bridge taxonomy based on the limited data fields available in the National Bridge Inventory (NBI). HAZUS fragility relationships suffer major drawbacks which are discussed in detail in this chapter. It has been noted that using HAZUS relationships leads to non-realistic estimation of the seismic risk. Also, HAZUS framework is not well aligned with Caltrans seismic design philosophy or the California bridge inventory. There is a need for the generation of fragility curves that can lead to a realistic estimation of seismic risk in California. High fidelity three-dimensional analytical models will be used in the current research to develop fragility curves for highway bridge classes.

The literature review also reveals the need for a sensitivity study on box-girder bridges that can identify the significant input parameters and the relative impact of these parameters on seismic demand models and fragilities. Such a sensitivity study would help Caltrans to spend their resources (e.g. data collection, field investigations, censoring) judiciously on parameters that have a significant influence on bridge fragilities.

CHAPTER 3 MODELING OF BRIDGE COMPONENTS

This section presents the various bridge components and the adopted numerical modeling strategies. Consistent with the previous work of Ramanathan et al. (2015), bridges are classified into pre 1971 design era (Era 11, hereafter), 1971-1990 design era (Era 22, hereafter), post 1990 design era (Era 33, hereafter) based on evolutions in the seismic design philosophy.

Highway bridges, as illustrated in Figure 3.1, have a number of bridge components. The components can be primarily classified into as superstructure and substructure. The super structure includes the girders, deck slab, and parapet, while the substructure consists of abutments, footing, bents (beam and columns), bearings, and shear key.

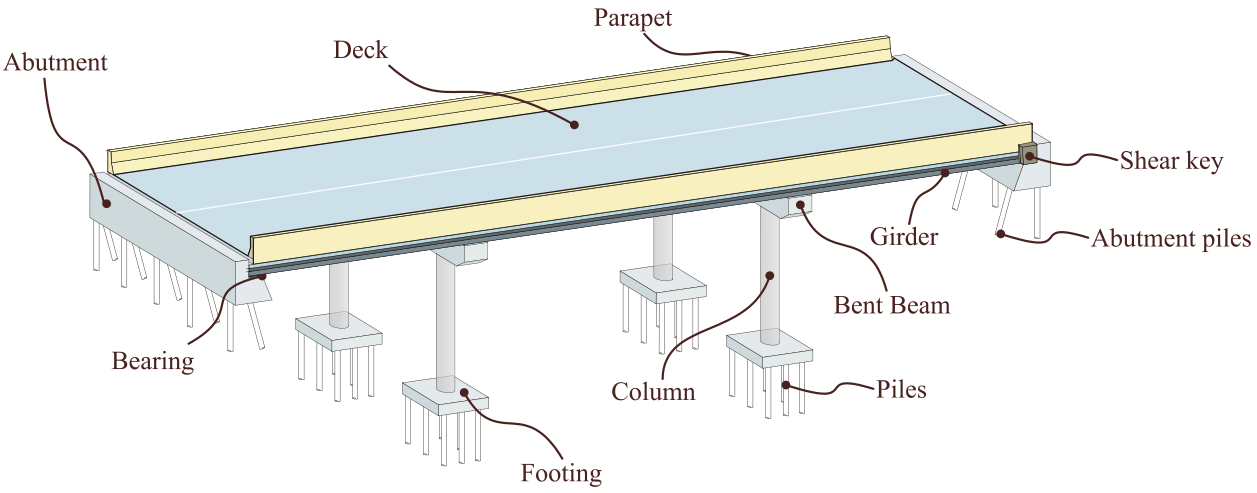

Figure 3.1 – Illustration of major bridge components.

A typical layout of the numerical modeling for a two-span bridge is shown in Figure 3.2. The bridge is modeled in three dimensions to capture responses in both the longitudinal and transverse directions, as well as their interactions. The modeling is carried out with the finite element package OpenSees (Mazzoni et al. 2006), incorporating geometric and material nonlinearities. Rayleigh damping is used in the non-linear time history analysis.

The ground motions representative of seismic risk in California are used in this study. The two horizontal components of the ground motions are assigned simultaneously to the longitudinal and transverse direction of the bridge, and the orientation is assigned randomly. The effects of vertical acceleration and spatially variable ground motions are not considered in this study. The following section explains the numerical modeling of various bridge components.

3.1 Superstructure

The superstructure of bridges is modeled as a spine with elastic beam-column elements since it is expected that the deck will remain elastic during earthquake loading. Transverse deck elements are modeled using elastic beam-column elements (rigid and massless) and are connected to the columns using rigid links to ensure the moment and force transfer between members. Translational and rotational springs are added to the base of the column to simulate the behavior of the footing. Zero length elements capturing the response of the abutment back fill soil and bi-directional force (abutment piles or frictional surface) are connected in parallel and are connected to the transverse deck elements in the case of diaphragm abutments. The abutment pile or friction surface model is selected based on the type of footing, whether the abutment is resting on piles or on a spread footing. In the case of cantilever abutments, the wall stem flexure is connected in series with the bi-directional force springs. Bearing pad elements and pounding elements are also modeled with zero length spring elements and are connected in parallel.

The following section presents detailed modeling considerations for various bridge components. In general, the bridge components are divided into superstructure and substructure.

The superstructure (bridge deck) typically remains elastic during an earthquake. The superstructure in this study is modeled using elastic beam-column elements and is shown in Figure 3.2.

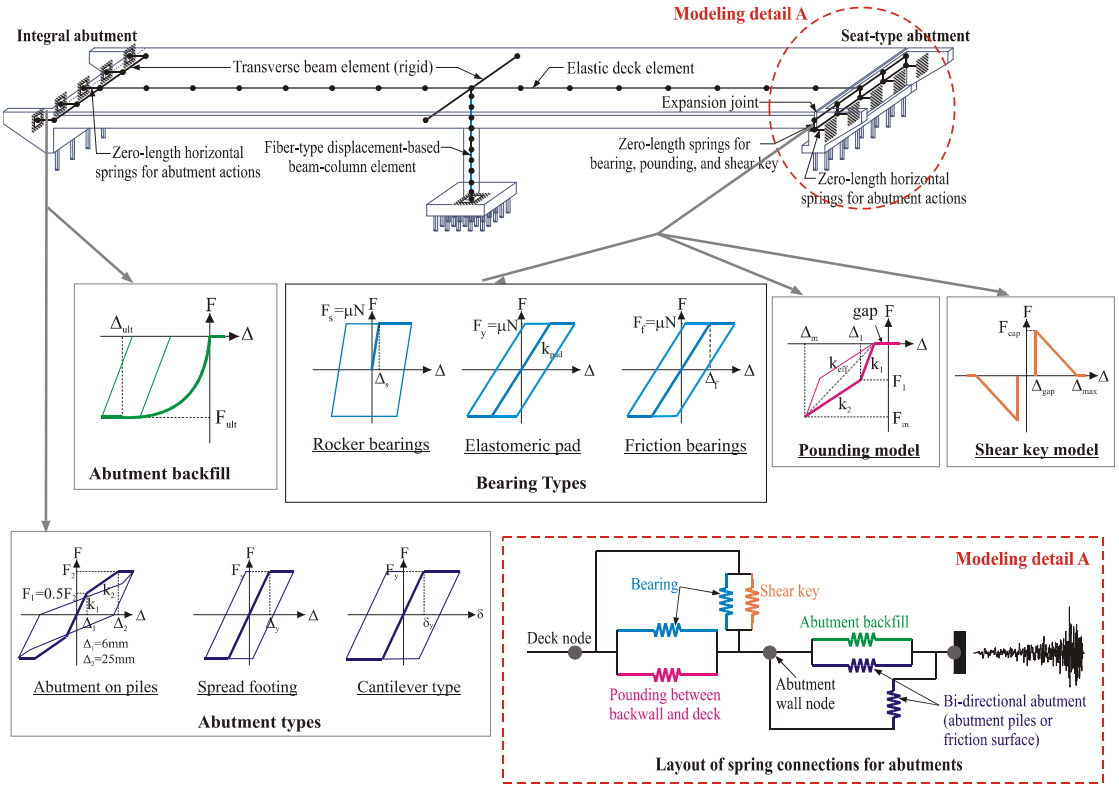

Figure 3.2 – Numerical modeling of various bridge components.

3.2 Substructure

California bridges have different pier types (single column bents (SCB), multi-column bents (MCB), pier walls or pile shafts), footing types (spread footing, shaft pile, or footing on piles), and abutment types (abutment on piles or abutment on footing).

3.2.1 Bents

The bents are modeled using a combination of displacement based beam column elements and rigid links to cause moment and force transfer between the members of the bent. The

finite element discretization of a single column and two-column bent is shown in Figure 3.3.

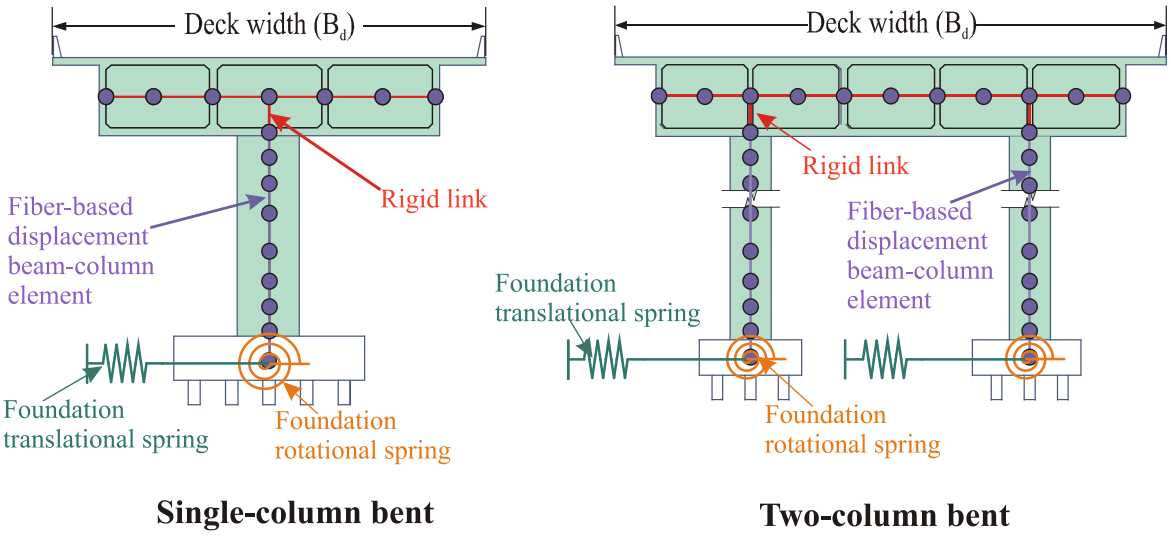

Figure 3.3 – Finite element discretization of bents.

3.2.2 Columns

Columns are one of the most vulnerable components in the event of an earthquake; the majority of bridge seismic failures in the past have been attributed to column failures. Displacement-based beam column elements with fiber-defined cross-sections are used in this study to model the columns (Figure 3.3). Fiber cross-sections have the distinct advantage of specification of unique material properties for different locations across a member's cross-section. For instance, confined concrete is used to represent the concrete behavior in the core section of the column, while unconfined concrete is used to represent the unconfined cover concrete. The Chang and Mander (1994) model is used to define the monotonic stress-strain curves of confined and unconfined concrete. Material models for the concrete section are shown in Figure 3.4, and Figure 3.5 shows the effectively confined core concrete area for the circular and rectangular section. Suppose, f_c represents the unconfined strength of concrete, the maximum concrete stress (f_{cc}) and corresponding strain (ε_{cc}) can be calculated as (Mander et al. 1988):

$$
\begin{aligned}
f_{cc} &= f_c + f_l k_e \\
&= f_c(1 + k_e \frac{f_l}{f_c}) \\
&= f_c CF \\
\varepsilon_{cc} &= \varepsilon_{co}(1 + k_2 \frac{f_l}{f_c})
\end{aligned}
\qquad \textbf{(3-1)}
$$

where f_l is the effective lateral confinement factor, k_e and k_2 are coefficients that are functions of the concrete mix and lateral pressure, and ε_{co} is the unconfined strain in concrete.

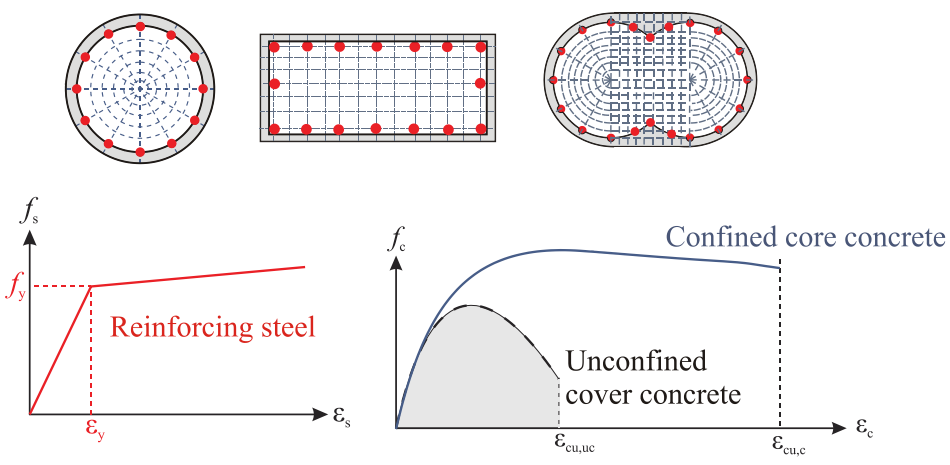

Figure 3.4 – Fiber based discretization of the columns.

The effective lateral confining pressure (f_l, Equation 3.2) for a circular column can be calculated as:

$$
f_l = \frac{1}{2}\rho_s f_{yh}; \qquad \rho_s = \frac{4A_{sp}}{d_s s} \qquad \textbf{(3-2)}
$$

where A_{sp} is the area of transverse reinforcement bar, f_{yh} is the yield strength of the transverse reinforcement, s is the center to center spacing or pitch of spiral or circular hoop, and d_s is the diameter of spiral bar centers. This is shown in Figure 3.5. The ratio of the

area of the effectively confined concrete core to the area of core of section enclosed by the perimeter lines of the perimeter spiral or hoop (Equation 3.3), k_e can be calculated as

$$k_e = \frac{1 - \frac{s'}{2d_s}}{1 - \rho_{cc}} \tag{3.3}$$

where ρ_{cc} is the ratio of area of longitudinal reinforcement to the area of core of section. k_2 is given as $5k_1$.

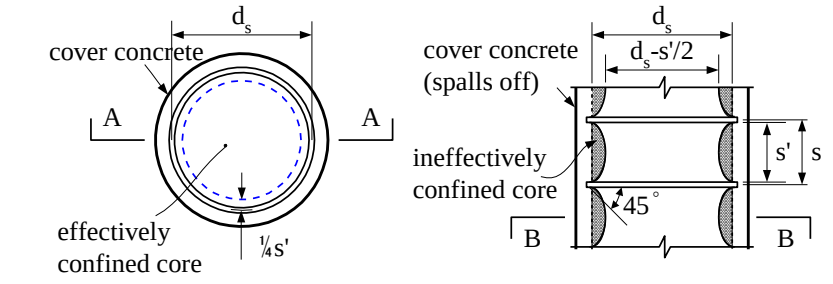

a)

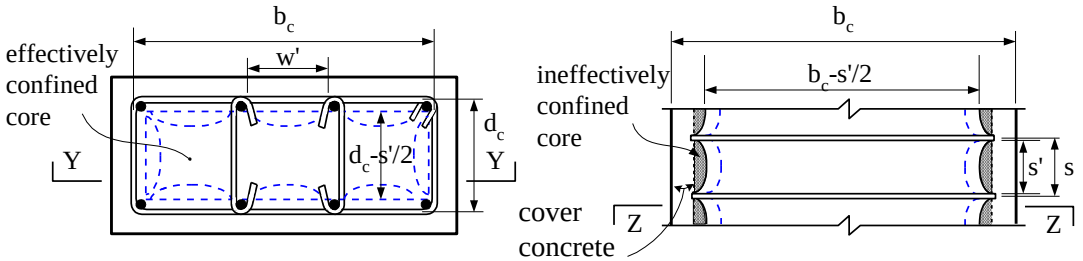

b)

Figure 3.5 – Effectively confined core for a) circular hoop reinforcement and, b) rectangular hoop reinforcement (Mander et al. 1988).

For a rectangular $b_c \times d_c$ (Figure 3.5), the area of effectively confined concrete core to the area of core of section (k_e) for a rectangular section can be calculated as

$$k_e = \frac{\left(1 - \sum_{i=1}^{n} \frac{(w_i')^2}{6 b_c d_c}\right)\left(1 - \frac{s'}{2b_c}\right)\left(1 - \frac{s'}{2d_c}\right)}{1 - \rho_{cc}} \tag{3.4}$$

The lateral confining stress of concrete in x and y directions (Figure 3.5) is given as

$$\begin{aligned} f_{l\,x} &= \rho_x f_{yh}; \qquad \rho_x = \frac{A_{sx}}{d_c s} \\ f_{l\,y} &= \rho_y f_{yh}; \qquad \rho_y = \frac{A_{sy}}{b_c s} \end{aligned} \tag{3.5}$$

where A_{sx} and A_{sy} are the total area of transverse bars running in the *x* and *y* direction.

The Menegotto and Pinto (1973) model, later modified by Filippou et al. (1983), is used to add isotropic strain hardening for steel (Figure 3.4).

3.2.2.1 Columns Types

Various cross sections such as circular, rectangular, wide perimeter, and wide circular are noted from the plan review. The typical details of some column cross-sections are shown in Figure 3.6. The wide perimeter cross-section corresponds to the section in which the reinforcement is laid around the perimeter, while the wide circular cross-section corresponds to the multi-circular reinforcement pattern. Regular cross-sections are classified as circular, rectangular, or oblong depending on the cross-section shape of their concrete core.

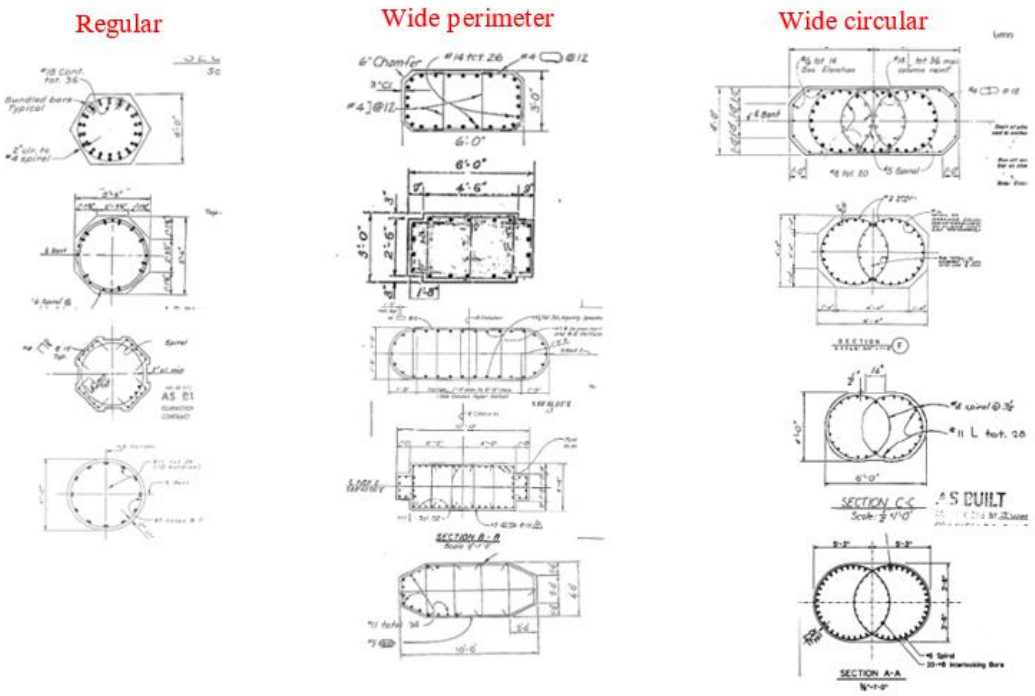

Figure 3.6 – Typical cross-sections noted from the bridge plan review (Caltrans, 2017).

3.2.2.2.1 Circular columns

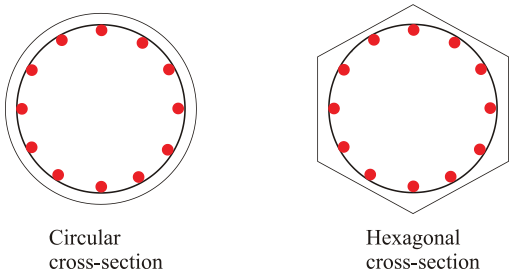

Figure 3.7 – Circular confined core concrete sections.

Figure 3.7 represents the common choice for columns with circular distribution of longitudinal reinforcement contained within transverse spirals or hoops. The area outside the core concrete can be circular, hexagonal, octagonal, or any other shape. In the case of a circular cross-section, flexural strength, shear strength, and moment capacity are independent of the direction of loading.

3.2.2.2 Rectangular columns

Rectangular columns of various sizes are noted from the plan review of bridges. Figure 3.8 shows some of the typical rectangular cross sections noted from the plan review. It is noteworthy to mention that the strength and stiffness of the rectangular columns depend on the direction of loading.

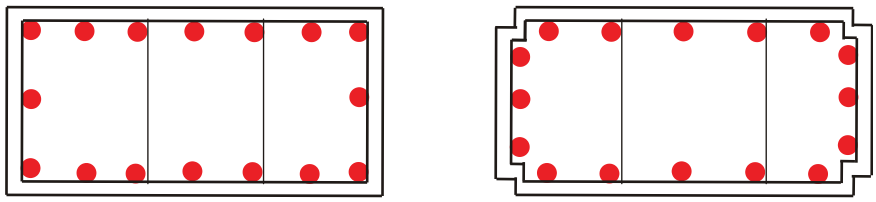

Figure 3.8 – Typical rectangular cross sections.

3.2.2.1.3 Oblong columns

The superior performance of the spiral reinforcement over the rectilinear tie transverse reinforcement led to the development of columns with interlocking spirals (also called oblong columns, Figure 3.9). The confinement factor of a single column fiber is applicable to the oblong columns as most of the confined concrete in double-spirals is confined by a single spiral and the interlocking region is a relatively small area (Correal et al. 2007).

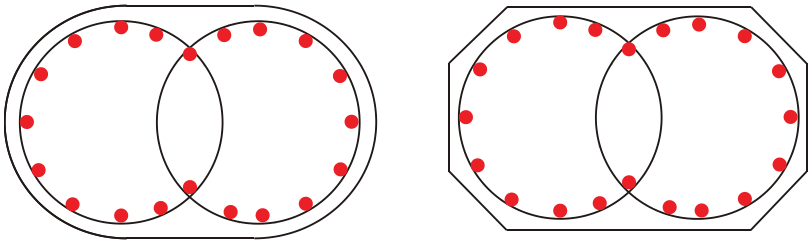

Figure 3.9 – Oblong columns.

3.2.3 Idealization of bridge columns

As the California bridge inventory consists of wide range of column cross-sections, some idealizations are used in this study. The idealization is carried out in such a way as to mimic the bridge inventory noted from plan review and is detailed in Table 3.1. The idealization of the cross-sections is carried out based on the area of confined concrete, as the core concrete will continue to carry stress at higher strains. The cover concrete becomes ineffective once the compressive strength is attained in the flexural deformation, and the effect of cover concrete is neglected in idealizing the cross-sections.

Table 3.1 – Idealization of bridge columns.

	Column cross-section from the bridge inventory	Idealized cross-section shape	Remarks*
Symmetric	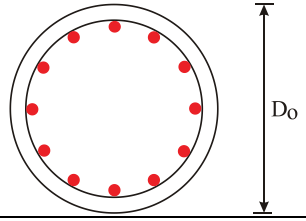	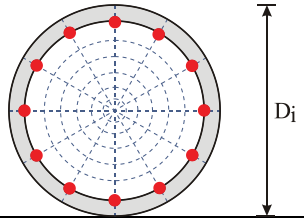	No idealization needed $D_o = D_i$ CF= circular
	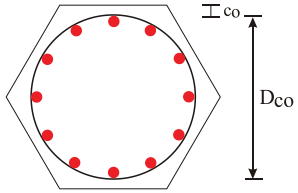	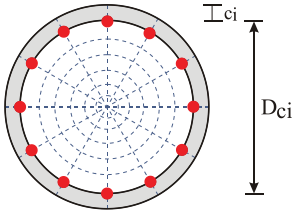	Idealized to circular cross-section. Area of core concrete remains the same $Dc_o = Dc_i$ $c_o = c_i$ CF= circular
	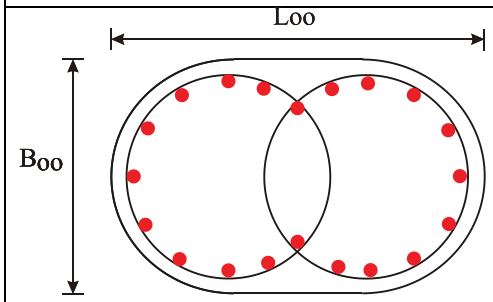	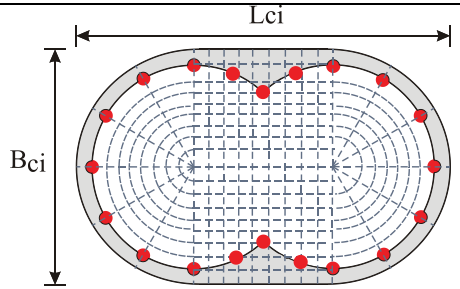	No idealization needed $L_{oo} = L_{co}$ $B_{oo} = B_{co}$ CF= circular

	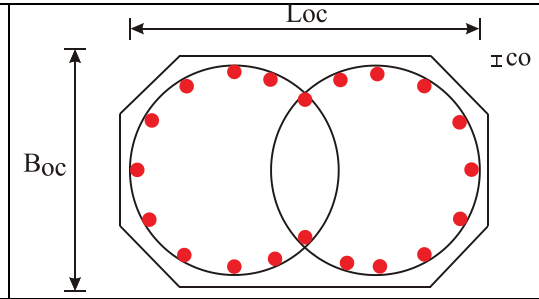	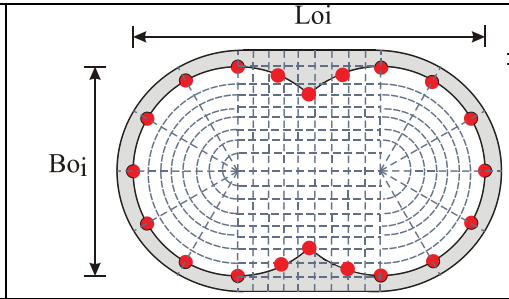	Idealized to oblong cross-section. Area of core concrete remains the same $L_{oc} = L_{oi}$ $B_{oc} = B_{oi}$ co = ci CF= circular
Wide perimeter	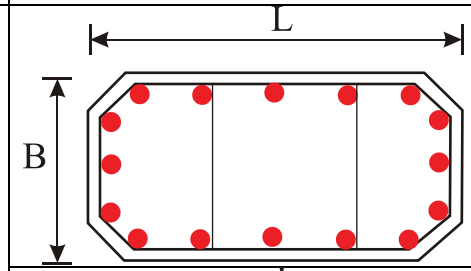	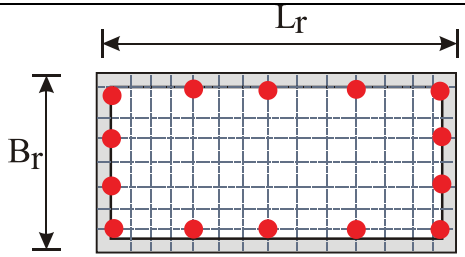	Idealized to rectangular cross-section. $L = L_r$ $B = B_r$ CF= rectangular
	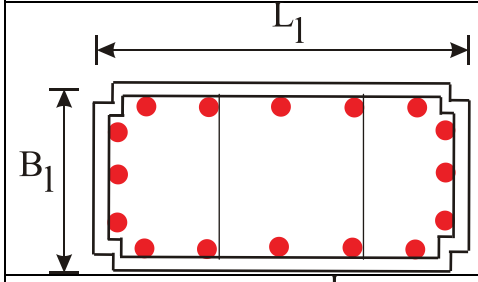	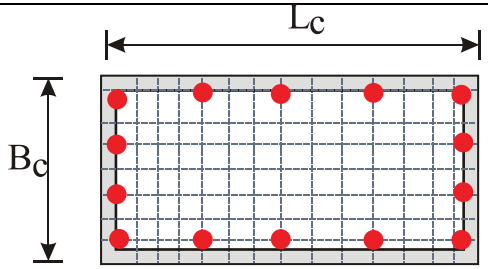	Idealized to rectangular cross-section. $L_l = L_c$ $B_l = B_c$ CF= rectangular
	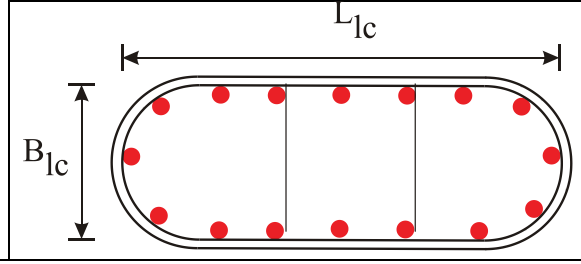	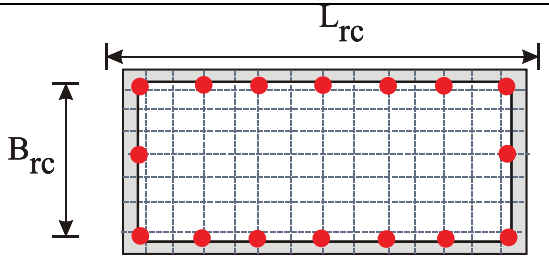	Idealized to rectangular cross-section. (Area of two sections remains the same) $B_{lc} = B_{rc}$ CF= rectangular

	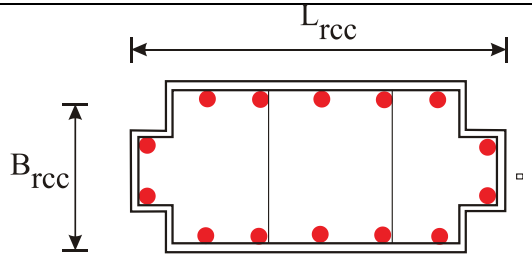	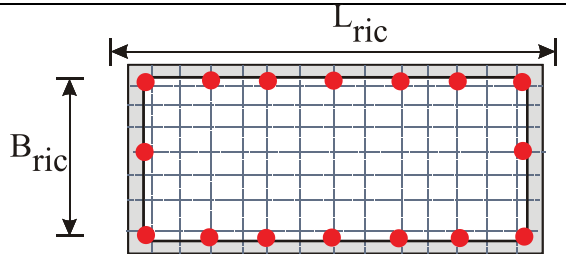	Idealized to rectangular cross-section. (Area of two sections remains the same) $B_{rcc} = B_{ric}$ CF= rectangular
	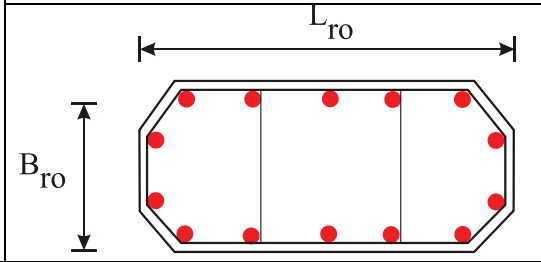	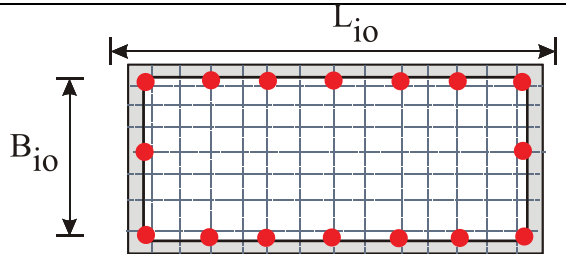	Idealized to rectangular cross-section. (Area of two sections remains the same) $B_{ro} = B_{io}$ CF= rectangular
Wide circular	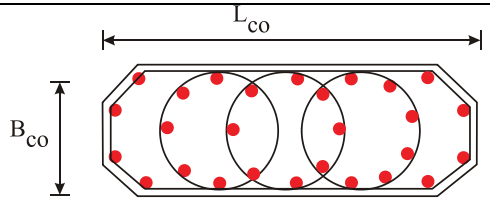		Planning to exclude as the count is less than 5% of total inventory

3.2.4 Validation of bridge columns

Figure 3.10 shows the comparison of the numerical model with the experimental results for Era 33 columns. The geometric and reinforcement details are obtained from Lehman and Moehle (2000), and the modeling details are outlined in section 3.2.2. It is seen from the comparison that the numerical model is able to capture the key responses fairly well.

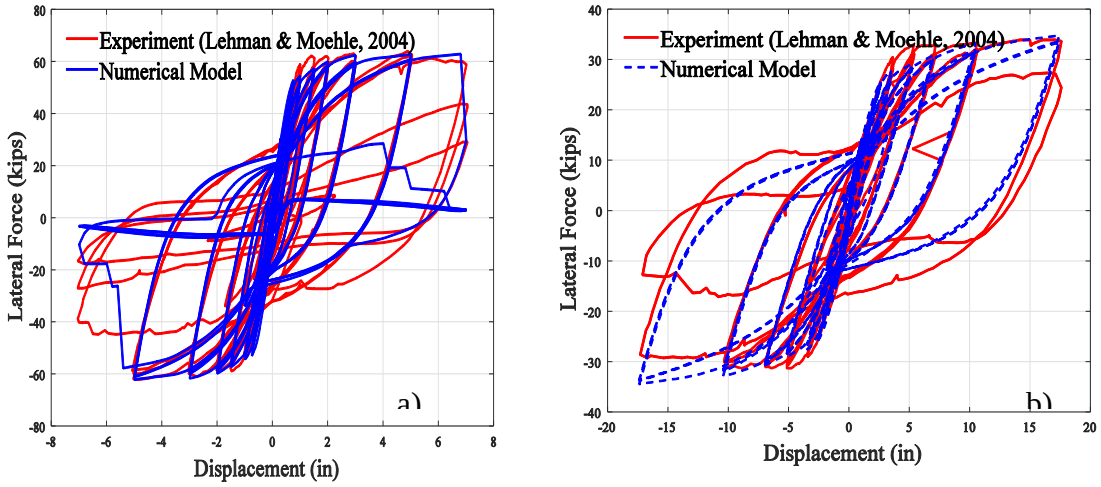

Figure 3.10 – Comparison of experimental and numerical results for era 33 columns (Lehman and Moehle, 2000) a) Specimen No. 415 b) Specimen No. 815.

3.3 Abutments

Abutments can be classified in two basic types: diaphragm abutments and seat abutments (Ramanathan, 2012). Diaphragm abutments are cast monolithic with the superstructure. As they engage the backfill soil during seismic action, diaphragm abutments provide a good source of energy dissipation and reduce the likelihood of span unseating. Seat abutments provide a bearing support to the superstructure, which is restrained longitudinally by the abutment backwall and transversely by the piles and the shear key. The stiffness and resistance to the seismic action increases when the deck is in contact with the abutment backwall in the longitudinal direction. However, as the

superstructure moves away from the abutment, the resistance depends primarily on the bearing pads, which makes it susceptible to unseating. The backwall of the seat abutment is typically designed to fail under impact and passive response, before damaging forces are transmitted to the lower portion of the abutment.

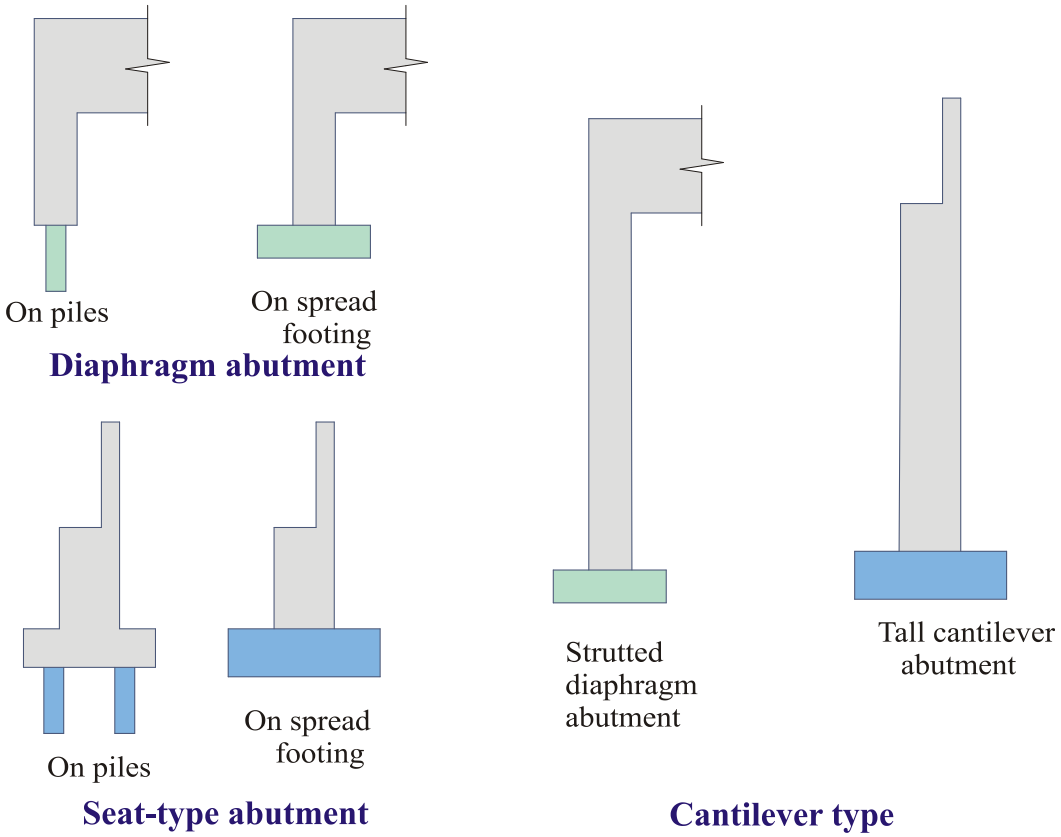

Figure 3.11 – Various types of abutments.

The major configurations of abutments noted from the review of bridge plans in various design eras are shown in Figure 3.11. Abutment can be on piles, on spread footing or cantilever. Abutments resting on piles are the major configuration for both diaphragm and seat abutments. However, the review of bridge plans also revealed a variety of unusual abutment wall details (Figure 3.12) which seemed to be designed to provide a weak link in the stem wall above the footing which could either translate along a construction joint or rotate on an intermediate section of the stem wall. These details were found on about 15-20% of the diaphragm-type abutments.

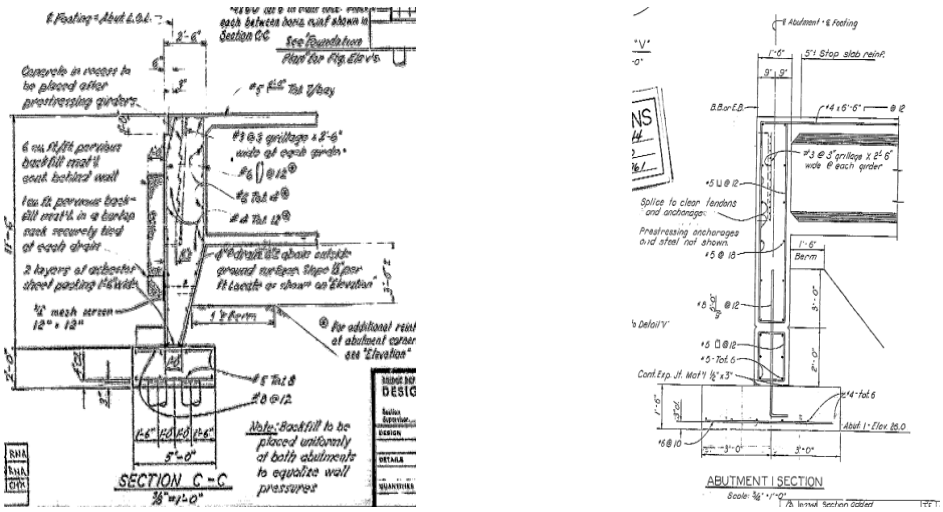

Figure 3.12 – Unusual abutment types (Caltrans, 2017).

Abutment responses to seismic actions include earth pressure response and structural response. The earth pressure on the abutment is due to the longitudinal response of the bridge deck and includes passive and active resistance. Passive resistance is provided by the backfill soil and piles/friction surface (depending on the abutment footing type); it develops when the abutment moves toward the backfill soil. Piles/friction surface alone contribute the active resistance, which is activated when the abutment moves away from the backwall soil. The passive response of the abutment backwall is simulated using the hyperbolic soil model proposed by Shamsabadi and Yan (2008) and is given in Figure 3.13. The model is based on experimental testing of bridge abutments conducted at the University of California Los Angeles with 5.5 ft. high backwalls and typical non-cohesive and cohesive backfill soils. The test results were then extended to develop closed form solutions for the abutment backfill soil response for a range of backwall heights based on a series of analyses using the limit-equilibrium method which implements mobilized logarithmic-spiral failure surfaces coupled with a modified hyperbolic soil stress strain behaviour. F_{ult} is the maximum abutment force developed at maximum displacement Δ_{ult}.

Equation 3.6 presents the closed form solution for the force displacement response of the backfill soil, where F is the force expressed in kip/ft width of the backwall, Δ is the displacement expressed in inches, and H is the height of the backwall expressed in feet.

$$\begin{aligned} F(\Delta) &= \frac{8\Delta}{1+3\Delta} H^{1.5} && \textit{Granular backfills} \\ &= \frac{8\Delta}{1+1.3\Delta} H && \textit{Cohesive backfills} \end{aligned} \tag{3.6}$$

The maximum displacement of the backwall is 0.05H and 0.1H (expressed in inches) for granular (sandy soils) and cohesive (clay soils) backfills, respectively, and substitution of these values in Equation 3.6 yields the ultimate force in the abutment. The backfill soil response is modeled using *HyperbolicGapMaterial* provided by OpenSees, which corresponds to the model proposed by Shamsabadi and Yan (2008). The force-displacement response of the *HyperbolicGapMaterial* is given in Equation 3.7.

$$F(\Delta) = \frac{\Delta}{\frac{1}{K_{max}} + R_f \frac{\Delta}{F_{ult}}} \tag{3.7}$$

where, the failure ratio R_f is 0.7, K_{max} is secant stiffness at half of the maximum abutment force.

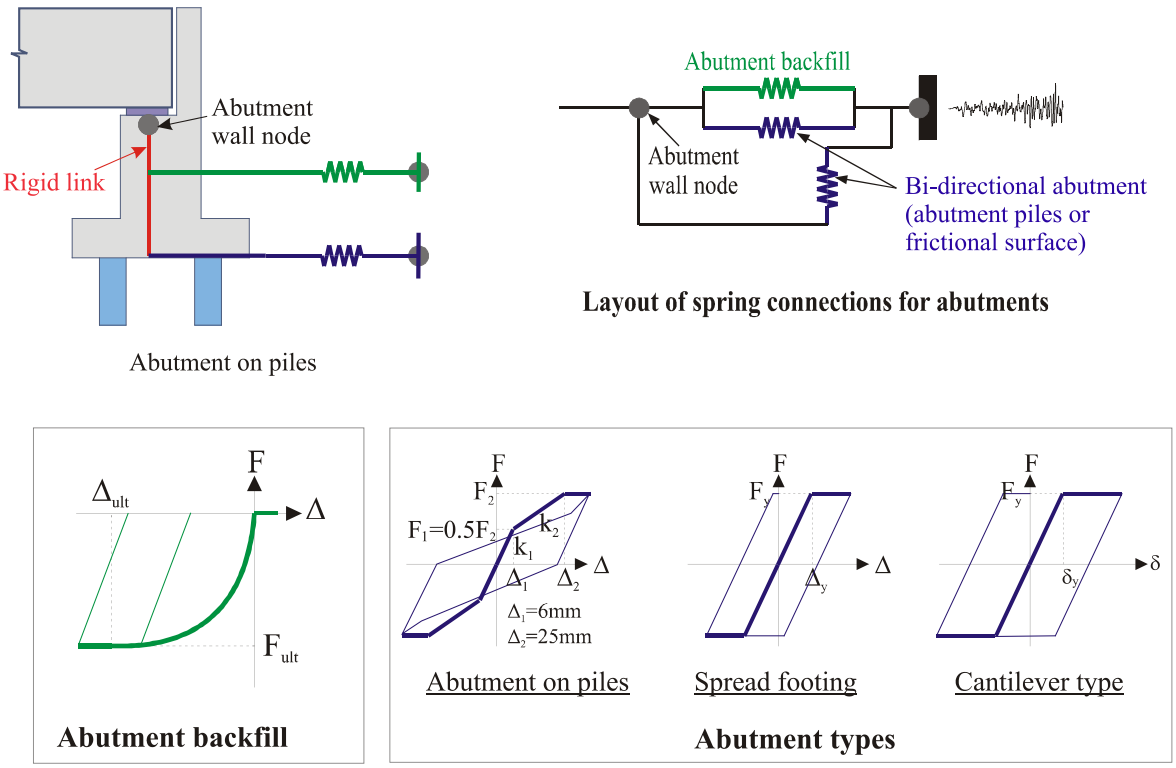

Figure 3.13 – Modeling of the abutments.

Piles provide longitudinal and transverse stiffness to the abutments when abutments rest on piles. The trilinear force-deformation response of the pile, along with the associated modeling parameters, are presented in Figure 3.13. The initial yield parameters (Δ_1, F_1) are determined following the design recommendations of the Caltrans 2014 draft of bridge design aids on 'Permissible Horizontal Loads for Standard Plan and Steel HP Piles' (Caltrans, 2015). The plastic yielding parameters (Δ_2, F_2) are calculated based on results of modeling various pile systems simulated in LPILE (Caltrans, 2015). The hysteretic behavior of piles is captured using the *Hysteretic* material in OpenSees with the hysteretic parameters *pinchX* and *pinchY* as 0.75 and 0.5 (Ramanathan, 2012). In contrast, for abutments supported on spread footings, a frictional response model is used. The maximum force (F_s) is calculated as the product of the coefficient of friction (μ_f) and the dead load reaction on the abutment. For cantilever abutments, the bi-linear model is obtained from numerical modelling of various cantilever type abutments in OpenSees.

3.4 Bearings

The bearings most commonly used for seat abutment bridges are rocker or elastomeric bearings, as shown in Figure 3.14. These bearings are characterized by different response mechanisms. Rocker bearings shown in Figure 3.14 (a) are considered vulnerable due to non-ductile transverse keeper plate failure and longitudinal instability (Mander et al., 1996). The elastomeric bearings shown in Figure 3.14(b) usually transfer horizontal forces using friction, and their behavior is characterized by sliding. Elastomeric bearings decouple the superstructure from the substructure, and thus the superstructure is susceptible to large deformations. Additionally, a special type of bearing called friction bearing can also be found in Era 11 bridges. The predominant difference between the Era 11 and the later design eras is the replacement of steel rocker bearings with elastomeric steel bearings. This shift in the bearing type is due to advancement in the seismic design philosophies.

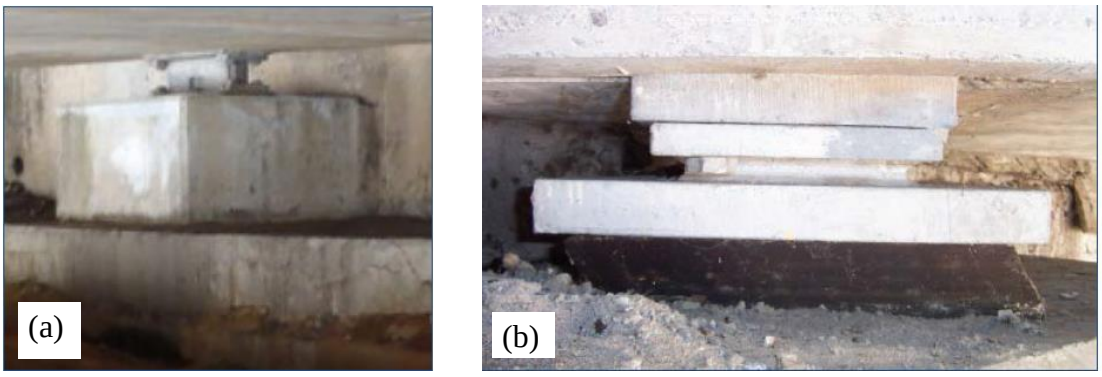

Figure 3.14 – Types of bearings: (a) rocker bearing and (b) elastomeric bearing (Mangalathu et al. 2016).

The elastomeric bearing is assumed to be elasto–plastic and the yield force, Fy, is obtained by multiplying the normal force by the coefficient of friction (Figure 3.15). The

rocker bearing is modeled following the experimental work of Mander et al. (1996). This material model includes a frictional component, and its longitudinal force-deformation behavior is shown in Figure 3.15. An elasto–plastic behavior is assumed for the friction bearings. The bearings are modeled using the *Steel01* material in OpenSees.

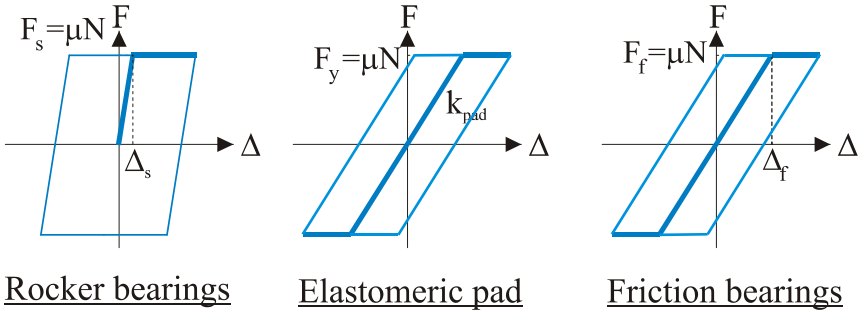

Figure 3.15 – Modeling of various bearings.

3.5 Shear Keys

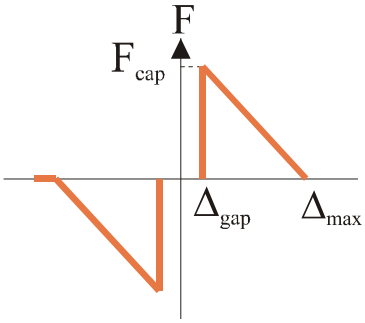

Figure 3.16 – Modeling of shear key.

Shear keys help restrain the relative transverse movement between the deck and the bridge abutments. A shear key can fail through four mechanisms in the event of an earthquake, namely shear friction, flexure, shear, and bearing (Megally et al. 2002). The shear key designs are categorized as isolated (emerging designs) or non-isolated

(conventional designs) (Caltrans 2017). Since the isolated shear key is a new type of design and does not exist in the current inventory, this study will focus only on the non-isolated shear keys. The nonlinear model of the shear key is also depicted in Figure 3.16. F_{cap} denotes the capacity of the shear key, which is computed as the product of the dead-load reaction and the acceleration (Caltrans 2015). Megally et al. (2002) conducted a series of experiments on the shear keys and found that Δ_{max} minus Δ_{gap} equal to 3.5 in. is the deformation at which the capacity of the shear keys essentially degrades to zero.

3.6 Pounding

Seismic pounding is the impact between the bridge decks, between deck and abutment, or between the adjacent decks in a multi-frame bridge in the longitudinal direction. Impact occurs when the relative displacement between adjacent decks or deck and abutment exceeds the gap between them. Significant pounding damage was noticed at the I-5/SR-14 interchange during the 1994 Northridge earthquake (Muthukumar and DesRoches, 2006). Some instances of pounding damage, ranging from superficial to complete collapse, are shown in Figure 3.17.

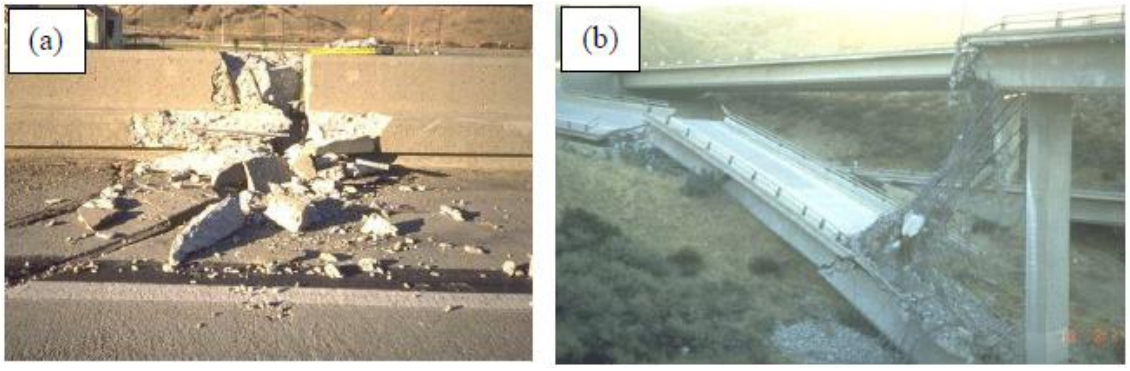

Figure 3.17 – Pounding damage in bridges during the 1994 Northridge earthquake: (a) barrier rail damage and, (b) connector collapse (Muthukumar and DesRoches, 2006).

The contact element developed by Muthukumar and DesRoches (2006) is used to model the pounding between superstructures and abutments. This material model explicitly

accounts for the loss of hysteretic energy (Figure 3.18). The maximum deformation, Δ_m, is assumed to be 1.0 in. The yield deformation, Δ_1, is assumed to be $0.10\Delta_m$. The stiffnesses, k_1 and k_2, are recommended to be 1022.3 kip/in/ft and 351.755 kip/in/ft, respectively.

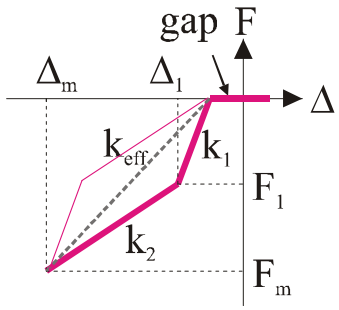

Figure 3.18 – Analytical Model for pounding between deck and abutment back wall.

3.7 Foundation

The foundation provides a means to transmit service and ultimate loads from the structure to the underlying soil. Foundations can be classified as either shallow or deep. As the name implies, the loads from the structure are transferred to the underlying soil at a shallow depth for shallow foundations. Deep foundations are used when soil conditions are not favourable to shallow foundations and transfer the load through piles. The type of foundation for a particular bridge is determined by various factors such as soil conditions, overhead clearance, existing utilities, and proximity to existing facilities such as buildings and railroads (Caltrans 2017). The possible types of footings are shown in Figure 3.19. Foundations are modeled using elastic translational and rotational springs (Figure 3.20) and are added at the base of the column.

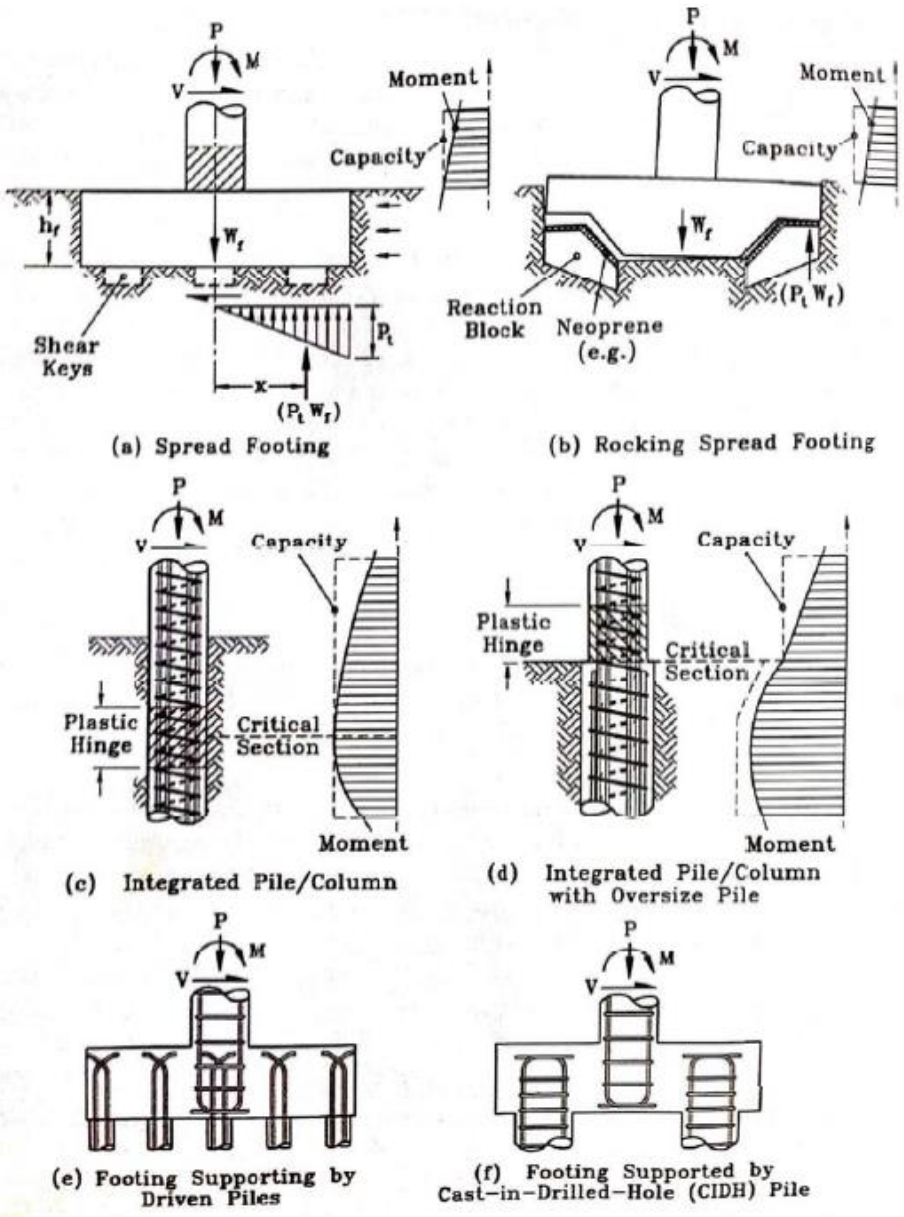

Figure 3.19 – Bridge foundation types (Priestley et al. 1996).

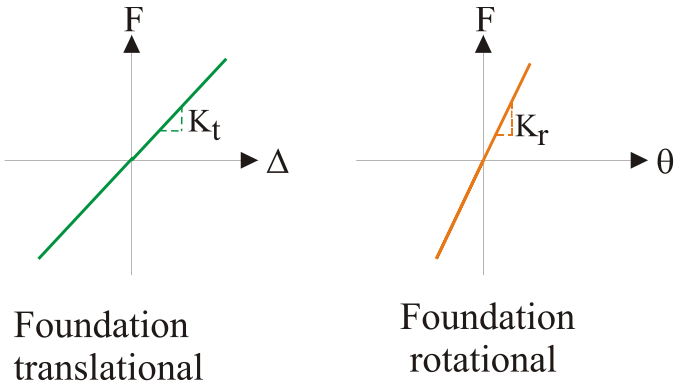

Figure 3.20 – Modelling of foundations.

3.8 Closure

The numerical modeling of various bridge components, and the integration of various component models, to generate a global analytical model of the bridge for fragility analysis. Displacement-based beam column elements are used to model the columns. Translational and rotational springs are added to the base of the column to simulate the behavior of the footing. Zero length elements capturing the response of the abutment back fill soil and bi-directional force (abutment piles or frictional surface) are connected in parallel and to the transverse deck elements in the case of diaphragm abutments. Bearing pad elements and pounding elements are also modeled with zero length spring elements and are connected in parallel to abutment springs in the case of seat abutments.

Interested readers are directed to the study from our research group members (Ramanathan et al. 2015; Soleimani 2017), for the validation of the global analytical model of the bridges. Ramanathan et al. (2015) compared the efficacy of the nonlinear dynamic analysis of the bridge models with the recorded ground motion data. The authors compared the response of a two span reinforced concrete box-girder bridge built in 1971 (Meloland Road Overpass) with the recorded ground motion during the 1970 Imperial Valley Earthquake. The bridge is instrumented with twenty-six channels of accelerometers and

peak ground acceleration (PGA) values of the ground motions that strike the bridges were of intensity, 0.32 g, 0.30 g, and 0.23 g in the longitudinal, transverse, and vertical directions, respectively. The authors concluded that the analytical model yield comparable results to the sensor data for the Meloland bridge. Note that the lack of data prevents the comparison of the bridge model with the ground motions that can cause significant nonlinear response. Soleimani (2017) compared the dynamic response of bridge columns with the full scale shake table test on single column bridge bent (Schoettler et al. 2012) to the various ground motions. It is noted from their study that the analytical model can predict the shear force and deformation of the column fairly well for various damages states.

CHAPTER 4 PERFORMANCE BASED GROUPING OF BRIDGE CLASSES

One of the critical aspects of seismic risk assessment of highway bridge infrastructure systems is the generation of fragility curves that are applicable to a class of bridges. California, a state with a high seismic hazard and a history of damaging earthquakes, has close to 29,000 bridges that vary in age based on their construction. However, it is cumbersome and time-consuming to develop unique fragility curves for each structure across a regional portfolio. One strategy that has been adopted to address this challenge is to group bridges into classes with similar design or structural performance. The bridges in a particular class (or group) are expected to have similar performance or damages during an earthquake. The identification of specific bridge parameters or bridge design attributes that yield distinct seismic performance to bridges is an important step in this procedure.

Traditionally, this grouping has been performed based on a relatively subjective identification of sub-classes. However, such subjective identification leads to a number of bridge classes with unwarranted grouping (HAZUS, 2013). The limitation of the HAZUS grouping is discussed in detail in the literature review of this thesis. This chapter explains the various performance based grouping strategies such as analysis of variance (ANOVA), analysis of Covariance (ANCOVA) and Kruskal–Wallis (KW) approach. Although these approaches are used widely in many disciplines such as biology, medical, and industrial engineering (Vidakovic 2011; Vickers 2005), the application, relevance, and advantages of these grouping techniques for the grouping of bridge classes for probabilistic seismic performance assessment have not been fully explored. The selected methods have different approaches and underlying assumptions to grouping structures, which are reviewed and compared on the basis of statistical power to identify attributes that dictate distinct bridge

sub-classes of structural performance. The comparison is based on case studies of two-span and three-span bridges in California. The assumptions underlying each approach are investigated in detail in this chapter. It is noteworthy to mention that the comparison is conducted in order to select a rational grouping procedure. A performance-based grouping approach is suggested in this chapter to group the California bridge inventory. A review of the application of ANOVA, ANCOVA, and KW in grouping the bridge classes is given in the next section.

4.1 Review of ANOVA, ANCOVA, and Kruskal–Wallis approach

This section briefly introduces the ANOVA, ANCOVA, and KW methods for grouping bridge classes. The grouping is achieved by comparing bridge responses of various bridge sub-classes and by identifying whether they are statistically different. The response considered in this study includes (1) maximum column curvature ductility, (2) maximum abutment passive deformation, (3) maximum abutment active deformation, (4) maximum abutment transverse deformation, (5) maximum unseating deformation, and (6) maximum bearing deformation. The maximum responses are obtained from a set of NLTHAs. Figure 4.1 shows the scatter plot of seismic demand or response (*D*) of two typical bridge groups with the *IM,* along with the probability distribution of their seismic demands. PSDMs are usually obtained by performing a linear regression for a pair of *D* and *IM,* using a suite of *N* ground motions. In a mathematical form, PSDM can be written as

$$\ln(S_d) = \ln(a) + b\ln(IM) \tag{4.1}$$

where *a* and *b* are the regression coefficients and, S_d is the median estimate of the demand in terms of an *IM*. The coefficients *a* and *b* are obtained by performing a linear regression analysis on *D* and *IM* pairs in the log–transformed space. Dispersion, $\beta_{d/IM}$, is evaluated based on statistical analysis of *D* and *IM* pairs:

$$\beta_{d/\mathrm{IM}} = \sqrt{\frac{\sum_{i=1}^{N}\left(\ln d_i - \ln\left(S_d\right)\right)^2}{N-2}} \tag{4.2}$$

where d_i is the demand for the i^{th} ground motion.

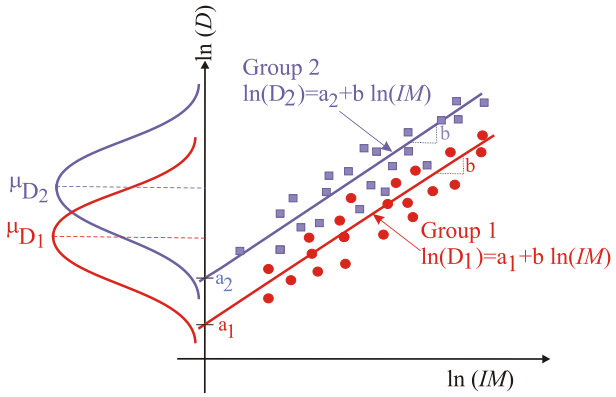

Figure 4.1 – Illustration of PSDM and grouping strategy.

4.2 ANOVA based grouping

Analysis of covariance (ANOVA) is generally utilized to determine whether there are any significant differences between the means of two or more independent, unrelated groups (Miller Jr 1997; Keselman et al., 1998; Vidakovic 2011; Mangalathu et al., 2017a; Mangaalthu et al., 2017b). It tests the hypothesis ($H_0 : \mu_{D_1} = \mu_{D_2}, \ldots, = \mu_{D_k}$) that the mean seismic responses of different bridge classes are equal (Figure 4.2) and can group the bridge classes accordingly. The assumptions underlying ANOVA are: (1) the responses are mutually independent, (2) homogeneity of response variance, and (3) samples are mutually independent. If the assumptions are violated, ANOVA is not a powerful test and the results may be incorrect or misleading.

Let D_{i1}, $D_{i2}, \ldots, D_{in}$, be the samples of bridge responses and n be the sample size, then $N = \sum_{i=1}^{k} n_i$ is the total sample size and k the number of groups to be compared. ANOVA can be used to test the hypothesis (Figure 4.2)

$$H_0 : \mu_{D_1} = \mu_{D_2} = \ldots = \mu_{D_k}$$
$$H_1 = (H_0)^c \qquad (\text{or } \mu_i \neq \mu_j \text{ for atleast one pair } i, j) \tag{4.3}$$

The total sum of squares (*SST*) is represented as a sum of the treatment sum of squares (SST_r) and the sum of squares due to error

$$SST = SST_r + SSE$$
$$\sum_{i=1}^{k}\sum_{j=1}^{n_i}(\mathrm{D}_{ij} - \bar{D})^2 = \sum_{i=1}^{k} n_i(\bar{D}_i - \bar{D})^2 + \sum_{i=1}^{k}\sum_{j=1}^{n_i}(\mathrm{D}_{ij} - \bar{D}_i)^2 \tag{4.4}$$

The test H_0 (treatment effect is zero) is based on the *F*–statistic,

$$F = \frac{SST_r / (\mathrm{k}-1)}{SSE / (N-k)} \tag{4.5}$$

with *k-1* and *N – k* degrees of freedom. The null hypothesis is rejected if the *F* - statistic is large compared to (1 - α) quantile of an *F* – distribution. The results can be inferred more easily though *p* - value.

$$p - \text{value} = 1 - Fcdf\left(F, k-1, N-k\right) \tag{4.6}$$

The *p*–value is the evidence against a null hypothesis or the probability that the variation between groups occurred by chance. The *p*–value can be interpreted as the probability of such an 'extreme' value of the test statistic when H_0 is true.

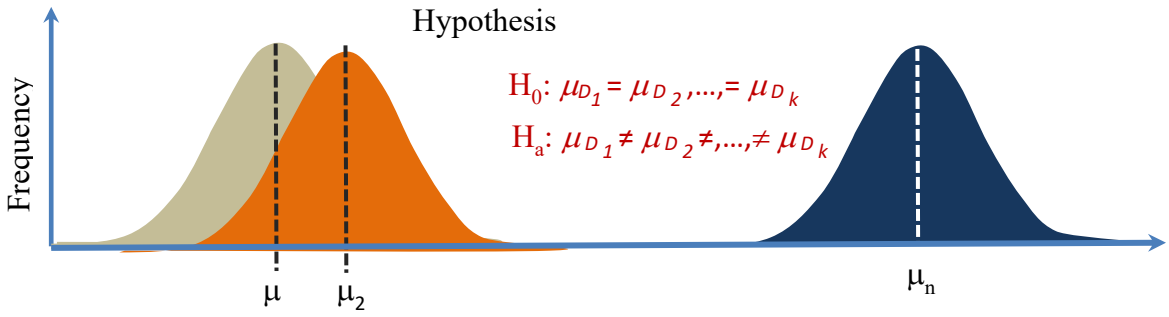

Figure 4.2 – ANOVA hypothesis.

4.3 ANCOVA based grouping

Analysis of covariance (ANCOVA) mainly checks whether two or more population means are equal, similar to analysis of variance (ANOVA). However, ANCOVA formulation includes the bridge response, bridge sub-class, and ground motion intensity (covariate). The first step in performing ANCOVA is to establish a linear regression relationship between the bridge response and the intensity measure for different bridge sub-classes (or PSDMs) and to identify whether slopes of the regression lines are significantly different. If the slopes are not significantly different, a regression line is drawn through each group of points with the same slope. The intercept of the regression lines is then checked, and if they are different, it can be concluded that the response of the bridge sub-classes is different (Figure 4.1). The statistical significance of treatment is more likely to be identified in an ANCOVA *F*-test than ANOVA. Two important assumptions in ANCOVA, in addition to the assumptions in ANOVA, are the independence of the treatment effect and the homogeneity of regression slopes.

In ANCOVA, the model is assumed as

$$\ln(S_d)_{ij} = \mu_{\ln(IM)} + \alpha_{si} + b_s(\ln(IM)_{ij} - \overline{\ln(IM)}) + \varepsilon_{ij},\ i=1,...,a_t;\ j=1,...,n \qquad (4.7)$$

where ln*(Sd)* is the response variable, $\mu_{\ln(IM)}$ the overall population mean of the intensity measure, a_t the number of treatments, n the common sample size, $\overline{\ln(IM)} = \frac{1}{a_t n}\sum_{i,j}\ln(IM)_{ij}$ the overall mean of ln*(IM)*'s, b_s the regression slope, and α_{si} the treatment effect. The error term ε_{ij} is assumed to be an independent normal distribution with zero mean and variance σ^2. $\overline{\ln(IM)}_i = \frac{1}{n}\sum_j \ln(IM)_{ij}$ is the *i*th bridge attribute effect for the ln*(IM)*'s. The means $\overline{\ln(S_d)}$ and $\overline{\ln(S_d)}_i$ are defined analogously to $\overline{\ln(IM)}$ and $\overline{\ln(IM)}_i$, respectively. The sum of squares and mixed-product sums can be calculated as

$$S_{\ln(IM)\ln(IM)} = \sum_{i=1}^{a_t}\sum_{j=1}^{n}(\ln(IM)_{ij} - \overline{\ln(IM)})^2,\ S_{\ln(IM)\ln(S_d)} = \sum_{i=1}^{a_t}\sum_{j=1}^{n}(\ln(IM)_{ij} - \overline{\ln(IM)})(\ln(S_d)_{ij} - \overline{\ln(S_d)})$$

$$S_{\ln(S_d)\ln(S_d)} = \sum_{i=1}^{a_t}\sum_{j=1}^{n}(\ln(S_d)_{ij} - \overline{\ln(S_d)})^2, T_{\ln(IM)\ln(IM)} = \sum_{i=1}^{a_t}(\overline{\ln(IM)}_i - \overline{\ln(IM)})^2$$

$$T_{\ln(IM)\ln(S_d)} = \sum_{i=1}^{a_t}(\overline{\ln(IM)}_i - \overline{\ln(IM)})(\overline{\ln(S_d)}_i - \overline{\ln(S_d)}),\ T_{\ln(S_d)\ln(S_d)} = \sum_{i=1}^{a_t}(\overline{\ln(S_d)}_i - \overline{\ln(S_d)})^2 \quad (4.8)$$

$$Q_{\ln(IM)\ln(IM)} = \sum_{i=1}^{a_t}\sum_{j=1}^{n}(\ln(IM)_{ij} - \overline{\ln(IM)}_i)^2,\ Q_{\ln(IM)\ln(S_d)} = \sum_{i=1}^{a_t}\sum_{j=1}^{n}(\ln(IM)_{ij} - \overline{\ln(IM)}_i)(\ln(S_d)_{ij} - \overline{\ln(S_d)}_i),$$

$$Q_{\ln(S_d)\ln(S_d)} = \sum_{i=1}^{a_t}\sum_{j=1}^{n}(\ln(S_d)_{ij} - \overline{\ln(S_d)}_i)^2$$

The estimator of the variance is

$$s^2 = MSE = \frac{SSE}{(a_t(n-1)-1)}, \text{ where } SSE = Q_{\ln(S_d)\ln(S_d)} - \frac{Q^2_{\ln(IM)\ln(S_d)}}{Q_{\ln(IM)\ln(IM)}} \quad (4.9)$$

If there are no treatment effects, i.e., $\alpha_{si} = 0$, then the model is

$$\ln(S_d)_{ij} = \mu_{\ln(IM)} + b_s(\ln(IM)_{ij} - \overline{\ln(IM)}) + \varepsilon_{ij},\ i = 1,...,a_t;\ j = 1,...,n \quad (4.10)$$

In this case, the error sum of squares is

$$SSE' = S_{\ln(S_d)\ln(S_d)} - \frac{S^2_{\ln(IM)\ln(S_d)}}{S_{\ln(IM)\ln(IM)}},\ \text{with } a_t n - 2 \text{ degrees of freedom} \quad (4.11)$$

Thus, the test $H_0 : \alpha_{si} = 0$ (treatment effect is zero) is based on the *F*–statistic,

$$F = \frac{(SSE' - SSE)/(a_t - 1)}{SSE/(a_t(n-1)-1)} \quad (4.13)$$

which has an *F*–distribution with $a_t - 1$ and $a_t(n-1)-1$ degrees of freedom.

The *p*–value of the *F*–statistic (upper trail area of the *F*–distribution) can be calculated as

$$p - \text{value} = 1 - Fcdf\left(F, a_t - 1, a_t(n-1)-1\right) \quad (4.14)$$

where *Fcdf* is the cumulative distribution function of the *F*–distribution. The *p*–value is the evidence against a null hypothesis, $H_0 : \alpha_{si} = 0$; in other words, the effect of treatment in Equation 4.7 is zero. The inclusion of ground motion intensity in the grouping of bridge sub-classes has several advantages: there is a higher probability that the test will reject a false H_0; there is a reduction in bias caused by chance differences between groups; and there is a conditionally unbiased estimate of treatment effects (Mangalathu et al. 2016a; Huietema 1980). ANCOVA assumes the homogeneity of regression slopes; and if the relationship assumed in the ANCOVA comparison is non–linear, there will be a significant reduction in the statistical power (Owen and Froman, 1998). This limitation can be averted in some cases by a transformation of the data.

4.4 KW-based grouping

The stringent assumptions on the response data placed in ANOVA and ANCOVA are often difficult to satisfy, which has led the development of non–parametric and semi–parametric approaches. The non–parametric approaches help to relax the restrictive assumptions on the ANOVA and ANCOVA. The Kuruskal-Wallis (KW) is a non–parametric version of ANOVA. KW tests place no restriction on the population data, and are applicable to complex experiments and messy sampling plans. The KW test statistic (H') for k bridge sub-classes with sample sizes, $n_1,\ldots,n_k$ is (Kruskal and Wallis, 1952)

$$H' = \frac{1}{S^2}\left(\sum_{i=1}^{k}\frac{R_i^2}{n_i} - N\frac{(N+1)^2}{4}\right) \tag{4.15}$$

where, $N = \sum n_i$, and R_i is the sum of the ranks for the i^{th} sample, and

$$S^2 = \frac{1}{N-1}\left(\sum_{i=1}^{k}\sum_{j=1}^{n_i} R_{ij}^2 - N\frac{(N+1)^2}{4}\right) \tag{4.16}$$

where R_i is the sum of the ranks for the i^{th} sample across the sample size j. If there are no ties in the data, Equation 4.15 can be simplified to

$$H = \frac{12}{N(N+1)} \sum_{i=1}^{k} \frac{1}{n_i} \left(R_i - \frac{n_i(N+1)}{2} \right)^2 \tag{4.17}$$

which approximately follows a χ^2 distribution with $k-1$ degrees of freedom. KW tests the hypothesis that responses from different bridge sub-classes have identical distribution functions against the alternate hypothesis that the samples differ only with respect to the median, if at all. Despite all its advantages over ANOVA and ANCOVA, the power of the KW is restricted in the case of normally distributed data (Vickers, 2005).

4.5 Case Study: Two-and Three-Span Box-Girder Bridges in California

Two-span and three-span box girders bridges, which possess a major portion of the California bridge inventory (Ramanathan, 2012) are the subject bridges in this study. The selected bridges were designed and constructed prior to 1970. A typical layout of a two-span box-girder bridge is shown in Figure 4.3. The current study adopts six different bridge attributes such as (1) bearing type (elastomeric or rocker bearings), (2) column cross–section (circular or rectangular), (3) abutment configuration (abutment on piles or on spread footing), (4) abutment backfill (clay or sand), (5) interior bent type (single–column or multi–column), and (6) material type of superstructure (reinforced or prestressed concrete).

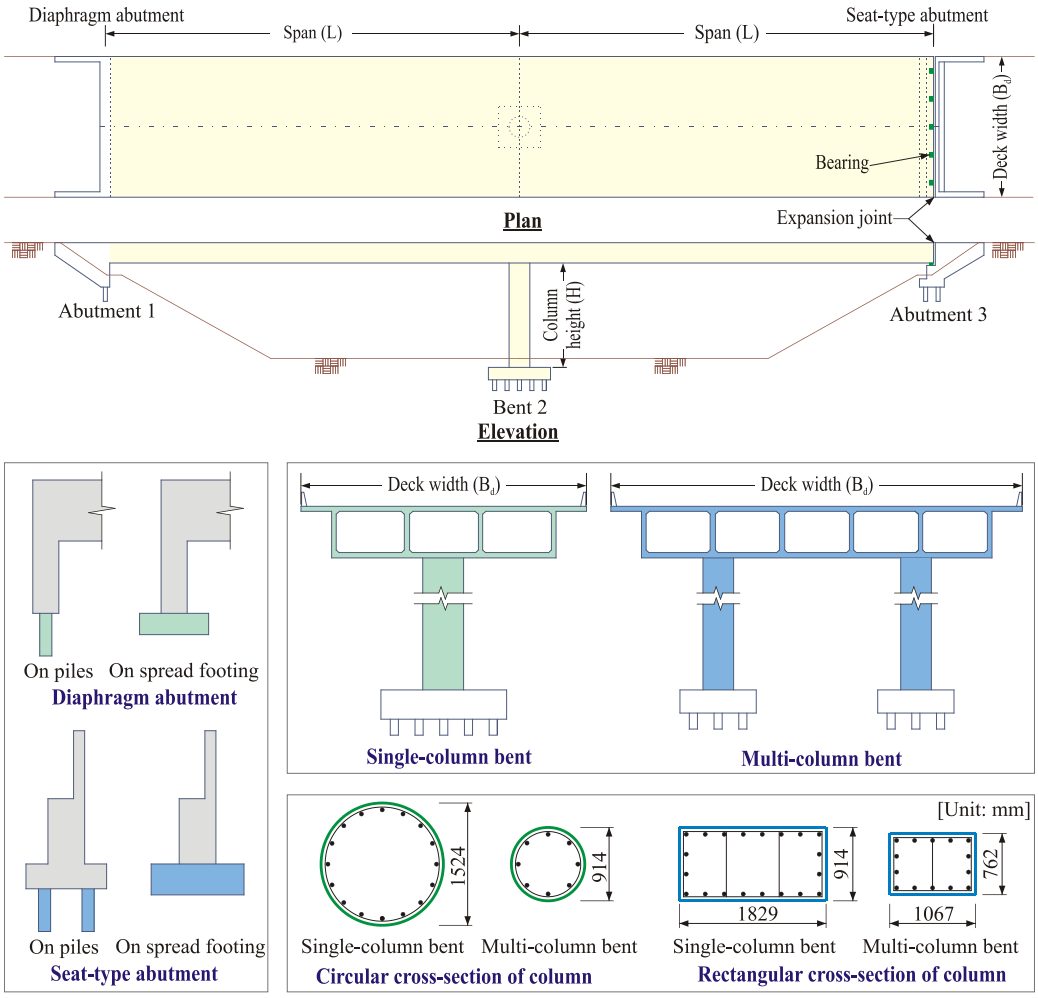

Figure 4.3 – General layout of a two–span concrete box–girder bridge.

The analytical modeling of the bridges is explained in detail in Chapter 3. A number of sources of uncertainties (aleatoric or epistemic) are present in the selected class of bridges, and are given in Table 4.1, which shows the mean value (μ), standard deviation (σ), and the associated probability distribution of various input variables. These variables are determined based on an extensive plan review of California bridges. In addition to the uncertainties related to structures, the uncertainty in ground motions are accounted for using the suite of ground motions assembled by Baker et al. (2011). The entire suite of ground motions are scaled by a factor of two (Ramanathan, 2012) to have sufficient

response data of *IM*s higher than Palmdale spectrum (the highest probabilistic design hazard level in California), and thus the expanded suite of 320 ground motions is used for the current study. Additionally, the spectral acceleration at 1.0 sec ($S_{a-1.0s}$) is the optimal intensity measure for the class of concrete box–girder bridges (Ramanathan, 2012), and is adopted as the *IM* in the current study.

As mentioned before, the objective of this study is to identify whether all of the grouping techniques lead to similar sub-classes. To compare the responses with different bridge attributes, the total simulation is split amongst the bridge attributes. For example, to identify the significance of cross–section on seismic response, 50% of the simulations (160) are carried out for bridges with rectangular columns, while the remaining simulations are performed for bridges with circular columns. The response variable and the ground motion intensity measure are transformed into the lognormal space to produce a linear relationship between the two (Cornell et al. 2002; Managalathu et al. 2016b). Using the relationship between the transformed response variable and intensity measure, ANOVA, ANCOVA, and KW grouping techniques are carried out. In all the grouping methods, *p*–values are computed to interpret the results of the hypothesis test. A smaller *p*–value indicates stronger evidence for rejecting the null hypothesis (H_0), and a cut–off *p*–value of 0.05 (Mangalathu et al. 2016a) is adopted in the current study. For example, at a cut–off value of 0.05, if the *p*–value is less than 0.05, it can be concluded with a 95% degree of confidence that the variation in the demand measure is not due to random chance, but due to the influence of the different bridge attributes. *p*–values less than 0.05 are highlighted in Table 4.2. The table indicates that the various demand parameters are typically sensitive to different bridge attributes. Among six bridge attributes, the type of interior bent is a significant parameter for all cases. It can be explained that the transverse moment demands in single column bents are higher than the longitudinal moment demands and have less redundancy than multi–column bents (Priestley et al. 1996).

The grouping pattern identified by the three methods is the same for 80% of the cases. ANOVA and KW yield the same identification of significant bridge attributes in 96% of the cases. The results of ANCOVA are different from those of ANOVA and KW in approximately 17% of cases. ANCOVA identifies more design attributes as significant in comparison to ANOVA and KW tests, which is shown in italics in Table 4.2. While comparing the ANOVA and KW grouping methods, ANOVA identifies more relevant parameters. The reason for such a discrepancy is investigated in detail in the following section.

Table 4.1 – Uncertainty distribution considered in the bridge models

Parameter	Units	Distribution		
		Type	μ	σ
Concrete compressive strength (f_c)	MPa	Normal	29.03	3.59
Reinforcing steel yield strength (f_y)	MPa	Lognormal	465.0	37.30
Span length (L)				
Two-span	mm	Lognormal	31775	8738
Approach to main span ratio (three-span bridge)	–	Normal	0.57	0.13
Deck width (B_d)				
Single column bent	mm	Lognormal	9780	1980
Multi-column bent	mm	Lognormal	11970	2418
Column height (H)	mm	Lognormal	6625	865
Abutment backwall height (H_a)				
Diaphragm abutments				
On piles	mm	Lognormal	3234	488
On spread footings	mm	Lognormal	2925	1056
Seat-type abutments				
On piles	mm	Lognormal	2186	441
On spread footings	mm	Lognormal	2186	441
Abutments on piles - Lateral capacity/deck width (K_{pa})				
Diaphragm abutment	N/mm	Lognormal	1120	404
Seat-type abutment	N/mm	Lognormal	1498	540
Abutments on spread footing				
Coefficient of friction (μ_{as})	–	Normal	0.40	0.075
Yield displacement (δ_y)	mm	Uniform	19.0	13.4
Elastomeric bearing pad				
Stiffness per deck width (K_b)	N/mm/m	Lognormal	908	327
Coefficient of friction for bearing pad (μ_b)	–	Normal	0.30	0.10
Rocker bearing				
Coefficient of friction (μ_l, longitudinal direction)	–	Normal	0.04	0.01
Coefficient of friction (μ_t, transverse direction)	–	Normal	0.10	0.02
Gap (g)				
Longitudinal (btw. deck and abutment wall)	mm	Lognormal	23.5	12.5
Transverse (btw. deck and shear key)	mm	Lognormal	12.8	2.58
Mass factor (m)		Uniform	1.25	0.007
Damping (ξ)		Normal	0.045	0.0125
Acceleration for shear key capacity (a_s)	g	Lognormal	1.00	0.20
Longitudinal reinforcement ratio (ρ)	(%)	Uniform	2.25	0.52
Pile group – pile cap and piles				
Translational stiffness (K_{ft})				
Single column – 1% long. rebar	N/mm	Normal	297716	140101
Single column – 3% long. rebar	N/mm	Normal	245178	105076
Multi column – 1.5% long. rebar	N/mm	Normal	140101	105076
Rotational stiffness (K_{fr})				
Single column – 1% long. rebar	N-m/rad	Normal	4.5×10^9	1.1×10^9
Single column – 3% long. rebar	N-m/rad	Normal	6.8×10^9	1.1×10^9

Table 4.2 – *p*–values by ANCOVA, ANOVA and KW test

Type		Bridge attribute	Column (μ_ϕ)			Passive (δ_p)			Active (δ_a)			Transverse (δ_t)			Unseating (δ_s)			Bearing (δ_b)		
			ANCOVA	ANOVA	KW	ANCOVA	ANOVA	KW	ANCOVA	ANOVA	KW	ANCOVA	ANOVA	KW	ANCOVA	ANOVA	KW	ANCOVA	ANOVA	KW
Two–span bridges	Diaphragm abutment	Column cross–section	**0.000**	**0.000**	**0.000**	0.834	0.667	0.567	0.897	0.720	0.631	0.908	0.723	0.686	–	–	–	–	–	–
		Interior bent	**0.000**	**0.000**	**0.000**	***0.038***	*0.233*	*0.326*	***0.046***	*0.315*	*0.417*	**0.000**	**0.000**	**0.000**	–	–	–	–	–	–
		Abutment	**0.000**	**0.000**	**0.000**	0.494	0.354	0.322	0.382	0.359	0.332	**0.000**	0.021	0.033	–	–	–	–	–	–
		Backfill	0.458	0.635	0.856	**0.000**	**0.000**	**0.000**	**0.000**	**0.000**	**0.000**	***0.018***	*0.209*	*0.387*	–	–	–	–	–	–
		Superstructure	0.438	0.775	0.875	0.715	0.464	0.639	0.832	0.467	0.680	0.703	0.230	0.269	–	–	–	–	–	–
	Seat–type abutment	Column cross–section	***0.043***	*0.317*	*0.343*	0.149	0.446	0.554	0.463	0.727	0.800	**0.005**	**0.048**	0.064	0.263	0.466	0.509	0.116	0.223	0.318
		Bearing	**0.005**	**0.003**	**0.002**	**0.043**	**0.008**	**0.001**	*0.124*	***0.031***	***0.003***	**0.008**	**0.002**	**0.000**	**0.000**	**0.000**	**0.000**	**0.002**	**0.000**	**0.008**
		Interior bent	**0.000**	**0.000**	**0.000**	**0.001**	**0.000**	**0.000**	**0.000**	**0.000**	**0.000**	**0.007**	**0.000**	**0.000**	**0.000**	**0.000**	**0.000**	**0.000**	**0.000**	**0.000**
		Abutment	0.302	0.988	0.943	0.252	0.052	**0.038**	0.469	0.125	0.085	0.116	0.507	0.548	0.600	0.200	0.209	0.194	0.494	0.315
		Backfill	**0.045**	**0.032**	**0.012**	0.148	0.401	0.478	0.145	0.486	0.537	0.549	0.892	0.831	0.722	0.844	0.887	0.641	0.667	0.747
		Superstructure	0.631	0.413	0.321	***0.039***	*0.609*	*0.686*	0.084	0.583	0.667	***0.036***	*0.643*	*0.646*	***0.001***	*0.438*	*0.451*	0.351	0.600	0.600
Three–span bridges	Diaphragm	Column cross–section	*0.010*	*0.135*	*0.070*	0.690	0.882	0.873	0.709	0.897	0.859	0.426	0.405	0.470	–	–	–	–	–	–
		Interior bent	**0.000**	**0.000**	**0.000**	***0.000***	*0.093*	*0.151*	***0.000***	*0.077*	*0.128*	**0.000**	**0.000**	**0.000**	–	–	–	–	–	–
		Abutment	0.095	0.520	0.356	0.317	0.298	0.529	0.440	0.368	0.620	0.441	0.954	0.953	–	–	–	–	–	–
		Backfill	0.799	0.637	0.771	**0.000**	**0.002**	**0.002**	**0.000**	**0.007**	**0.005**	0.228	0.568	0.626	–	–	–	–	–	–
		Superstructure	0.155	0.347	0.498	0.419	0.850	0.807	0.314	0.763	0.723	0.877	0.593	0.551	–	–	–	–	–	–
	Seat–type abutment	Column cross–section	0.097	0.451	0.459	0.582	0.548	0.625	0.858	0.853	0.881	***0.001***	*0.027*	*0.025*	0.637	0.907	0.935	0.669	0.569	0.914
		Bearing	0.258	0.378	0.482	***0.005***	***0.043***	*0.357*	**0.000**	**0.002**	**0.048**	0.006	0.066	0.173	**0.000**	**0.000**	**0.003**	0.128	0.168	0.754
		Interior bent	**0.000**	**0.000**	**0.000**	**0.000**	**0.000**	**0.000**	**0.000**	**0.000**	**0.000**	**0.000**	**0.000**	**0.000**	**0.000**	**0.000**	**0.000**	**0.000**	**0.000**	**0.000**
		Abutment	***0.003***	*0.104*	*0.065*	***0.002***	*0.334*	*0.739*	***0.000***	*0.153*	*0.376*	***0.000***	*0.174*	*0.158*	**0.000**	**0.000**	**0.000**	*0.014*	*0.050*	*0.034*
		Backfill	**0.000**	**0.001**	**0.001**	0.388	0.565	0.952	0.918	0.958	0.836	0.142	0.272	0.259	***0.001***	*0.059*	*0.072*	***0.023***	*0.117*	*0.058*
		Superstructure	0.172	0.961	0.678	0.088	0.776	0.815	0.067	0.885	0.994	***0.005***	*0.321*	*0.327*	***0.004***	*0.718*	*0.779*	0.083	0.732	0.931

4.6 Comparison of various grouping techniques

ANCOVA shows that some of the design attributes are significant, while ANOVA and KW tests identify the same attributes as non–significant, as noted in Table 4.2. This non–significance can be interpreted in two ways. Firstly, the lack of attribute significance may be obtained because there is indeed very little or no true effect of the design attribute on the seismic response. Alternatively, the finding suggesting a lack of significance can be attributed to the grouping technique having less power to identify the effects of the design attribute (Huitema, 1980). To evaluate the power and efficiency of various grouping techniques, the current study selects three bridge sub–classes: (1) three-span diaphragm abutment bridges grouped by the cross–section shape based on the curvature ductility response, (2) two-span seat-type abutment bridges grouped by the cross–section shape based on the transverse abutment response, and (3) two-span seat-type abutment bridges grouped by the abutment type based on the passive abutment response. The three sub classes are carefully chosen such that one of the grouping techniques identifies the design attribute as non–significant.

4.6.1 Case 1: Significant per ANCOVA

For the three-span diaphragm abutment bridge, two sub–classes are formed based on the curvature ductility response according to the column cross–section: (1) with circular cross–section (hereafter, 3SDC) and (2) with rectangular cross–section (hereafter, 3SDR). The ANCOVA result (p–value of 0.010) reveals that the cross–section is significant for this bridge, while the ANOVA (p–value of 0.135) and KW (p–value of 0.070) tests conclude it is not significant. Figure 4.4 shows the data analysis results of the curvature ductility for 3SDC and 3SDR. The power of ANOVA and the ANCOVA depends on the three or four assumptions and is evaluated initially. One of the critical assumptions in both ANOVA and ANCOVA is that the data is normally distributed. The normality of 3SDC and 3SRC is checked using the Kolmogorov–Smirnov test (KS test) (Kolmogorov, 1933), which identifies the null hypothesis that the data is normally distributed. If

the *p*–value is less than $\alpha = 0.05$, the null hypothesis is rejected. Thus, there is enough evidence that the data do not follow a normally distributed population. The *p*–value of normality check for 3SDC and 3SDR is 0.067 and 0.099, respectively, and hence one fails to reject the null hypothesis. The assumption that each observation is mutually independent is valid because of the random sampling and pairing of the bridge and ground motions. The validity of the assumption of the independence of the treatment effect lies in the fact that the different bridge attributes are independent of each other. ANCOVA has one additional assumption regarding the homogeneity of regression slopes. As the demand measure increases with the intensity of ground motions, it implies a monotonic relationship between the two.

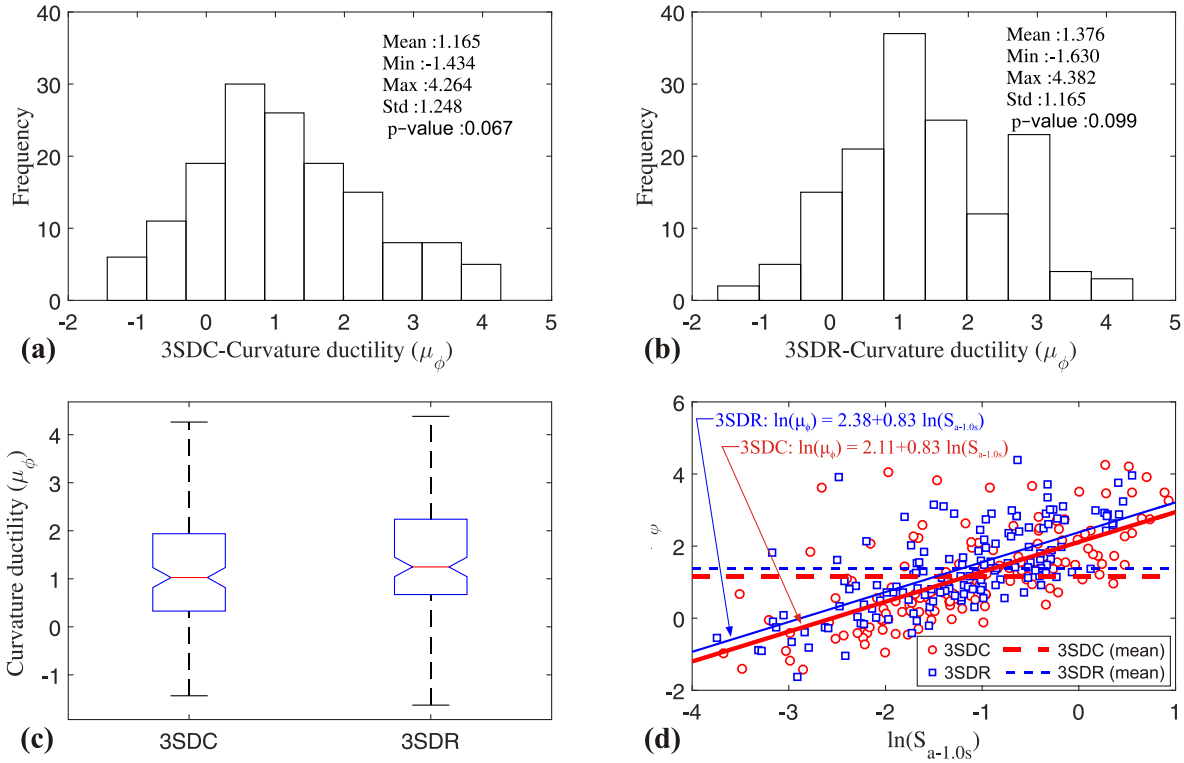

Figure 4.4 – Histograms and descriptive statistics for case 1: a) 3SDC, b) 3SDR, c) box plot of 3SDC and 3SDR, and d) ANCOVA regression lines of 3SDC and 3SDR.

The homogeneity of regression slopes is checked in the current study using the *F*-test for the equality of slopes (Vidakovic, 2005) and also seems to hold. ANCOVA and ANOVA have a

greater power than the KW test when the above assumptions are satisfied (Vidakovic, 2005; Vickers 2005).

Figure 4.4 (c) shows box plots of the curvature ductility for 3SDC and 3SDR. The mean value of intensity measure in the logarithmic scale for 3SDC and 3SDR is –1.14 and –1.21, respectively. The ground motions are randomly assigned in this study because it is computationally intensive and almost impractical to produce responses for all the cases with the same suite of ground motions. The experiment has been designed in a way that the design attributes are randomly sampled in the 320 simulations from a practical perspective. Such an assignment also helps assess the combined effect of two or more different design attributes; for example, the combined effect of the abutment type and column cross-section. The question arising from this case is whether the column response of 3SDC and 3SDR can be compared as there is a clear variation in the *IM* and the column response is highly related to *IM*. It is possible that the results are skewed if the column responses are compared as the mean values of *IM* are different. ANOVA and KW tests neglect such variation in *IM* and such a comparison leads to erroneous results. The mean value of the curvature ductility for3SDC and 3SDR is shown in dashed lines in Figure 4.4(b). It can be seen from Figure 4.4 (c) and Figure 4.4(d) that the mean values are very close; their comparison without reflecting the effect of *IM* leads to erroneous conclusions. ANOVA and KW tests neglect the variation of *IM* in their comparison and this ignorance leads to *p*–values higher than 0.05. On the other hand, ANCOVA compares the treatment means after adjusting the variation in *IM*, i.e., what would be the response means, if the two bridge sub-classes have the same *IM*. In other words, ANCOVA tests the null hypothesis whether the 'adjusted population' means are equal. It can also be formulated as whether the regression intercept of the two bridge sub-classes is equal (Mangalathu et al. 2016a; 2017a). Under the assumption of the homogeneity of regression slopes, the difference between the intercept means is equal to the difference between the adjusted means. The regression lines of the curvature ductility for 3SDC and 3SDR are plotted in Figure 4.4(d). ANCOVA yields the cross–section as significant (*p*–value of 0.010) because of the difference

between the intercepts. The adjusted and unadjusted means are equal only when the *IM* means are same. In such a scenario, ANOVA and ANCOVA yield similar results.

4.6.2 Case 2: Significant per ANOVA and ANCOVA

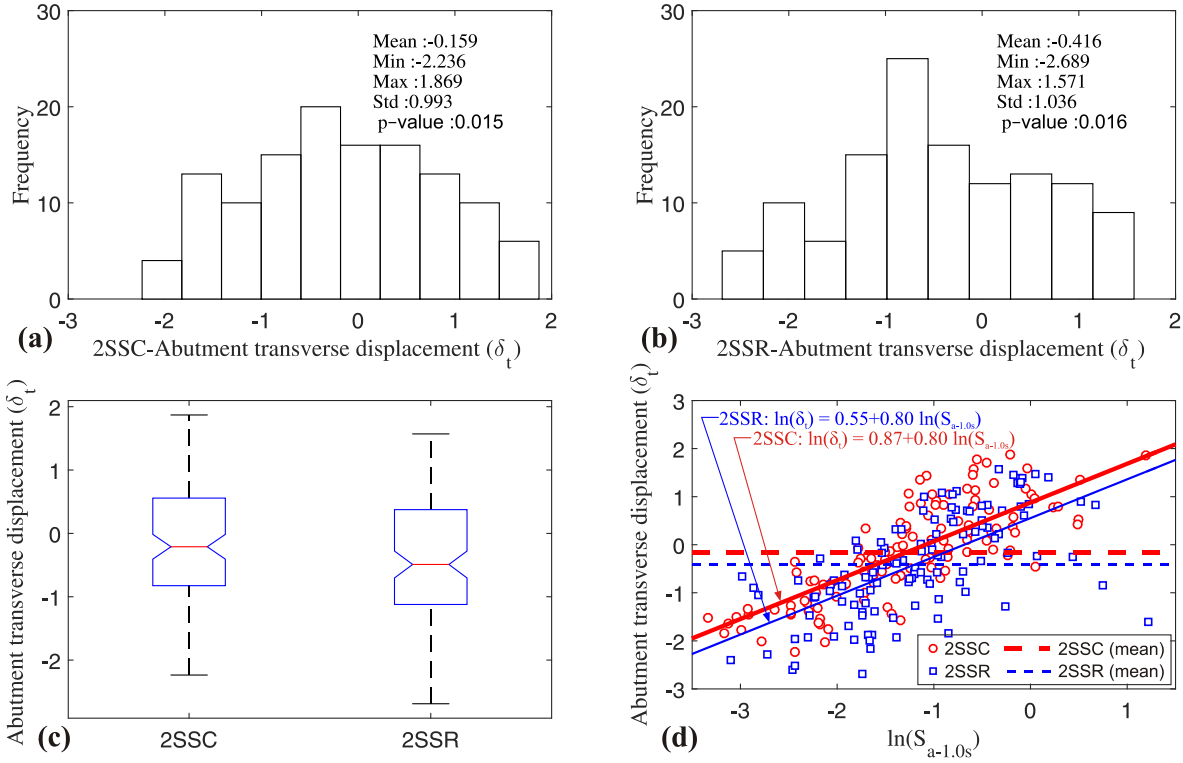

Figure 4.5 – Data analysis for case 2: a) histogram of 2SSC, b) histogram of 2SSR, c) box plot of 2SSC and 2SSR, and d) ANCOVA regression lines of 2SSC and 2SSR.

The two-span seat-type abutment bridges grouped by the cross–section shape based on the transverse abutment response are 1) with circular cross–sections (hereafter, 2SSC) and (2) with rectangular cross–sections (hereafter, 2SSR). ANOVA and ANCOVA identify this cross-section shape as a significant design attribute with *p*–value of 0.005 and 0.048, respectively. The KS test shows a *p*–value greater than 0.015 and 0.016 for 2SSC and 2SSR, and hence fails to reject the null hypothesis that they are normally distributed. As seen from Figure 4.5(c) and Figure 4.5(d), there is a statistically significant difference between the mean values, and both ANOVA and ANCOVA method can capture this difference. The reason why the KW test suggests it as non-

significant might be due to the limited power when the data is normally distributed, which has also been pointed out by other researchers (Vickers 2005; Kvam and Vidakovic 2007).

4.6.3 Case 3: Significant per KW

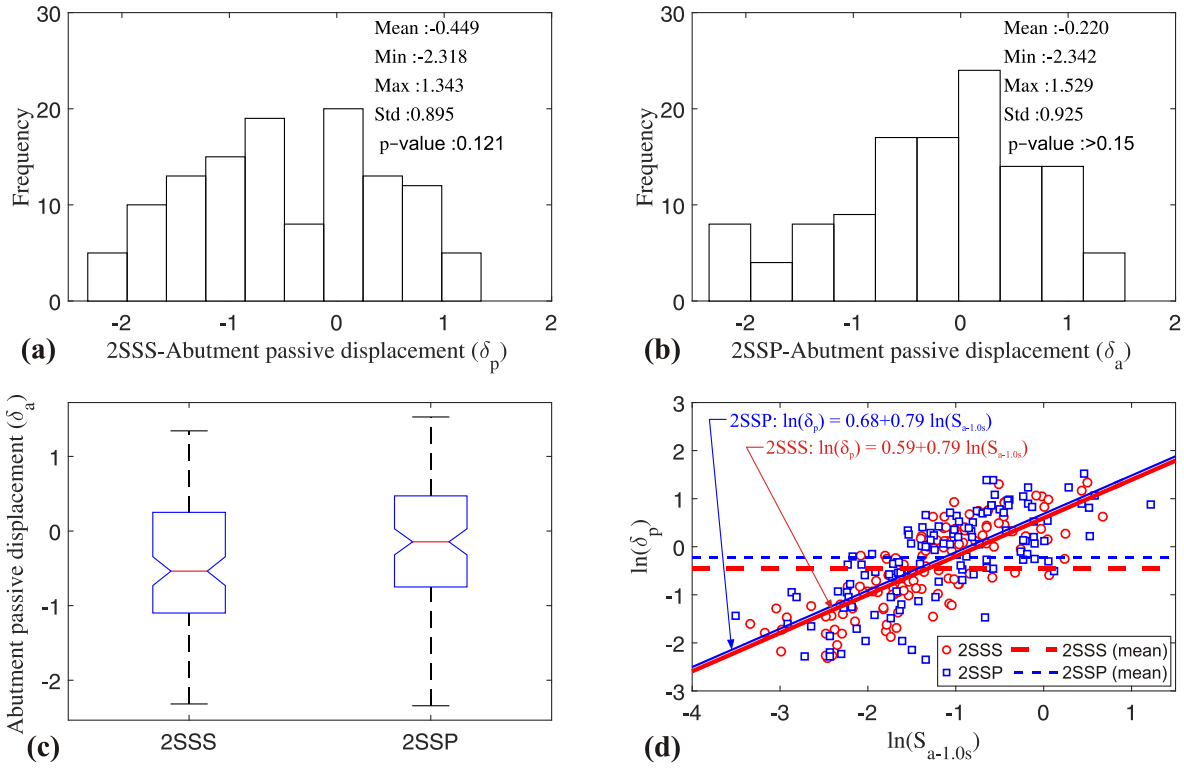

Figure 4.6 – Data analysis for case 3: a) histogram of 2SSS, b) histogram of 2SSP, c) box plot of 2SSS and 2SSP, and d) ANCOVA regression lines of 2SSS and 2SSP.

The two span seat-type abutment bridges are categorized by the abutment type based on the passive response of the abutments (1) with spread abutments (hereafter, 2SSS) and (2) with abutment on piles (hereafter, 2SSP). The results (Figure 4.6) underscore the importance of ANCOVA–based grouping compared to other methods. The KW identifies abutment type as a significant design attribute, while other grouping methods suggest it as non–significant. The mean value of *IM* (in a logarithmic scale) for the passive abutment action of 2SSS and 2SSP is –1.31 and –1.13, respectively, and the comparison of the adjusted means identifies this attribute as non–significant (Figure 4.6d). Although ANOVA identifies it as insignificant, the KW test fails here.

All of the above cases identify the statistical power of ANCOVA to provide an unbiased estimator compared to ANOVA and KW methods by accounting for the variation in *IM*s. Although not shown here, similar conclusions are also drawn for the other cases. To evaluate whether the bridge sub-classes identified by ANCOVA yield a distinct response, fragility curves are developed in the next section.

The following points can be inferred from the comparison of various grouping techniques:

1. ANCOVA compares the linear regression between the component response and the intensity measure. In a logarithmic space, it corresponds to probabilistic seismic demand models (PSDMs). The PSDMs are one of the core steps in the generation of fragility curves. Thus, ANCOVA compares the PSDMs and the group's bridge sub-classes based on the difference in PSDMs. ANOVA compares the responses based on mean value of the responses.

2. ANOVA and ANCOVA yield similar results when the mean value of ground motions associated with the groups to be compared is the same. If there is a variation in the *IM*s mean value, ANCOVA is more likely to catch the significant parameter than ANOVA.

3. The normality assumptions in ANOVA and ANCOVA seem to be satisfied in the case of seismic responses of bridges. Hence, the statistical power in identifying the significant attributes is greater in ANOVA and ANCOVA than the KW. It seems from the current study that the KW is not a reliable performance based grouping approach for bridges.

4. The pairwise comparison is difficult in the case of ANCOVA than ANOVA.

5. Where the ground motions associated with the bridge groups to be compared are the same, ANOVA yields the same results as ANCOVA.

In light of the inferences from the various grouping strategies, the current study adopts ANOVA from the point of pair-wise comparisons and the extent of numerical simulations needed to group the California bridge inventory.

The grouping strategy adopted in the current study is given below:

Step 1: Select possible combinations of bridge configurations.

Step 2: Using Latin Hypercube Sampling method, select N ground motions from the suite of ground motions assembled for the fragility analysis. The ground motions are selected based on the distribution of Sa-1.0s of ground motions.

Step 3: Analyze each bridge configuration in OpenSees for the selected N ground motions.

Step 4: Collect output of interest (or response) including curvature ductility, bearing displacement, abutment active/passive/transverse displacement, etc.

Step 5: Conduct an ANOVA to evaluate the sensitivity of each component to the variation in bridge configurations. The results can be inferred more easily though *p*–value. The *p*–value is the evidence against a null hypothesis or the probability that the variation between groups occurred by chance. The *p*–value can be interpreted as the probability of such an 'extreme' value of the test statistic when H_0 is true.

Step 6: Perform Fischer Method on the ANOVA output to group the bridge configurations that have a statistically similar response. The Fisher Method compares all pairs of groups while controlling the individual error rate. It identifies the group with the highest sensitivity and checks a null hypothesis whether the mean values of other groups match with the most sensitive one. If there is a match, they will be grouped together. If not, it will check the group with the second highest sensitivity and check whether the mean value of the

remaining groups matches the group with second highest sensitivity. The procedure is repeated until all the members are grouped.

4.7 Grouping of bridge classes

ANOVA-based grouping strategy is used to group the bridge classes in California. To group the bridge classes, the uncertain parameters in Table 4.1 are kept at their mean values. Nonlinear time history analysis (NLTHA) is carried out for the bridge models for the selected ground motions and the maximum response of the various bridge components are recorded. Thirty ground motions are selected from the expanded suite of 320 ground motions by Latin Hypercube Sampling (LHS) for the grouping of bridge classes and is chosen based on a sensitivity study. The histogram of the peak ground acceleration (PGA) and the acceleration response spectrum of the ground motion suite are shown in Figure 4.7.

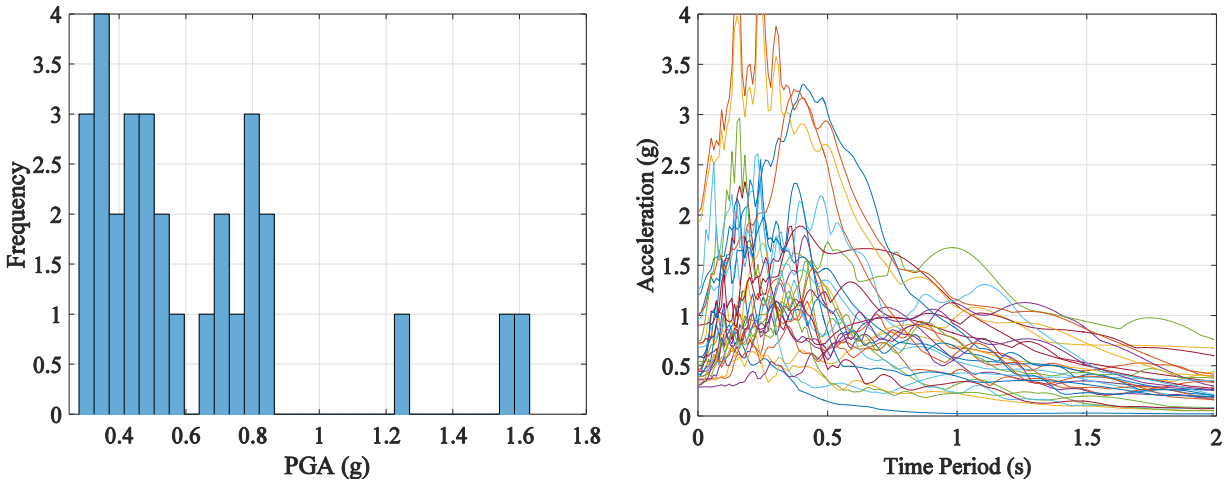

Figure 4.7 – a) Histogram of the PGA values of the ground motion suite, b) Acceleration response spectrum of the ground motion suite.

Various demand parameters such as column curvature ductility (μ_ϕ, -), passive abutment displacement (δ_p, mm), active abutment displacement (δ_a, mm), transverse abutment displacement

(δ_t , mm), bearing displacement (δ_b, mm), and superstructure unseating (δ_c, mm) are used to group the bridge classes. As mentioned before, the results are inferred in terms of *p*–value. A smaller *p*–value refers to stronger evidence for rejecting the null hypothesis (H_1). If the *p*–value is less than 0.05, it can be concluded that not all of the population means are equal. The sensitivity of the seismic demand on two-span bridge configurations to the various design eras and bent configurations are evaluated using ANOVA and is given in Table 4.3. It is clearly observed from Table 4.3 that all of the demand parameters in rigid abutments are highly sensitive to the design eras and bent configurations, and hence cannot be grouped together. In the case of seat abutments, column curvature ductility and bearing displacement are the most sensitive parameters affected by the design eras and bent configurations. The Fischer Method is carried out on ANOVA to group the bridges that have similar seismic demands; those results are shown in Table 4.3.

Table 4.3 – *p*–values from ANOVA.

Bridge type	*p*–value				
	μ_ϕ	δ_p	δ_a	δ_t	δ_b
Rigid abutments	**0.000**	**0.001**	**0.002**	**0.001**	–
Seat abutments	**0.037**	0.857	0.888	0.503	**0.050**

Table 4.4 presents the Fischer Method grouping results for two span box-girder bridges and Table 4.5 shows the grouping results of Era 11 bridges to number of spans. The inferences obtained from the sensitivity study results, presented in Table 4.4 and Table 4.5, are summarized below:

1. For the two-span seat and diaphragm abutment bridges, Era 11 shows behavior that is distinct from the other design eras (Table 4.4). It can be inferred that the changes in the seismic design philosophy from Era 22 to Era 33 don't significantly change the seismic demand of bridge components.

2. In the case of two-span bridge configurations, the seismic demand of columns (μ_ϕ) is the component greatly influenced by the design eras and number of columns per bent. It requires special attention as column vulnerability governs bridge vulnerability in most bridge configurations (Mangalathu et al. 2016a).

3. By comparing the seismic demand on abutments, it can be inferred that the bridge design philosophy and number of columns per bent have more influence on the diaphragm abutment bridge than the seat abutment bridge. It might be due to the integral connection of the diaphragm abutment bridges at the ends which causes the abutment to share a significant portion of the seismic demand. In the case of seat abutment bridges, the seismic demand on the abutments is less influenced by the design eras and number of columns per bent.

4. The seismic demand of single–column bent, two– column bent, and multi–column bent (bent with greater than two columns) bridges are statistically different from the selected two span bridge configurations (Table 4.5) and thus cannot be grouped together from a seismic demand perspective.

5. In the case of diaphragm abutment bridges, two-span bridges have distinct seismic demands that are distinct from three-to six-span bridge configurations for all bridge components. Although not shown here, similar conclusions have also been noted for bridges with seat abutments.

6. The bridges with diaphragm abutments and seat abutments have different seismic demand for all of the design eras and bent configurations.

Table 4.4 – Results of the grouping for two-span box girder bridges.

Bridge configurations		Column ductility		Abutment passive		Abutment active		Abutment transverse		Bearing/ Unseating displacement	
		Mean*	Grouping[#]	Mean	Grouping	Mean	Grouping	Mean	Grouping	Mean	Grouping
Diaphragm abutments	Era 11 - 1 column bent	0.86	B C	0.00	B	0.08	B	0.75	C	–	– –
	Era 11 - 2 column bent	1.96	A	0.39	A	0.45	A	1.58	A	–	– –
	Era 22 - 1 column bent	0.10	D	0.00	B	0.08	B	0.67	C	–	– –
	Era 22 - 2 column bent	1.13	B	0.45	A	0.51	A	1.17	B	–	– –
	Era 22 - 3 column bent	0.90	B C	0.42	A	0.48	A	1.00	B C	–	– –
	Era 22 - 4 column bent	0.73	B C	0.48	A	0.53	A	0.90	B C	–	– –
	Era 33 - 1 column bent	0.10	D	0.00	B	0.09	B	0.67	C	–	– –
	Era 33 - 2 column bent	1.13	B	0.45	A	0.51	A	1.17	B	–	– –
	Era 33 – 3 column bent	0.91	B C	0.42	A	0.48	A	1.01	B C	–	– –
	Era 33 - 4 column bent	0.73	B C	0.48	A	0.53	A	0.90	B C	–	– –
	Era 33 - 5 column bent	0.65	C	0.49	A	0.54	A	0.83	B C	–	– –
Seat abutments	Era 11 - 1 column bent	1.26	B	-0.02	A	0.01	A	-0.05	A	0.94	B
	Era 11 - 2 column bent	1.99	A	0.32	A	0.35	A	0.65	A	1.60	A
	Era 22 - 1 column bent	0.51	C	0.07	A	0.10	A	-0.02	A	0.93	B
	Era 22 - 2 column bent	1.26	B	0.36	A	0.39	A	0.42	A	1.22	A B
	Era 22 - 3 column bent	1.03	B C	0.31	A	0.33	A	0.33	A	1.09	B
	Era 22 - 4 column bent	0.92	B C	0.25	A	0.28	A	0.23	A	1.04	B
	Era 33 - 1 column bent	0.51	C	0.07	A	0.10	A	-0.03	A	0.93	B
	Era 33 - 2 column bent	1.26	B	0.36	A	0.39	A	0.42	A	1.22	A B
	Era 33 – 3 column bent	1.04	B C	0.31	A	0.33	A	0.33	A	1.09	B
	Era 33 - 4 column bent	0.92	B C	0.25	A	0.27	A	0.23	A	1.04	B
	Era 33 - 5 column bent	0.76	B C	0.23	A	0.24	A	0.06	A	0.99	B

*Mean is shown in logarithmic scale. [#]Bridge configurations that do not share common alphabet cannot be grouped together as the seismic demand of these bridges are statistically different.

Table 4.5 – Results of the grouping for multi-span bridges

Bridge configurations	Column ductility		Abutment passive		Abutment active		Abutment transverse		Bearing/Unseating displacement	
	Mean*	Grouping#	Mean	Grouping	Mean	Grouping	Mean	Grouping	Mean	Grouping
Era 11 – 2 span	1.26	A	-0.02	A	0.01	A	-0.05	A	0.93	A
Era 11 – 3 span	0.82	A B	-0.49	A B	-0.47	A B	-0.70	A B	0.61	A B
Era 11 – 4 span	0.55	B	-0.88	B	-0.87	B	-0.85	B	0.40	B
Era 11 – 5 span	0.53	B	-0.99	B	-0.97	B	-0.97	B	0.36	B
Era 11 – 6 span	0.52	B	-1.04	B C	-1.02	B	-1.03	B	0.36	B

*Mean is shown in logarithmic scale. #Bridge configurations that do not share common alphabet cannot be grouped together as the seismic demand of these bridges are statistically different.

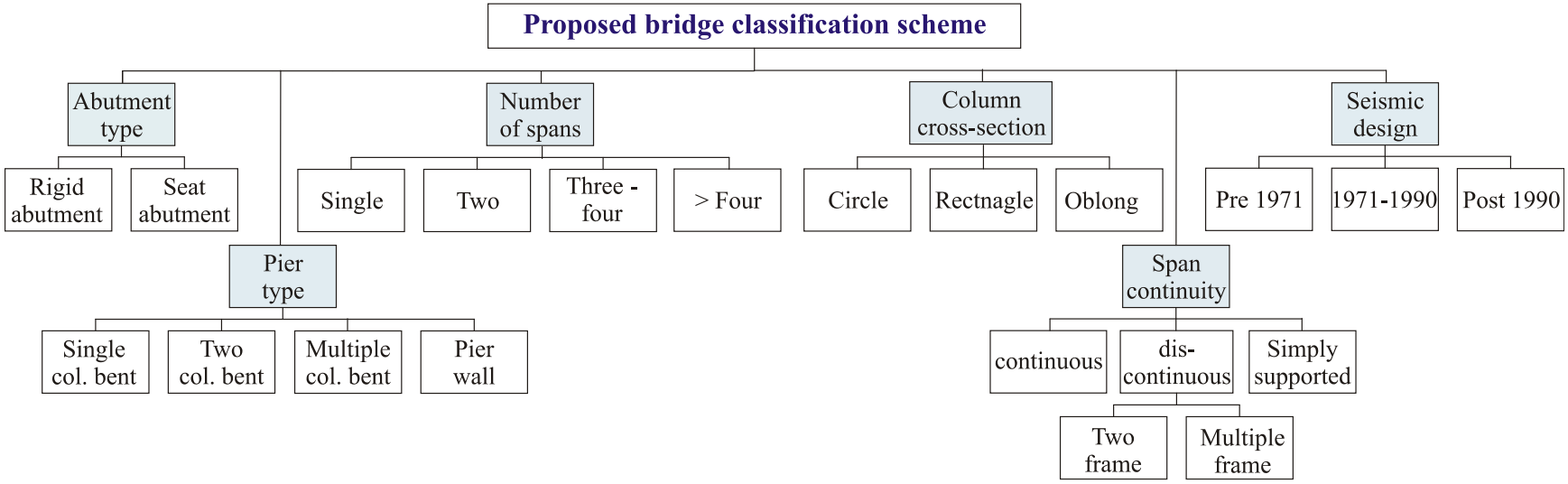

Figure 4.8 – Proposed classification scheme.

It is noteworthy to mention that only the abutment types, design code eras, interior support and number of columns per bent, column cross-section, span-range and frame-system are adopted as design attributes in this study to group bridge classes. These attributes are selected based on the current sensitivity study, insights from the previous research on the bridge's seismic responses for regional risk assessment (Shinozuka et al. 2000; Mackie and Stojadinovic 2001; Avsar et al. 2001; Choi 2002; Nielson 2005; Padgett 2007; Ramanathan 2012; Moschonas et al. 2008; Banerjee and Shinozuka 2008; Mehr and Zaghi 2016; Managalathu et al 2016a, 2016b; Zelaschi et al. 2016) and the input from Caltrans (Caltrans, 2017). Figure 4.8 shows the proposed grouping; classification is carried out based on the abutment type, column cross–section, pier type, number of spans, span continuity and seismic design. They are explained below:

- **Abutment types:** It has been noted that the response of rigid abutments is different from seat type abutments and hence cannot be grouped together.

- **Column cross-section**: On the basis of the column cross-section shape, the bridges are classified into circular, rectangular, and oblong bridges. Soleimani et al. (2017) showed different demands for bridges with circular, rectangular, and oblong cross sections.

- **Interior support and number of columns per bent (Pier type)**: Sensitivity results showed that the number of columns greater than three in a multi-column support does not significantly impact response and therefore does need to be considered as separate classes. The responses for bridge models having from 3-5 columns-per-bent were most consistent (MCB, hereafter) and can be grouped together. Responses for 2-column bents (TCB, hereafter) were statistically different from MCB and hence grouped separately. The response of bridges supported on single-column bents (SCB, hereafter) was shown to be distinct for each era and therefore cannot be grouped with other support systems. Although pier-wall supports (PW, hereafter) were not explicitly

modelled, engineering judgment indicated this support system would also yield distinct responses.

- **Design code era**: Sensitivity results showed that bridges built or rebuilt within either of the two later design code eras (i.e. Era 22 and Era 33) had statistically similar responses and could be grouped as 'E22/E33' Era for purposes of establishing demand models (note: capacity models, particularly for the columns, are different for these eras and hence the fragilities). Era 11 bridges were shown to have distinct response (also capacity) and require the development of separate demand models. Mixed-era bridges are not addressed in this study.

- **Span range:** Single-span bridges need to be treated as a separate class due to their unique and limited combination of demand parameters. Sensitivity studies considered single-frame systems having more spans (from 2-span to 6-span) to determine if any range could be grouped. Depending on other factors such as era and abutment, the responses varied from being similar for all span ranges to being distinct for various combinations. As a practical compromise, 2-span bridges (S22, hereafter) were to be treated separately, while span-groups of two (i.e. three- and four-span bridges (S34, hereafter), and spans greater than 4 (S4x, hereafter) were adopted for longer bridges.

- **Multi-Frame System:** The sensitivity studies also considered various simplified framing configurations. Responses for 2-frame systems were clearly unique, but the distinctions between bridges with a higher numbers of frames were less clear. The 'two-frame' system was therefore retained as a distinct class. Larger numbers of frames such as three frames four frames et al., are combined into the 'multi frame' It is noteworthy to mention that very less number of multiple frame system are noted from the extensive plan review and such a compromise is reasonable.

4.8 Conclusion

Regional risk assessment relies on fragilities that are applicable to a portfolio of structures, as it is cumbersome and time consuming to generate fragility curves for each structure in a specific region. Also the generation of each structure-specific fragility curve is not warranted as some structures have similar performance or fragilities. Currently, the grouping of structures is typically conducted based on engineering judgment and there is a lack of systematic strategy for binning/grouping structures. These limitations can be addressed by performance based grouping techniques, which lead to more reliable sub-classes of bridges relative to the traditional subjective lumping of bridges. The current study explores the various performance based grouping techniques such as analysis of variance (ANOVA), analysis of Covariance (ANCOVA) and non–parametric Kruskal-Wallis test (KW) for the grouping of structures of similar performance. The selected grouping methods have different underlying assumptions and approaches in grouping the structures. The comparison of various grouping techniques is carried out with the case study of two span and three span concrete box girder bridges in California with seat-type and diaphragm abutments.

In the light of these studies, a new performance-based grouping methodology utilizing analysis of variance (ANOVA) is suggested in this chapter. Thirty ground motions are selected by Latin hypercube sampling from the suite of ground motions assembled for California for the nonlinear time history analysis (NLTHA) of bridge models. Consistent with the ground motions, 30 three-dimensional bridge models are created in OpenSees and the maximum component responses are noted for each NLTHA. ANOVA is carried out for the recorded maximum bridge responses to determine if the mean responses are statistically similar. If they are not, the bridges are grouped by pairwise comparison using the Fischer method.

The insights from the performance based grouping method, Caltrans engineering experience regarding bridge-design features affecting seismic performance, and the population size of the sets of bridges sharing a particular combinations of design features are used to group the of box-girder bridge classes in California.

CHAPTER 5 CALIFORNIA BRIDGE INVENTORY

To have a reliable estimate of the vulnerability or fragility of highway bridges in California, it is necessary to understand and characterize the California bridge inventory. This chapter presents an in-depth study of the California bridge inventory using the in-house database called BIRIS, assembled by California Department of Transportation (Caltrans) engineers.

Bridge design philosophy in California has been significantly influenced by the historic 1971 San Fernando and the 1989 Loma Prieta earthquakes. Based on the unique design attributes and the evolution in seismic design philosophy, California bridges can be separated by three design eras: Era 11 (pre-1971), Era 22 (1971-1990), and Era 33 (post-1990) (Ramanathan, 2012). In Era 11 seismic design philosophy, seismic forces were proportional to the dead weight of the structure. Bridges were designed for a lateral seismic force equal to 6% of the dead weight of the structures. Column shear failure and pull-out of the longitudinal reinforcement were predominant due to the lack of ductility, as was revealed in the 1971 San Fernando earthquake. After the 1971 San Fernando earthquake, capacity design principles were added to the design standards. The lateral load-carrying capacity of the bridges was increased by a factor of 2 or 2.5 and the aspects of fault proximity, site conditions, dynamic structural response, and ductile details were considered in the design of bridge columns. However, column shear failure in the plastic hinge regions was typical in Era 22 due to the lack of confinement in this zone. The extensive damage from the 1989 Loma Prieta earthquake forced Caltrans to solicit the Applied Technology Council (ATC) to conduct a detailed study and to provide recommendations for design standards, performance criteria, and practices. The recommendations from ATC described in ATC-32 were incorporated in the Caltrans design manuals and led to the Era 33 design details. The fundamental emphasis in Era 33 design philosophy was on displacement-based

or capacity design approach, which ensures a ductile failure mode in the columns. A detailed review of the design details pertinent to various design eras is presented in this chapter.

5.1 Bridge classification based on BIRIS

BIRIS is the bridge inventory assembled by Caltrans engineers for the purpose of having a unified database for bridges; it contains bridge types, materials, operational conditions, geometric data, functional details and other data. Table 5.1 shows the distribution of various bridge classes in California obtained from BIRIS. Bridges are classified based on the material and the bridge type. Box girder bridges account for the majority of the California bridge inventory. The current study is limited to concrete box girder, which accounts for more 30% of the California bridge inventory.

Table 5.1 – Bridge classes in California and their proportion in the overall inventory.

	Materials			Total
	Concrete	Steel	Mixed	
Box girder	***7839***	***23***	***166***	**8028**
Tee Girder	2901	0	16	2917
I girder	1015	2133	603	3751
Slab	5703	15	64	5782
Culvert	3307	264	22	3593
Others	837	378	798	2013
				Total: **26084**

5.2 Box girder bridge class statistics

The various components of a three-span box girder bridge are illustrated in Figure 5.1. An extensive plan review was carried out to identify the design attributes and are explained below:

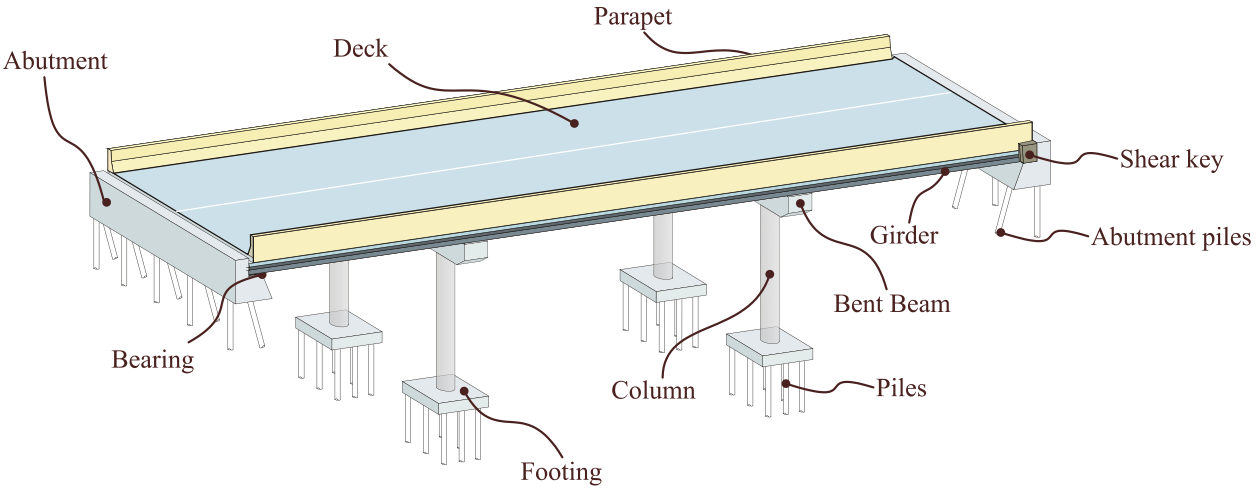

Figure 5.1 – Illustration of major bridge components.

5.3 Abutments

Abutments can be classified into two basic types: seat abutments and diaphragm abutments (Ramanathan 2012). Diaphragm abutments are cast monolithic with the superstructure. As the diaphragm abutments readily engage the backfill soil during the seismic action, it provides a great source of energy dissipation and reduces the likelihood of span unseating. Seat-type abutments provide a bearing support to the superstructure, which is restrained longitudinally by the abutment backwall and transversely by the shear key. Mixed abutments are supported by a diaphragm abutment at one end and seat abutment at other end. The distribution of the abutments for various design eras are shown in Figure 5.2. Rigid abutments are the most common type in Era 11, while seat abutments are more common in Era 33. Era 22 contains an approximately equal mix of rigid and seat abutments.

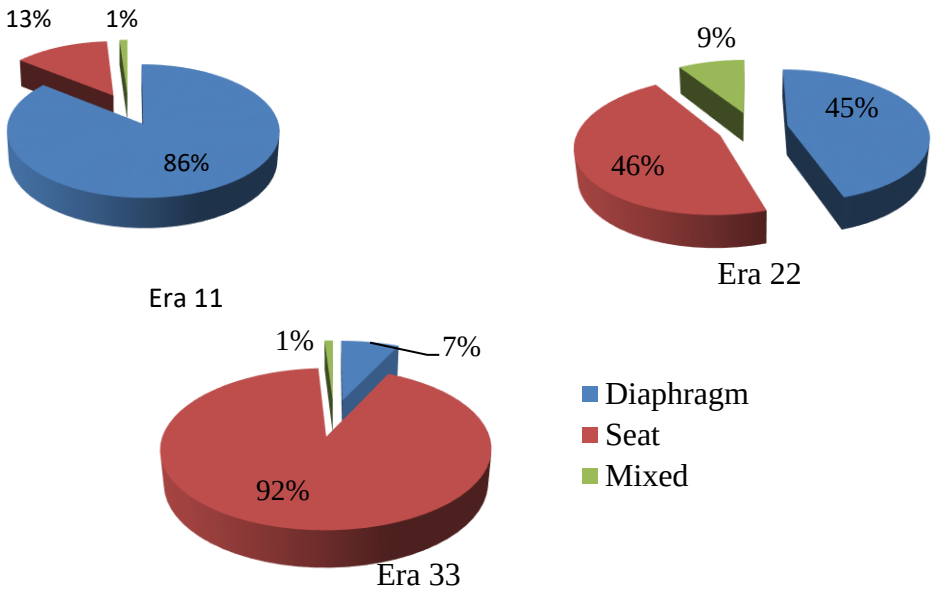

Figure 5.2 – Distribution of abutments for various eras.

Based on the support type, the abutment can be (1) on piles, (2) on spread footing or (3) cantilever type. The distribution of the abutment based on the support type is shown in Figure 5.3. Abutments resting on piles are the major configuration for both diaphragm and seat-type abutments.

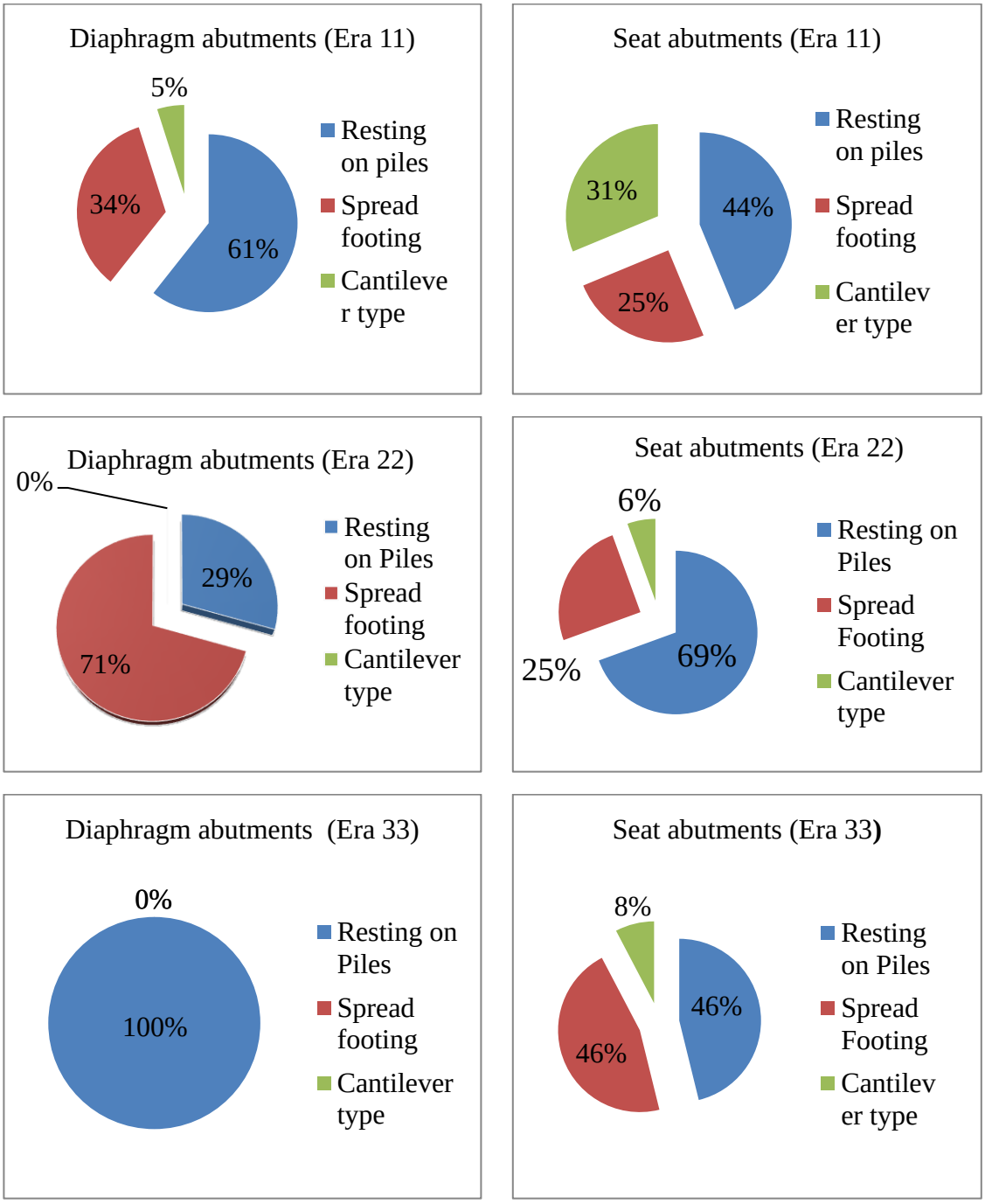

Figure 5.3 – Distribution of abutments for various bridge eras.

Table 5.2 shows the statistics summary of abutment parameters for various design eras and abutment types. The development of abutment parameter values was based on manual review of bridge details found in plans downloaded through the BIRIS search. It is seen from Table 5.2 that the abutment backwall height varies depending on the design era, abutment type, and the abutment support type. Caltrans 2014 draft of bridge design aids (BDA, hereafter) on 'Permissible Horizontal Loads for Standard Plan and Steel HP Piles' (Caltrans, 2017) was used to establish a typical value and representative range of pile capacity for various types of standard piles in both sands and clays. BDA defines the permissible load corresponding to a deflection of 0.25-inch. The mean value of approximately 25 kips per pile was determined from BDA for a 5-foot cutoff, and the representative range of 15-50 kips per pile showed the variability to be approximately a factor of two above and below the central value. These ranges of values are used to derive the abutment pile stiffness and are given in Table 5.2. To derive the coefficient of friction for abutments on spread footing, concrete-soil and concrete-concrete friction coefficient were considered (Potyondy, 1961), and the range is modeled as a normal distribution with mean of 0.40 and standard deviation of 0.075. A slip as little as 0.04-0.10 inch can mobilize the full friction in an abutment on spread footing and hence yield displacement is assumed to be uniformly distributed with an upper bound of 0.10 in. and lower bound of 0.04 in.

Table 5.2 – Distribution of parameters for abutments.

Parameter	Design era	Type of abutment		Units	Distribution				
					Type [§]	Parameters[†]		Lower bound (L)	Upper Bound (U)
						Mean (α)	Standard Deviation (β)		
Abutment backwall height	Era11	Diaphragm	On piles	feet	LN	2.35	0.15	8.0	14.0
			On spread	feet	LN	2.20	0.35	4.5	18.0
			Cantilever	feet	U	25.0	8.33	20.0	30.0
		Seat	On piles	feet	LN	1.95	0.20	5.0	10.5
			On spread	feet	LN	1.95	0.20	5.0	10.5
			Cantilever	feet	U	25.0	8.33	20.0	30.0
	Era22	Diaphragm	On piles	feet	LN	2.39	0.20	6.5	13.0
			On spread	feet	LN	2.37	0.09	9.5	12.5
			Cantilever	feet	-	-	-	-	-
		Seat	On piles	feet	LN	2.45	0.18	9.5	20.0
			On spread	feet	LN	2.50	0.09	10.5	14.5
			Cantilever	feet	-	-	-	-	-
	Era33	Diaphragm	On piles	feet	LN	2.45	0.18	9.5	20.0
			On spread	feet	-	-	-	-	-
			Cantilever	feet	-	-	-	-	-
		Seat	On piles	feet	LN	2.63	0.22	10.5	23.5
			On spread	feet	LN	2.58	0.14	11.0	19.0
			Cantilever	feet	-	-	-	-	-
Abutment pile stiffness (lateral capacity /deck width)	All Eras	Diaphragm	On piles	kip/ft	LN	1.79	0.35	2.5	12.0
	All Eras	Seat	On piles	kip/ft	LN	2.08	0.35	4.0	16.0
Coefficient of friction	All Eras	Diaphragm /Seat	On spread	_	N	0.40	0.075	0.25	0.55
Yield displacement	All Eras	Diaphragm /Seat	On spread	in.	U	0.75	0.02	0.50	1.0
Abutment backfill soil (clay vs sand)	All Eras	Diaphragm /Seat	All types		B	Equally split among all simulations			

[§] N = normal, LN = lognormal, U = uniform, and B = Bernoulli distribution.

[†] α and β are the parameters of the distribution. These denote mean and standard deviation for a normal and uniform distribution, and mean and standard deviation of the associated normal distribution (in log space) in the case of a lognormal distribution.

Table 5.3 – Distribution of parameters for bearings.

Design era	Type of bearings	Parameter	Units	Distribution				
				Type§	Parameters†		Lower bound (L)	Upper Bound (U)
					Mean (α)	Standard Deviation (β)		
Era11	Rocker	Coefficient of friction (longitudinal direction)	-	N	0.04	0.01	0.02	0.06
		Coefficient of friction (transverse direction)	-	N	0.10	0.02	0.06	0.14
	Elastomeric	Stiffness per feet of deck width	kip/in/ft	LN	0.40	0.35	0.70	3.0
		Coefficient of friction	-	N	0.30	0.10	0.10	0.50
	Friction	Coefficient of friction	-	U	0.50	0.03	0.20	0.80
		Yield displacement	In.	U	0.07	0.0003	0.04	0.10
Era22	Elastomeric	Stiffness per feet of deck width	kip/in/ft	LN	0.77	0.52	0.7	6.0
		Coefficient of friction	-	N	0.30	0.10	0.10	0.50
Era33	Elastomeric	Stiffness per feet of deck width	kip/in/ft	LN	0.00	0.45	0.4	2.5
		Coefficient of friction	-	N	0.30	0.10	0.10	0.50

§ N = normal, LN = lognormal, U = uniform, and B = Bernoulli distribution.

† α and β are the parameters of the distribution. These denote mean and standard deviation for a normal and uniform distribution, and mean and standard deviation of the associated normal distribution (in log space) in the case of a lognormal distribution.

5.4 Bearings

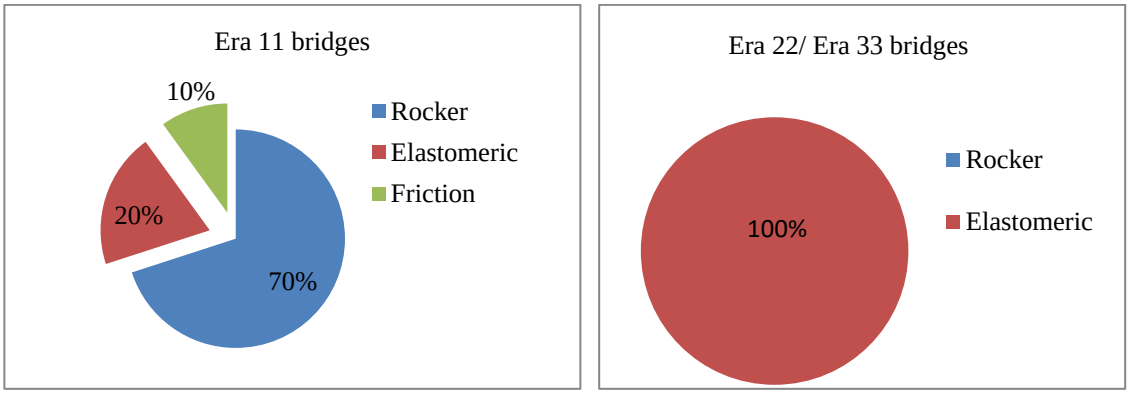

Figure 5.4 – Percentage distribution of bearings based on design eras.

Bridges with seat abutments are rest on bearings at the abutments. Era 11 consists of various bearing such as rocker bearings, elastomeric bearings, and friction bearings

(Figure 3.14), while Era 22 and Era 33 consists only of elastomeric bearings. The motion associated with elastomeric and friction bearings are based on sliding. On the other hand, motion is characterized by rocking in case of rocker bearings. The distribution of the bearings of various eras is shown by percentage in Figure 5.4. The statistical distribution of the uncertain parameters for the bearings is given in Table 5.3.

5.5 Box girder deck

The important uncertain parameters in the modeling of superstructure are the span length, deck-width, and type of girder (reinforced or pre-stressed). The distribution of these parameters is derived based on an extensive plan review of bridges pertinent to the design eras. As explained in Chapter 4, bridges are grouped based on the span length as S11 (single span), S22 (two-span), S34 (three and four spans), and S5x (spans greater than 4). Also, Era 22 and Era 33 bridges are grouped together from a demand perspective.

5.5.1 Span length

Span length is a critical parameter that governs the seismic responses of bridges; the parameters of the span length distribution for box girder bridges are given in Table 5.4. The span length is defined as a function of the design era, type of superstructure, and the number of spans. Interested readers are directed to the memo on the span length models for box girder bridges (Roblee, 2016a) and a brief summary is given in this section. Some notable trends in the distribution of span length are given below:

- In general, the span value associated with reinforced concrete (RC) girder is less than the pre-stressed concrete (PC) girder.
- The mean span value for multi-span PC bridge models is 135-feet for 2-span bridges and 155-feet for 3- to 6-span bridges, independent of the design era.

However, the mean span length of RC bridge models is not independent of design era.

- Two-span RC bridges are somewhat longer than other span ranges for each era.
- In the case of single-span bridges, both RC and PC have somewhat shorter span length than their multi-span counterparts.

The ratio of the approach span to the main span for multi-span bridges is defined as the span ratio and its properties are also given in Table 5.4. The span ratio model for PC bridges has a higher mean (0.75) than that for RC bridges (0.60), but the overall range is comparable (0.35-1.00 for RC, 0.40-1.00 for PC).

5.5.2 Deck width

Deck width parameters are determined based on the extensive plan review of bridges (Roblee 2016b) and are given in Table 5.5. Deck width distribution is a function of the design era and number of columns per bent. Era 22 and Era 33 are combined for deck width distribution as the plan review suggested similar trends in Era 22 and Era 33.

Table 5.4 – Distribution of span length and span ratio (approach span/main span) for box girder bridges.

Design era	Span range	No. of spans	Mix %	Type of superstructure: Reinforced (RC) or Pre-stressed (PC)	Units	Span length distribution					Span ratio distribution				
						Type[§]	Parameters[†]		Lower bound (L)	Upper Bound (U)	Type[§]	Parameters[†]		Lower bound (L)	Upper Bound (U)
							Mean (α)	Standard Deviation (β)				Mean (α)	Standard Deviation (β)		
Era11	S11	1	50	RC	feet	N	80	25	35	130	-	-	-	-	-
			50	PC	feet	N	110	35	40	180	-	-	-	-	-
	S22	2	75	RC	feet	N	95	20	55	140	-	-	-	-	-
			25	PC	feet	N	135	35	75	230	-	-	-	-	-
	S34	3	55	RC	feet	N	90	25	50	160	N	0.60	0.20	0.35	1.00
		4	45	RC	feet	N	90	25	50	160	N	0.60	0.20	0.35	1.00
	S5x	5	80	RC	feet	N	90	20	60	125	N	0.60	0.20	0.35	1.00
		6	20	RC	feet	N	90	20	60	125	N	0.60	0.20	0.35	1.00
Era22	S11	1	10	RC	feet	N	80	25	35	130	-	-	-	-	-
			35	PC	feet	N	130	35	50	220	-	-	-	-	-
Era 33			15	RC	feet	N	105	40	35	200	-	-	-	-	-
			40	PC	feet	N	130	35	50	220	-	-	-	-	-
Era22	S22	2	5	RC	feet	N	95	20	55	140	-	-	-	-	-
			35	PC	feet	N	135	35	75	230	-	-	-	-	-
Era 33	S22		10	RC	feet	N	135	35	85	200	-	-	-	-	-
			50	PC	feet	N	135	35	75	230	-	-	-	-	-
Era22	S34	3	10	RC	feet	N	90	25	50	160	N	0.60	0.20	0.35	1.00
			20	PC	feet	N	155	45	75	250	N	0.75	0.20	0.40	1.00
		4	5	RC	feet	N	90	25	50	160	N	0.60	0.20	0.35	1.00
			10	PC	feet	N	155	45	75	250	N	0.75	0.20	0.40	1.00
Era 33	S34	3	5	RC	feet	N	110	35	55	190	N	0.60	0.20	0.35	1.00
			30	PC	feet	N	155	45	75	250	N	0.75	0.20	0.40	1.00
		4	5	RC	feet	N	110	35	55	190	N	0.60	0.20	0.35	1.00
			15	PC	feet	N	155	45	75	250	N	0.75	0.20	0.40	1.00
Era22	S5x	5	10	RC	feet	N	90	20	60	125	N	0.60	0.20	0.35	1.00
			10	PC	feet	N	155	35	95	240	N	0.75	0.20	0.40	1.00
		6	5	RC	feet	N	90	20	60	125	N	0.60	0.20	0.35	1.00
			5	PC	feet	N	155	35	95	240	N	0.75	0.20	0.40	1.00
Era 33	S5x	5	15	RC	feet	N	125	35	75	165	N	0.60	0.20	0.35	1.00
			30	PC	feet	N	155	35	95	240	N	0.75	0.20	0.40	1.00
		6	5	RC	feet	N	125	35	75	165	N	0.60	0.20	0.35	1.00
			20	PC	feet	N	155	35	95	240	N	0.75	0.20	0.40	1.00

[§] N = normal, LN = lognormal, U = uniform, and B = Bernoulli distribution.

[†] α and β are the parameters of the distribution. These denote mean and standard deviation for a normal and uniform distribution, and mean and standard deviation of the associated normal distribution (in log space) in the case of a lognormal distribution.

Table 5.5 – Distribution of deck width for box girder bridges.

Design era	Column type (no. of columns)	Mix %	Distribution						Cell distribution					
			Unit	Type§	Parameters		Lower bound (L)	Upper Bound (U)	Type	% distr.	Type	% distr.	Type	% distr.
					Mean (α)	Standard Deviation (β)								
Era 11	1	25	feet	N	26.5	1.5	22	30	3 cell	100	-	-	-	-
		50	feet	N	34	1.2	30	38	3 cell	70	5 cell	30	-	-
		25	feet	N	40	1.5	38	46	3 cell	40	5 cell	60	-	-
	2	15	feet	N	34	2.0	30	38	3 cell	50	5 cell	50	-	-
		25	feet	N	41	5	38	48	3 cell	25	5 cell	75		
		15	feet	N	58	26	48	74	5 cell	25	7 cell	50	9 cell	25
	3	10	feet	N	48	18	38	56	5 cell	65	7 cell	35	-	-
		15	feet	N	66	9	56	74	7 cell	50	9 cell	50	-	-
		5	feet	N	80	9	74	92	9 cell	70	11 cell	30	-	-
	4	5	feet	N	60	34	38	72	5 cell	25	7 cell	35	9 cell	40
		10	feet	N	88	34	72	106	9 cell	25	11 cell	75	-	-
Era 22/Era 33	1	15	feet	N	28	1.2	22	30	3 cell	100	-	-	-	-
		20	feet	N	34	4	30	38	3 cell	85	5 cell	15		
		55	feet	N	42	2	38	46	3 cell	75	5 cell	25	-	-
		10	feet	N	50	14	46	60	3 cell	30	5 cell	50	7 cell	20
	2	20	feet	N	43	7	36	50	3 cell	40	5 cell	60		
		15	feet	N	57	8	50	66	5 cell	80	7 cell	20		
		10	feet	N	73	22	66	88	5 cell	25	7 cell	50	9 cell	25
	3	10	feet	N	59	18	50	68	5 cell	50	7 cell	50		
		15	feet	N	79	20	68	88	7 cell	50	9 cell	50		
		10	feet	N	98	20	88	108	7 cell	20	9 cell	40	11 cell	40
	4	5	feet	N	75	32	58	90	5 cell	25	7 cell	40	9 cell	35
		15	feet	feet	107	38	90	128	9 cell	40	11 cell	35	13 cell	25

§ N = normal, LN = lognormal, U = uniform, and B = Bernoulli distribution.

†α and β are the parameters of the distribution. These denote mean and standard deviation for a normal and uniform distribution, and mean and standard deviation of the associated normal distribution (in log space) in the case of a lognormal distribution

5.5.3 Deck cross-section properties

Figure 5.5 illustrates the typical cross-section of box girder bridges. The height of the box girder is a function of the span length; the acceptable depth-to span ratios are 0.055 and 0.04 for RC and PC concrete boxes, respectively. The cross-section details noted from the plan review are presented in Table 5.4. It has been noted that the wall thickness (t_{wall}) is constant across the design eras and type of superstructure (RC or PC). A constant value is adopted for the bottom flange thickness (t_{bot}) for each design era and is given in Table 5.6. The top flange thickness is a function of the center-to-center spacing of the girders (MTD, 2008) and is given in Table 5.7.

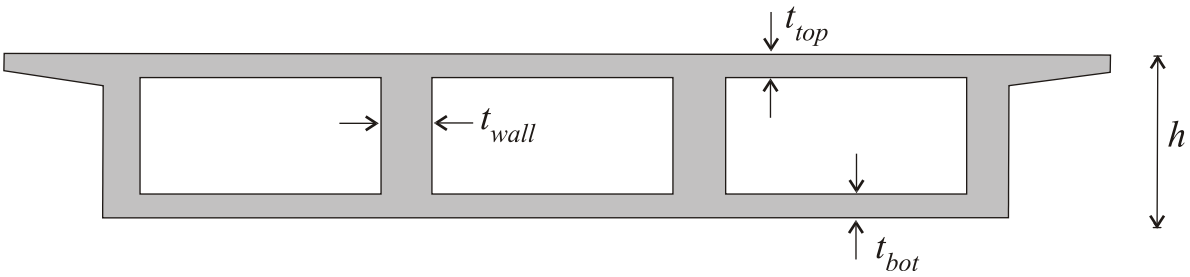

Figure 5.5 – Cross-section details of box-girder bridges.

Table 5.6 – Deck cross-section properties.

Deck cross-section properties	Era 11	Era 22	Era 33
Bottom flange thickness (t_{bot}, in.)	6.0	6.5	7.0
Wall thickness	12.0	12.0	12.0

Table 5.7 – Box-girder deck slab thickness (MTD, 2008).

REINFORCED CONCRETE BOX & STEEL GIRDERS w/ flange width >12"and < 24"						
"S"	"t"	Dimension	Transverse Bars		"D" Bars	"G" Bars
Girder CL to CL Spacing	Top Slab Thickness	"F"	Size	Spacing [1]	#5 Bars	#4 Bars
4'- 0"	7"	6"	#5	12"	3	2
4'- 3"	7"	6"	#5	12"	3	2
4'- 6"	7"	6"	#5	12"	3	2
4'- 9"	7"	7"	#5	12"	3	2
5'- 0"	7"	7"	#5	12"	4	2
5'- 3"	7"	7"	#5	12"	4	3
5'- 6"	7"	8"	#5	12"	4	3
5'- 9"	7"	8"	#5	11"	4	3
6'- 0"	7 1/8"	9"	#5	11"	5	3
6'- 3"	7 1/8"	9"	#5	11"	5	3
6'- 6"	7 1/4"	9"	#5	11"	5	3
6'- 9"	7 3/8"	10"	#5	11"	5	3
7'- 0"	7 1/2"	10"	#5	10"	6	3
7'- 3"	7 1/2"	11"	#5	10"	6	3
7'- 6"	7 5/8"	11"	#5	10"	6	3
7'- 9"	7 3/4"	11"	#5	10"	6	3
8'- 0"	7 3/4"	1'- 0"	#5	10"	7	3
8'- 3"	7 7/8"	1'- 0"	#5	10"	7	4
8'- 6"	8"	1'- 1"	#5	10"	7	4
8'- 9"	8 1/8"	1'- 1"	#5	10"	7	4
9'- 0"	8 1/8"	1'- 1"	#5	10"	7	4
9'- 3"	8 1/4"	1'- 2"	#5	10"	8	4
9'- 6"	8 3/8"	1'- 2"	#5	10"	8	4
9'- 9"	8 3/8"	1'- 2"	#5	10"	8	4
10'- 0"	8 1/2"	1'- 3"	#6	12"	10	4
10'- 3"	8 5/8"	1'- 3"	#6	11"	11	4
10'- 6"	8 5/8"	1'- 4"	#6	11"	11	4
10'- 9"	8 3/4"	1'- 4"	#6	11"	11	4
11'- 0"	8 7/8"	1'- 4"	#6	11"	11	4
11'- 3"	8 7/8"	1'- 5"	#6	11"	12	5
11'- 6"	9"	1'- 5"	#6	11"	12	5
11'- 9"	9 1/8"	1'- 6"	#6	11"	12	5
12'- 0"	9 1/8"	1'- 6"	#6	10"	13	5
12'- 3"	9 1/4"	1'- 6"	#6	10"	13	5
12'- 6"	9 3/8"	1'- 7"	#6	10"	13	5
12'- 9"	9 1/2"	1'- 7"	#6	10"	14	5
13'- 0"	9 1/2"	1'- 7"	#6	10"	14	5
13'- 3"	9 5/8"	1'- 8"	#6	10"	14	5
13'- 6"	9 3/4"	1'- 8"	#6	10"	14	5
13'- 9"	9 3/4"	1'- 9"	#6	10"	14	5
14'- 0"	9 7/8"	1'- 9"	#6	10"	14	5
14'- 3"	10"	1'- 9"	#6	10"	14	5
14'- 6"	10 1/8"	1'- 10"	#6	10"	15	5
14'- 9"	10 1/4"	1'- 10"	#6	10"	15	5
15'- 0"	10 3/8"	1'- 11"	#6	10"	15	5

CIP PRESTRESSED BOX, PRECAST-I, & STEEL GIRDERS w/ flange width>=24"						
"S"	"t"	Dimension	Transverse Bars		"D" Bars	"G" Bars
Girder CL to CL Spacing	Top Slab Thickness	"F"	Size	Spacing [1]	#5 Bars	#4 Bars
4'- 0"	7"	5"	#5	12"	3	2
4'- 3"	7"	5"	#5	12"	3	2
4'- 6"	7"	6"	#5	12"	3	2
4'- 9"	7"	6"	#5	12"	3	2
5'- 0"	7"	6"	#5	12"	3	2
5'- 3"	7"	7"	#5	12"	3	2
5'- 6"	7"	7"	#5	12"	4	2
5'- 9"	7"	7"	#5	12"	4	3
6'- 0"	7"	8"	#5	12"	4	3
6'- 3"	7"	8"	#5	12"	4	3
6'- 6"	7 1/8"	9"	#5	12"	4	3
6'- 9"	7 1/8"	9"	#5	11"	5	3
7'- 0"	7 1/4"	9"	#5	11"	5	3
7'- 3"	7 3/8"	10"	#5	11"	5	3
7'- 6"	7 1/2"	10"	#5	11"	5	3
7'- 9"	7 1/2"	11"	#5	11"	5	3
8'- 0"	7 5/8"	11"	#5	11"	6	3
8'- 3"	7 3/4"	11"	#5	11"	6	3
8'- 6"	7 3/4"	1'- 0"	#5	11"	6	3
8'- 9"	7 7/8"	1'- 0"	#5	11"	6	4
9'- 0"	8"	1'- 1"	#5	11"	6	4
9'- 3"	8 1/8"	1'- 1"	#5	11"	7	4
9'- 6"	8 1/8"	1'- 1"	#5	11"	7	4
9'- 9"	8 1/4"	1'- 2"	#5	10"	8	4
10'- 0"	8 3/8"	1'- 2"	#5	10"	8	4
10'- 3"	8 3/8"	1'- 2"	#5	10"	8	4
10'- 6"	8 1/2"	1'- 3"	#5	10"	8	4
10'- 9"	8 5/8"	1'- 3"	#5	10"	8	4
11'- 0"	8 5/8"	1'- 4"	#6	11"	11	4
11'- 3"	8 3/4"	1'- 4"	#6	11"	11	4
11'- 6"	8 7/8"	1'- 4"	#6	11"	11	4
11'- 9"	8 7/8"	1'- 5"	#6	11"	12	5
12'- 0"	9"	1'- 5"	#6	11"	12	5
12'- 3"	9 1/8"	1'- 6"	#6	11"	12	5
12'- 6"	9 1/8"	1'- 6"	#6	11"	12	5
12'- 9"	9 1/4"	1'- 6"	#6	11"	12	5
13'- 0"	9 3/8"	1'- 7"	#6	10"	13	5
13'- 3"	9 1/2"	1'- 7"	#6	10"	14	5
13'- 6"	9 1/2"	1'- 7"	#6	10"	14	5
13'- 9"	9 5/8"	1'- 8"	#6	10"	14	5
14'- 0"	9 3/4"	1'- 8"	#6	10"	14	5
14'- 3"	9 3/4"	1'- 9"	#6	10"	14	5
14'- 6"	9 7/8"	1'- 9"	#6	10"	14	5
14'- 9"	10"	1'- 9"	#6	10"	14	5
15'- 0"	10 1/8"	1'- 10"	#6	10"	15	5

5.6 Columns

As mentioned before, the column details vary depending on the design era due to the changes in design philosophy. The design philosophies adopted for California bridges have been significantly influenced by the historic 1971 San Fernando and the 1989 Loma Prieta earthquakes. In seismic design philosophy during Era 11, seismic forces were proportional to the dead weight of structures. Bridges were designed to resist a lateral seismic force equal to 6% of the dead weight of the structures. After the 1971 San Fernando earthquake, capacity design principles were introduced in the seismic design standards. The lateral load-carrying capacity of the seismically designed bridges increased by a factor of 2 or 2.5. In addition, several aspects, including fault proximity, site conditions, dynamic structural response, and ductile details were considered in the design of bridge columns. The extensive damage from the 1989 Loma Prieta earthquake forced Caltrans to solicit the Applied Technology Council (ATC) to conduct a detailed study and provide recommendations for design standards, performance criteria, and practices. The recommendations described in ATC-32 were incorporated in the Caltrans design manuals, leading to the Era 33 columns. The design attributes and statistical properties of bridge columns are identified by an in-depth review of bridge plans pertinent to the design eras for the chosen box girder bridge classes.

5.6.1 Column height

In this study, column heights are measured as the height between the underside of the bridge deck and the top of column footing by manual plan review. The basic statistics of the column height are provided in Table 5.8. As noted in Table 5.8, the median column height increases from Era 11 to Era 33.

Table 5.8 – Column height distribution.

Design era	Units	Distribution					
		Type [§]	Parameters[†]		Median	Lower bound (L)	Upper Bound (U)
			Mean (α)	Standard Deviation (β)			
Era11	ft	LN	3.06	0.13	21.5	16.5	28.0
Era 22	ft	LN	3.14	0.16	23.2	17.0	32.0
Era 33	ft	LN	3.22	0.18	25.0	17.5	36.0

[§] N = normal, LN = lognormal, U = uniform, and B = Bernoulli distribution.

[†] α and β are the parameters of the distribution. These denote mean and standard deviation for a normal and uniform distribution, and mean and standard deviation of the associated normal distribution (in log space) in the case of a lognormal distribution

5.6.2 Column cross-section

Various cross sections such as circular, rectangular, and oblong are noted from the plan review. Era 11 consists of circular and rectangular cross-sections while Era 22 and Era 33 contain circular and oblong cross-sections. As seen in Figure 5.6, where the cross-section details of various design eras are presented, each era consists of a wide range of cross-sections. The percentage distribution of the Era 11 columns is given in Table 5.9.

Table 5.9 – Distribution of column cross-sections.

Design era	Type of bent	Column cross-section	Diameter (D, in.)*	Length (L_c, in.)*	Breadth (B_c, in.)*	Mix %
Era 11	Single	Circular	48	-	-	10
			60	-	-	20
			72	-	-	20
		Rectangular	-	72	36	10
			-	96	36	15
			-	120	36	10
			-	96	48	15
	Multi	Circular	36	-	-	15
			48	-	-	20
			60	-	-	5
		Rectangular	-	42	30	20
			-	48	36	25
			-	60	42	10
			-	96	36	5
Era 22	Single	Circular	60	-	-	10
			66	-	-	25
			72	-	-	15
			84	-	-	10
		Oblong	-	72	48	10
			-	96	48	15
			-	99	66	15
	Multi	Circular	48	-	-	35
			60	-	-	10
			66	-	-	20
			72	-	-	10
		Oblong	-	60	36	10
			-	72	48	15
Era 33	Single	Circular	60	-	-	5
			66	-	-	15
			84	-	-	20
			108	-	-	10
		Oblong	-	72	48	5
			-	96	48	10
			-	99	66	25
			-	108	72	10
	Multi	Circular	48	-	-	30
			60	-	-	10
			66	-	-	25
			84	-	-	5
		Oblong	-	72	48	15
			-	99	66	10
			-	126	84	5

*Refer figure 5.6

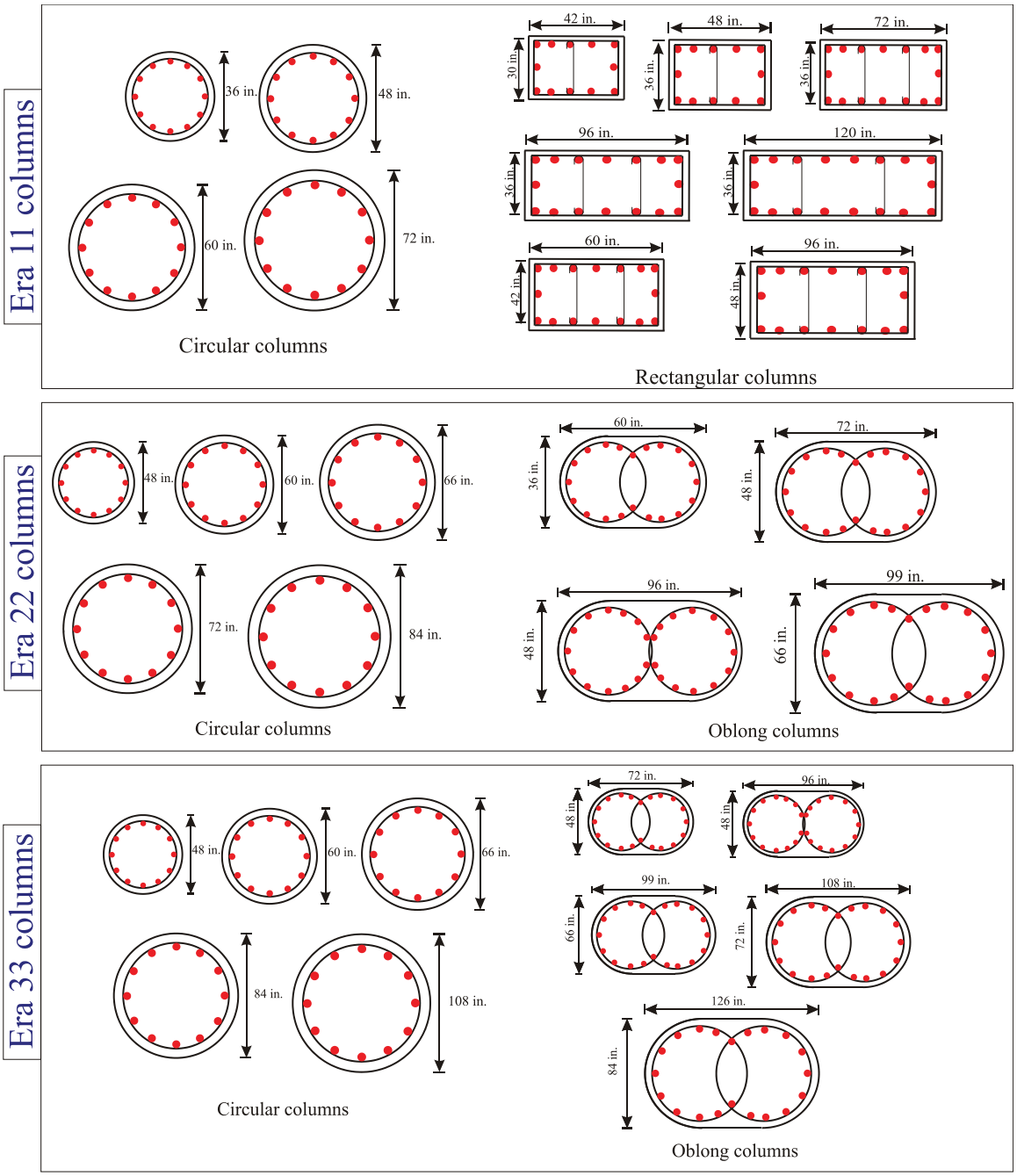

Figure 5.6 – Column cross-sections for various design eras of box girder bridges.

5.6.3 Column material properties

The bridge classes considered in this study use concrete as the construction material and the statistical properties of the concrete are given in Table 5.10. Following the recommendations of Choi (2002), the compressive strength of concrete is modeled using a normal distribution. The statistical properties of the yield strength of the reinforcing steel are also presented in Table 5.10.

Table 5.10 – Statistical distribution of column material properties.

Parameter	Design era	Units	Distribution				
			Type§	Parameters†		Lower bound (L)	Upper Bound (U)
				Mean (α)	Standard Deviation (β)		
Concrete compressive strength	Era11	ksi	N	3.90⊗ (4.23)	0.48 (0.52)	2.94 (4.86)	5.19 (5.36)
	Era 22/ Era33	ksi	N	4.55	0.56	3.43	5.67
Steel yield strength	Era11	ksi	N	57.3⊗ (69.0)	4.5 (5.5)	49.0 (58.0)	67.0 (80.0)
	Era 22/ Era33	ksi	N	69.0	5.5	58.0	80.0

§ N = normal, LN = lognormal, U = uniform, and B = Bernoulli distribution.

⊗80% simulations with 3.9 ksi and remaining 20% with 4.23 ksi, same the case for reinforcing steel yield strength.

†α and β are the parameters of the distribution. These denote mean and standard deviation for a normal and uniform distribution, and mean and standard deviation of the associated normal distribution (in log space) in the case of a lognormal distribution.

5.6.4 Column reinforcement details

The statistical properties of the column reinforcement identified from the plan review of bridges are given in Table 5.11. In Era 11, the column shear reinforcement consisted of #4 transverse stirrups spaced at 12 in. on center regardless of the column size or the size of the longitudinal reinforcing bars. Uniform distribution is assumed for the longitudinal and transverse reinforcement ratio.

Table 5.11 – Statistical distribution of column reinforcement details.

Parameter	Design era	Units	Distribution			Lower bound (L)	Upper Bound (U)
			Type[§]	Parameters[†]			
				Mean (α)	Standard Deviation (β)		
Longitudinal steel reinforcement ratio	All	-	U	2.00	0.33	1.0	3.0
Transverse steel reinforcement ratio	Era11	-	#4 @ 12 in. irrespective of the cross-section				
	Era 22/ Era33	-	U	0.85	0.07	0.4	1.3

[§] N = normal, LN = lognormal, U = uniform, and B = Bernoulli distribution.

[†] α and β are the parameters of the distribution. These denote mean and standard deviation for a normal and uniform distribution, and mean and standard deviation of the associated normal distribution (in log space) in the case of a lognormal distribution.

5.7 Foundations

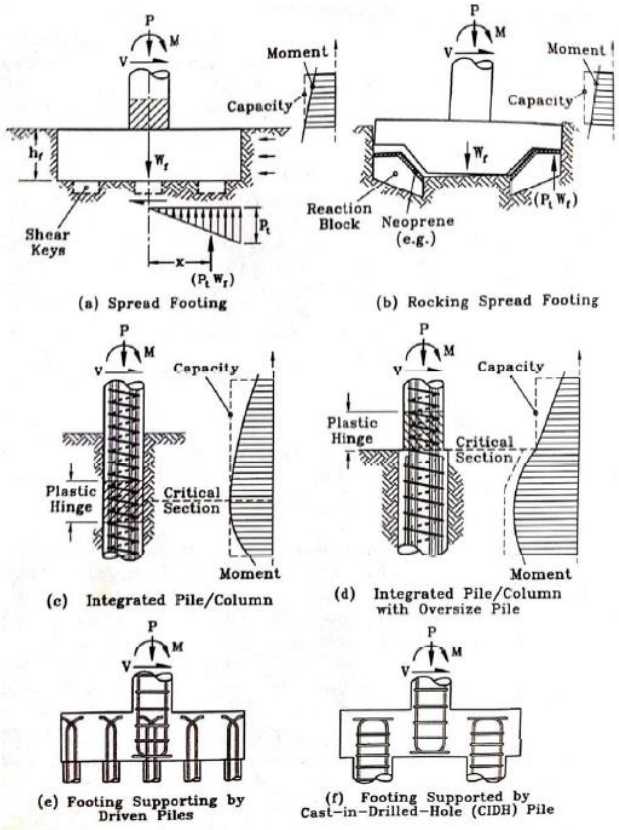

Figure 5.7 – Bridge foundation types (Priestley et al. 1996).

The foundation provides a means to transmit service and ultimate loads from the structure to the underlying soil. Foundations can be classified into two types: shallow

foundations and deep foundations. As the name implies, the loads from the structure are transferred to the underlying soil at a shallow depth for shallow foundations. Deep foundations are provided when soil conditions are not favorable to shallow foundations and transfer the load through piles. The type of foundation for a particular bridge is determined by various factors such as soil conditions, overhead clearance, existing utilities, and proximity to existing facilities such as buildings and railroads. The possible types of footings are shown in Figure 5.7 and the statistical distribution of foundations across the design eras is shown in Figure 5.8. The rotational and translational stiffness of the foundations are presented in Tables 5.12 and 5.13, respectively.

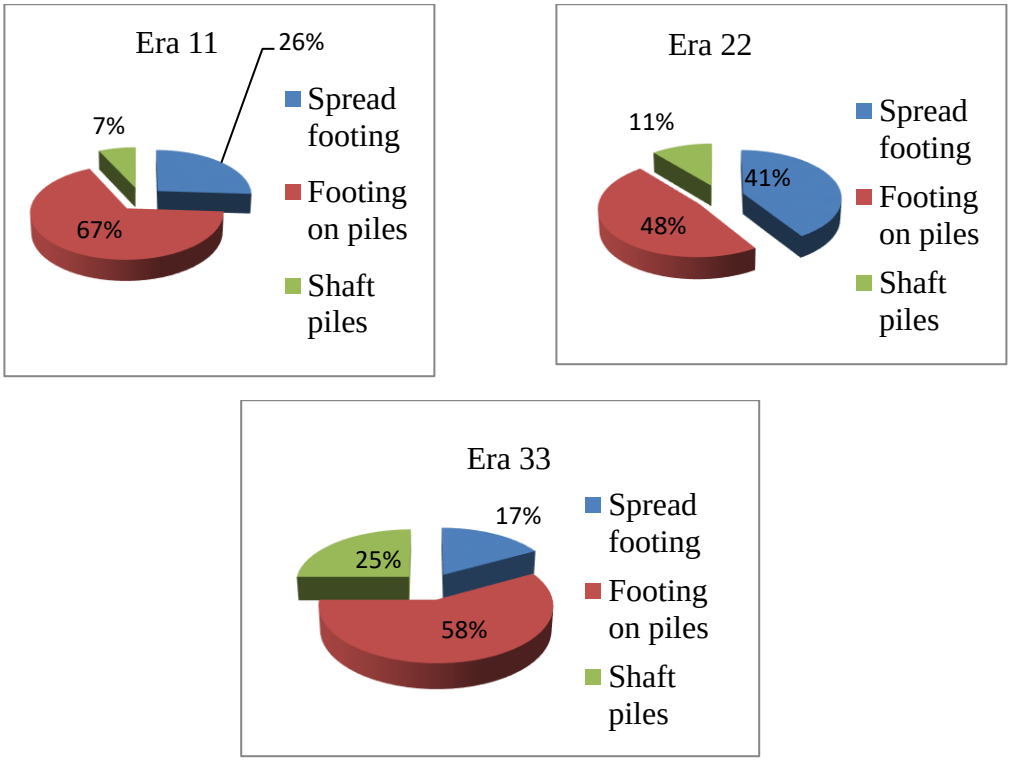

Figure 5.8 – Statistical distribution of foundation for various eras.

Table 5.12 – Distribution of foundation rotational stiffness (×10^6 kip-in/rad).

Design era	Type of bent	Type of footing	Foundation fixity	Mix %	Transverse to bridge direction					Trans/Long stiffness ratio				
					Type§	Parameters		Lower bound (L)	Upper Bound (U)	Type§	Parameters		Lower bound (L)	Upper Bound (U)
						Mean (α)	Standard Deviation (β)				Mean (α)	Standard Deviation (β)		
Era 11	single	pile	fixed	100	LN	25.0	2.5	10	62.5	LN	1.5	1.5	1.0	2.25
		spread	fixed		LN	25.0	2.5	10	62.5	LN	1.5	1.5	1.0	2.25
	multiple	pile	pinned	37.5	LN	2.5	2.5	1.0	6.3	LN	1.0	1.5	0.67	1.50
			fixed	12.5	LN	4.0	2.5	1.6	10.0	LN	1.0	1.5	0.67	1.50
		spread	pinned	37.5	LN	2.5	2.5	1.0	6.3	LN	1.0	1.5	0.67	1.50
			fixed	12.5	LN	4.0	2.5	1.6	10.0	LN	1.0	1.5	0.67	1.50
Era 22	single	pile	fixed	50	LN	80.0	2.5	32.0	200.0	LN	1.5	1.5	1.0	2.25
		spread	fixed	50	LN	50.0	2.5	20.0	125.0	LN	1.3	1.3	1.0	1.70
	multiple	pile	pinned	25	LN	12.0	2.5	4.8	30.0	LN	1.0	1.5	0.67	1.5
			fixed	25	LN	18.0	2.5	7.2	15.0	LN	1.0	1.5	0.67	1.5
		spread	pinned	25	LN	12.0	2.5	4.8	30.0	LN	1.0	1.5	0.67	1.5
			fixed	25	LN	18.0	2.5	7.2	15.0	LN	1.0	1.5	0.67	1.5
Era 33	single	pile	fixed	90	LN	190.0	2.5	76.0	475.0	LN	1.15	1.15	1.00	1.32
		spread	fixed	10	LN	50.0	2.5	20.0	125.0	LN	1.15	1.15	1.00	1.32
	multiple	pile	pinned	50	LN	20.0	2.5	8.0	50.0	LN	1.20	1.25	0.96	1.50
			fixed	0	LN	30.0	2.5	12.0	75.0	LN	1.20	1.25	0.96	1.50
		spread	pinned	50	LN	20.0	2.5	8.0	50.0	LN	1.20	1.25	0.96	1.50
			fixed	0	LN	30.0	2.5	12.0	75.0	LN	1.20	1.25	0.96	1.50

Table 5.13 – Distribution of foundation translational stiffness (kip/in).

Design era	Type of bent	Type of footing	Foundation fixity	Mix %	Transverse to bridge direction					Trans/Long stiffness ratio				
					Type§	Parameters		Lower bound (L)	Upper Bound (U)	Type§	Parameters		Lower bound (L)	Upper Bound (U)
						Mean (α)	Standard Deviation (β)				Mean (α)	Standard Deviation (β)		
Era 11	single	pile	fixed	100	LN	1250.0	2.5	500.0	3125.0	LN	1.0	1.0	1.0	1.0
		spread	fixed		LN	1250.0	2.5	500.0	3125.0	LN	1.0	1.0	1.0	1.0
	multiple	pile	pinned	37.5	LN	625.0	2.5	250.0	1562.5	LN	1.0	1.0	1.0	1.0
			fixed	12.5	LN	625.0	2.5	250.0	1562.5	LN	1.0	1.0	1.0	1.0
		spread	pinned	37.5	LN	625.0	2.5	250.0	1562.5	LN	1.0	1.0	1.0	1.0
			fixed	12.5	LN	625.0	2.5	250.0	1562.5	LN	1.0	1.0	1.0	1.0
Era 22	single	pile	fixed	50	LN	2000.0	2.5	800.0	5000.0	LN	1.0	1.0	1.0	1.0
		spread	fixed	40	LN	2000.0	2.5	800.0	5000.0	LN	1.0	1.0	1.0	1.0
	multiple	pile	pinned	25	LN	1000.0	2.5	400.0	2500.0	LN	1.0	1.0	1.0	1.0
			fixed	12.5	LN	1000.0	2.5	400.0	2500.0	LN	1.0	1.0	1.0	1.0
		spread	pinned	25	LN	1000.0	2.5	400.0	2500.0	LN	1.0	1.0	1.0	1.0
			fixed	12.5	LN	1000.0	2.5	400.0	2500.0	LN	1.0	1.0	1.0	1.0
Era 33	single	pile	fixed	65	LN	2500.0	2.5	1000.0	6250.0	LN	1.0	1.0	1.0	1.0
		spread	fixed	10	LN	2500.0	2.5	1000.0	6250.0	LN	1.0	1.0	1.0	1.0
	multiple	pile	pinned	35	LN	1000.0	2.5	400.0	2500.0	LN	1.0	1.0	1.0	1.0
			fixed	0	LN	1000.0	2.5	400.0	2500.0	LN	1.0	1.0	1.0	1.0
		spread	pinned	35	LN	1000.0	2.5	400.0	2500.0	LN	1.0	1.0	1.0	1.0
			fixed	0	LN	1000.0	2.5	400.0	2500.0	LN	1.0	1.0	1.0	1.0

5.8 Other uncertain parameters

The distribution of other uncertain parameters is given in this section.

5.8.1 Damping

Bavirisetty et al. (2003) estimated the 2nd and 98th percentile of damping ratios in bridges to be 0.02 and 0.07 respectively. The recommendations of Feng et al. (1999) for tall buildings are extended to bridges by the researchers (Nielson 2005; Padgett 2007) and the damping uncertainty is modeled using a normal distribution. Based on these studies, damping is modeled as normal distribution (mean = 4.5%, standard deviation = 1.25%) and is shown in Table 5.14.

5.8.2 Mass factor

Mass sources such as parapets and barrier rails, variable deck slab thickness, electric poles and other equipment, re-pavement procedures, and variation in material densities are not considered in the OpenSees bridge model; because of this, it has been decided to account for these mass sources explicitly with the addition of a mass factor. The mass factor is assumed to be uniformly distributed with bounds of 0.95 and 1.15.

5.8.3 Shear key acceleration

Per Caltrans, designs of shear keys are categorized as either *isolated*, as new emerging designs, or *non-isolated*, as older conventional designs. Since the isolated design is a new type of design that does not appear in the existing inventory, the current study will focus only on the non-isolated type. The non-isolated shear keys were designed to withstand dead-load reaction for 0.3 to 0.5g. However, they have been shown in reality to be on the order of 3 times stronger (Caltrans, 2017). Based on the recommendation from Caltrans, shear key is modeled using lognormal distribution, with a mean value of 1.0 and standard deviation of 0.20.

5.8.4 Gap

Lognormal distribution is adopted for the gap between the deck and the superstructure with a median value of -0.20 and standard deviation of 0.50. Further, the gap between the superstructure and shear keys is assumed to be uniformly distributed between 0 and 1.5 in.

5.8.5 Earthquake direction

The ground motions considered in the present study have fault-normal and fault-parallel components. Mackie et al. (2011) concluded that there is a negligible effect of the angle of incidence on the mean ensemble response of bridge components and hence the incident angle is not considered as a major source of uncertainty in the study. As such, the two horizontal components of ground motions are assigned simultaneously to the longitudinal and transverse direction of the bridge and the orientation is assigned randomly. The effects of vertical acceleration and spatially-variable ground motions are not considered in this study.

Table 5.14 – Distribution of other uncertain parameters.

Design era	Parameter	Units	Distribution				
			Type[§]	Parameters[†]		Lower bound (L)	Upper Bound (U)
				Mean (α)	Standard Deviation (β)		
All eras	Damping	-	N	0.045	0.0125	0.02	0.07
	Mass factor		U	1.05	0.0033	0.95	1.15
	Shear key acceleration	g	LN	0.0	0.20	0.8	1.20
	Gap						
	deck and superstructure	in.	LN	-0.20	0.50	0.30	2.20
	superstructure and shear key	in	U	0.75	0.19	0.00	1.50

[§] N = normal, LN = lognormal, U = uniform, and B = Bernoulli distribution.

[†] α and β are the parameters of the distribution. These denote mean and standard deviation for a normal and uniform distribution, and mean and standard deviation of the associated normal distribution (in log space) in the case of a lognormal distribution.

5.9 Closure

This chapter presents the extensive plan review and analysis of the California box girder bridge inventory using the BIRIS assembled by Caltrans engineers. The bridges are divided into three

eras: Era 11 (pre 1971), Era 22 (1971 – 1990), and Era 33 (post 1990), based on the seismic design principles and column detailing. Details pertinent to abutments, bearing, foundations, superstructure, and columns are gathered across the three design eras to aid in the development of stochastic finite element models for the generation of probabilistic seismic demand models (PSDMs) and fragility curves. Also, the bridge design details and physical characteristics identified in this chapter help to capture the vulnerabilities associated with various components. The input parameters are assumed to be uncorrelated in the current study and further studies are needed to address the correlation effects.

CHAPTER 6 SYSTEM AND COMPONENT FRAGILITY CURVES FOR BOX-GIRDER BRIDGES

The economic and social impacts of earthquakes on civil infrastructure have increased awareness of potential seismic hazards and the associated vulnerability of structures. The evaluation of economic losses after earthquakes is primarily based on the prediction of structural damage. These damage assessments can be represented probabilistically by fragility curves, a statistical function that gives the conditional probability of exceeding a certain damage state given a certain ground motion intensity measure (*IM*). Component and system fragility curves can be useful in prioritizing both post-earthquake emergency responses and field inspections.

Generating seismic fragility curves involves the convolution of demand models and capacity models. This chapter explains the fragility framework, including the formulation of probabilistic seismic demand models (PSDMs) and capacity models. The methodology presented in this section is used in this study to develop system and component fragility curves for single frame multi-span box-girder bridges in California. Comparisons are conducted among various bridge classes to assess the relative vulnerability of each class, and are presented in detail in this chapter.

6.1 Fragility Framework

The multiphase framework used by numerous researchers (Nielson 2005, Padgett 2007, Ramanathan et al. 2015, Jeon et al. 2015) is adopted in the current study to shed light on the fragilities of various bridge classes and the effects of various bridge components on bridge fragilities. This methodology also helps to generate system as well as component fragilities. The parameters listed in Chapter 5 are varied to capture uncertainties in bridge classes. Input variables are sampled across the range of parameters presented in the Chapter 5 using Latin Hypercube

Sampling technique in order to generate statistically significant yet nominally identical three–dimensional bridge models. The variables are randomly paired with the selected suite of ground motions. The two orthogonal components of the ground motions are randomly assigned to the longitudinal and transverse direction of the bridge axis. A set of 320 simulations of nonlinear time history analyses (NLTHAs) is performed for all bridge-ground motion pairs to monitor the maximum response of various bridge components. Figure 6.1 shows the schematic of the procedure that was adopted to capture the demand of various bridge components due to the ground motions.

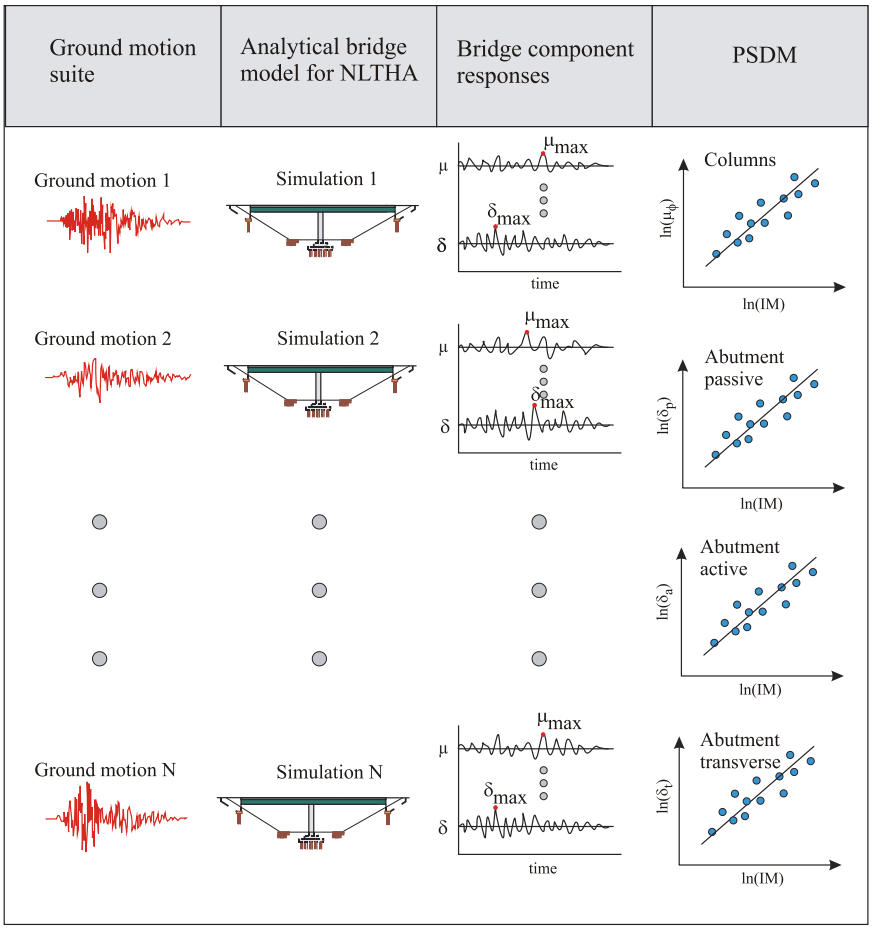

Figure 6.1 – Schematic representation of the NLTHA procedure used to derive the PSDMs.

Table 6.1 − Engineering demand parameters for bridge components monitored in NLTHA.

Component	Engineering demand parameter	Notation	Units
Columns	Curvature ductility	ϕ_c	-
Abutment seat	Displacement	δ_{seat}	Inches
Unseating	Displacement	δ_u	Inches
Elastomeric bearing	Displacement	δ_b	Inches
Deck	Displacement	δ_d	Inches
Foundation translation	Displacement	δ_{fnd}	Inches
Foundation rotation	Rotation	θ_f	
Passive abutment	Displacement	δ_p	Inches
Active abutment	Displacement	δ_a	Inches
Transverse abutment	Displacement	δ_t	Inches
Shear key	Displacement	δ_{key}	Inches

The current study considers the vulnerability of multiple components: columns, abutment seat (seat type abutments), elastomeric bearings, joint seal, restrainer cables (retrofitted bridges), deck displacement, foundations, abutments, and shear keys. The engineering demand parameters (EDP) representing the above components are indicated in Table 6.1. The following section explains the estimation of the seismic demand and capacity models.

6.1.1 Probabilistic seismic demand models

Fragility curves require the convolution of the demand model and capacity models. As mentioned before, the seismic demands on bridge components are obtained by the three-dimensional NLTHAs of bridge models. The peak response of the components (d_i, e.g., column curvature ductility, bearing deformations, and abutment deformations) is recorded for each NLTHA. Based on Cornell et al. (2002), PSDMs are defined as the linear regression of pairs of *D* and *IM* in the log-transformed space, as illustrated in Figure 6.2. These can be written as

$$\ln(S_d) = \ln(a) + b\ln(IM) \tag{6.1}$$

where a and b are the regression coefficients. The coefficients a and b are obtained by performing a linear regression analysis on *D-IM* pairs in the log-transformed space. Dispersion, $\beta_{d/IM}$, is evaluated based on statistical analysis:

$$\beta_{d/\mathrm{IM}} = \sqrt{\frac{\sum_{i=1}^{N}\left(\ln d_i - \ln\left(S_d\right)\right)^2}{N-2}} \tag{6.2}$$

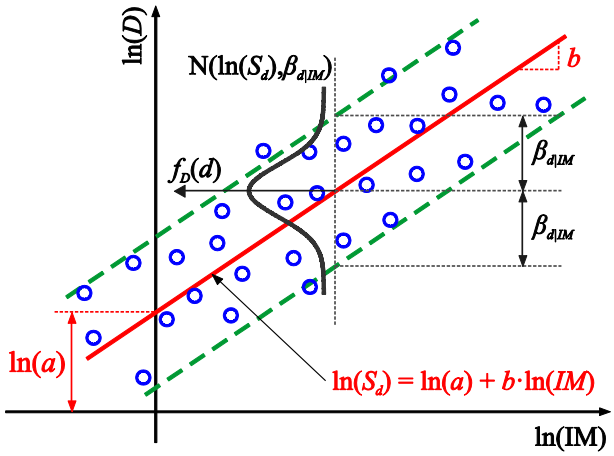

Figure 6.2 – Illustration of a typical PDSM.

6.1.2 Capacity models

The development of a probabilistic seismic demand model using the results of the NLTHA forms the demand side of the fragility formulation. The next crucial step in the fragility formulation is the formulation of capacity, or limit state, models. The capacity models are described by a two-parameter lognormal distribution with median, S_c and dispersion, βc. Discrete damage states are defined for each component corresponding to the significant change in its response and consequent to its own performance and the performance of the bridge at both the global and system levels. A general description of the component damage thresholds (CDT) and bridge system-level damage states (BSST) is given in Table 6.2 and 6.3, respectively (Ramanathan et al. 2015).

The bridge components are categorized as either primary or secondary. Primary components include the columns and abutment seat; these are the components that affect the vertical stability and load carrying capacity of the bridge. Secondary components are those whose failure will not force the closure of the bridge; this includes abutment deformations, shear key displacement, and others. As the failure of a primary component affects the load carrying capacity and stability of the bridge system, CDTs of primary components map directly into BSSTs. Only two broad CDTs, CDT-0 and CDT-1, are defined for the secondary components and these map directly into BSST-0 and BSST-1. CDTs and BSSTs were developed in close collaboration with Caltrans. The number of components used to integrate the system fragility varies based on the BSST under consideration. Such mapping ensures similar consequences in terms of repair and traffic implications at the system level.

Table 6.2– Component level damage state descriptions – Component Damage Thresholds (CDT).

	CDT-0	CDT-1	CDT-2	CDT-3	
Component damage states	No damage	Aesthetic damage	Repairable minor functional	Repairable major	Component replacement

Table 6.3 – General description of BSSTs along with CDTs.

Bridge system damage states	BSST-0 MINOR	BSST-1 MODERATE	BSST-2 EXTENSIVE	BSST-4 COMPLETE
ShakeCast Inspection Priority levels	Low	Medium	Medium-High	High
Likely Immediate Post-Event Traffic State	Open to normal public traffic – No Restrictions	Open to Limited public traffic – speed/weight/lane restrictions	Emergency vehicles only – speed/weight/lane restrictions	Closed (until shored/braced) – potential for collapse
Traffic Operation Implications Is closure/detour needed? Are traffic restrictions needed?	 Very unlikely Unlikely	 Unlikely Likely	 Likely Very Likely	 Very likely Very Likely - Detour
Emergency Repair Implications Is shoring/bracing needed? Is roadway leveling needed?	 Very unlikely Unlikely	 Unlikely Likely	 Likely Very Likely	 Very likely Very Likely - Detour
Component Damage Range Primary components Secondary components	 CDT-0 to 1 CDT-0	 CDT-1 to 2 CDT-1	 CDT-2 to 3 NA	 Above CDT-3 NA

A significant contribution of the present study is the suggestion of capacity limit states for columns (CCLS) based on extensive experimental review. A review of the existing research pertinent to various design eras was conducted to collect the experimental data for bridge columns, and statistical analysis was carried out to suggest the CCLS for bridge columns. Such an exercise helps to support seismic risk evaluation of bridges in California by developing a new generation of more accurate and useful bridge fragility models for incorporation into the ShakeCast earthquake alerting system developed by the California Department of Transportation (Caltrans). As mentioned before, the intention of the current study is to suggest fragility relationships for damage states that range from minor spalling of concrete to complete bridge collapse. The definitions of these limit states and their operational consequences are given in Table 6.4.

Table 6.4 – General definition of column capacity limit states.

Column capacity limit states (CCLS)	Component state	Component damage	Component repair
CCLS-0 (Slight)	None or aesthetic	EQ-related minor cracking	Seal and paint
CCLS-1 (Moderate)	Minor repairs needed	Minor spalling of cover concrete	Epoxy inject, minor removal/patch
CCLS-2 (Extensive)	Major repairs needed, but function intact	Exposed core, confinement yield	Major removal/patch. Add jacket.
CCLS-3 (Complete)	Irreparable damage, function compromised	Bar bucking, large drift, core crushing	Remove/Replace column (or bridge)

6.1.2.1 Experimental data analysis for various design eras

The design philosophies for California bridges have been significantly influenced by the historic 1971 San Fernando and the 1989 Loma Prieta earthquakes. Based on unique design attributes and evolutions in seismic design philosophy, California bridges are categorized into three design eras: Era 11 (pre-1971), Era 22 (1971-1990), and Era 33 (post-1990). In Era 11 seismic design philosophy, seismic forces were proportional to the dead weight of structures. Bridges were designed to resist a lateral seismic force equal to 6% of the dead weight of the structures. Shear failure and pull-out of the longitudinal reinforcement in columns were predominant due to the lack of ductility, as was revealed by the 1971 San Fernando earthquake.

After the 1971 San Fernando earthquake, capacity design principles were introduced in the seismic design standards. The lateral load carrying capacity of seismically-designed bridges increased by a factor of 2 or 2.5. In addition, several aspects, including fault proximity, site conditions, dynamic structural response, and ductile details, were considered in the design of

bridge columns. However, shear failure in the columns was still observed in Era 22 columns due to the insufficient confinement in the plastic hinge regions.

The extensive damage from the 1989 Loma Prieta earthquake forced Caltrans to solicit the Applied Technology Council (ATC) to conduct a detailed study and provide recommendations for design standards, performance criteria, and practices. The recommendations described in ATC-32 were incorporated in Caltrans design manuals, leading to the distinctive Era 33 columns. The fundamental emphasis in the Era 33 design philosophy was on the displacement-based or capacity design approach, which ensures a ductile failure mode in the columns. The design details pertinent to various design eras are given in Table 6.5, 6.6, and 6.7 respectively.

Table 6.8, 6.9, and 6.10, respectively, summarize the extensive literature review on experimental investigations of bridge columns. The tables also present the geometric features of the test column, and the values of displacement and curvature ductility limit states for various levels of damage.

Table 6.5 – Design details for columns in Era 11 (pre-1971).

Design details	Typical column reinforcement layout
Lateral seismic force 6% of structural dead weight **Column shear reinforcement** #4 @ 12 in. irrespective of column size **Other notable features** • Lap-splice of column longitudinal bars near footing. • Inadequate development length of the column longitudinal bars into the footing without any standard hooks. • Concept of ductility was absent (failure modes are brittle, shear or lap-splice failure) • Strength of column degrades rapidly once yield moment is attained • Column bars are embedded into footing without 90 degree hook • Splice length of longitudinal bars was too short	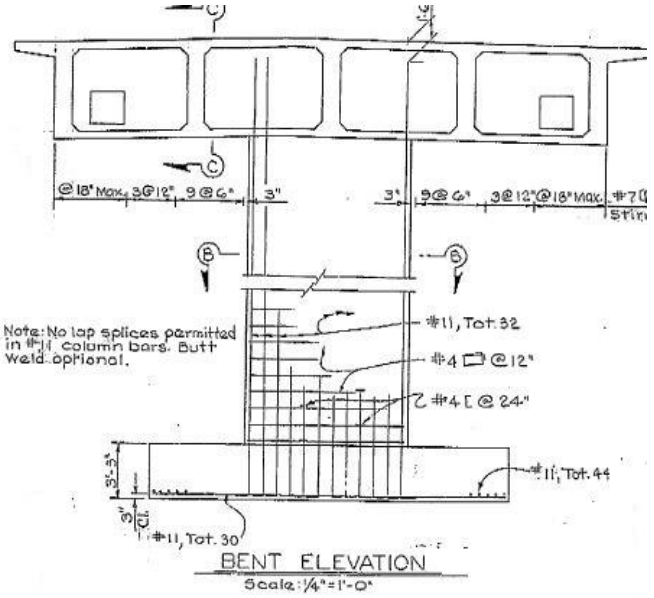 Caltrans (2017)

Table 6.6 – Design details of columns in Era 22 (1971-1990).

Design details	Typical column reinforcement layout
Lateral seismic force 2 to 2.5 times higher than era 11. Based on ATC-6 guidelines. **Column shear reinforcement** Spacing: 3-6 in. However, confinement in the plastic hinge region is absent. **Other notable features** • Bar lap-splice is not permitted at the location of maximum moment. • Increase in the negative moment reinforcement in footing and pile caps without any shear reinforcement. • Joint reinforcement between the column and the bent cap, and the column and the footing was absent. • Column shear in the plastic hinge region is typical. • Due to the poor flare details, shear failure was seen in columns with flares.	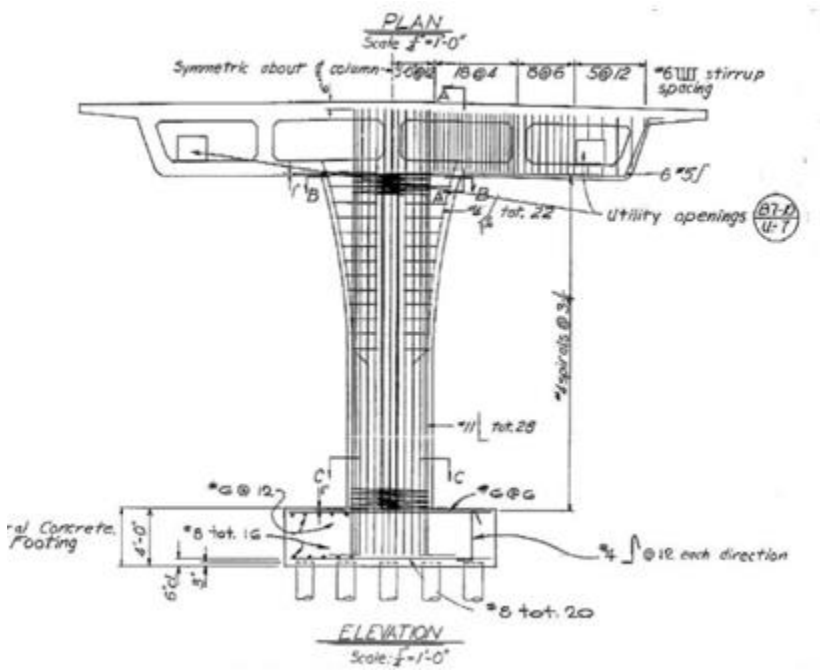 Caltrans (2017)

Table 6.7 – Design details for columns in Era 33 (post-1990).

Design details	Typical column reinforcement layout
Lateral seismic force Based on ATC-32. Capacity based design to ensure the ductile mode of failure. **Column shear reinforcement** Spacing: <6 times the longitudinal bar diameter. **Other notable features** • Usage of column flares was very minimal. • Tight confinement reinforcement was provided in the column plastic hinge zones. • Improvised flare details were provided by isolating the flare from the superstructure, i.e., a gap of 2–4 in. • No lap splices were provided in the plastic hinge zones. • Shear reinforcement was provided in the footing and pile caps. • Joint reinforcement was provided between the column and the bent cap, and the column and the footing.	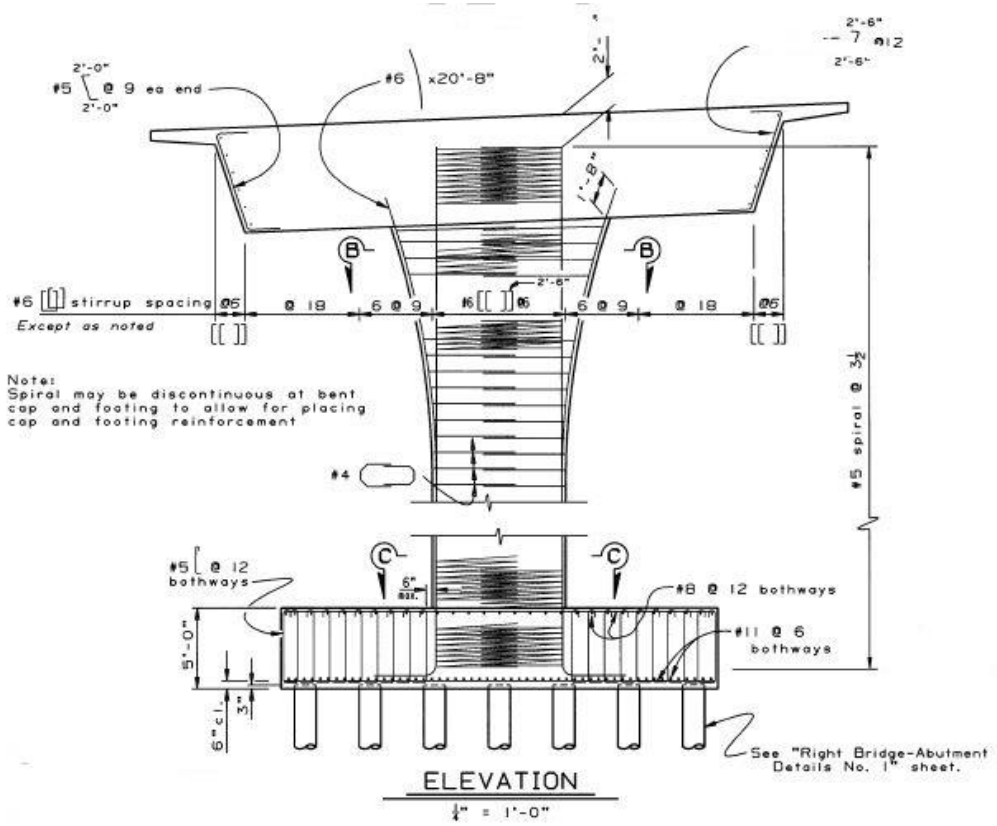 Caltrans (2017)

Table 6.8 – Summary of limit states for Era 11 columns.

Section properties								Displacement ductility				Curvature ductility				Reference
Column model	**Cross-section**	**Column diameter (in.)**	**Length * breadth (in.)**	**Column height (ft.)**	**Scale**	**Design code**	**Long. Steel ratio (%)**	**CCLS-0**	**CCLS--1**	**CCLS--2**	**CCLS--3**	**CCLS--0**	**CCLS--1**	**CCLS--2**	**CCLS--3**	
R-I	Rectangle	-	28.75 ×19.25	12.0	0.4	Caltrans	2.55	0.80	1.00	2.00	3.00	0.80	2.00	6.00	10.00	Sun et al. (1993)
R-5	Rectangle	-	28.75 × 19.25	12.0	0.4	Caltrans	5.00	0.80	2.00	3.00	4.00	0.80	2.50	3.50	6.00	
SRPH-6	Circular	24	-	7.0	0.4	Caltrans	5.4	0.80	1.00	1.50	2.00	0.80	1.00	1.54	2.56	Hose et al. (1997)
col #2	Circular	24	-	6.0	0.4	ACI	1.06	0.80	1.50	2.00	4.00	0.80	2.26	3.52	8.56	Priestley et al. (1996)
col-1	Circular	24	-	12	0.4	Caltrans	2.53	0.80	1.00	1.50	4.00	0.80	1.00	2.31	8.87	Chai et al. (1991)
col-3	Circular	24	-	12	0.4	Caltrans	2.53	1.00	1.50	3.00	5.00	1.00	2.31	6.25	11.49	
T1	Circular	10	-	3.33	0.28	Caltrans	2	0.80	2.00	3.00	5.00	0.80	2.93	4.85	8.71	Jaradat et al. (1998)
T2	Circular	10	-	3.33	0.28	Caltrans	1.1	0.80	2.00	4.00	5.00	0.80	2.93	6.78	8.71	
T3	Circular	10	-	3.33	0.28	Caltrans	2	0.80	2.00	3.00	4.00	0.80	2.93	4.85	6.78	
S1	Circular	10	-	5.83	0.28	Caltrans	2	0.80	1.00	1.50	2.00	0.80	1.00	2.33	3.65	
S2	Circular	10	-	5.83	0.28	Caltrans	1.1	0.80	2.00	3.00	5.00	0.80	3.65	6.31	11.62	
S3	Circular	10	-	5.83	0.28	Caltrans	1.1	1.00	2.00	3.00	4.00	1.00	3.65	6.31	8.96	
S1	Circular	20	-	5.0	0.33	Washington	0.99	0.8	1.82	5.04	8.27	0.8	2.48	8.28	14.10	Ranf et al. (2006)
S3	Circular	20	-	5.0	0.33	Washington	0.99	0.8	1.34	2.45	3.56	0.8	1.61	3.61	5.61	
S15	Circular	20	-	5.0	0.33	Washington	0.99	0.8	2.05	4.03	6	0.8	2.89	6.46	10.01	
C2	Circular	20	-	5.0	0.33	Washington	0.99	0.8	1.47	2.65	3.83	0.8	1.85	3.97	6.10	
C4	Circular	20	-	5.0	0.33	Washington	0.99	0.8	1.52	4.6	7.68	0.8	1.94	7.49	13.04	
C3R	Circular	20	-	5.0	0.33	Washington	0.99	0.8	1.32	3.51	5.7	0.8	1.58	5.52	9.47	

Table 6.9 – Summary of limit states for Era 22 columns.

Section properties								Displacement ductility				Curvature ductility				Reference
Column model	**Cross-section**	**Column diameter (in.)**	**Length * breadth (in.)**	**Column height (ft.)**	**Scale**	**Design code**	**Long. Steel ratio (%)**	**CCLS--0**	**CCLS--1**	**CCLS--2**	**CCLS--3**	**CCLS--0**	**CCLS--1**	**CCLS--2**	**CCLS--3**	
SRPH-1	Circular	24	-	-	0.4	Caltrans	2.7	0.77	1.00	6.00	8.00	0.77	2.77	7.00	9.26	Hose et al. (1997)
SRPH-2	Circular	24	-	-	0.4	Caltrans	5.4	0.72	1.50	3.00	4.50	0.72	1.60	4.15	7.80	
SRPH-3	Circular	24	-	-	0.4	Caltrans	5.4	0.69	2.50	5.00	7.30	0.69	3.10	5.80	9.23	
SRPH-7	Circular	24	-	-	0.4	Caltrans	5.4	0.75	2.00	4.00	6.00	0.75	1.60	4.56	7.32	
MG-2	Circular	28.8	-	8.8	0.4	Caltrans	2.0	0.86	2.3	2.88	3.45	0.86	4.48	6.04	7.57	Sanchez et al. (1997)
RDS-2	Oblong	-	24 ×36	13.0	0.4	Caltrans	2.0	2.0	6.0	8.0	10.0	3.75	14.77	20.28	25.79	
PEER-COL-1	Circular	16	-	6.0	0.33	Caltrans	1.17	1.3	5.08	4.16	5.55	1.75	11.27	8.95	12.46	Asad and Xiao (2005)
PEER-COL-3	Circular	16	-	6.0	0.33	Caltrans	1.17	1.11	2.80	4.17	5.55	1.277	5.534	8.984	12.46	
Flexure	Circular	60	-	30.0	1.0	Caltrans	2.0	1.0	3.00	5.00	6.60	3.87	6.74	12.49	17.08	Stone and Cheok (1989)
Shear	Circular	60	-	15.0	1.0	Caltrans	2.0	1.0	4.00	6.00	10.00	3.09	7.26	11.44	19.79	

Table 6.10 – Summary of limit states for Era 33 columns.

Section properties								Displacement ductility				Curvature ductility				Reference
Column model	**Cross-section**	**Column diameter (in.)**	**Length * breadth (in.)**	**Column height (ft.)**	**Scale**	**Design code**	**Long. Steel ratio (%)**	**CCLS--0**	**CCLS--1**	**CCLS--2**	**CCLS--3**	**CCLS--0**	**CCLS--1**	**CCLS--2**	**CCLS--3**	
328	Circular	24	-	6.0	0.5	Caltrans	2.72	1.40	3.51	4.91	9.12	2.07	7.64	11.36	22.51	Calderone et al. (2001)
328T	Circular	24	-	6.0	0.5	Caltrans	2.72	1.57	4.71	7.84	10.20	2.51	10.81	19.12	25.35	
828	Circular	24	-	16.0	0.5	Caltrans	2.72	1.26	4.41	4.41	7.77	1.91	12.90	12.90	24.63	
1028	Circular	24	-	20.0	0.5	Caltrans	2.72	1.81	5.81	6.46	9.04	3.94	18.47	20.82	30.19	
ISL 1.0	Oblong	-	12 × 17.5	4.83	0.2	Caltrans	2.00	0.8	1.5	5.6	9.6	0.50	2.24	12.40	22.31	Correal. et al. (2007)
ISL 1.5	Oblong	-	12 × 20.25	6	0.2	Caltrans	2.00	1.5	2.4	7.5	10.4	2.35	4.78	18.53	26.35	
ISH 1.0	Oblong	-	10 × 14.5	7.62	0.2	Caltrans	2.90	0.9	1.4	3.6	4.7	1.00	2.19	8.72	11.99	
ISH 1.25	Oblong	-	10 × 16.75	8.15	0.2	Caltrans	2.80	0.7	1.4	3.7	4.7	1.00	2.22	9.22	12.26	
ISH 1.5	Oblong	-	10 × 15.62	8.79	0.2	Caltrans	2.90	1	1.6	2.2	4.7	1.00	2.86	4.72	12.46	
ISH1.5T	Oblong	-	10 × 16.75	8.79	0.2	Caltrans	2.90	1.0	1.7	2.8	3.8	1.00	3.18	6.60	9.71	
415	Circular	24	-	8.0	0.33	Caltrans	1.5	1.0	2.7	5.0	8.0	1.00	5.04	10.59	17.78	Lehman and Moehle (2000)
407	Circular	24	-	8.0	0.33	Caltrans	0.75	1.0	2.5	3.0	6.0	1.00	4.60	5.80	12.99	
430	Circular	24	-	8.0	0.33	Caltrans	1.5	1.0	3.0	5.0	7.0	1.00	5.88	10.59	15.41	
815	Circular	24	-	8.0	0.33	Caltrans	1.5	1.0	2.0	3.0	5.0	1.00	3.47	5.94	10.89	
1015	Circular	24	-	8.0	0.33	Caltrans	1.5	1.0	2.0	3.0	5.0	1.00	3.47	5.94	10.89	
SRPH-4	Circular	24	-	7.0	0.4	Caltrans	5.4	1.00	2.50	8.00	-	1.00	2.00	14.60	-	Hose et al. (1997)
VP-2	Circular	16	-	6.0	0.4	Caltrans	1.17	1.0	3.4	7.0	8.3	1.00	5.10	10.80	13.85	Orozco et al. (1999)
RDS-1	Oblong	-	24 ´ 36	13	0.4	Caltrans	1.64	2.0	4.0	8.0	12.0	2.30	4.50	10.90	17.30	Sanchez et al. (1997)
RDS-6	Oblong	-	24 ´ 36	13	0.4	Caltrans	2.00	2.0	6.0	8.0	12.0	1.50	5.30	11.40	17.40	
H/D (6)	Circular	24	-	12.0	0.5	Caltrans	2.10	0.75	4.50	6.0	18.0	0.75	8.71	12.01	38.43	Shanmugam (2009)
H/D (3)	Circular	24	-	6.0	0.5	Caltrans	2.10	0.75	4.33	13.75	17.0	0.75	5.03	16.42	20.36	

Table 6.11 presents the summary of the ductility values for various design eras. Column curvature ductility (μ_ϕ) is chosen as the EDP for columns and the median values for various design eras are highlighted in Table 6.11.

Table 6.11– Statistical summary of ductility values for various design eras.

Design era	No. of experiments	Properties	**Displacement ductility**				**Curvature ductility**			
			CCLS-0	CCLS-1	CCLS-2	CCLS-3	CCLS-0	CCLS-1	CCLS-2	CCLS-3
Era 11	18	Mean	0.82	1.58	2.93	4.56	0.82	2.25	4.99	8.57
		Median	0.80	1.51	3.00	4.00	**0.80**	**2.30**	**5.20**	**8.80**
		lower bound	0.80	1.00	1.50	2.00	0.80	1.00	1.54	2.56
		upper bound	1.00	2.05	5.04	8.27	1.00	3.65	8.28	14.10
Era 22	9	Mean	1.02	3.02	4.65	6.29	1.32	5.64	8.22	11.49
		Median	1.00	2.65	4.59	6.30	**1.00**	**5.00**	**8.00**	**11.00**
		Lower bound	0.69	1.00	2.88	3.45	0.69	1.60	4.15	7.32
		Upper bound	2.00	6.00	8.00	10.00	3.75	14.77	20.28	25.79
Era 33	21	Mean	1.20	2.98	5.45	7.86	1.45	5.63	11.73	18.05
		Median	1.00	2.68	5.00	8.13	**1.00**	**5.00**	**11.00**	**17.50**
		lower bound	0.70	1.40	2.20	3.80	0.50	2.00	4.72	9.71
		upper bound	2.00	6.00	10.00	12.00	3.94	18.47	23.67	30.19

6.1.3 Abutments

In addition to columns, seat is also considered a primary component in the current study to account for the unseating potential. Bridge seat widths chronologically increased from the 4 – 12 inch range in Era 11, to the 12 – 24 inch range in Era 22, to greater than 24 inches in Era 33. Table 6.12 gives the median CDT values for abutment seats for various

design eras. The values were developed based on previous studies (Ramanathan, 2012) and discussion with Caltrans engineers.

Table 6.12– Median value of CDT for abutment seat.

Design era	Units	CDT-0	CDT-1	CDT-2	CDT-3
Era 11	Inches	0.5	1.0	2.0	3.0
Era 22	Inches	1.0	4.5	10.0	15.0
Era 33	Inches	1.5	4.5	14.0	21.0

The CDT values for other components such as superstructure deck, abutment displacement in the passive, active, and transverse directions, foundation displacements, shear keys, and joint seals are consistent with previous research conducted by Ramanathan (2012). Interested readers are directed to Ramanathan (2012) for a more detailed explanation of the CDT values of these components. Table 6.13 provides the summary values of the CDT and CCLS value for various bridge components. The capacity models are described by a two-parameter lognormal distribution with median, S_c and dispersion, β_c. β_c is assigned as 0.35 in a subjective manner due to lack of sufficient information and is adopted as the same across the components and the respective damage states.

Table 6.13– Summary of CDT values for various bridge components.

Components	EDP	Units	Median value, S_c				β_c
			CDT-0	CDT-1	CDT-2	CDT-2	
Primary Components							
Columns							
Era 11	Curvature ductility	NA	0.8	2.0	5.0	8.0	0.35
Era 22	Curvature ductility	NA	1.0	5.0	8.0	11.0	0.35
Era 33	Curvature ductility	NA	1.0	5.0	11.0	17.0	0.35
Abutment seat							
Era 11	Displacement	Inches	0.5	1.0	2.0	3.0	0.35
Era 22	Displacement	Inches	1.0	4.5	10.0	15.0	0.35
Era 33	Displacement	Inches	1.5	4.5	14.0	21.0	0.35
Secondary Components							
Joint Seal	Displacement	Inches	2.0	5.0	NA	NA	0.35
Bearings	Displacement	Inches	1.0	4.0	NA	NA	0.35
Shear keys	Displacement	Inches	1.0	5.0	NA	NA	0.35
Deck	Displacement	Inches	4.0	12.0	NA	NA	0.35
Bent foundation							
Translation	Displacement	Inches	1.0	4.0	NA	NA	0.35
Rotation	Rotation	Radian	1.5	6.0	NA	NA	0.35
Abutments							
Passive	Displacement	Inches	3.0	10.0	NA	NA	0.35
Active	Displacement	Inches	1.5	4.0	NA	NA	0.35
Transverse	Displacement	Inches	1.0	4.0	NA	NA	0.35

6.2 Fragility methodology

The probability that the seismic demands (*D*) placed on a component exceed the capacity (*C*) conditioned on a chosen intensity measure (*IM*) can be assessed by a fragility function. Assuming a lognormal distribution for the *D* and *C*, component fragility curves, defined here as the probability of reaching or exceeding a specified damage state for a particular component, are estimated as

$$P[D > C / IM] = \Phi\left[\frac{\ln(S_d / S_c)}{\sqrt{\beta_{d/IM}^2 + \beta_c^2}}\right] \quad (6.3)$$

where, S_d is the median estimate of the demand as a function of the *IM*, S_c is the median estimate of the capacity, $\beta_{d/IM}$ is the dispersion of the demand conditioned on the *IM*, β_c is the dispersion of the capacity, and $\Phi(\bullet)$ is the standard normal cumulative distribution function. As presented in equation 6.3, a component fragility curve is computed through a convolution of a PSDM and a limit state model. A set of component fragility curves computed in equation 6.3 has to be integrated into a system fragility (or bridge fragility), which is facilitated through the development of joint probabilistic seismic demand models (JPSDMs) (Nielson 2005, Padgett 2007, Ramanathan et al. 2015, Jeon et al. 2015). The JPSDM recognizes the correlation between various components. If the vector demands, X_i, placed on the *n* components of the system are expressed as $\underline{X} = (X_1, X_2, ..., X_n)$, then the vector, $\underline{Y} = \ln(\underline{X})$ represents the vector of component demands in the log-transformed space. The JSPDM is formulated in this space by assembling the vector of means $\mu_{\underline{Y}}$ and the covariance matrix, $\sigma_{\underline{Y}}$. A Monte Carlo simulation (10^6 in the current study) in which samples are drawn from both the demand and capacity models is used to estimate the probability of demand exceeding the capacity value for each *IM*. This procedure is repeated for the increasing value of the *IM*, and regression analysis is used afterwards to estimate the lognormal parameters, median, and dispersion, which characterize the bridge fragility. The system fragilities are helpful to measure the correlation between various bridge components and determine which component is dominating the overall system vulnerability. The system or bridge fragilities are useful for risk assessment on a regional level, where it would be computationally burdensome to calculate the probability of failure of each bridge component, and then combine them to form the probability of failure of the system. Moreover, it is found that using the fragility

of any single bridge component to represent the overall vulnerability of the bridge would likely result in a significant underestimation of that vulnerability (Nielson 2007). Figure 6.3 shows a schematic of the fragility framework adopted in the current study.

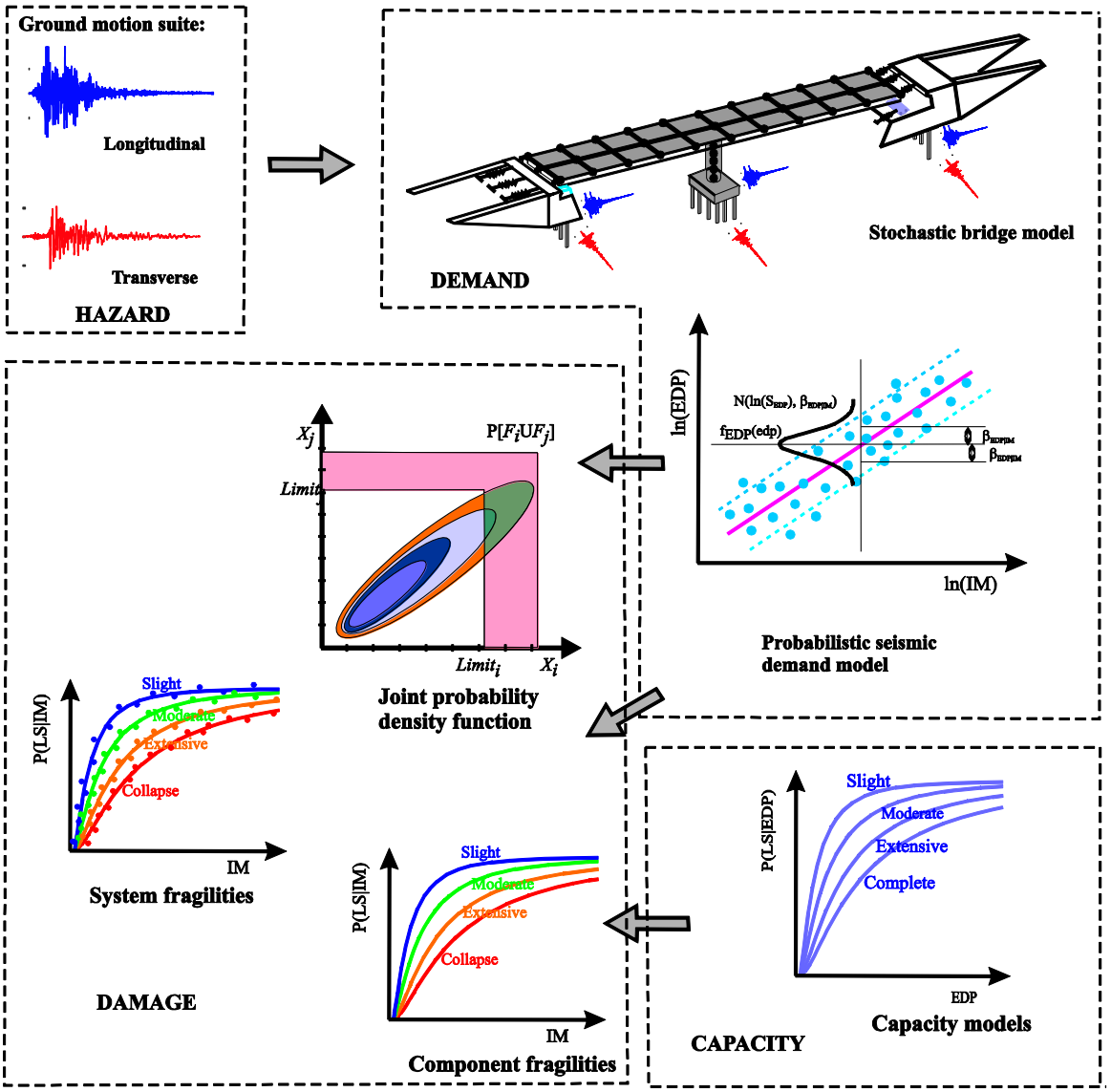

Figure 6.3 – Schematic of the fragility framework.

The input for the fragility framework is presented in the following section.

6.2.1 Ground motion suite

It is important to have a wide range of ground motions with a large variation of peak ground accelerations to ensure the evaluation of a sufficient range of bridge responses. The current study utilizes the ground motions from the NGA-2 database assembled by Caltrans (2017). These motions were developed specifically for this project and consist of 320 ground motions. The ground motion details are given in Appendix A, and the response spectra for the ground motions are presented in Figure 6.4. The work of Ramanathan (2012) indicated that spectral acceleration at 1.0 sec ($S_{a\text{-}1.0s}$) is the optimal intensity measure for the class of concrete box-girder bridges. Based on this observation, the current study selected $S_{a\text{-}1.0s}$ as the IM.

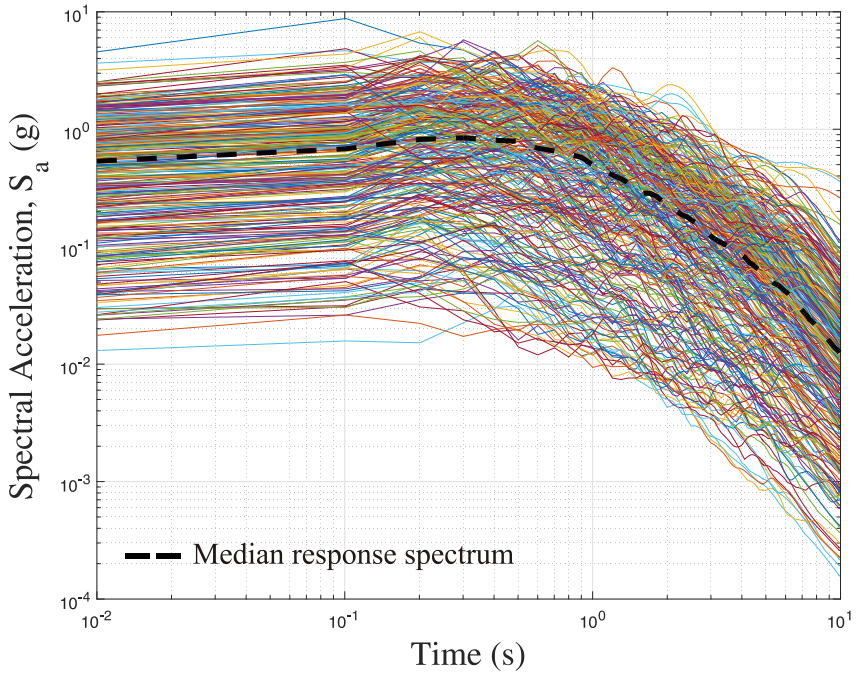

Figure 6.4 – Response spectra for the selected ground motions.

6.2.2 Material and geometric uncertainties and parameterized stochastic bridge models

Geometric and material uncertainties considered in the current study are discussed in detail in Chapter 5. As mentioned before, most of the parameters were chosen based on the plan review of more than 1,000 bridges, using in-house database obtained from Caltrans. Having identified all key modeling assumptions and the uncertainty distribution of the bridge models, the next step was to develop representative bridge models that could capture the entire range of material and geometric uncertainties. Statistically significant yet nominally identical three-dimensional bridge models were generated by sampling across the range of parameters using Latin Hypercube Sampling technique, and were then paired randomly with the selected suite of ground motions. 320 analytical bridge models were generated, consistent with the number of ground motions. These were then paired randomly to create the bridge model-ground motion pair. NLTHA was performed on each case and the peak component demands are noted for each. The responses from the NLTHA were used to generate the PSDMs. The PSDMs were then convolved with capacity models to generate the fragility curves.

6.3 Fragility curves for multi-span continuous concrete single frame box-girder bridges

The intent of this research is to generate fragility curves for multi-span continuous concrete box-girder (MSCC-BG) bridge classes in California in order to identify the relative vulnerabilities of various bridge groupings. Some nomenclatures were adopted for this study and are detailed in Table 6.14. For example, S-E1-S22-R-D corresponds to single-column bent (S) in design era Era11 (E1) with two spans (S22), rectangular cross-sections, (R) and diaphragm abutments (D).

One simple technique to evaluate the differences in fragility curves is to evaluate the relative change in the median value of the fragility curves. An increase in the median value means a less vulnerable structure, while a decrease in the median value indicates a more vulnerable structure, and is illustrated in Figure 6.5. In Figure 6.5, bridge 2 is less vulnerable than bridge 1 for the limit state BSST-3.

Table 6.14 – Nomenclature adopted in the current study.

Design attributes	Nomenclature
Bent type	
Single column bent	S
Two column bent	T
Multi column bent	M
Design era	
Era 11 (pre 1970)	E1
Era 22 (1971-1990)	E2
Era 33 (post 1990)	E3
Span range	
Two span	S22
Three-four span	S34
Column cross-section	
Rectangle	R
Circular	C
Oblong	O
Abutment type	
Diaphragm	D
Seat	S

Fragility curves were generated for the 72 single frame box-girder bridge classes and are presented in Table 6.15 - 6.18. These classifications cover more than 75% of the California box-girder bridge inventory. Tables 6.15 – 6.18 also give the dispersion, ζ, a single value of dispersion characterizing the fragility across the four limit states. Appendix B documents the fragility values in terms of PGA. The system and component fragility curves for two bridge classes, S-E1-S22-C-D and S-E2-S22-C-S, are presented in Figure 6.6. It is seen from Figure 6.6 that the column is the most vulnerable component for bridges

with diaphragm abutments. In the case of bridges with seat abutments, columns and bearing each contribute to the system vulnerability. The median and dispersion values for the component fragility curves for the bridge classes are documented in Appendix C.

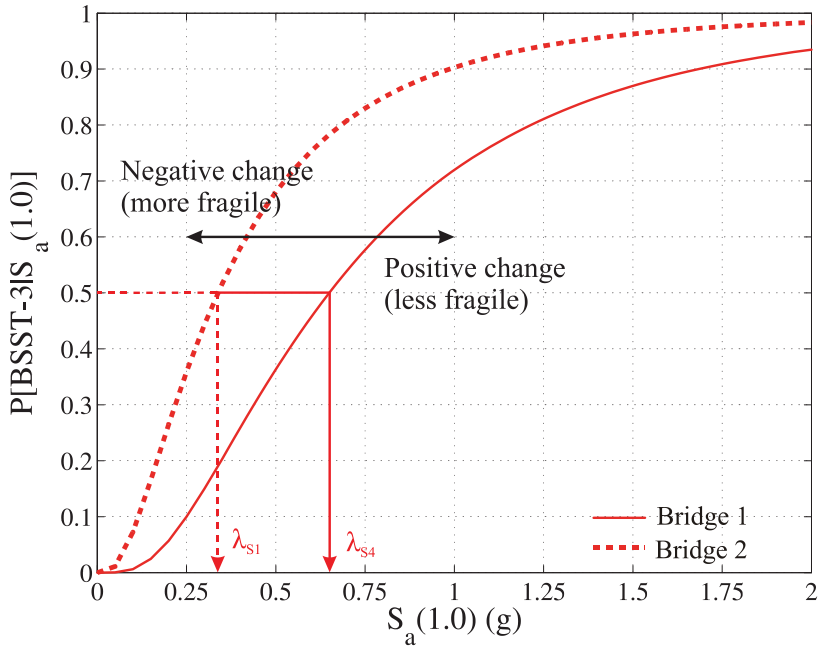

Figure 6.5 – Illustration of change in median value and relative vulnerability.

Table 6.15 – Fragility values for two span continuous concrete box-girder fragilities with diaphragm abutments.

Design era	Bridge class	BSST-0		BSST-0		BSST-0		BSST-0		ζ^*
		λ	ζ	λ	ζ	λ	ζ	λ	ζ	
Era 11	S-E1-S22-C-D	0.12	0.60	0.30	0.61	0.70	0.63	1.06	0.62	0.61
	S-E1-S22-R-D	0.17	0.63	0.41	0.64	0.82	0.65	1.18	0.66	0.65
	T-E1-S22-C-D	0.08	0.63	0.20	0.66	0.47	0.71	0.72	0.70	0.68
	T-E1-S22-R-D	0.10	0.69	0.21	0.73	0.43	0.75	0.62	0.76	0.73
	M-E1-S22-C-D	0.07	0.82	0.17	0.87	0.44	1.11	0.69	1.11	0.98
	M-E1-S22-R-D	0.06	0.88	0.15	1.06	0.41	1.36	0.69	1.36	1.17
Era 22	S-E2-S22-C-D	0.15	0.68	0.63	0.68	1.45	0.69	1.93	0.69	0.68
	S-E2-S22-O-D	0.16	0.64	0.71	0.64	2.36	0.73	3.07	0.65	0.67
	T-E2-S22-C-D	0.11	0.62	0.42	0.61	0.97	0.66	1.27	0.66	0.63
	T-E2-S22-O-D	0.15	0.58	0.55	0.57	1.17	0.57	1.47	0.57	0.57
	M-E2-S22-C-D	0.10	0.61	0.33	0.60	0.67	0.74	0.86	0.74	0.68
	M-E2-S22-O-D	0.10	0.61	0.33	0.60	0.67	0.74	0.86	0.74	0.68
Era 33	S-E3-S22-C-D	0.15	0.68	0.63	0.68	1.91	0.70	2.86	0.72	0.69
	S-E3-S22-O-D	0.16	0.64	0.71	0.64	3.10	0.67	4.39	0.63	0.65
	T-E3-S22-C-D	0.11	0.62	0.41	0.61	1.27	0.66	1.84	0.66	0.64
	T-E3-S22-O-D	0.15	0.58	0.55	0.57	1.49	0.57	2.06	0.58	0.57
	M-E3-S22-C-D	0.10	0.63	0.33	0.60	0.86	0.75	1.20	0.74	0.68
	M-E3-S22-O-D	0.10	0.63	0.33	0.60	0.86	0.75	1.20	0.74	0.68

Table 6.16 – Fragility values for two span continuous concrete box-girder fragilities with seat abutments.

Design era	Bridge class	BSST-0		BSST-0		BSST-0		BSST-0		ζ^*
		λ	ζ	λ	ζ	λ	ζ	λ	ζ	
Era 11	S-E1-S22-C-S	0.08	0.61	0.15	0.59	0.29	0.58	0.42	0.58	0.59
	S-E1-S22-R-S	0.08	0.52	0.15	0.54	0.27	0.53	0.38	0.52	0.53
	T-E1-S22-C-S	0.06	0.57	0.11	0.60	0.21	0.59	0.30	0.59	0.59
	T-E1-S22-R-S	0.08	0.57	0.14	0.57	0.25	0.57	0.35	0.55	0.57
	M-E1-S22-C-S	0.04	0.63	0.08	0.62	0.18	0.60	0.26	0.60	0.61
	M-E1-S22-R-S	0.09	0.58	0.15	0.58	0.27	0.58	0.37	0.58	0.58
Era 22	S-E2-S22-C-S	0.11	0.58	0.53	0.57	0.99	0.65	1.32	0.65	0.61
	S-E2-S22-O-S	0.11	0.51	0.53	0.49	1.14	0.55	1.58	0.55	0.52
	T-E2-S22-C-S	0.08	0.51	0.38	0.49	0.77	0.55	1.08	0.56	0.53
	T-E2-S22-O-S	0.08	0.45	0.37	0.44	0.80	0.55	1.10	0.56	0.50
	M-E2-S22-C-S	0.07	0.49	0.36	0.48	0.73	0.59	1.02	0.62	0.54
	M-E2-S22-O-S	0.08	0.54	0.42	0.51	0.91	0.66	1.30	0.67	0.60
Era 33	S-E3-S22-C-S	0.11	0.57	0.53	0.56	1.25	0.63	1.88	0.63	0.60
	S-E3-S22-O-S	0.12	0.50	0.53	0.49	1.28	0.53	1.91	0.53	0.51
	T-E3-S22-C-S	0.08	0.51	0.38	0.50	0.94	0.53	1.41	0.54	0.52
	T-E3-S22-O-S	0.08	0.45	0.37	0.43	0.91	0.52	1.32	0.50	0.48
	M-E3-S22-C-S	0.07	0.49	0.36	0.49	0.89	0.58	1.35	0.58	0.53
	M-E3-S22-O-S	0.08	0.54	0.42	0.52	1.07	0.60	1.64	0.61	0.56

Table 6.17 – Fragility values for multi-span continuous concrete box-girder fragilities with diaphragm abutments.

Design era	Bridge class	BSST-0		BSST-0		BSST-0		BSST-0		ζ^*
		λ	ζ	λ	ζ	λ	ζ	λ	ζ	
Era 11	S-E1-S34-C-D	0.12	0.61	0.33	0.65	0.83	0.70	1.33	0.69	0.66
	S-E1-S34-R-D	0.06	0.89	0.25	1.11	1.00	1.32	2.04	1.31	1.16
	T-E1-S34-C-D	0.06	0.72	0.15	0.77	0.36	0.89	0.56	0.89	0.82
	T-E1-S34-R-D	0.07	0.75	0.17	0.79	0.41	0.91	0.66	0.92	0.84
	M-E1-S34-C-D	0.01	1.04	0.04	0.98	0.19	1.13	0.40	1.13	1.07
	M-E1-S34-R-D	0.01	1.04	0.04	0.98	0.19	1.13	0.40	1.13	1.07
Era 22	S-E2-S34-C-D	0.15	0.56	0.59	0.54	1.34	0.71	1.79	0.71	0.63
	S-E2-S34-O-D	0.19	0.67	0.93	0.66	3.04	0.93	4.26	0.87	0.78
	T-E2-S34-C-D	0.09	0.62	0.39	0.59	0.82	0.89	1.12	0.89	0.75
	T-E2-S34-O-D	0.11	0.71	0.56	0.73	1.79	1.12	2.64	1.16	0.93
	M-E2-S34-C-D	0.09	0.54	0.35	0.50	0.68	0.71	0.93	0.71	0.61
	M-E2-S34-O-D	0.03	0.82	0.47	0.73	2.00	1.59	4.00	1.66	1.20
Era 33	S-E3-S34-C-D	0.15	0.55	0.58	0.54	1.78	0.71	2.63	0.69	0.62
	S-E3-S34-O-D	0.20	0.67	0.93	0.66	4.47	0.94	6.44	0.82	0.77
	T-E3-S34-C-D	0.09	0.62	0.39	0.60	1.12	0.89	1.72	0.89	0.75
	T-E3-S34-O-D	0.11	0.73	0.56	0.73	2.59	1.12	4.34	1.12	0.93
	M-E3-S34-C-D	0.08	0.54	0.35	0.50	0.92	0.70	1.40	0.71	0.61
	M-E3-S34-O-D	0.03	0.86	0.47	0.74	3.74	1.47	9.02	1.50	1.14

Table 6.18 – Fragility values for multi-span continuous concrete box-girder fragilities with seat abutments.

Design era	Bridge class	BSST-0		BSST-0		BSST-0		BSST-0		ζ^*
		λ	ζ	λ	ζ	λ	ζ	λ	ζ	
Era 11	S-E1-S34-C-S	0.10	0.50	0.20	0.49	0.38	0.49	0.54	0.49	0.49
	S-E1-S34-R-S	0.05	0.64	0.13	0.61	0.29	0.58	0.44	0.56	0.60
	T-E1-S34-C-S	0.05	0.62	0.11	0.62	0.22	0.60	0.31	0.59	0.61
	T-E1-S34-R-S	0.02	0.77	0.07	0.73	0.20	0.67	0.31	0.65	0.70
	M-E1-S34-C-S	0.01	1.15	0.02	0.99	0.11	0.82	0.22	0.81	0.94
	M-E1-S34-R-S	0.01	1.15	0.02	0.99	0.11	0.82	0.22	0.81	0.94
Era 22	S-E2-S34-C-S	0.10	0.66	0.52	0.65	0.96	0.80	1.34	0.81	0.73
	S-E2-S34-O-S	0.11	0.62	0.65	0.66	1.52	0.85	2.27	0.90	0.76
	T-E2-S34-C-S	0.03	0.75	0.28	0.66	0.63	1.11	1.02	1.20	0.93
	T-E2-S34-O-S	0.05	0.67	0.39	0.63	1.02	0.88	1.64	0.88	0.77
	M-E2-S34-C-S	0.07	0.66	0.32	0.66	0.57	0.88	0.79	0.92	0.78
	M-E2-S34-O-S	0.01	1.06	0.28	0.72	0.78	0.94	1.43	0.90	0.90
Era 33	S-E3-S34-C-S	0.10	0.65	0.52	0.65	1.30	0.77	2.05	0.77	0.71
	S-E3-S34-O-S	0.11	0.63	0.65	0.66	1.82	0.76	2.87	0.79	0.71
	T-E3-S34-C-S	0.03	0.72	0.28	0.66	0.88	1.02	1.56	0.98	0.84
	T-E3-S34-O-S	0.05	0.67	0.40	0.63	1.26	0.76	2.06	0.69	0.69
	M-E3-S34-C-S	0.07	0.66	0.32	0.66	0.76	0.85	1.18	0.87	0.76
	M-E3-S34-O-S	0.01	1.01	0.28	0.72	1.13	0.78	1.93	0.69	0.80

S-E1-S22-C-D

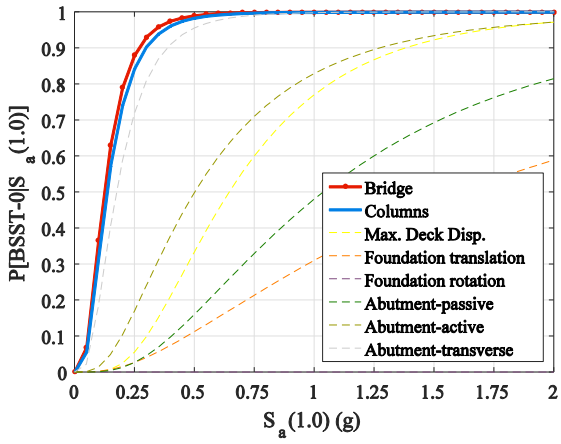

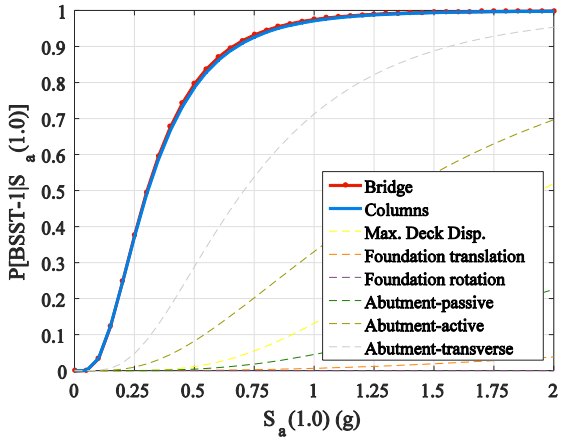

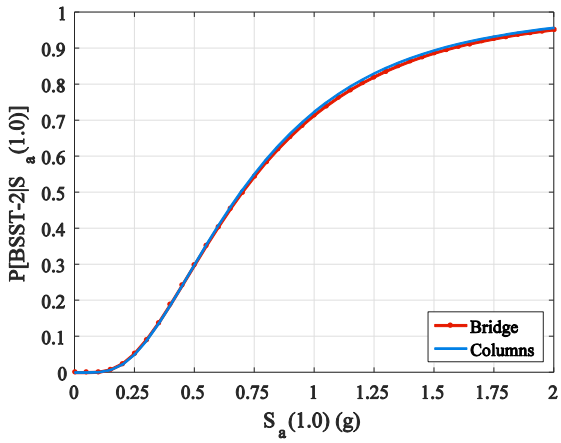

S-E2-S22-C-S

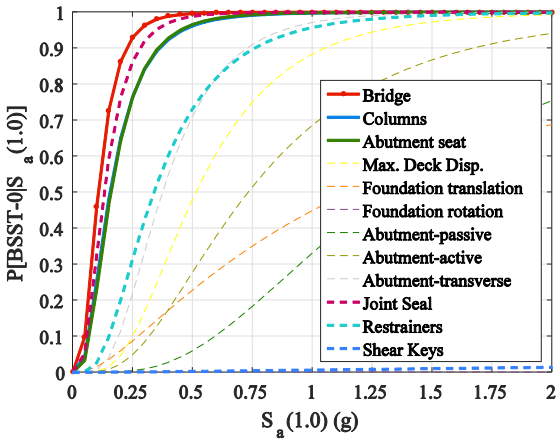

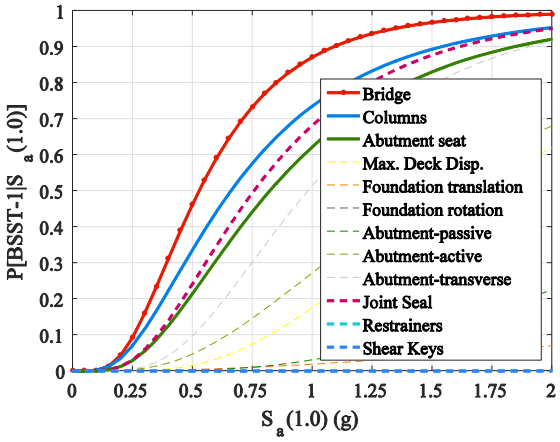

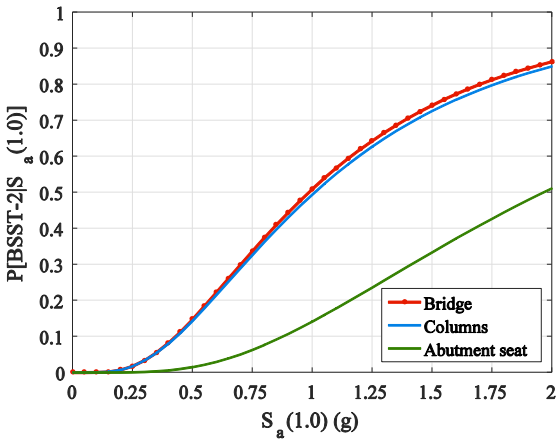

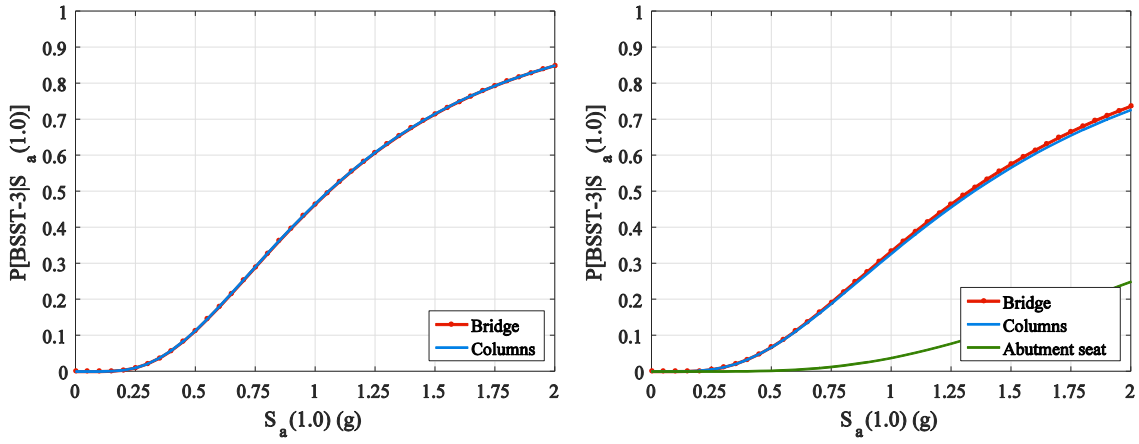

Figure 6.6 – System and component fragility curves for bridge classes S-E1-S22-C-D and S-E2-S22-C-S.

6.3.1 Trends based on design era

The plot of the median value of bridge fragility curves for two bridge classes, S-E-S22-C-D and T-E-S34-C-S is presented in Figure 6.7, and the trend is similar across the different bridge classes. The following are the salient inferences noted from bridge fragilities across the design eras:

- In general, Era 11 bridges are more vulnerable than Era 22 and Era 33 bridges. This trend is valid irrespective of the type of abutments, cross-section, and number of columns per bent.
- Era 22 bridges are more vulnerable than Era 33 bridges. The lower vulnerability of Era 33 is due to the high ductility that is associated with Era 33 bridge columns. This highlights the importance of seismic design detailing.
- Across the design eras for a particular abutment type, it is seen that single column bents are more vulnerable than the multi-column bents. This trend is consistent with a previous study (Mangalathu et al. 2016a). Amongst the bridges with multi-column bents, two-column bents are the least vulnerable.

- In general, diaphragm abutment bridges are less vulnerable than seat abutment bridges for all design eras. The lower vulnerability of the diaphragm abutment bridges might be attributed to the complete engagement of the superstructure and the abutments in the load transfer mechanism.

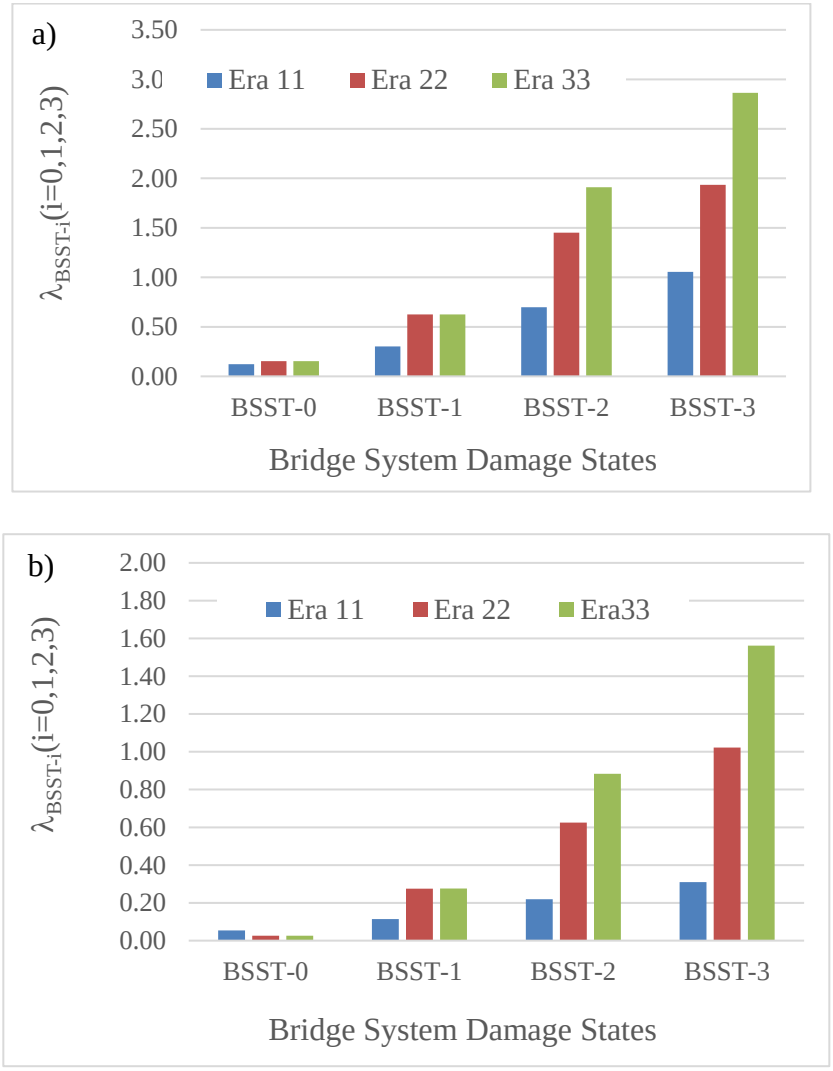

Figure 6.7 – Plot of median values of bridge classes across the design eras for a) S-E(1/2/3)-S22-C-D, and b) T-E(1/2/3)-S34-C-S.

6.3.2 Trends based on spans

The variation of the median value of fragility curves for bridge classes with number of spans is presented in Figure 6.8. The following inferences can be made from the data presented in Tables 6.15 – 6.18 and Figure 6.8:

- The relative vulnerability between the bridge classes with different spans depends on the column cross-section, abutment type, design era, and number of columns per bent. For example, it is seen in Figure 6.8 that the multi-span Era 22 bridge class with circular cross-section resting on diaphragm abutments (S-E2-S34-C-D) is more vulnerable than its two-span counterpart S-E2-S22-C-D for all limit states. The percentage change in median values between two-span and multi-span bridges are 1%, 7%, 8%, and 8% for BSST-0, -1, -2, and -3 respectively. However, the trend is different for the Era 22 bridge class with oblong cross-section resting on diaphragm abutments. In this case, multi-span bridges are less vulnerable than two-span bridges, and the relative vulnerabilities of two-span bridges (S-E2-S22-O-D) compared to multi span bridges (S-E2-S34-O-D) are 19%, 32%, 29%, and 39% for BSST-0, -1, -2, and -3 respectively.
- The differences in vulnerabilities for two-span and multi-span bridges underscore the necessity to account for the number of spans in the generation of fragility curves, which is not currently captured by the existing HAZUS classifications. It also substantiates the performance-based grouping of the bridge classes suggested in Chapter 4.

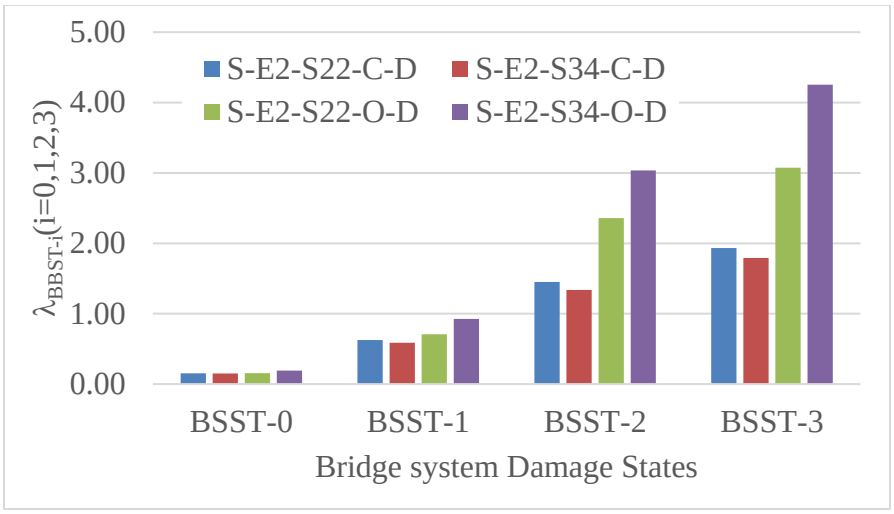

Figure 6.8 – Plot of median values of bridge classes across the number of spans for bridge classes S-E2-S(22/34)-C-D and S-E2-S(22/34)-O-D.

6.3.3 Trends based on abutment type

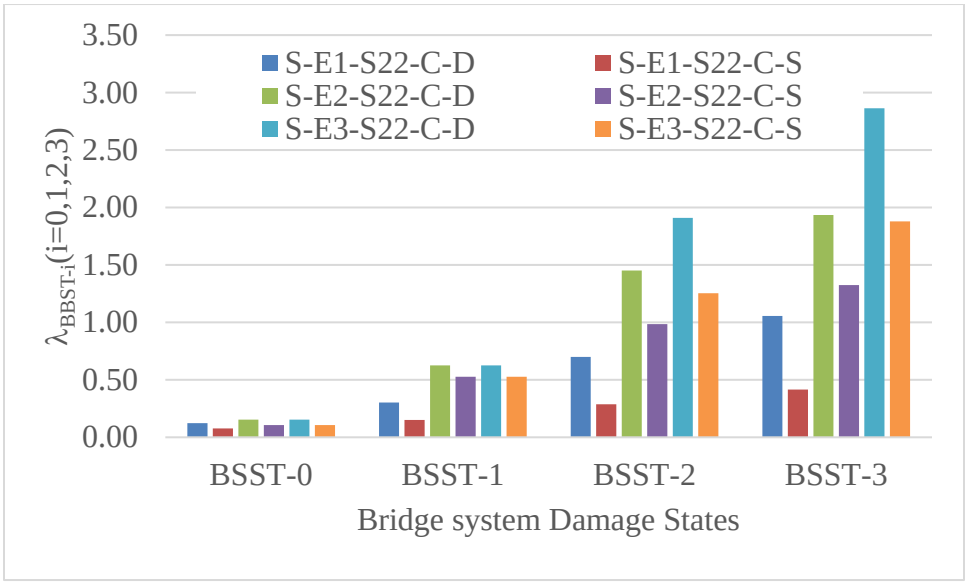

Figure 6.9 – Plot of median values of bridge classes across the type of abutments for the selected bridge classes.

The following inferences can be deduced from the comparison of fragilities for bridge classes with various abutment types:

- For all design eras, diaphragm abutment bridges are less vulnerable than seat abutment bridges. A general trend is shown in Figure 6.9 for selected bridge classes. The lower vulnerability of the diaphragm abutment bridges might be attributed to the complete engagement of the superstructure and the abutments in the load transfer mechanism.
- The columns are the most vulnerable component of bridges with diaphragm abutments. However, in the case of seat abutment bridges, bearings as well as columns contribute to the overall vulnerability. This highlights the need for adequate seat width in the case of bridges with seat abutments.
- The vulnerability of bridges reduces with the evolution of column design philosophy. The trend is the same irrespective of the type of cross-section and number of columns per bent.
- HAZUS suggests the same fragility relationships for bridges with seat and diaphragm abutments. The fragility curves generated in the current study outline the need to account for the type of abutments. For example, the bridge class with seat abutment (S-E3-S22-C-S) is 36%, 19%, 53% and 53% more vulnerable than the bridge class with diaphragm abutment (S-E3-S22-C-D) for the limit states BSST-0, -1, -2, and -3, respectively. Note that the only difference between the bridge class S-E3-S22-C-S and S-E3-S22-C-D is the type of abutments.

6.3.4 Trends based on column cross-section

As mentioned in Chapter 5, Era 11 bridges consist of circular and rectangular column cross-sections, while Eras 22 and 33 utilize circular and oblong cross-sections. The

following inferences are noted from the comparison of median fragilities for bridges classes (Tables 6.15 – 6.18, and Figure 6.10) with various cross-sections:

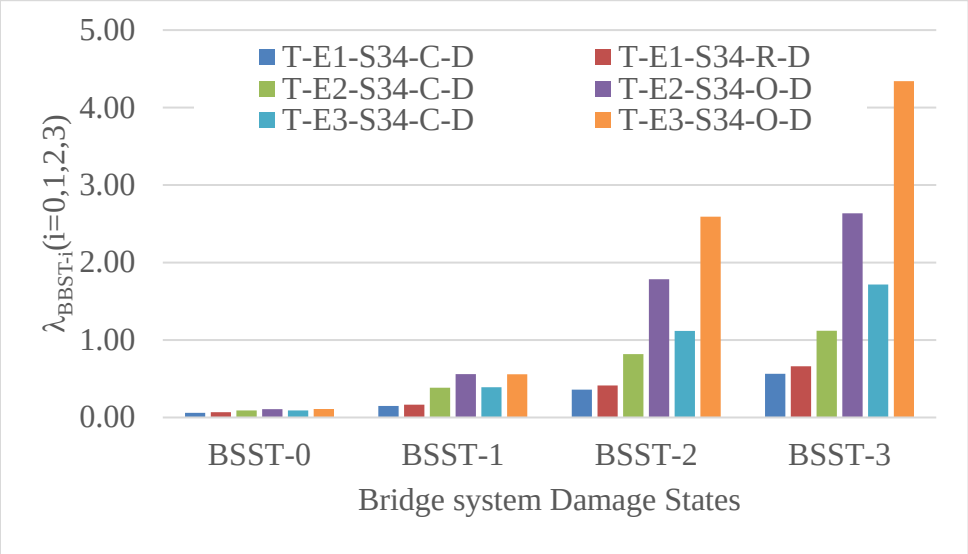

Figure 6.10 – Plot of median values of bridge classes across various column cross-sections for the selected bridge classes.

- In the case of bridges from Eras 22 and 33, columns with oblong cross-sections are less vulnerable than columns with circular cross-sections. This trend is the same irrespective of the type of abutment and number of columns per bent.
- No general trend is observed in the case of Era 11 bridges. For example, bridges with rectangular cross-sections performed better in the case of two-span bridges with single column bent and multi-column bent bridges with diaphragm abutments. However, the trend is reversed in the case of two-span bridges with two-column bents resting on diaphragm abutments. Also, there is no trend observed in the case of bridges resting on seat abutments.

6.3.5 Trends based on number of columns per bent

The general trend of the change in the median value of the fragility curves is presented in. The following inferences can be drawn from the comparison of the median values of fragility curves:

- Multi-column bents are more vulnerable than bridges with single column bents. The increased vulnerability of bridges with multi-column bents is mainly due to the bridge width and modeling assumptions, as a significant portion of multi-column bents are pinned at the base, while single-column bents have a significant amount of rotational restraint (see Chapter 5).
- For a given design era and number of spans, multi-column bents with circular cross-section are more vulnerable. For example, M-E2-S34-C-D is 34%, 194%, and 331% more vulnerable than M-E2-S34-O-D for the limit states BSST -1, -2, and -3, respectively. BSST-0 for the two bridge classes is significantly low.
- It is seen that the vulnerability of single, two-column, and multi-column bridges decreases with the evolution is seismic design philosophy. Also, there in a tremendous reduction in the vulnerability of bridges from Eras 22 and 33, compared to their Era 11 counterparts.
- Further, the differences in the median value of bridge classes with different numbers of columns per bent underscore the necessity to capture the number of columns per bent in the fragility curves. Such a classification is not currently available in HAZUS.

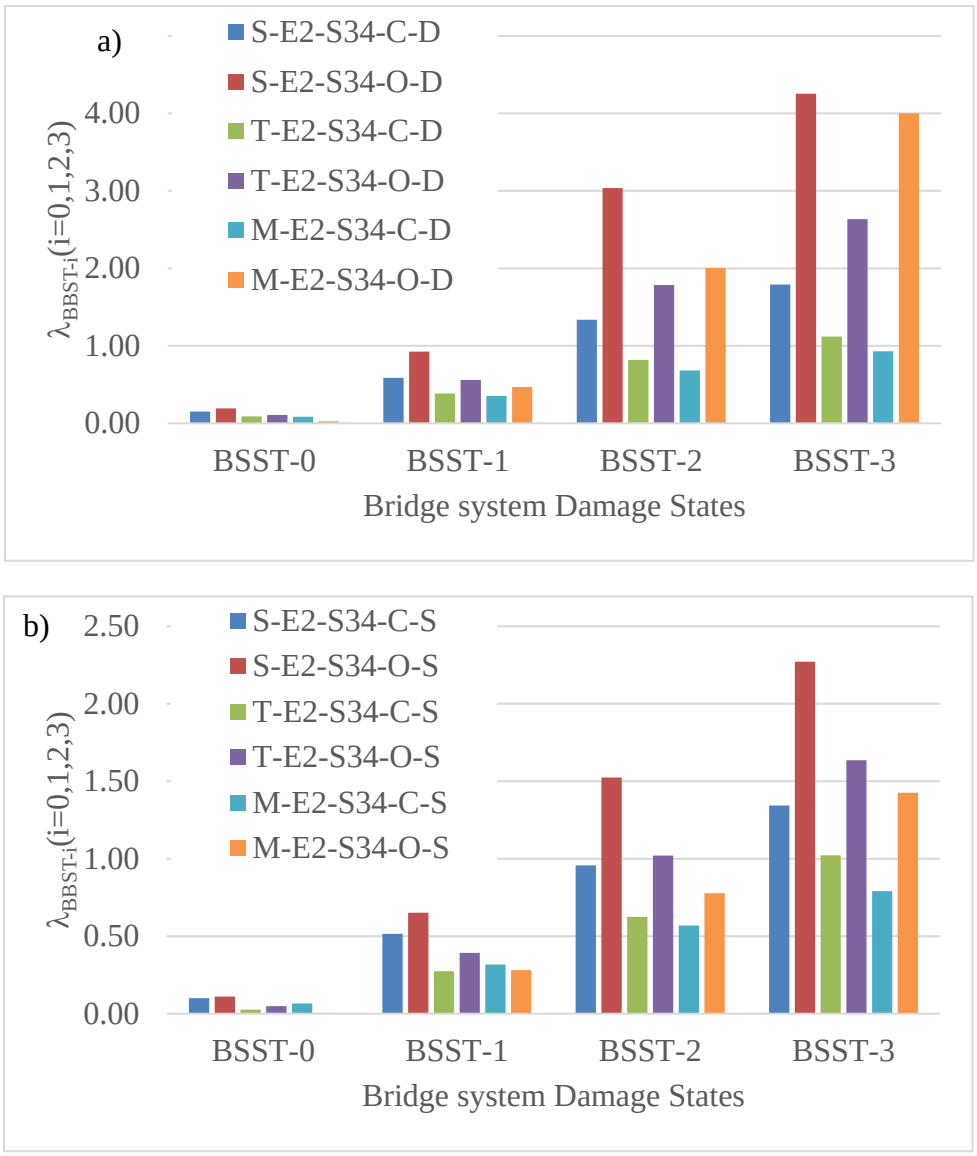

Figure 6.11 – Plot of median values of bridge classes across the number of columns per bent for the selected bridge classes with a) diaphragm abutments and b) seat abutments.

6.4 HAZUS comparison

A detailed discussion on the classification, assumptions, and methodologies of the HAZUS fragilities is given in Chapter 2. HAZUS utilized a subjective classification of bridges based on seismic design, span length, bent type, and span discontinuity. However,

the current study utilized a performance-based grouping strategy. HAZUS failed to consider the variability of geometric and material attributes, which this study incorporated. Despite the differences between the present study and HAZUS, S_a (1.0s) is adopted as the intensity measure in both cases. Also the number of damage states characterizing the bridge system vulnerability is similar in both studies. Table 6.19 presents the median values of HAZUS fragility curves corresponding to slight (λ_s), moderate (λ_m), extensive (λ_e), and complete (λ_c) damage states. HAZUS suggests a single value of dispersion (β_{ds}) across all bridge classes and damage states. The equivalent bridge class notations between HAZUS and the current study are presented in Table 6.19 to facilitate comparison. The comparison of HAZUS and the present study's selected bridge class fragilities are shown in Figures 6.12 and 6.13.

Table 6.19 – Comparison of bridge classes.

Bridge class notation		Median fragilities				β_{ds}
Present study	HAZUS	λ_s	λ_m	λ_e	λ_c	
S-E1-S22/S33-C/R-D/S	HWB8/HWB20	0.35	0.45	0.55	0.80	0.60
S-E2-S22/S33-C/O-D/S S-E3-S22/S33-C/O-D/S	HWB9/HWB21	0.60	0.90	1.30	1.60	0.60
T-E1-S22/S33-C/R-D/S M-E1-S22/S33-C/R-D/S	HWB10/HWB22	0.60	0.90	1.10	1.50	0.60
T-E2-S22/S33-C/R-D/S M-E3S22/S33-C/R-D/S T-E2-S22/S33-C/R-D/S M-E3-S22/S33-C/R-D/S	HWB11/HWB23	0.90	0.90	1.10	1.50	0.60

By comparing the HAZUS fragilities with the fragilities generated in this study, the following inferences can be made:

- For the lower limit states BSST-0 and BSST-1, bridges are more vulnerable than is currently predicted by HAZUS. This trend is the same across all of the bridge classes considered in the present study.
- Single column bent seat abutment bridges in Era 11 are more vulnerable than is currently predicted by HAZUS (Figure 6.12). For example, for the respective limit states BSST -1, -2, and -3, bridges in the S-E1-S22-C-S class are 338%, 200%, 90%, and 90% more vulnerable than HAZUS predicts.
- For all bridge classes, HAZUS either over-estimates or under-estimates the fragilities for higher limit states BSST-2 and BSST-3. The over-estimation or under-estimation depends on the column cross-section, design era, number of spans, and number of columns per bent.
- HAZUS fragilities are unreliable for Era 11 two-span and multi-span bridges (Figure 6.13) resting on seat and diaphragm abutments for all the limit states. For example, HAZUS overestimates the bridge fragilities by 650%, 543%, 340% and 330%, compared to T-E1-S22-R-S for the limit states BSST -1, -2, and -3 respectively.
- Era 33 two-column bridges with diaphragm abutments are less vulnerable than is predicted by HAZUS.
- The dispersions obtained in the current study are close to the HAZUS values, except for classes of multi-column bent bridges, where the dispersions are higher than HAZUS values.
- Based on the current study, it is reasonable to conclude that existing HAZUS bridge groupings and their associated fragilities lead to a non-realistic estimation of seismic fragilities for bridges in California.

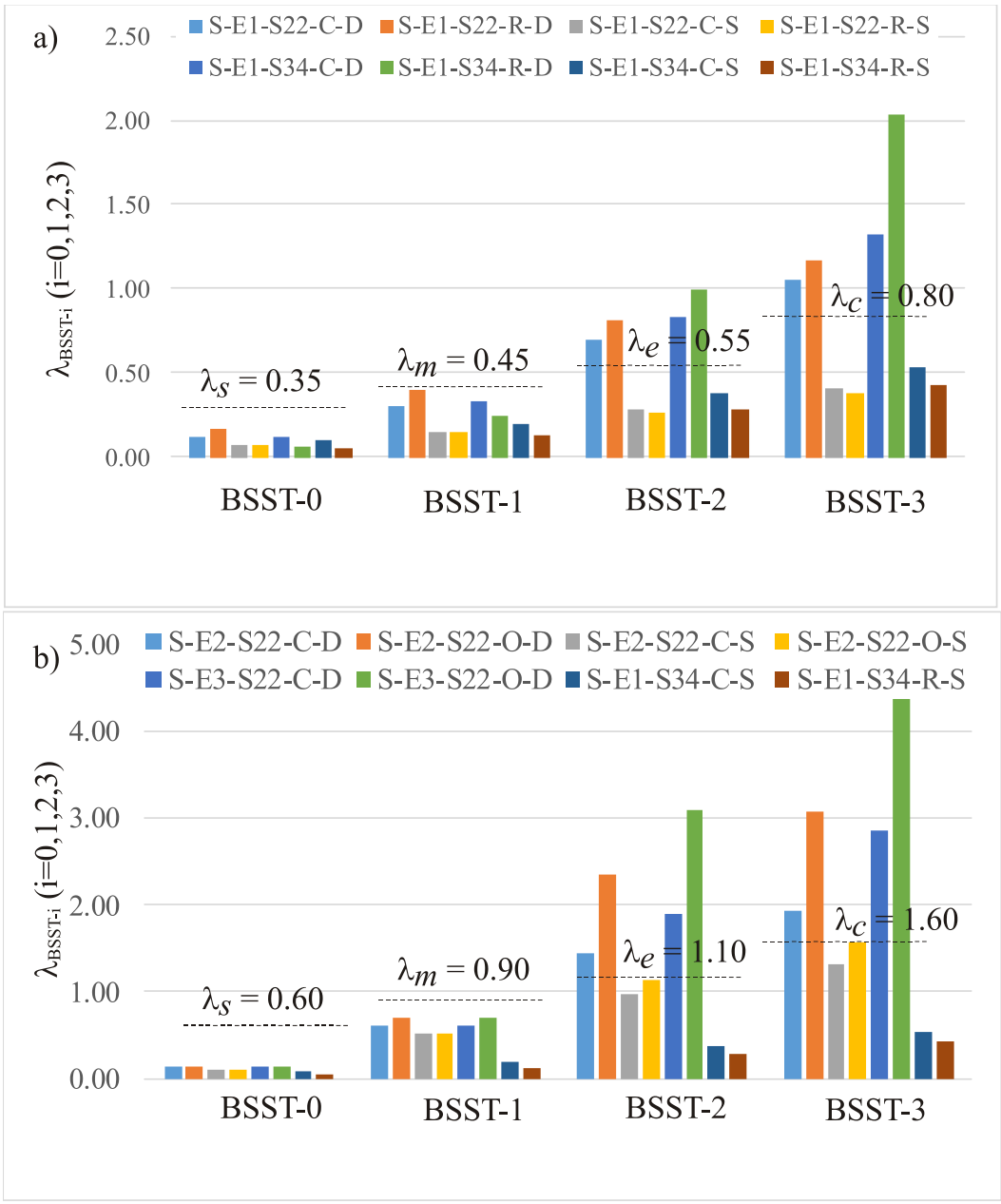

Figure 6.12– Comparison of HAZUS and selected bridge class fragilities for a) Era 11 bridges with single column bent and b) Era 22 and Era 33 bridges with single column bent.

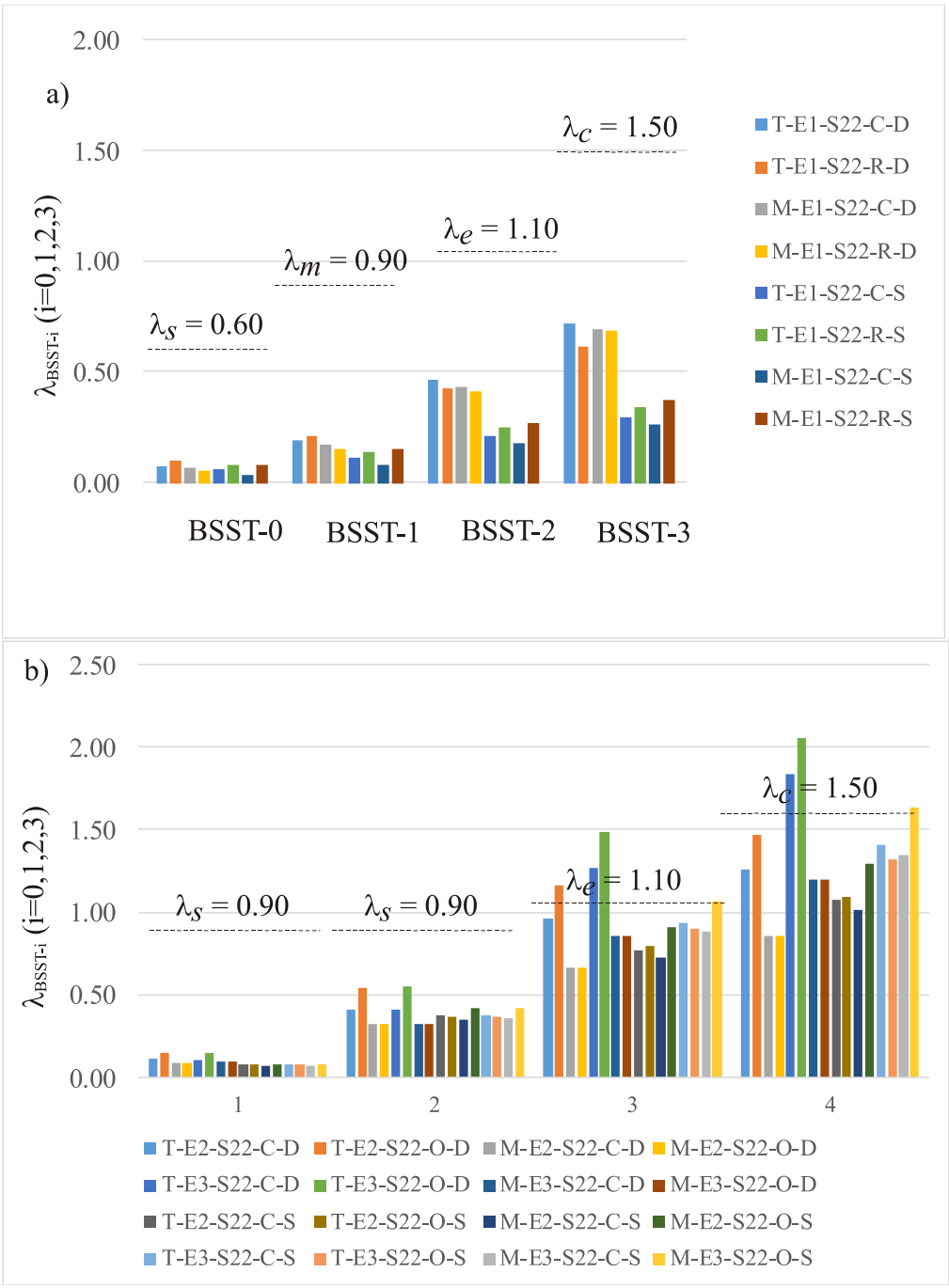

Figure 6.13– Comparison of HAZUS and selected bridge class fragilities a) Era 11 two-span bridges with two- and multi-column bents and b) Era 22 and Era 33 two-span bridges with single and multi-column bents.

6.5 Closure

This chapter presents the multi-phase framework for the generation of fragility curves, and the fragility curves for selected bridge classes. The framework includes the selection of a bridge class, characterization of bridge attributes such as material and geometric uncertainties, creation of numerical component models, non-linear time history analysis, convolution with limit-state models, and generation of system fragility curves through joint probabilistic seismic demand models (JPSDMs). The variations in the material and geometric properties of the bridges were accounted for on the basis of the plan review of California bridges. A set of numerical bridge models reflecting these uncertainties and nonlinear responses of various bridge components was created using OpenSees, and each of the bridge models obtained from a Latin hypercube sampling (LHS) was randomly paired with one of ground motions. The response data of each component, monitored from dynamic analyses, was used to develop the associated probabilistic seismic demand models (PSDMs). An important aspect presented in this chapter is the suggestion of limit-state models based on the literature review of experimental studies on bridge columns.

Bridge component and system fragilities were generated for 72 bridge classes and are presented in detail in this chapter. The generated fragility curves were compared with the existing HAZUS fragility curves. The following are some of the significant findings presented in this chapter:

- The seismic vulnerability for all bridge classes reduced with evolutions in column design philosophy (ductile detailing).
- Multi-column bents are more vulnerable than single column bents. The increased vulnerability of multi-column bents is mainly due to the bridge width and modeling assumptions.

- Across the various design eras, diaphragm abutment bridges are less vulnerable than seat abutment bridges.
- Columns are the most vulnerable components in the case of bridges with diaphragm abutments. In seat abutment bridges, columns and bearings are significant contributors to the overall vulnerability.
- There is a wide disparity between the fragility curves generated in the present study and the existing HAZUS fragility curves. Based on the current study, it is reasonable to state that existing HAZUS bridge groupings and their associated fragility curves lead to a non-realistic estimation of the seismic fragilities.

.

CHAPTER 7 PARAMETERIZED FRAGILITY CURVES: LASSO APPROACH

This chapter explores the relative impact of various uncertain input variables and level of treatment needed for these variables in the estimation of seismic demand models and fragility curves. As seen in the previous chapters, the seismic fragility of bridges has been expressed with one-dimensional (1-D) fragility curves developed with low-degree polynomial demand models (linear regression models) conditioned a single-parameter (IM). It is difficult to estimate the sensitivity of seismic demand models to input parameters in traditional single parameter fragility analysis, as the demand model is conditioned only on IM. Also, as stated in Ghosh et al. (2013), single-parameter demand models and fragility curves have some limitations: (1) the inability to account for the influence of uncertainty (modeling) parameters on structural performance during earthquakes without extensive re-simulations for each new set of parameter combinations, (2) the inability to explicitly address the effect of uncertainty parameters on fragility curves, and (3) the lack of flexibility to incorporate field instrumentation data resulting from monitoring of highway bridges to enable updating of fragility estimates.

Recently, to alleviate the limitations of the single-parameter demand models, logistic regression in conjunction with multi-parameter demand models comprising various predictor variables has been gradually increased in the realm of seismic vulnerability and loss estimation of bridges (Seo and Linzell, 2012; Dukes, 2013; Dukes et al. 2017 Ghosh et al., 2013; Kameshwar and Padgett, 2014; Park and Towashiraporn 2014; Mangalathu et al., 2015; Jeon et al., 2017; Mangalathu et al. 2017c). Assuming that the input variables are statistically independent, a multi-parameter demand model of each bridge component (demand parameter) is constructed. Samples obtained from this demand model are compared with those of the associated limit-state model to obtain the binary survival-

failure vector. This vector is used to perform a logistic regression analysis to determine the regression coefficients and thus develop the multi-parameter fragility curve in the component. This chapter (1) identifies the variables that exhibit strongest influences on the seismic demand and seismic fragilities, (2) quantifies the relative impact of various sources of uncertainty on the seismic response of bridges, (3) compares the regression-based response surface models such as linear, stepwise, Lasso, Ridge, and elastic net in the estimation of seismic demand models, and (4) suggests a parameterized fragility methodology that accounts for the effect of uncertain input variables in the seismic demand models as well as seismic fragilities. Such a study (1) provides insight in quantifying whether the variation of uncertain parameters should be treated explicitly or be neglected, (2) eliminates the parameters which have a minimal influence on the seismic demand and reduces unnecessary and exhaustive efforts in statistical sampling, (3) identifies the parameters that can reduce the uncertainty in demand models and fragility curves by more explicit evaluation of the uncertainty distribution (e.g., by developing an extensive database), and (4) helps bridge owners, such as California Department of Transportation, spend their resources judiciously (e.g. data collection, field investigations, censoring) on parameters that have a significant influence on bridge fragilities.

The generation of the parameterized fragility curves for the bridge classes discussed in Chapter 6 is beyond the scope of this thesis. It is noteworthy to mention that the geometric, material, and structural uncertainties, ground motions, and fragility curves in this chapter are used to demonstrate the approach and are not consistent with the earlier chapters. Note that the purpose of this chapter is to suggest a methodology and demonstrate its application. The approach is explained with a case study of two-span box girder bridges in California. A brief review of various regression models, such as linear, stepwise, Lasso, Ridge, and elastic net, is given in the next section. The efficiency of these models in

estimating the seismic demand is then compared using the mean square error (MSE) and absolute error (ABS) in predicting the seismic demand models.

7.1 Regression models

The following subsections describe the various regression models used for estimation of seismic demand models. Five regression models such as linear regression, stepwise regression, Ridge regression, Lasso regression, and elastic net regression are used in this paper; this subsection describes their relevance to seismic demand modeling.

7.1.1 Linear Regression

The linear regression (or least squares fitting) is the simplest and most commonly applied form of regression technique and provides a solution to the problem of finding the best-fitting straight line through a set of points. In the case of the seismic demand model for bridges with input vector, $X = (X_1, X_2,..., X_p)$ and a real-valued seismic demand (output from NLTHA) D, the linear regression has the following form:

$$D = \beta_0 + \sum_{j=1}^{p} X_j \beta_j \tag{7.1}$$

where β_j's are the unknown parameters or coefficients and p is the number of input parameters. With a training data set $(x_1, d_1),...,(x_N, d_N)$ the most popular method for the estimation of β is to minimize the residual sum of squares (RSS, Equation 7.2). The training set data is explained in section 7.2.

$$\begin{aligned} RSS(\beta) &= \sum_{i=1}^{N} (d_i - \mathrm{f}(x_i))^2 \\ &= \sum_{i=1}^{N} (d_i - \beta_0 - \sum_{j=1}^{p} x_{ij} \beta_j)^2 \end{aligned} \tag{7.2}$$

The least square estimates of the parameter β have the smallest variance among all linear unbiased estimates (Guass–Markov Theorem).

7.1.2 Stepwise regression

In the stepwise regression approach, only a subset of the input variable is retained and the rest of the variables are eliminated by a selection criterion. Forward stepwise regression is used in this paper. Forward stepwise regression starts with the intercept, and subsequently adds the variables into the model that most improve the fit. The improvement in fit is often based on the *F* statistic (Equation 7.3) in which the variables are sequentially added until the model attains the largest value of *F*.

$$F = \frac{RSS(\hat{\beta}) - RSS(\tilde{\beta})}{RSS(\tilde{\beta}) / (N - k - 2)} \tag{7.3}$$

The parameter estimate $\hat{\beta}$ in Equation 7.3 is with *k* inputs and the estimate $\tilde{\beta}$ is with the addition of a predictor. The *F*-ratio stopping rule doesn't attempt to find the best model, as the stopping rule provides only local control of the model search (Friedman et al. 2001).

7.1.3 Ridge regression

The least square estimates often have low bias but suffer the drawback of large variance (Hoerl and Kennard, 1970). The search for a biased estimator with smaller mean square error (MSE) and significant reduction in variance led to the development of Ridge regression (Tibshirani, 1996). Regression coefficients are shrunk by the Ridge regression by imposing a penalty on their size; the Ridge regression minimizes a penalized residual sum of squares (Equation 7.4)

$$\hat{\beta}_{ridge} = \underset{\beta}{\operatorname{argmin}} \left\{ \sum_{i=1}^{N} (d_i - \beta_0 - \sum_{i=1}^{p} x_{ij}\beta_j)^2 + \lambda \sum_{j=1}^{p} \beta_j^2 \right\} \quad (7.4)$$

The λ in Equation 7.4 corresponds to the shrinkage parameter, as the larger the value of λ, the greater the shrinkage (towards zero) of the regression coefficients. The inputs have to be standardized before applying the Ridge regression because the Ridge solutions are not equivariant under the scaling of the input variables. Also, the intercept β_0 has not been penalized in the Ridge regression.

7.1.4 Lasso regression

Lasso regression is similar to Ridge regression, but can do variable selection (Tibshirani, 1996). Lasso regression minimizes the residual sum of squares, subjected to a constraint based on the sum of absolute values of regression coefficients (Equation 7.5). The Lasso estimate $\hat{\beta}_{lasso}$ is defined as

$$\hat{\beta}_{lasso} = \underset{\beta}{\operatorname{argmin}} \left\{ \sum_{i=1}^{N} (d_i - \beta_0 - \sum_{i=1}^{p} x_{ij}\beta_j)^2 + \lambda \sum_{j=1}^{p} \left|\beta_j\right| \right\} \quad (7.5)$$

In Lasso regression, the penalty is imposed on $\sum_1^p |\beta_j|$, and because of the form of the Lasso penalty, Lasso regression does variable selection and shrinkage of regression coefficients. In other words, the most significant variables are retained while the insignificant variables are removed from the model. Bias is more controllable in Lasso regression when compared to Ridge regression (Tibshirani, 1996).

7.1.5 Elastic net

Zou and Hastie (2005) suggested another regularization and variable selection technique called elastic net, which is given as

$$\hat{\beta}_{elastic} = \underset{\beta}{\operatorname{argmin}} \left\{ \sum_{i=1}^{N} (d_i - \beta_0 - \sum_{i=1}^{p} x_{ij}\beta_j)^2 + \frac{1-\lambda}{2} \sum_{i=1}^{p} \beta_j^2 + \lambda \sum_{j=1}^{p} |\beta_j| \right\} \tag{7.6}$$

The penalty is imposed on $\sum_1^p |\beta_j|$ and $\sum_1^1 \beta_j^2$ in elastic net regression and provides a bridge between Lasso regression and Ridge regression. It is particularly useful for analyzing high dimensional data. In Ridge, Lasso, and elastic net, λ needs to be specified by the analyst.

The relative advantages of the above-mentioned regression techniques in the evaluation of seismic demand model will be discussed in Section 7.3. More detailed descriptions of the various regression techniques can be found in Friedman et al. (2001).

7.2 Case-study bridges: numerical modeling, uncertainties, ground motion suite, and demand parameters

Two-span box girder bridges are the most common type of highway bridge inventory in California and account for more than 35% of the box girder bridge inventory. Two-span bridges with seat and diaphragm abutments are selected for the case study in this paper, and the selected bridges were designed and constructed prior to 1970. Figure 7.1shows the numerical modeling of various bridge components; three-dimensional numerical modeling is carried out with the help of the finite element package OpenSees. A detailed description of the modeling strategy is given in Chapter 3.

Different sources of geometric, material, and system uncertainties are included in this study. Table 7.1 shows the mean value (μ), standard deviation (σ), and the associated probability distribution of various input variables used in the current study. Mangalathu et al. (2016a) identified the input variables based on an extensive plan review and hence mimic the California bridge inventory. The current study selects the suite of ground motions developed by Baker et al. (2011), which was proposed as part of the PEER Transportation Research Program. The suite comprises 120 pairs of broadband ground motions and 40 pairs of near-fault ground motions. The entire suite of ground motions are scaled by a factor of two (Ramanathan, 2012) to have sufficient response data of IMs higher than the Palmdale spectrum (the highest probabilistic design hazard level in California), and thus the expanded suite of 320 ground motions is used for the current study. The spectral acceleration at 1.0 sec ($S_{a–1.0s}$) is adopted as the intensity as the *IM* in the current study based on the work of Ramanthan (2012).

The input variables are sampled across the range of parameters presented in Table 7.2 using Latin Hypercube Sampling technique to generate statistically significant yet nominally identical three–dimensional bridge models. The variables are randomly paired with the selected suite of ground motions. The two orthogonal components of the ground motions are randomly assigned to the longitudinal and transverse direction of the bridge axis. A set of NLTHAs (320 simulations) is performed for all bridge-ground motion pairs to monitor the maximum response of various bridge components. The various demand parameters considered in this study are presented in Table 7.2.

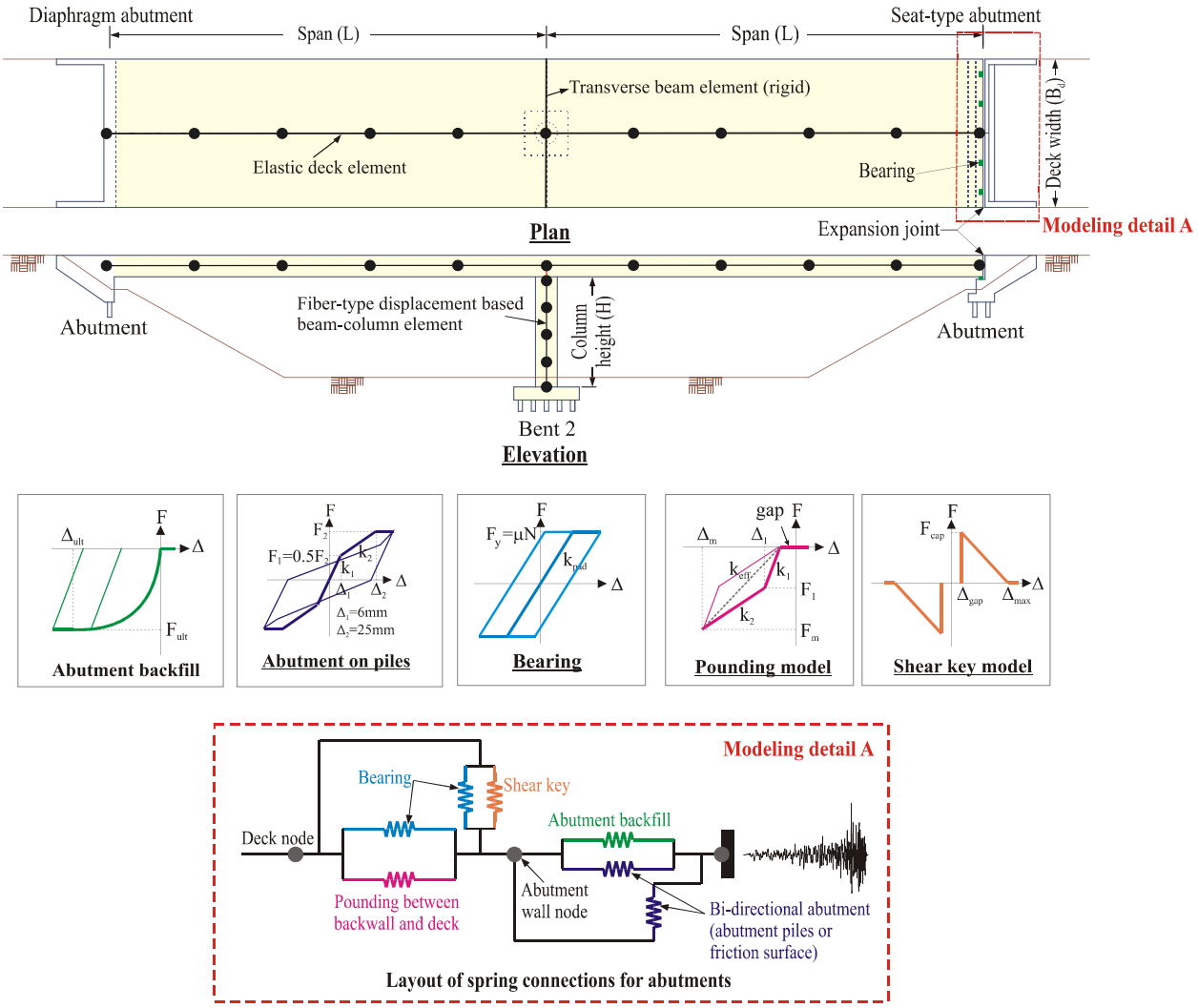

Figure 7.1 – Numerical modeling of various bridge components.

Table 7.1 – Uncertainty distribution considered in the bridge models.

Parameter	Units	Distribution		
		Type	μ^a	σ*
Concrete compressive strength (f_c)	MPa	Normal	29.03	3.59
Reinforcing steel yield strength (f_y)	MPa	Lognormal	465.0	37.30
Span length (L)	mm	Lognormal	31775	8738
Deck width (B_d)	mm	Lognormal	9780	1980
Column height (H)	mm	Lognormal	6625	865
Abutment backwall height (H_a)				
Diaphragm abutments				
On piles	mm	Lognormal	3234	488
On spread footings	mm	Lognormal	2925	1056
Seat-type abutments				
On piles	mm	Lognormal	2186	441
On spread footings	mm	Lognormal	2186	441
Abutments on piles - Lateral capacity/deck width (K_{pa})				
Diaphragm abutment	N/mm	Lognormal	1120	404
Seat-type abutment	N/mm	Lognormal	1498	540
Elastomeric bearing pad				
Stiffness per deck width (K_b)	N/mm/m	Lognormal	908	327
Coefficient of friction for bearing pad (μ_b)	–	Normal	0.30	0.10
Gap (g)				
Longitudinal (btw. deck and abutment wall, Δ_l)	mm	Lognormal	23.5	12.5
Transverse (btw. deck and shear key, Δ_t)	mm	Lognormal	12.8	2.58
Mass factor (m)		Uniform	1.25	0.007
Damping (ξ)		Normal	0.045	0.0125
Acceleration for shear key capacity (a_s)	g	Lognormal	1.00	0.20
Longitudinal reinforcement ratio (ρ)	(%)	Uniform	2.25	0.52
Pile group – pile cap and piles				
Translational stiffness (K_{ft})				
Single column – 1% long. rebar	N/mm	Normal	297716	140101
Single column – 3% long. rebar	N/mm	Normal	245178	105076
Multi column – 1.5% long. rebar	N/mm	Normal	140101	105076
Rotational stiffness (K_{fr})				
Single column – 1% long. rebar	N-m/rad	Normal	4.5×10^9	1.1×10^9
Single column – 3% long. rebar	N-m/rad	Normal	6.8×10^9	1.1×10^9
Multi column – 1.5% long. rebar	N-m/rad	Normal	0	0
Superstructure box type				
Reinforced vs. cast-in-place prestressed concrete(BT)		Bernoulli	Equally split**	
Abutment backfill type (sand vs. clay, ST)		Bernoulli	Equally split**	
Ground motion direction (fault parallel)				
Longitudinal vs. transverse (ED)		Bernoulli	Equally split**	
Column diameter (1524 mm vs. 1828.8 mm, D)		Bernoulli	Equally split**	

**μ and σ denotes the mean and standard deviation of the distribution. ** 160 simulations are carried out by one type and the remaining 160 simulations are carried out by other type and are chosen randomly*

Table 7.2 – Bridge component demand parameters.

Bridge component	Demand parameter	Abbreviation	Units
Column	Curvature ductility	COL	–
Abutment	Passive abutment displacement	ABP	mm
	Active abutment displacement	ABA	mm
	Transverse abutment displacement	ABT	mm
Deck	Displacement	DEC	mm
Bearing	Superstructure unseating displacement	UST	mm
	Bearing deformation	BRD	mm
Foundation	Translation	FNT	mm
	Rotation	FNR	rad

7.3 Comparison of the regression models

As the variable of interest ranges over several orders of magnitude (Table 7.1), the demand and input variable are transformed into the logarithmic space (Cornell et al. 2000; Mangalathu et al. 2016b). Also, because Ridge, Lasso, and elastic net regression models are sensitive to the scaling of input variables, the input variables are transformed (after the logarithmic transformation) into standard space (zero mean and unit variance). It is assumed that all of the input parameters are independent of each other and are therefore non-correlated. As mentioned before, Ridge, Lasso, and elastic net models identify the variables that have less influence on the regression model by penalizing the regression coefficient associated with the variable to zero. The regression coefficient of the input variable that has a minimal variance on the regression is penalized and the penalization procedure depends on the type of regression formulation (Equation 7.4, 7.5 and 7.6). A detailed description of the penalization procedure and algorithms can be found in Friedman et al. (2001). In general, the larger the penalty applied, the greater the shrinkage of regression coefficients (or setting the regression coefficient associated with the least

significant variables in the regression model to zero). However, an increase in penalization beyond a certain point might lead to the removal of variables that have a significant influence on the demand model. Hence, an investigation is carried out to find the optimal penalty factor.

7.3.1 Investigation of penalty factor

The performance or penalization of Ridge, Lasso, and elastic net regression models depends on the shrinkage factor λ (Equation 7.4, 7.5 and 7.6). Thus, this study is carried out to (1) understand the variation of MSE with λ and (2) determine the optimal value of λ for the estimation of seismic demand models. The MSE for a vector $\hat{D}$ with *n* predictors can be estimated as

$$\text{MSE} = \frac{1}{n}\sum_{i=1}^{n}(\hat{D}_i - D_i)^2 \tag{7.7}$$

As mentioned before, λ controls the amount of shrinkage of regression coefficients. MSE is estimated in this study through tenfold cross validation: the data is fitted on nine-tenths of the data, and the prediction error is computed for the remaining data. An in-depth discussion on the cross-validation techniques can be found in Friedman et al. (2001). Note that λ = 0 corresponds to the linear regression model, and in the case of λ = ∞, all the regression coefficients except intercept are shrunk to zero. The results of the investigation of shrinkage factor are presented in Figure 7.2 and Figure 7.3. Figure 7.2 shows some bridge components for the variation of MSE with λ, while Figure 7.3 shows the shrinkage of the regression coefficients with λ. Figure 7.3 measures the number of regression coefficients (or significant parameters) retained in the model with the increase in λ. The following inferences obtained from Figure 7.2 and Figure 7.3 are summarized below.

- MSE decreases with λ until reaching an optimal value for Ridge, Lasso and elastic net regressions and starts increasing beyond this value.
- The MSE of Ridge, Lasso, and elastic net regressions decreases with the increase of λ up to the optimal value, and thus the Ridge, Lasso, and elastic net regressions produce better performance until the optimal λ.
- The optimal λ varies depending on the component demand parameter. For example, in the case of diaphragm abutment bridges, the optimal λ for COL is 0.014 in the case of Lasso, while it is 0.032 for ABP.
- The optimal λ is different for different regression methods.
- The shrinkage of regression coefficients increases with an increase in λ; however, it also increases the MSE of the demand model once λ is beyond the optimal λ.
- As the recommended values of λ (Friedman et al. 2001) are very low (in the order of 10^{-2} to 10^{-3}), Ridge regression is not able to shrink the regression coefficients.

Although only selected component demand parameters are shown in Figure 7.2, similar observations are also noted for other demand models.

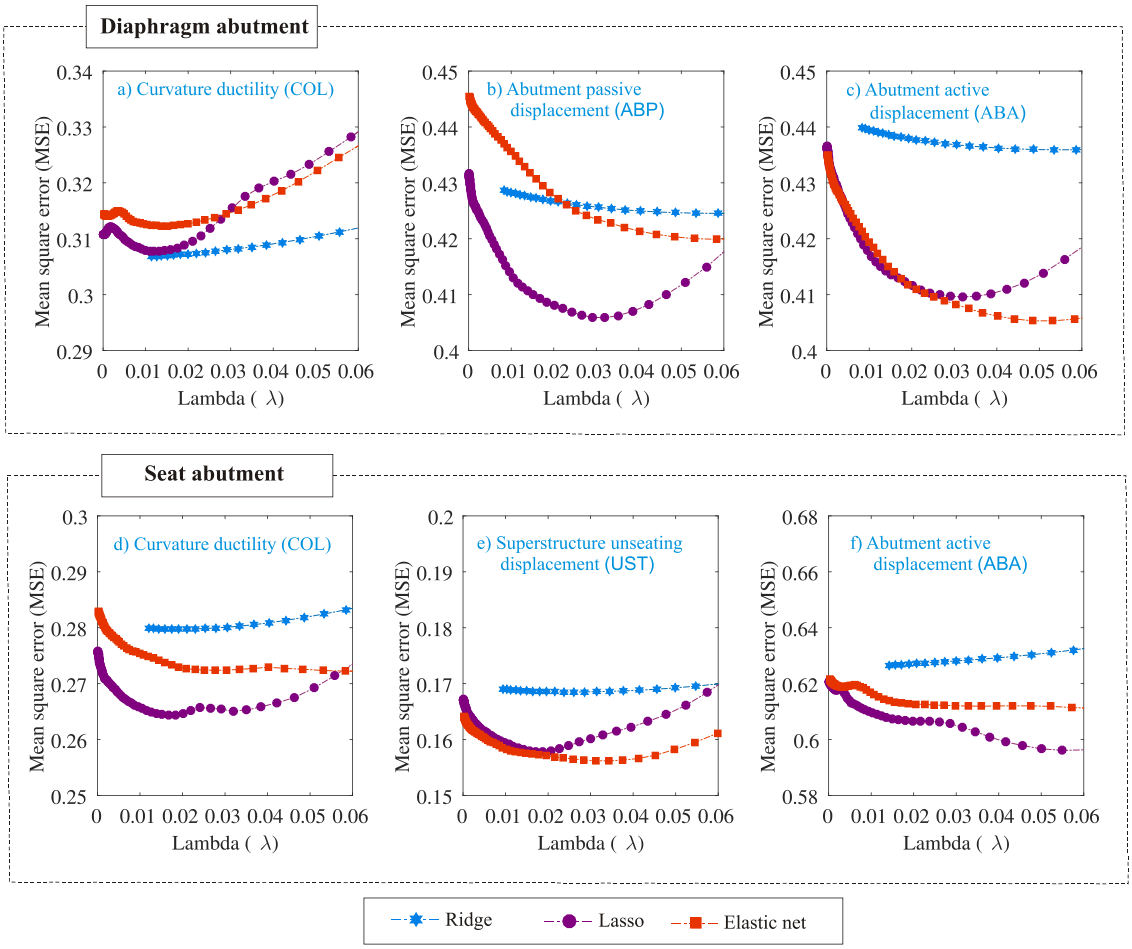

Figure 7.2 – Comparison of MSE with λ.

The optimal value of λ is adopted as 0.01 in the current study because it is found to be the lower bound for all the optimal λ values in the estimation of seismic demand parameters. However, such an estimate fails to identify many insignificant variables (or fails to shrink the regression coefficient), and thus overestimates the shrinkage coefficients. Nevertheless, the criteria adopted for the selection of λ is that the MSE of the models should (1) be less than the linear regression, (2) shrink highly insignificant regression coefficients, and (3) serve as a uniform value of λ for all the demand parameters. The optimal choice of λ for each demand model is beyond the scope of this paper.

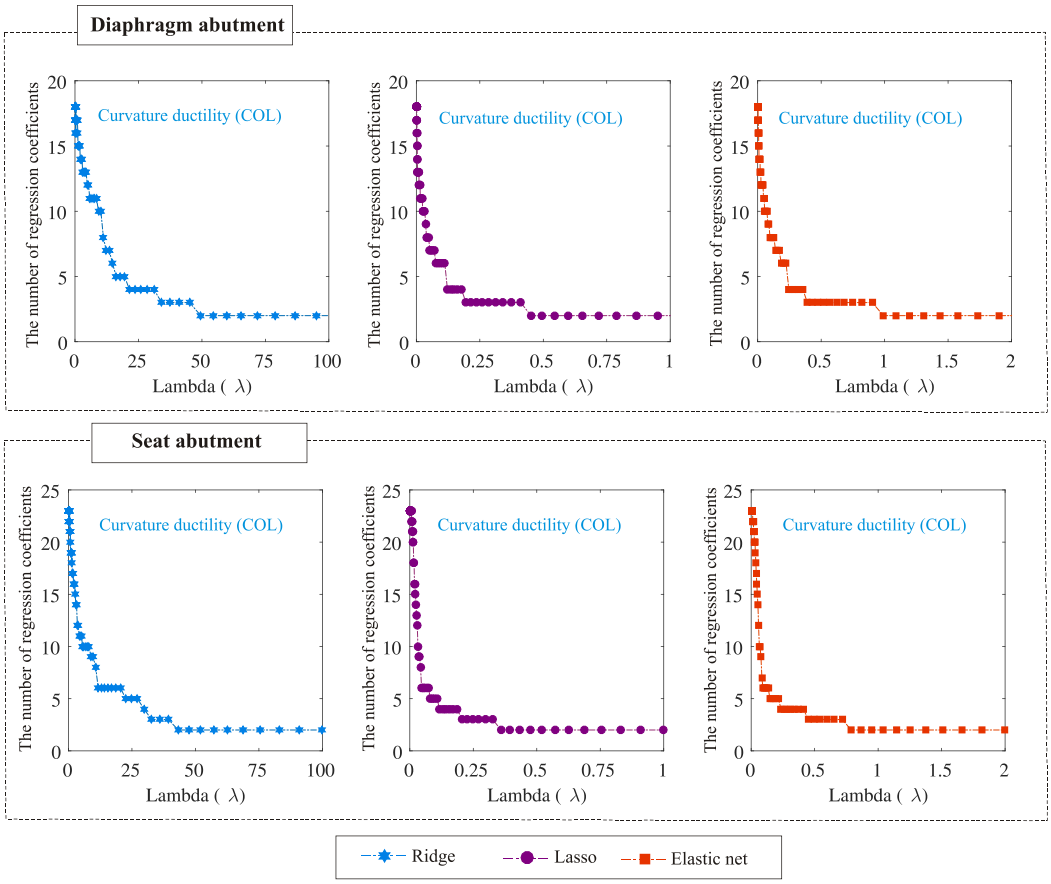

Figure 7.3 – Shrinkage of regression coefficients with λ.

7.3.2 Comparison of the regression models

The criteria adopted for evaluating the model-fitting procedure must be (1) able to more accurately predict the future data and (2) a simple model with less number of regression coefficients (Zou and Hastie, 2005). To evaluate the accuracy in predicting the future data, the current database is split into two: training set and test set. 75% of the data is assigned to the training set and is used to fit the model (Friedman et al. 2001). The remaining 25% of the data is used as the test set to estimate the accuracy of the fitted model. The assignment of data to the training set and test set is carried out randomly. The reason to split the data into training set and test set is to avoid the over-fitting of data (Friedman et al. 2001), which is a common problem if we use the entire data as training set. Table 7.3

shows the coefficients from five different regression models for COL with the training set for the diaphragm abutment bridge. The estimated fit is used to check the error in the test set. To achieve this goal, two types of error, MSE and absolute error (ABS), are selected in this paper. The ABS for a vector $\hat{Y}$ with n predictors can be estimated as

$$\text{ABS} = \frac{1}{n}\left|(\hat{Y}_i - Y_i)\right| \tag{7.7}$$

Table 7.3 – Estimated coefficients and test error for COL for the bridge with diaphragm abutments by various regression techniques

Parameter	Linear regression	Stepwise regression	Ridge regression	Lasso regression	Elastic net
Intercept	0.376	0.376	0.376	0.376	0.376
$S_{a-1.0s}$	1.129	1.120	1.119	1.117	1.118
ST	-0.034		-0.035	-0.031	-0.033
BT	-0.007		-0.005		
L	0.179	0.176	0.180	0.173	0.177
H	0.033		0.033	0.022	0.028
B_d	0.169	0.162	0.163	0.126	0.146
D	-0.243	-0.232	-0.235	-0.199	-0.219
ρ	-0.411	-0.415	-0.395	-0.407	-0.407
H_a	0.003		0.000		
K_{pa}	-0.055		-0.058	-0.028	-0.032
K_{ft}	0.022		0.033		
K_{fr}	-0.002		-0.017		-0.003
f_c	-0.810	-0.899	-0.228	-0.066	-0.072
f_y	0.734	0.821	0.151		
m	0.115	0.107	0.117	0.104	0.110
ξ	0.006		0.010	0.005	0.009
ED	0.014		0.015	0.001	0.007
MSE (test set)	0.474	0.471	0.459	**0.444**	0.447
Std. MSE	0.079	0.079	0.077	**0.075**	0.075
ABS (test set)	0.534	0.527	0.528	**0.518**	0.519
Std. ABS	0.049	0.049	0.048	**0.047**	0.047

The standard error of the mean value of the MSE (std.MSE) and ABS (std.ABS) is estimated as

$$\begin{aligned} \text{Std.MSE} &= \frac{\text{standard deviation (MSE)}}{n} \\ \text{Std.ABS} &= \frac{\text{standard deviation (ABS)}}{n} \end{aligned} \tag{7.8}$$

Table 7.3 also gives the MSE, Std.MSE, ABS, and Std.ABS value of the various regression models. The comparison of MSE and ABS helps to demonstrate how well the fit explains a given set of test data. The results from Table 7.3 show that (1) linear and Ridge regressions identify all the input variables as significant; (2) stepwise regression is the one which identifies the least number of significant parameters; (3) Lasso regression model has the minimum of MSE, Std. MSE, ABS, and Std. ABS, and thus is the best fit amongst the selected regression models; (4) among Lasso, Ridge, and elastic net, Lasso regression identifies more insignificant parameters; (5) these three regression methods identify that f_y, K_{ft}, and BT have less effect on the seismic demand model for COL, and thus it can be deduced that these input parameters are the least significant parameters; (6) all the regression methods identify $S_{a-1.0s}$ as the most significant parameter; and (7) standard error for all of the models are fairly similar. MSE and ABS are compared for the different regression models for the various demand parameters and are plotted in Figure 7.4. Lasso regression is the one having the least MSE and ABS for all the demand models. The MSE and ABS associated with COL, UST, and BRD are low for all of the regression models, which shows the good predictive capability. However, the MSE and ABS for ABA and ABP are higher for all the models. Previous studies (Ramanathan 2012; Mangalathu et al. 2016a) pointed out that columns and bearings are the components that govern the system fragility, and thus the adopted models are good enough to capture the seismic demand of COL and UST. Note that the results shown in Table 7.3and Figure 7.4 are for $\lambda = 0.01$ and the results can be significantly improved by selecting a better optimal value for λ. However, the selected λ yields good results and is able to remove insignificant parameters from the regression model. In addition, stepwise regression might result in the data over-fitting and instability (Vidakovic 2011), so Lasso regression is adopted as the regression model for further part of this study. Lasso regression leads to low values of MSE and ABS and has the ability to shrink the regression coefficients.

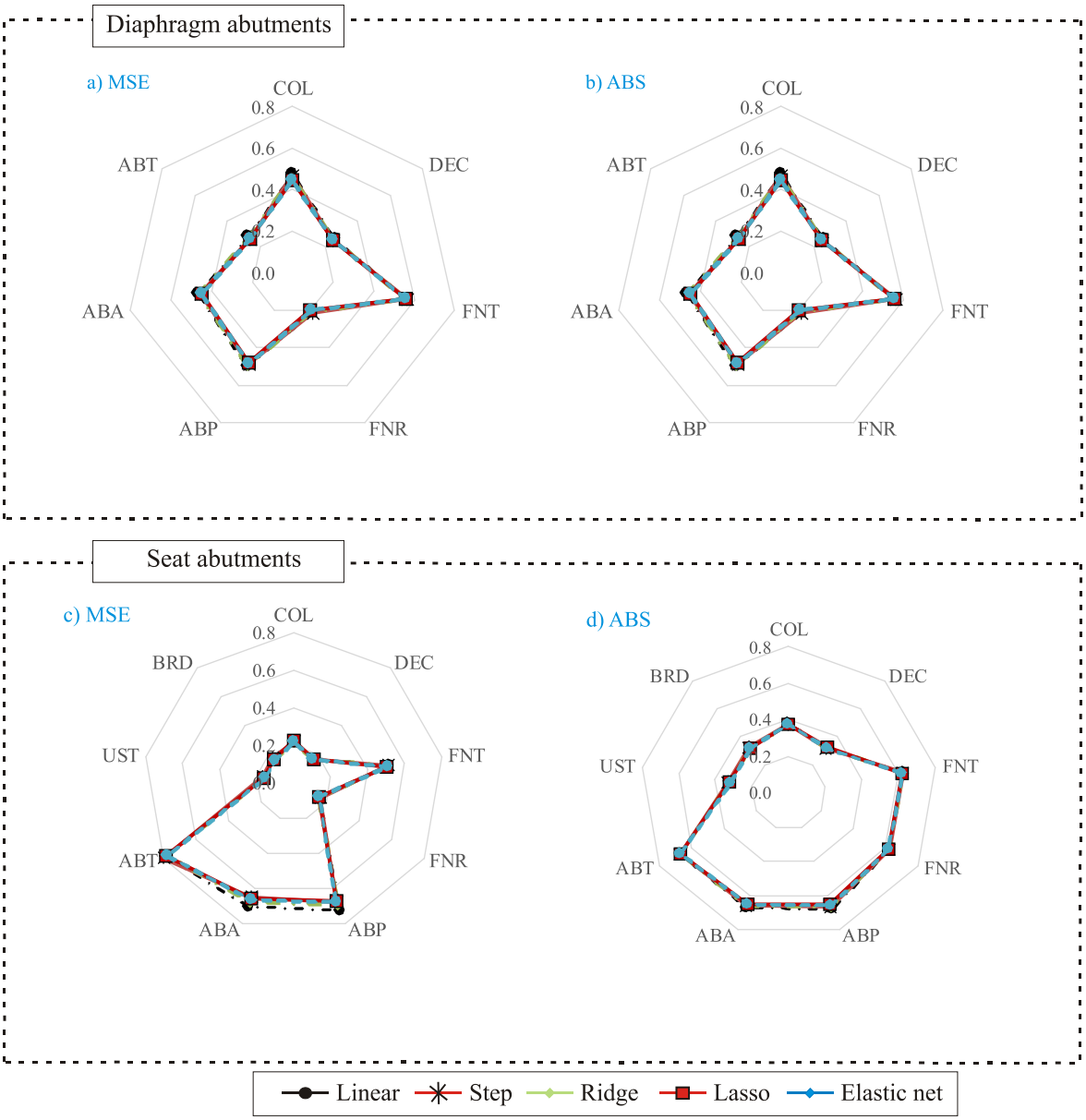

Figure 7.4 – Radar plot depicting the comparison of accuracy of fit obtained from the various regression models.

7.4 Sensitivity of input parameters to the seismic demand model

The regression coefficients from Lasso regression are also a measure of sensitivity of input parameters to the seismic demand model or fragilities because the input parameters

are converted to a standard space (after a logarithmic transformation of the data) in Lasso regression. A positive regression coefficient for a particular variable indicates that the seismic demand increases with a positive increase in the variable, and a negative regression coefficient shows that an increase in that variable reduces the seismic demand. Figure 7.5 shows the sensitivity of demand models for bridges with diaphragm and seat abutments. It is noted from Figure 7.5 that the significant parameters for both bridges tend to vary from component to component. In general, the IM (here, $S_{a-1.0s}$) has the greatest influence on the demand model for all the demand parameters. Span length (*L)* is the second most sensitive parameter for all the demand parameters. Soil type has a significant influence on the ABA and ABP in the case of the diaphragm abutment bridges. The influence of soil type is due to the fact that diaphragm abutments are stiffer than the adjacent bent and attract a large portion of the seismic demand. Similar conclusions are also noted in previous studies (Ramanathan 2012; Mangalathu et al. 2016a). COL is significantly affected by the reinforcement ratio (ρ) and the column diameter (D) for the two case-study bridges. L and IM are the most significant parameters for UST.

Concrete strength (f_c), steel strength (f_y), damping ratio (ξ), superstructure box type (BT), earthquake direction (ED), abutment height (H_a), acceleration for shear key capacity (a_s), gap between the deck and shear key (Δ_t), and coefficient of bearing (μ_b) all have a minimal impact on all the seismic demand models. In addition, Jeon et al. (2017) used a Bayesian parameter estimation method coupled with stepwise regression to identify significant parameters affecting the seismic response of curved concrete box girder bridges. Their work concluded that f_c, f_y, ED, μ_b, H_a, and Δ_t are the least significant parameters on the seismic demand model of the bridges. The current sensitivity study shows that other variables, except for IM, also have a significant influence on the seismic demand. The demand model conditioned only on the IM, as used in traditional fragility analysis, might not lead to a realistic estimation of the seismic demand and the fragility curves. Hence, a

fragility methodology accounting for the influence of significant parameters in the demand model as well as the fragility is given in the next section.

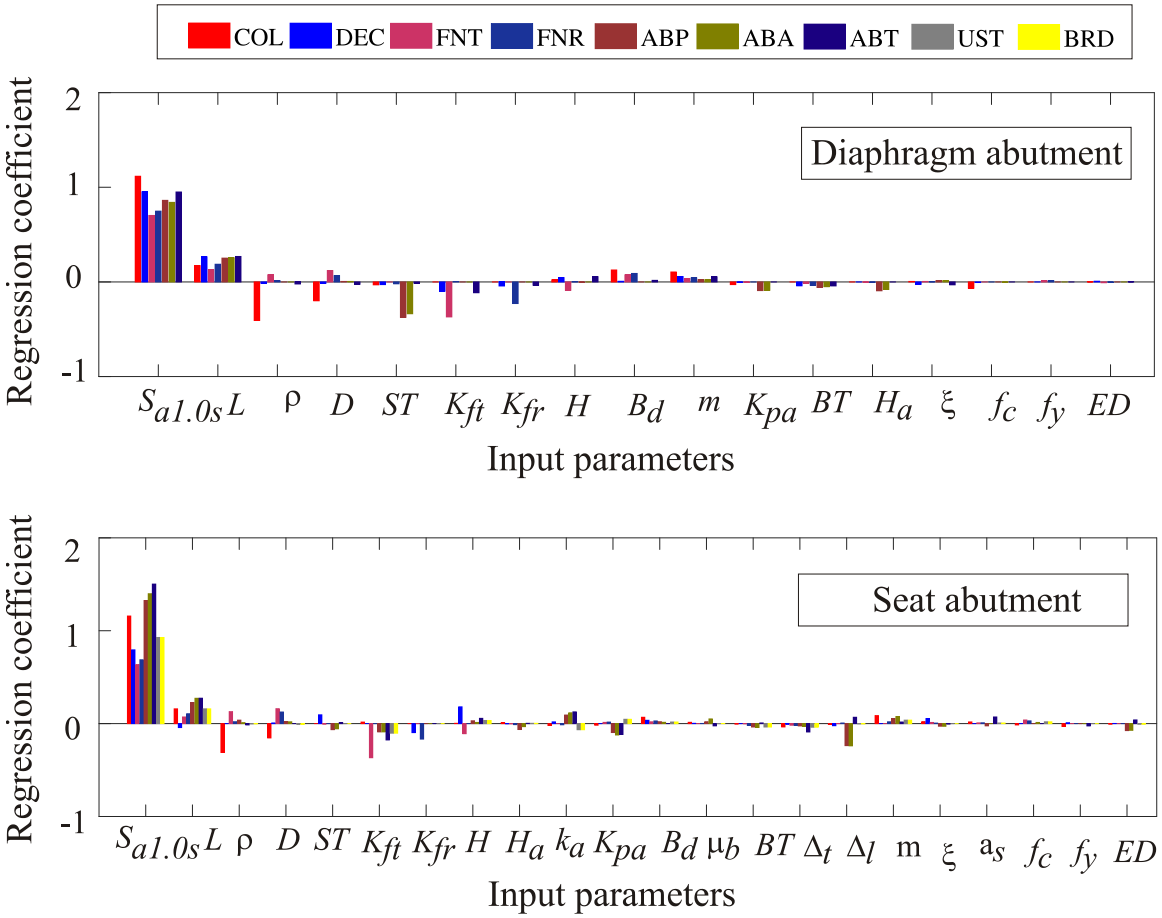

Figure 7.5 – Sensitivity of input parameters.

7.5 Multi-Parameter fragility curves

Recently, a number of studies (Seo and Linzell, 2012; Dukes, 2013; Ghosh et al., 2013; Kameshwar and Padgett, 2014; Park and Towashiraporn 2014; Jeon et al., 2015; Mangalathu et al., 2015) generated parameterized component and system fragility curves of highway bridges using multi-parameter demand models in conjunction with logistic regression technique. A modified approach stemming from the previous research is

suggested in this paper. Unlike the previous studies, the proposed approach helps to identify the relative impact of the various input parameters on the seismic demand as well as fragilities. Also, the proposed approach removes the less significant variable from the generation of seismic demand model and the seismic fragilities without much computational effort. The outline of the proposed approach is given below, for uncertain input parameters ($x_1,\ldots,x_n$, IM) and the demand measures ($d_1,\ldots,d_{ns}$).

Step 1: Evaluate the linear regression coefficients (β_{li}) by performing Lasso regression analysis for each component (k_i, $i = 1,\ldots,m$) with the input parameters ($x_1,\ldots,x_n$, IM), assuming that the input variables are statistically independent.

Step 2: Generate a large number of demand estimates (N, 1 million in this study) for each component, k_i, using their respective Lasso regression model by generating N values of randomly generated input parameters based on their probabilistic distribution.

Step 3: Generate N capacity values for a specific damage state for each bridge component based on the assumed distribution of the limit states (Table 7.1).

Step 4: Obtain the binary survive-failure ($N \times 1$) vector by comparing the capacity values (step 3) with the demand values (step 2).

Step 5: Conduct a Lasso logistic regression on the survive-failure vector to determine the k^{th} component probability model, conditioned on the input parameters as

$$PF_{\mathrm{k|IM},x_1,x_2,..x_{n_l}} = \frac{e^{\theta_{k,0}+\theta_{k,\mathrm{IM}}\ln(\mathrm{IM})+\sum_{j=1}^{n_l}\theta_{k_j}\ln(x_j)}}{1+e^{\theta_{k,0}+\theta_{k,\mathrm{IM}}\ln(\mathrm{IM})+\sum_{j=1}^{n_l}\theta_{k_j}\ln(x_j)}}, \quad n_l \le n \tag{7.9}$$

where $\theta_{k,0}$, $\theta_{k,sa}$, and $\theta_{k,j's}$ ($j = 1,\ldots,n_l$) are the Lasso logistic regression coefficients of the k^{th} bridge component. This step helps to identify the sensitivity of bridge component fragility curves to the uncertain input parameters.

Step 6: Assuming that the bridge failure is a series system (the system fails if one or more components fail), estimate the binary survive-failure vector, and conduct a Lasso logistic regression to obtain the system failure. This step helps to identify the sensitivity of bridge system fragility to the uncertain input parameters

$$PF_{SYS|S_a,x_1,x_2,\ldots x_{n_s}} = \frac{e^{\theta_{SYS,0}+\theta_{SYS,IM}\ln(IM)+\sum_{j=1}^{n_s}\theta_{SYS,j}\ln(x_j)}}{1+e^{\theta_{SYS,0}+\theta_{SYS,IM}\ln(IM)+\sum_{j=1}^{n_s}\theta_{SYS,j}\ln(x_j)}}, \quad n_s \le n \tag{7.10}$$

where $\theta_{SYS,0}$, $\theta_{SYS,sa}$, and $\theta_{SYS,j's}$ ($j = 1,\ldots, n_s$) are the Lasso logistic regression coefficients for the system failure.

Step 7: For a particular bridge with significant input parameters, $x_1,\ldots,x_{n_s}$, the classical one-dimensional fragility curves can be obtained as

$$PF_{SYS|IM} = \int_{x_1}\int_{x_2}\ldots\int_{x_{n_s}} \frac{e^{\theta_{SYS,0}+\theta_{SYS,IM}\ln(IM)+\sum_{j=1}^{n_s}\theta_{SYS,j}\ln(x_j)}}{1+e^{\theta_{SYS,0}+\theta_{SYS,IM}\ln(IM)+\sum_{j=1}^{n_s}\theta_{SYS,j}\ln(x_j)}} f(x_1)\ldots f(x_{n_s})\,dx_1\ldots dx_{n_s} \tag{7.11}$$

where $f(x_1),\ldots, f(x_9)$ are the probability density parameters for parameters, $x_1,\ldots,x_{n_s}$.

The limit state models for the various bridge components are given in Table 7.4, and are consistent with the limit states presented in Chapter 6. The limit states were derived

in such a way as to align with the California Department of Transportation (Caltrans) design and operational experience. This will facilitate Caltrans' evaluation of repair–related decision variables, repair cost, and repair time.

Table 7.4 – Limit state models of various bridge components.

Component	Median value, S_c				β_c
	Slight	Moderate	Extensive	Complete	
Column curvature ductility (COL, –)	0.80	2.0	5.00	8.00	0.35
Passive abutment response (ABP, mm)	76	254	–	–	0.35
Active abutment response (ABA, mm)	38	102	–	–	0.35
Transverse abutment response (ABT, mm)	25	102	–	–	0.35
Deck displacement (DEC, mm)	102	305	–	–	0.35
Bearing displacement (BRD, mm)	25	76	–	–	0.35
Superstructure unseating (UST, mm)	–	–	152	229	0.35

Based on the approach mentioned in this section, multi-parameter demand model and fragility curves are generated for the bridges with diaphragm and seat abutments for various limit states. Figure 7.6 shows the single parameter fragility curves (conditioned on $S_{a\text{-}1.0s}$) for the diaphragm and seat abutments for the moderate damage state. It is clear from Figure 7.6 that the bridge fragility is mostly dominated by column fragilities for the moderate damage state. ABT and BRD, respectively, are the second most vulnerable components in the case of diaphragm abutment bridges and seat abutment bridges. Although not shown here, similar conclusions are observed for other limit states. Interested readers are directed to previous studies (Mangalathu et al. 2015, Jeon et al. 2017) for the comparison of the fragility curves through the multi-parameter demand model with the traditional single-parameter demand model.

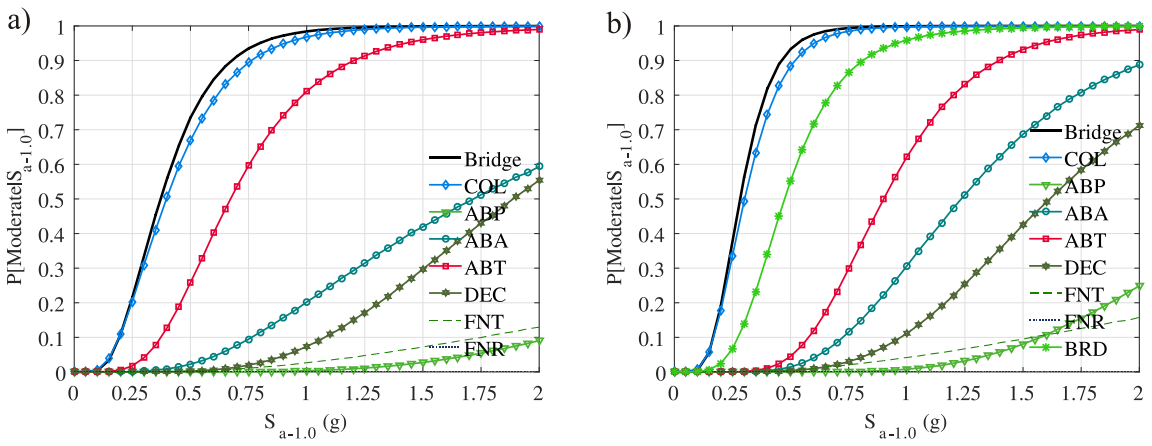

Figure 7.6 – System and component fragility curves for moderate damage state: a) diaphragm abutment bridge, b) seat abutment bridge.

As mentioned before, the proposed approach also helps identify the sensitivity of the fragility curves to the input parameters. Figures 7.7 and 7.8 show the sensitivity of the fragility curves to the input parameters for the diaphragm and seat abutment bridges, respectively. The uncertainty in IM dominated over all the other uncertainties in the fragility curves. In the case-study bridges where the fragility of COL determines the bridge fragility, $S_{a-1.0s}$, L, ρ, D, B_d, and m are the most sensitive parameters for the diaphragm abutment bridges for system fragility, while $S_{a-1.0s}$, L, ρ, D, B_d, m, and Δ_l are the sensitive parameters in the case of seat abutment bridges. f_y, ξ, ED, and K_{fr} are the least significant parameters for all the components for all the damage states. Another advantage of the proposed approach is the ability to identify the sensitivity of input variables based on the limit state under consideration. For example, the sensitivity of IM is higher for ABP at the moderate damage state when compared to the slight damage state in the case of diaphragm abutment bridges. It is deduced from the comparison of the magnitude of regression coefficients.

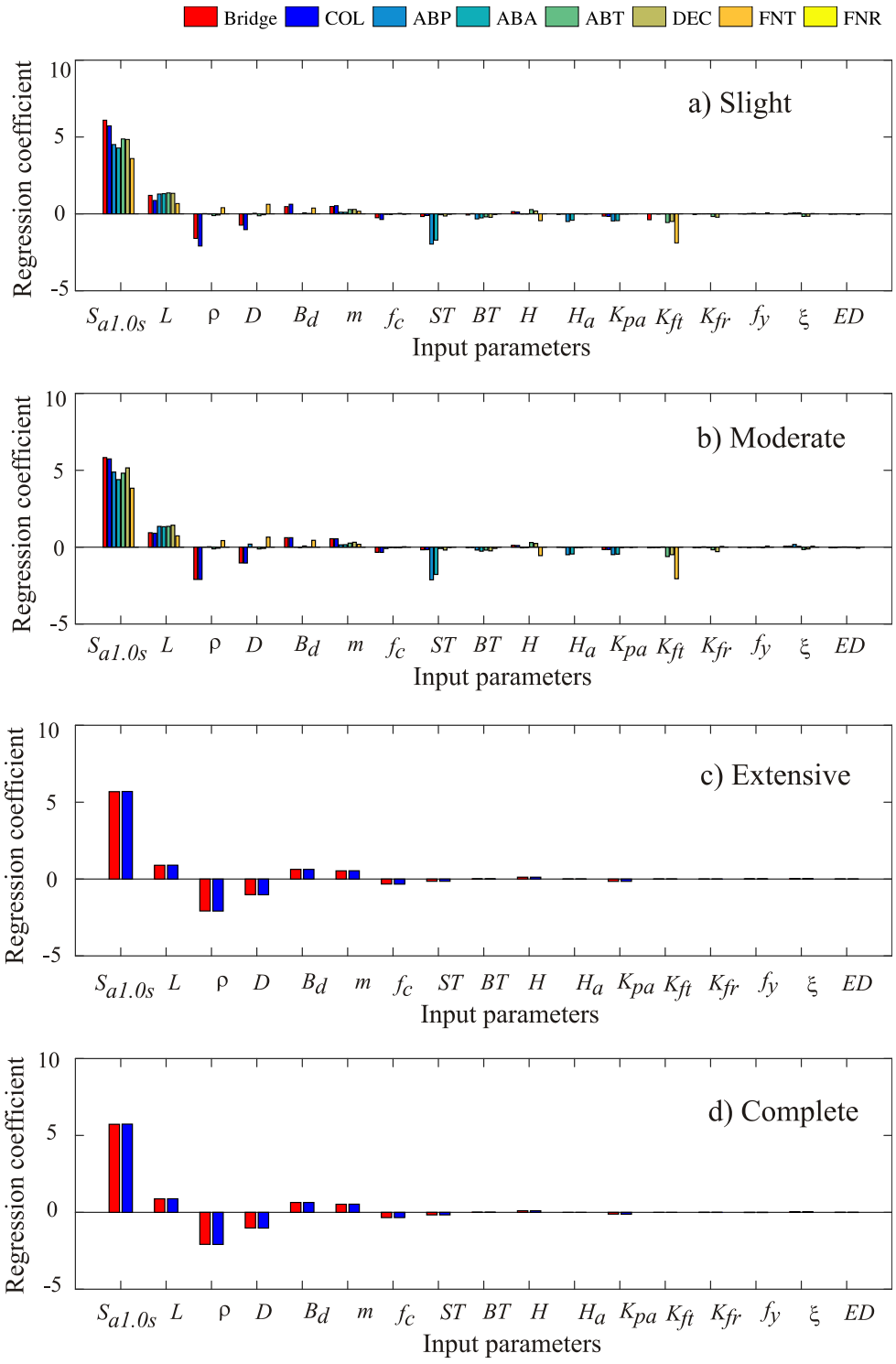

Figure 7.7 – Sensitivity of fragility curves to input parameters for diaphragm abutment bridge for various limit states

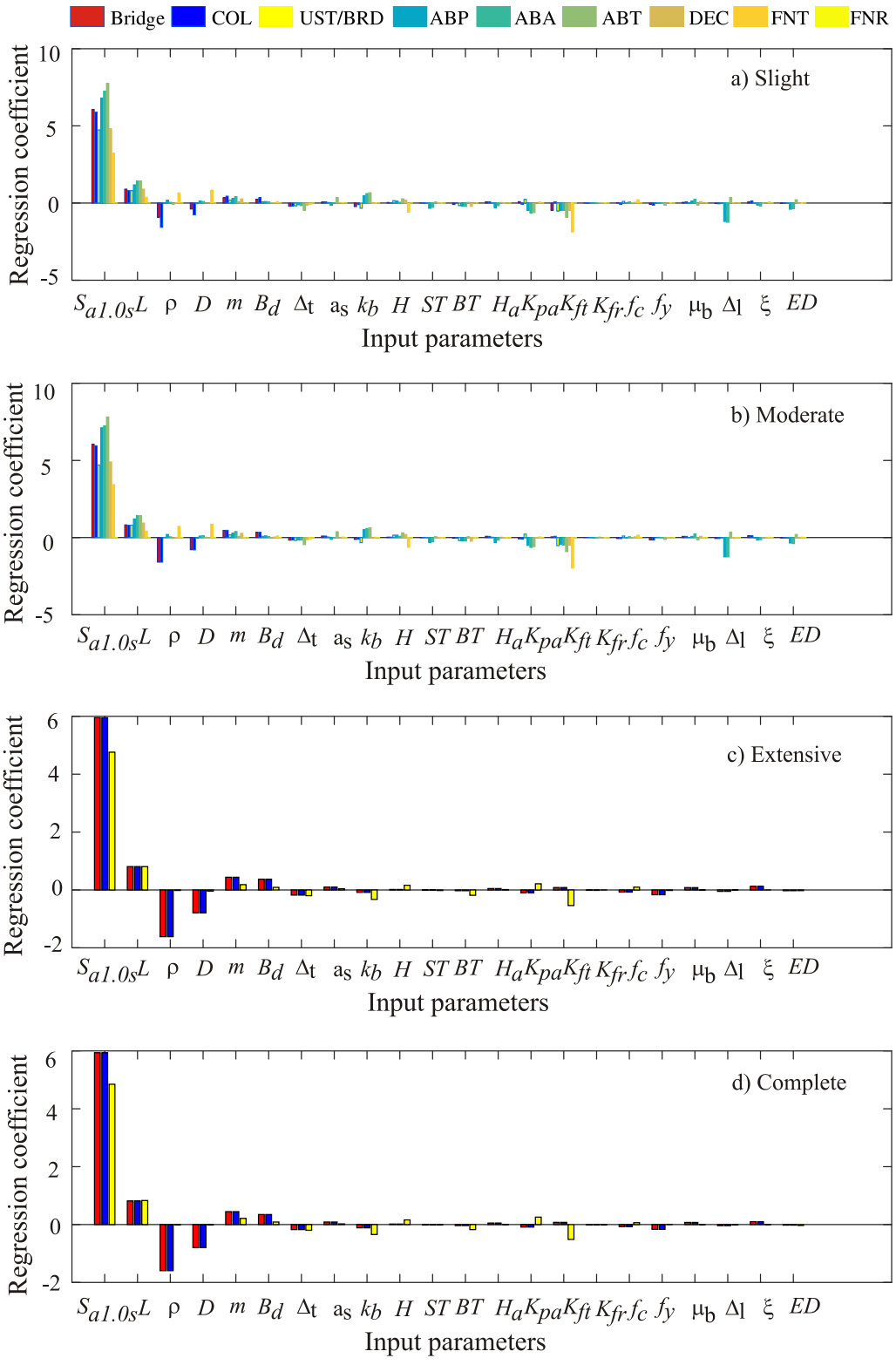

Figure 7.8 – Sensitivity of fragility curves to input parameters for seat abutment bridge for various limit states

7.6 Conclusions

This chapter identifies the relative impact of various uncertain input parameters on the seismic response of various bridge components. The efficiency of various regression models such as linear, stepwise, Ridge, Lasso, and elastic net in the generation of seismic demand models are evaluated in the initial part of the paper. The comparison is carried out for two-span box girder bridges with seat and diaphragm abutments. Nonlinear time history analysis (NLTHA) is carried out for the bridge models accounting for the material, geometric, and system uncertainties. Various demand parameters such as curvature ductility demand, abutment displacements in the passive, active, and transverse directions, deck displacement, foundation translation and rotation, superstructure unseating displacement, and elastomeric bearing displacement are recorded for each NLTHA. Multi-parameter demand models are generated for each demand parameter by using 75% of the data from the NLTHA. The efficiency of the regression methods are compared in terms of the mean square error (MSE) and absolute error (ABS) in predicting the remaining 25% of the NLTHA data. It is observed that the Lasso regression model is the most effective with regard to lowest MSE and ABS in predicting the data. Also, the Lasso regression model is able to remove insignificant variables from the demand model. As the Lasso regression coefficients are a measure of the sensitivity of the input variables, the results of the Lasso regression is used to identify the significance of the input variables in the estimation of seismic demand models for various bridge components. Ground motion intensity measure (IM, here, spectral acceleration at 1 sec) and span length (L) are identified as the most sensitive variables in the demand models for various demand parameters. In general, the steel strength (f_y), damping ratio (ξ), superstructure box type (BT), earthquake direction (ED), abutment height (H_a), acceleration for shear key capacity (a_s), gap between the deck and shear key (Δ_t), and coefficient of bearing (μ_b) all have a minimal impact on all the seismic demand models.

The sensitivity results reveal that the generation of demand models without considering the uncertainties in the significant parameters might lead to inaccurate estimates of the demand models. To include the effect of significant uncertain variables in the generation of demand models and fragility curves, a multi-parameter fragility methodology using Lasso regression is suggested in this paper. The proposed fragility approach helps to identify the relative impact of the various input parameters on the demand as well as fragility curves of various structural components. Hence, the proposed approach provides additional perspectives for the decision makers or the owners in prioritizing their resources in the database development or structural monitoring. The sensitivity study on fragility curves indicates that IM, L, reinforcement ratio (ρ), column diameter (D), deck width (B_d), mass factor (m), and gap between the deck and shear key (Δ_l) are the parameters significantly affecting on the bridge fragilities. In general, the component as well as system fragilities are minimally affected by f_y, ξ, ED, and foundation rotational stiffness (K_{fr}). The finding of the sensitivity study is helpful in evaluating the level of uncertainty treatment required for each variable. Depending on the user requirement and whether the intention is to have system or component vulnerability, the proposed approach notifies whether the uncertainty in a particular variable should be treated explicitly or be neglected.

Although the findings observed from this study are based on the case studies of two-span concrete box girder bridges in California, the methodology is relevant and applicable to other structures as well. As the level of uncertainty treatment is a common challenge in regional risk assessment, the proposed approach helps to identify whether the uncertainty for a particular variable needs to be treated explicitly or be neglected. The identification of level of uncertainty treatment required for a particular variable also helps bridge owners spend their resources judiciously and develop a more reliable database of the uncertain input variables for the seismic risk assessment.

CHAPTER 8 CONCLUSIONS AND FUTURE WORK

8.1 Summary and Conclusions

Regional seismic risk assessment relies on fragilities that are applicable to a portfolio of structures, as it is time consuming and impractical to generate fragility curves for each individual structure in a specific region. Also the generation of structure-specific fragility curves is not warranted as some structures have similar performance or fragilities. The grouping of structures is carried out in most cases based on engineering judgment and there is a lack of systematic strategy for binning/grouping structures. In the existing grouping methodology, HAZUS grouping is the widely accepted approach. However, a critical review of HAZUS based on recent research revealed many drawbacks and showed that the HAZUS bridge grouping and associated fragilities leads to an unrealistic estimation of the seismic demand and the associated losses. These limitations in the traditional engineering judgment based grouping can be addressed by performance based grouping techniques. The performance based grouping leads to more reliable sub-classes of bridges relative to the traditional subjective lumping of bridges. The current study explores various performance based grouping techniques such as Analysis of Variance (ANOVA), Analysis of Covariance (ANCOVA) and non-parametric Kruskal-Wallis test (KW) towards the grouping of structures of similar performance. Based on the insights from the comparison, a new performance grouping methodology based on ANOVA is suggested in this study. This study improved bridge classifications of HAZUS by considering various structural attributes such as column cross-section, design era, number of spans, abutment type, pier type and span continuity. Although the current study groups the box-girder bridge classes

in California, the proposed grouping approach can also be applied to other regions by fine-tuning the grouping based on the evolution in seismic design philosophy and other attributes which are different from California.

A major task in the current research was to understand and characterize the California bridge inventory. California is a state with a high seismic hazard, a history of damaging earthquakes, and has close to 29,000 bridges which vary in age based on their construction. Bridge plans pertinent to various design eras and structural configurations were reviewed in detail, and descriptive statistics were calculated for the material, geometric and structural parameters of the box-girder bridges in California. Such a characterization helps to make the fragility models applicable to a wide geographic area. More than 1000 bridge plans were reviewed for this process with the help of California Department of Transportation (Caltrans) in-house database.

Numerical bridge models accounting for geometric, material, and system uncertainties are created in OpenSees. The numerical models incorporate a high degree of detail with respect to the component modeling strategies and their ability to capture the damage due to the seismic demand. The input variables are sampled across the range of parameters using the Latin Hypercube Sampling technique to generate statistically significant yet nominally identical three–dimensional bridge models. The variables are randomly paired with the selected suite of ground motions. The two orthogonal components of the ground motions are randomly assigned to the longitudinal and transverse direction of the bridge axis. A set of NLTHAs (320 simulations) is performed for all bridge-ground motion pairs to monitor the maximum response of various bridge components. Various demand parameters considered in the current study are curvature

ductility, abutment displacements in the passive, active and transverse direction, superstructure unseating displacement, and elastomeric bearing displacement. The demand models are convolved with the capacity models to generate the component fragility curves. A significant contribution of the present study is to suggest the capacity limit states (CCLS) for columns based on extensive experimental review. Pertinent to various design eras, literature review was carried out to collect the experimental data for bridge columns and statistical analysis was carried out to suggest the CCLS of bridge columns. Such an exercise helps to develop a new generation of more accurate and useful bridge fragility models for incorporation into the ShakeCast earthquake alerting system developed by the California Department of Transportation (Caltrans) and to support seismic risk evaluation of bridges in California. System fragility curves are generated afterwards using Monte Carlo simulations and joint probabilistic seismic demand models (JPSDMs) incorporating the correlation between the components.

Bridge component and system fragilities are generated for 72 bridge classes and the selected bridge classes cover more than 75% of the California box-girder bridge inventory. The following are some of the notable findings from the fragility analysis:

- The seismic vulnerability of all the bridge classes reduced with the evolution in column design philosophy (ductile detailing).
- Multi-column bents are more vulnerable than the single column bents. The increased vulnerability of the multi-column bents is mainly due to the bridge width and modeling assumptions.
- Across the various design eras, diaphragm abutment bridges are less vulnerable than seat abutment bridges for all the design eras.

- Columns are the most vulnerable component in the case of bridges with diaphragm abutments. However, in the case of seat abutment bridges, bearings also contribute significantly to the overall vulnerability in addition to the columns.
- Comparison with HAZUS fragilities revealed the wide disparity between the fragility curves generated in the present study and the HAZUS fragilities. Based on current study, HAZUS bridge grouping and associated fragilities leads to an-unrealistic estimation of the seismic fragilities.

Another contribution in the present study is the generation of bridge-specific fragility curves through machine learning techniques. The framework includes the selection of a bridge class, characterization of bridge attributes such as material and geometric uncertainties, creation of numerical component models, construction of multi-parameter demand models using the Lasso regression method, and development of parameterized (multi-dimensional) fragility models using logistic regression. The parameterized fragility models are used (1) to produce bridge-specific (one-dimensional) fragility curves when the uncertainty parameters are available and (2) to develop bridge-class (one-dimensional) fragility curves using a Monte Carlo integration. The advantage of the Lasso regression model is that it is able to remove insignificant variables from the demand model. As the Lasso regression coefficients are a measure of the sensitivity of the input variables, the results of the Lasso regression are used to identify the significance of the input variables in the estimation of seismic demand model for various bridge components. Ground motion intensity measure (IM, here, spectral acceleration at 1 sec) and span length (L) are identified as the most sensitive variables in the demand models for various demand parameters. In general, the steel strength (f_y), damping ratio (ξ), superstructure box type (BT), earthquake

direction(ED), abutment height (H_a), acceleration for shear key capacity (a_s), gap between the deck and shear key (Δ_t), and coefficient of bearing (μ_b) have a minimal impact on all the seismic demand models. The proposed fragility approach helps to identify the relative impact of the various input parameters on the demand as well as fragility curves of various structural components. Hence, the proposed approach provides additional perspectives for the decision makers or the owners in prioritizing their resources in the data base development or structural monitoring.

8.2 Research Impact

This study presents a performance based grouping methodology to group the box-girder bridge classes in California and generated component and system fragility curves for single frame multi-span box girder bridges in California. This resulted in a significant number of contributions which are as follows:

- The grouping has been traditionally performed based primarily on engineering judgment and prior experience. This work (1) presents an overview of various statistical techniques such as analysis of variance (ANOVA), analysis of covariance (ANCOVA), and Kruskal Wallis (KW) test for grouping the bridges of similar performance; (2) compares the groupings that emerge from the various grouping techniques; and (3) identifies the method that has more statistical power in creating bridge sub-classes of distinct structural performance. The grouping is achieved by comparing the structural responses of bridge classes obtained from the non-linear time history analysis of bridges.

- A simple performance based grouping methodology based on ANOVA is suggested in this work. The ANOVA-based grouping provides insight into the potential bridge attributes which significantly affect the seismic response and fragility curves, which to date has not been assessed thoroughly. The method can be used to group bridge classes depending upon the user requirement, i.e. whether the user would like to assess the system or component vulnerability. The grouping of bridge classes yields a more reliable estimation of the seismic vulnerability of various bridge classes. The proposed method helps to save considerable computational effort and simulation compared to the traditional subjective grouping.
- Extensive details are provided regarding the variability in the material, structural and geometric attributes of box-girder bridges in California. Such a characterization helps to make the fragility models applicable to a wide geographic area.
- Column capacity limit states are suggested based on the literature review of experimental studies on bridge columns. The proposed limit states are more reliable, and help to develop a new generation of more accurate and useful bridge fragility models for incorporation into the ShakeCast earthquake alerting system.
- Fragility curves and relative vulnerabilities are evaluated for the 72 box-girder bridge classes in California. The selected bridge classes cover more than 75% of the California box-girder bridge inventory. The generate fragility curves underscore the necessity to go beyond the traditional engineering judgment based grouping.
- The study suggests a methodology to evaluate the sensitivity of demand models and fragility curves to the uncertain input parameters. To include the effect of significant uncertain variables in the generation of demand models and fragility curves, a multi-

parameter fragility methodology using Lasso regression is suggested in this work. The proposed approach provides additional perspectives for the decision makers or the owners in prioritizing their resources in the data base development or structural monitoring.

8.3 Recommendations for future work

Potential areas in which this work can be extended through additional research include the following:

- Bridge foundations and abutments may be founded on liquefiable soil, and significant damage can be seen on bridges in regions with high liquefaction potential. Also, the random and non-liner behavior of soil can significantly affect the behavior of bridges. Further studies are needed to explore the effect of liquefaction, ground deformation hazard and soil-structure interaction on the fragility curves.
- The performance based strategy should be extended to other bridge class such as I-girder, T-girder, slab bridges, to mention a few.
- The study focused on the seismic risk assessment due to main-shock ground motions, and doesn't account for aging and deterioration mechanism. The effect of aftershock, aging and deterioration, and material degradation should be investigated further.
- The current study is limited to machine learning techniques such as Lasso, Ridge and Elastic net. Future work should investigate other machine learning techniques such as Random Forest, Support Vector Machine, to name a few. Also the

application of machine learning for fragility curves is limited to two-span box-girder bridges with circular columns in Era 11. Future work can focus on expanding the use of the method and tool to other bridge types common in California.

- The current study has adopted relevant capacity models for the bridge type and design era of interest. In theory, the subgrouping of bridges presented in this paper may also have slight variations in component capacities. However, such refined capacity estimates that are attribute-dependent for a range of damage states and components are still rather lacking and typically require extensive additional experimental testing for model building or validation. As a result, the current study has adopted capacity estimates appropriate for the bridge class and era, where uncertainty in these capacity models is generally a result of the attribute variation within the class. Further studies are needed for the development of refined capacity models per damage state and component associated with variations in bridge attributes. Currently these variations are generally reflected in the uncertainty in a general capacity model per component, overall bridge class, and design era.

APPENDIX A. EARTHQUAKE RECORDS USED FOR FRAGILITY ANALYSIS

Earthquake no:	PEER Record Sequence Number	Scale Factor	Sa (1.0, g)	V_s30 (m/sec)	Arias Intensity (m/sec)	Earthquake Name	Year	Station Name	Magnitude	Mechanism	R_{jb} (km)	R_{rup} (km)
1	0007	1.18	0.04	219.31	0	"Northwest Calif-02"	1941	"Ferndale City Hall"	6.6	strike slip	91.15	91.22
2	0009	1.17	0.06	213.44	0.1	"Borrego"	1942	"El Centro Array #9"	6.5	strike slip	56.88	56.88
3	0020	1.10	0.35	219.31	0.5	"Northern Calif-03"	1954	"Ferndale City Hall"	6.5	strike slip	26.72	27.02
4	0051	1.02	0.05	280.56	0	"San Fernando"	1971	"2516 Via Tejon PV"	6.61	Reverse	55.2	55.2
5	0056	0.90	0.03	235.00	0.1	"San Fernando"	1971	"Carbon Canyon Dam"	6.61	Reverse	61.79	61.79
6	0058	0.87	0.02	477.22	0	"San Fernando"	1971	"Cedar Springs Pumphouse"	6.61	Reverse	92.25	92.59
7	0065	1.20	0.07	308.35	0.1	"San Fernando"	1971	"Gormon - Oso Pump Plant"	6.61	Reverse	43.95	46.78
8	0068	0.92	0.16	316.46	0.7	"San Fernando"	1971	"LA - Hollywood Stor FF"	6.61	Reverse	22.77	22.77
9	0070	1.12	0.37	425.34	0.3	"San Fernando"	1971	"Lake Hughes #1"	6.61	Reverse	22.23	27.4
10	0078	1.04	0.14	452.86	0.3	"San Fernando"	1971	"Palmdale Fire Station"	6.61	Reverse	24.16	28.99
11	0092	0.81	0.01	347.67	0	"San Fernando"	1971	"Wheeler Ridge - Ground"	6.61	Reverse	68.38	70.23
12	0122	0.81	0.11	249.28	0.1	"Friuli Italy-01"	1976	"Codroipo"	6.5	Reverse	33.32	33.4
13	0126	2.11	1.33	259.59	5.7	"Gazli USSR"	1976	"Karakyr"	6.8	Reverse	3.92	5.46
14	0126	1.03	0.65	259.59	5.7	"Gazli USSR"	1976	"Karakyr"	6.8	Reverse	3.92	5.46

15	0160	2.27	1.01	223.03	6.1	"Imperial Valley-06"	1979	"Bonds Corner"	6.53	strike slip	0.44	2.66
16	0160	1.11	0.49	223.03	6.1	"Imperial Valley-06"	1979	"Bonds Corner"	6.53	strike slip	0.44	2.66
17	0161	1.01	0.26	208.71	0.4	"Imperial Valley-06"	1979	"Brawley Airport"	6.53	strike slip	8.54	10.42
18	0162	0.92	0.15	231.23	0.9	"Imperial Valley-06"	1979	"Calexico Fire Station"	6.53	strike slip	10.45	10.45
19	0172	1.04	0.08	237.33	0.3	"Imperial Valley-06"	1979	"El Centro Array #1"	6.53	strike slip	19.76	21.68
20	0174	2.45	0.58	196.25	2	"Imperial Valley-06"	1979	"El Centro Array #11"	6.53	strike slip	12.56	12.56
21	0174	0.91	0.22	196.25	2	"Imperial Valley-06"	1979	"El Centro Array #11"	6.53	strike slip	12.56	12.56
22	0175	0.91	0.16	196.88	0.4	"Imperial Valley-06"	1979	"El Centro Array #12"	6.53	strike slip	17.94	17.94
23	0179	2.13	1.14	208.91	1.4	"Imperial Valley-06"	1979	"El Centro Array #4"	6.53	strike slip	4.9	7.05
24	0179	0.86	0.46	208.91	1.4	"Imperial Valley-06"	1979	"El Centro Array #4"	6.53	strike slip	4.9	7.05
25	0180	2.25	1.33	205.63	1.7	"Imperial Valley-06"	1979	"El Centro Array #5"	6.53	strike slip	1.76	3.95
26	0180	1.09	0.65	205.63	1.7	"Imperial Valley-06"	1979	"El Centro Array #5"	6.53	strike slip	1.76	3.95
27	0181	2.37	1.15	203.22	1.8	"Imperial Valley-06"	1979	"El Centro Array #6"	6.53	strike slip	0	1.35
28	0181	1.05	0.51	203.22	1.8	"Imperial Valley-06"	1979	"El Centro Array #6"	6.53	strike slip	0	1.35
29	0182	2.27	1.53	210.51	1.7	"Imperial Valley-06"	1979	"El Centro Array #7"	6.53	strike slip	0.56	0.56
30	0182	0.98	0.66	210.51	1.7	"Imperial Valley-06"	1979	"El Centro Array #7"	6.53	strike slip	0.56	0.56
31	0183	2.24	0.78	206.08	1.6	"Imperial Valley-06"	1979	"El Centro Array #8"	6.53	strike slip	3.86	3.86
32	0183	0.90	0.31	206.08	1.6	"Imperial Valley-06"	1979	"El Centro Array #8"	6.53	strike slip	3.86	3.86

33	0184	1.85	0.79	202.26	2.1	"Imperial Valley-06"	1979	"El Centro Differential Array"	6.53	strike slip	5.09	5.09
34	0184	1.02	0.44	202.26	2.1	"Imperial Valley-06"	1979	"El Centro Differential Array"	6.53	strike slip	5.09	5.09
35	0188	0.96	0.04	316.64	0.1	"Imperial Valley-06"	1979	"Plaster City"	6.53	strike slip	30.33	30.33
36	0191	0.88	0.06	242.05	0.3	"Imperial Valley-06"	1979	"Victoria"	6.53	strike slip	31.92	31.92
37	0285	0.99	0.27	649.67	0.4	"Irpinia Italy-01"	1980	"Bagnoli Irpinio"	6.9	Normal	8.14	8.18
38	0287	0.86	0.04	356.39	0	"Irpinia Italy-01"	1980	"Bovino"	6.9	Normal	44.62	46.25
39	0288	1.00	0.10	561.04	0.5	"Irpinia Italy-01"	1980	"Brienza"	6.9	Normal	22.54	22.56
40	0294	0.87	0.05	496.46	0	"Irpinia Italy-01"	1980	"Tricarico"	6.9	Normal	51.74	53.16
41	0427	1.03	0.02	671.52	0	"Taiwan SMART1(25)"	1983	"SMART1 E02"	6.5	Reverse	91.54	92.04
42	0432	1.01	0.05	267.67	0	"Taiwan SMART1(25)"	1983	"SMART1 O01"	6.5	Reverse	97.16	97.63
43	0436	1.01	0.02	279.97	0	"Borah Peak ID-01"	1983	"CPP-601"	6.88	Normal	82.6	82.6
44	0440	0.91	0.01	324.20	0	"Borah Peak ID-01"	1983	"TRA-642 ETR Reactor Bldg(Bsmt)"	6.88	Normal	79.59	79.59
45	0441	1.07	0.02	324.20	0	"Borah Peak ID-01"	1983	"TRA-670 ATR Reactor Bldg(Bsmt)"	6.88	Normal	80	80
46	0587	0.99	0.21	551.30	0.7	"New Zealand-02"	1987	"Matahina Dam"	6.6	Normal	16.09	16.09
47	0721	2.27	0.66	192.05	1.1	"Superstition Hills-02"	1987	"El Centro Imp. Co. Cent"	6.54	strike slip	18.2	18.2
48	0721	0.95	0.28	192.05	1.1	"Superstition Hills-02"	1987	"El Centro Imp. Co. Cent"	6.54	strike slip	18.2	18.2
49	0723	2.22	1.60	348.69	3.7	"Superstition Hills-02"	1987	"Parachute Test Site"	6.54	strike slip	0.95	0.95
50	0723	1.08	0.78	348.69	3.7	"Superstition Hills-02"	1987	"Parachute Test Site"	6.54	strike slip	0.95	0.95
51	0724	1.06	0.16	316.64	0.6	"Superstition Hills-02"	1987	"Plaster City"	6.54	strike slip	22.25	22.25

52	0726	1.08	0.19	191.14	0.4	"Superstition Hills-02"	1987	"Salton Sea Wildlife Refuge"	6.54	strike slip	25.88	25.88
53	0730	1.07	0.32	343.53	0.3	"Spitak Armenia"	1988	"Gukasian"	6.77	Reverse Oblique	23.99	23.99
54	0737	0.95	0.16	239.69	0.5	"Loma Prieta"	1989	"Agnews State Hospital"	6.93	Reverse Oblique	24.27	24.57
55	0739	0.91	0.16	488.77	0.8	"Loma Prieta"	1989	"Anderson Dam (Downstream)"	6.93	Reverse Oblique	19.9	20.26
56	0741	2.30	1.23	476.54	5.4	"Loma Prieta"	1989	"BRAN"	6.93	Reverse Oblique	3.85	10.72
57	0741	0.85	0.46	476.54	5.4	"Loma Prieta"	1989	"BRAN"	6.93	Reverse Oblique	3.85	10.72
58	0745	0.90	0.05	422.79	0.2	"Loma Prieta"	1989	"Bear Valley #14 Upper Butts Rn"	6.93	Reverse Oblique	71.28	71.39
59	0747	0.81	0.03	509.87	0	"Loma Prieta"	1989	"Bear Valley #7 Pinnacles"	6.93	Reverse Oblique	68.22	69.38
60	0748	0.99	0.14	627.59	0.2	"Loma Prieta"	1989	"Belmont - Envirotech"	6.93	Reverse Oblique	43.94	44.11
61	0753	2.47	1.24	462.24	3.2	"Loma Prieta"	1989	"Corralitos"	6.93	Reverse Oblique	0.16	3.85
62	0753	1.20	0.61	462.24	3.2	"Loma Prieta"	1989	"Corralitos"	6.93	Reverse Oblique	0.16	3.85
63	0764	1.06	0.39	308.55	0.7	"Loma Prieta"	1989	"Gilroy - Historic Bldg."	6.93	Reverse Oblique	10.27	10.97
64	0767	2.11	0.67	349.85	2.1	"Loma Prieta"	1989	"Gilroy Array #3"	6.93	Reverse Oblique	12.23	12.82
65	0767	1.09	0.35	349.85	2.1	"Loma Prieta"	1989	"Gilroy Array #3"	6.93	Reverse Oblique	12.23	12.82
66	0776	1.77	1.26	282.14	2.2	"Loma Prieta"	1989	"Hollister - South and Pine"	6.93	Reverse Oblique	27.67	27.93
67	0776	1.04	0.74	282.14	2.2	"Loma Prieta"	1989	"Hollister - South and Pine"	6.93	Reverse Oblique	27.67	27.93
68	0779	1.58	1.19	594.83	7.9	"Loma Prieta"	1989	"LGPC"	6.93	Reverse Oblique	0	3.88
69	0779	1.08	0.82	594.83	7.9	"Loma Prieta"	1989	"LGPC"	6.93	Reverse Oblique	0	3.88

70	0800	1.00	0.10	279.56	0.2	"Loma Prieta"	1989	"Salinas - John and Work"	6.93	Reverse Oblique	28.66	32.78
71	0803	2.27	1.37	347.90	1.3	"Loma Prieta"	1989	"Saratoga - W Valley Coll."	6.93	Reverse Oblique	8.48	9.31
72	0803	0.84	0.51	347.90	1.3	"Loma Prieta"	1989	"Saratoga - W Valley Coll."	6.93	Reverse Oblique	8.48	9.31
73	0821	2.42	1.87	352.05	1.8	"Erzican Turkey"	1992	"Erzincan"	6.69	strike slip	0	4.38
74	0821	1.08	0.83	352.05	1.8	"Erzican Turkey"	1992	"Erzincan"	6.69	strike slip	0	4.38
75	0825	2.29	1.39	567.78	6	"Cape Mendocino"	1992	"Cape Mendocino"	7.01	Reverse	0	6.96
76	0825	1.12	0.68	567.78	6	"Cape Mendocino"	1992	"Cape Mendocino"	7.01	Reverse	0	6.96
77	0827	0.95	0.17	457.06	0.3	"Cape Mendocino"	1992	"Fortuna - Fortuna Blvd"	7.01	Reverse	15.97	19.95
78	0828	2.36	1.93	422.17	3.8	"Cape Mendocino"	1992	"Petrolia"	7.01	Reverse	0	8.18
79	0828	1.05	0.86	422.17	3.8	"Cape Mendocino"	1992	"Petrolia"	7.01	Reverse	0	8.18
80	0860	1.16	0.11	328.09	0.3	"Landers"	1992	"Hemet Fire Station"	7.28	strike slip	68.66	68.66
81	0880	1.01	0.09	355.42	0.4	"Landers"	1992	"Mission Creek Fault"	7.28	strike slip	26.96	26.96
82	0881	0.94	0.20	396.41	1.2	"Landers"	1992	"Morongo Valley Fire Station"	7.28	strike slip	17.36	17.36
83	0897	1.04	0.03	635.01	0.1	"Landers"	1992	"Twentynine Palms"	7.28	strike slip	41.43	41.43
84	0900	2.18	0.92	353.63	0.9	"Landers"	1992	"Yermo Fire Station"	7.28	strike slip	23.62	23.62
85	0900	0.88	0.37	353.63	0.9	"Landers"	1992	"Yermo Fire Station"	7.28	strike slip	23.62	23.62
86	0952	0.88	0.26	545.66	3	"Northridge-01"	1994	"Beverly Hills - 12520 Mulhol"	6.69	Reverse	12.39	18.36
87	0953	1.18	1.15	355.81	4.5	"Northridge-01"	1994	"Beverly Hills - 14145 Mulhol"	6.69	Reverse	9.44	17.15
88	0966	1.00	0.08	324.79	0.1	"Northridge-01"	1994	"Covina - W Badillo"	6.69	Reverse	53.21	53.45
89	0968	0.97	0.15	271.90	0.6	"Northridge-01"	1994	"Downey - Co Maint Bldg"	6.69	Reverse	43.2	46.74

90	0975	0.91	0.09	362.31	0.1	"Northridge-01"	1994	"Glendora - N Oakbank"	6.69	Reverse	53.71	53.94
91	0982	1.74	2.48	373.07	5.3	"Northridge-01"	1994	"Jensen Filter Plant Administrative Building"	6.69	Reverse	0	5.43
92	0982	0.93	1.32	373.07	5.3	"Northridge-01"	1994	"Jensen Filter Plant Administrative Building"	6.69	Reverse	0	5.43
93	0983	1.93	1.93	525.79	6.5	"Northridge-01"	1994	"Jensen Filter Plant Generator Building"	6.69	Reverse	0	5.43
94	0983	1.07	1.07	525.79	6.5	"Northridge-01"	1994	"Jensen Filter Plant Generator Building"	6.69	Reverse	0	5.43
95	0984	1.05	0.14	301.00	0.4	"Northridge-01"	1994	"LA - 116th St School"	6.69	Reverse	36.39	41.17
96	0990	0.98	0.15	365.22	1.1	"Northridge-01"	1994	"LA - City Terrace"	6.69	Reverse	35.03	36.62
97	0998	1.00	0.18	315.06	1.4	"Northridge-01"	1994	"LA - N Westmoreland"	6.69	Reverse	23.4	26.73
98	1001	0.98	0.19	285.28	0.7	"Northridge-01"	1994	"LA - S Grand Ave"	6.69	Reverse	29.52	33.99
99	1004	1.66	1.42	380.06	7	"Northridge-01"	1994	"LA - Sepulveda VA Hospital"	6.69	Reverse	0	8.44
100	1004	0.92	0.78	380.06	7	"Northridge-01"	1994	"LA - Sepulveda VA Hospital"	6.69	Reverse	0	8.44
101	1006	1.09	0.25	398.42	1.6	"Northridge-01"	1994	"LA - UCLA Grounds"	6.69	Reverse	13.8	22.49
102	1013	2.33	1.46	628.99	1.8	"Northridge-01"	1994	"LA Dam"	6.69	Reverse	0	5.92
103	1013	1.13	0.71	628.99	1.8	"Northridge-01"	1994	"LA Dam"	6.69	Reverse	0	5.92
104	1037	0.96	0.03	422.73	0	"Northridge-01"	1994	"Mojave - Oak Creek Canyon"	6.69	Reverse	75.64	75.8
105	1044	1.71	1.71	269.14	5.7	"Northridge-01"	1994	"Newhall - Fire Sta"	6.69	Reverse	3.16	5.92
106	1044	0.91	0.91	269.14	5.7	"Northridge-01"	1994	"Newhall - Fire Sta"	6.69	Reverse	3.16	5.92
107	1052	0.97	0.50	508.08	1.8	"Northridge-01"	1994	"Pacoima Kagel Canyon"	6.69	Reverse	5.26	7.26
108	1054	2.12	2.47	325.67	3.1	"Northridge-01"	1994	"Pardee - SCE"	6.69	Reverse	5.54	7.46
109	1054	1.17	1.37	325.67	3.1	"Northridge-01"	1994	"Pardee - SCE"	6.69	Reverse	5.54	7.46
110	1061	1.14	0.07	580.03	0.1	"Northridge-01"	1994	"Rancho Palos Verdes - Hawth"	6.69	Reverse	48.02	52.18

111	1063	1.86	2.72	282.25	7.5	"Northridge-01"	1994	"Rinaldi Receiving Sta"	6.69	Reverse	0	6.5
112	1063	0.91	1.33	282.25	7.5	"Northridge-01"	1994	"Rinaldi Receiving Sta"	6.69	Reverse	0	6.5
113	1080	2.32	1.66	557.42	4.1	"Northridge-01"	1994	"Simi Valley - Katherine Rd"	6.69	Reverse	0	13.42
114	1080	1.06	0.76	557.42	4.1	"Northridge-01"	1994	"Simi Valley - Katherine Rd"	6.69	Reverse	0	13.42
115	1084	1.62	2.24	251.24	6	"Northridge-01"	1994	"Sylmar - Converter Sta"	6.69	Reverse	0	5.35
116	1084	1.01	1.40	251.24	6	"Northridge-01"	1994	"Sylmar - Converter Sta"	6.69	Reverse	0	5.35
117	1086	1.75	1.14	440.54	5	"Northridge-01"	1994	"Sylmar - Olive View Med FF"	6.69	Reverse	1.74	5.3
118	1086	0.97	1.12	440.54	5	"Northridge-01"	1994	"Sylmar - Olive View Med FF"	6.69	Reverse	1.74	5.3
119	1097	0.98	0.03	506.00	0	"Northridge-01"	1994	"Wrightwood - Nielson Ranch"	6.69	Reverse	81.54	81.69
120	1101	1.87	1.58	256.00	2	"Kobe Japan"	1995	"Amagasaki"	6.9	strike slip	11.34	11.34
121	1101	0.97	0.82	256.00	2	"Kobe Japan"	1995	"Amagasaki"	6.9	strike slip	11.34	11.34
122	1106	1.69	2.34	312.00	8.4	"Kobe Japan"	1995	"KJMA"	6.9	strike slip	0.94	0.96
123	1106	1.16	1.61	312.00	8.4	"Kobe Japan"	1995	"KJMA"	6.9	strike slip	0.94	0.96
124	1107	0.97	0.33	312.00	1.7	"Kobe Japan"	1995	"Kakogawa"	6.9	strike slip	22.5	22.5
125	1109	0.91	0.03	609.00	0.1	"Kobe Japan"	1995	"MZH"	6.9	strike slip	69.04	70.26
126	1111	2.31	0.66	609.00	3.4	"Kobe Japan"	1995	"Nishi-Akashi"	6.9	strike slip	7.08	7.08
127	1111	1.06	0.30	609.00	3.4	"Kobe Japan"	1995	"Nishi-Akashi"	6.9	strike slip	7.08	7.08
128	1114	2.31	2.15	198.00	1.8	"Kobe Japan"	1995	"Port Island (0 m)"	6.9	strike slip	3.31	3.31
129	1114	1.13	1.05	198.00	1.8	"Kobe Japan"	1995	"Port Island (0 m)"	6.9	strike slip	3.31	3.31
130	1115	1.02	0.18	256.00	0.6	"Kobe Japan"	1995	"Sakai"	6.9	strike slip	28.08	28.08

131	1116	1.02	0.27	256.00	0.8	"Kobe Japan"	1995	"Shin-Osaka"	6.9	strike slip	19.14	19.15
132	1119	2.27	1.86	312.00	3.9	"Kobe Japan"	1995	"Takarazuka"	6.9	strike slip	0	0.27
133	1119	1.11	0.91	312.00	3.9	"Kobe Japan"	1995	"Takarazuka"	6.9	strike slip	0	0.27
134	1120	1.62	2.09	256.00	8.7	"Kobe Japan"	1995	"Takatori"	6.9	strike slip	1.46	1.47
135	1120	1.02	1.31	256.00	8.7	"Kobe Japan"	1995	"Takatori"	6.9	strike slip	1.46	1.47
136	1121	0.91	0.37	256.00	1.1	"Kobe Japan"	1995	"Yae"	6.9	strike slip	27.77	27.77
137	1154	1.00	0.12	612.78	0.1	"Kocaeli Turkey"	1999	"Bursa Sivil"	7.51	strike slip	65.53	65.53
138	1158	2.01	0.98	281.86	1.3	"Kocaeli Turkey"	1999	"Duzce"	7.51	strike slip	13.6	15.37
139	1158	0.92	0.45	281.86	1.3	"Kocaeli Turkey"	1999	"Duzce"	7.51	strike slip	13.6	15.37
140	1162	1.06	0.14	347.62	0.3	"Kocaeli Turkey"	1999	"Goynuk"	7.51	strike slip	31.74	31.74
141	1166	0.94	0.21	476.62	0.4	"Kocaeli Turkey"	1999	"Iznik"	7.51	strike slip	30.73	30.73
142	1176	2.33	0.90	297.00	1.3	"Kocaeli Turkey"	1999	"Yarimca"	7.51	strike slip	1.38	4.83
143	1176	1.14	0.44	297.00	1.3	"Kocaeli Turkey"	1999	"Yarimca"	7.51	strike slip	1.38	4.83
144	1197	1.49	1.51	542.61	5.9	"Chi-Chi Taiwan"	1999	"CHY028"	7.62	Reverse Oblique	3.12	3.12
145	1197	1.02	1.04	542.61	5.9	"Chi-Chi Taiwan"	1999	"CHY028"	7.62	Reverse Oblique	3.12	3.12
146	1231	1.11	2.34	496.21	9.3	"Chi-Chi Taiwan"	1999	"CHY080"	7.62	Reverse Oblique	0.11	2.69
147	1234	0.92	0.21	665.20	1	"Chi-Chi Taiwan"	1999	"CHY086"	7.62	Reverse Oblique	27.57	28.42
148	1244	2.35	1.73	258.89	3	"Chi-Chi Taiwan"	1999	"CHY101"	7.62	Reverse Oblique	9.94	9.94

149	1244	1.04	0.77	258.89	3	"Chi-Chi Taiwan"	1999	"CHY101"	7.62	Reverse Oblique	9.94	9.94
150	1289	1.07	0.26	484.97	0.3	"Chi-Chi Taiwan"	1999	"HWA041"	7.62	Reverse Oblique	43.37	47.76
151	1486	1.10	0.18	465.55	0.4	"Chi-Chi Taiwan"	1999	"TCU046"	7.62	Reverse Oblique	16.74	16.74
152	1492	2.22	2.27	579.10	2.9	"Chi-Chi Taiwan"	1999	"TCU052"	7.62	Reverse Oblique	0	0.66
153	1492	0.96	0.98	579.10	2.9	"Chi-Chi Taiwan"	1999	"TCU052"	7.62	Reverse Oblique	0	0.66
154	1503	1.90	2.22	305.85	7.7	"Chi-Chi Taiwan"	1999	"TCU065"	7.62	Reverse Oblique	0.57	0.57
155	1503	0.93	1.09	305.85	7.7	"Chi-Chi Taiwan"	1999	"TCU065"	7.62	Reverse Oblique	0.57	0.57
156	1505	1.51	1.06	487.34	3.3	"Chi-Chi Taiwan"	1999	"TCU068"	7.62	Reverse Oblique	0	0.32
157	1505	1.04	0.73	487.34	3.3	"Chi-Chi Taiwan"	1999	"TCU068"	7.62	Reverse Oblique	0	0.32
158	1507	2.05	1.43	624.85	9.5	"Chi-Chi Taiwan"	1999	"TCU071"	7.62	Reverse Oblique	0	5.8
159	1507	1.00	0.70	624.85	9.5	"Chi-Chi Taiwan"	1999	"TCU071"	7.62	Reverse Oblique	0	5.8
160	1509	1.85	2.11	549.43	6.4	"Chi-Chi Taiwan"	1999	"TCU074"	7.62	Reverse Oblique	0	13.46
161	1509	0.90	1.03	549.43	6.4	"Chi-Chi Taiwan"	1999	"TCU074"	7.62	Reverse Oblique	0	13.46
162	1510	1.99	0.69	573.02	3	"Chi-Chi Taiwan"	1999	"TCU075"	7.62	Reverse Oblique	0.89	0.89
163	1510	1.03	0.36	573.02	3	"Chi-Chi Taiwan"	1999	"TCU075"	7.62	Reverse Oblique	0.89	0.89
164	1513	1.39	0.88	363.99	7.7	"Chi-Chi Taiwan"	1999	"TCU079"	7.62	Reverse Oblique	0	10.97
165	1513	0.93	0.59	363.99	7.7	"Chi-Chi Taiwan"	1999	"TCU079"	7.62	Reverse Oblique	0	10.97
166	1517	1.06	1.99	665.20	20.3	"Chi-Chi Taiwan"	1999	"TCU084"	7.62	Reverse Oblique	0	11.48

167	1549	2.42	1.37	511.18	9.3	"Chi-Chi Taiwan"	1999	"TCU129"	7.62	Reverse Oblique	1.83	1.83
168	1549	0.95	0.54	511.18	9.3	"Chi-Chi Taiwan"	1999	"TCU129"	7.62	Reverse Oblique	1.83	1.83
169	1551	1.04	0.45	652.85	1.7	"Chi-Chi Taiwan"	1999	"TCU138"	7.62	Reverse Oblique	9.78	9.78
170	1602	2.23	2.16	293.57	3.7	"Duzce Turkey"	1999	"Bolu"	7.14	strike slip	12.02	12.04
171	1602	1.09	1.05	293.57	3.7	"Duzce Turkey"	1999	"Bolu"	7.14	strike slip	12.02	12.04
172	1605	2.36	1.51	281.86	2.9	"Duzce Turkey"	1999	"Duzce"	7.14	strike slip	0	6.58
173	1605	1.15	0.74	281.86	2.9	"Duzce Turkey"	1999	"Duzce"	7.14	strike slip	0	6.58
174	1620	1.12	0.02	411.91	0	"Duzce Turkey"	1999	"Sakarya"	7.14	strike slip	45.16	45.16
175	1626	1.07	0.05	649.67	0.2	"Sitka Alaska"	1972	"Sitka Observatory"	7.68	strike slip	34.61	34.61
176	1627	1.07	0.03	432.58	0.1	"Caldiran Turkey"	1976	"Maku"	7.21	strike slip	50.78	50.82
177	1628	0.97	0.27	306.37	0.9	"St Elias Alaska"	1979	"Icy Bay"	7.54	Reverse	26.46	26.46
178	1636	1.08	0.13	302.64	0.4	"Manjil Iran"	1990	"Qazvin"	7.37	strike slip	49.97	49.97
179	1767	0.97	0.02	667.42	0	"Hector Mine"	1999	"Banning - Twin Pines Road"	7.13	strike slip	83.43	83.43
180	1782	1.03	0.08	436.14	0.1	"Hector Mine"	1999	"Forest Falls Post Office"	7.13	strike slip	74.92	74.92
181	1794	0.92	0.28	379.32	0.6	"Hector Mine"	1999	"Joshua Tree"	7.13	strike slip	31.06	31.06
182	2093	1.08	0.02	382.50	0	"Nenana Mountain Alaska"	2002	"TAPS Pump Station #09"	6.7	strike slip	104.73	104.73
183	2111	0.88	0.09	341.56	0.1	"Denali Alaska"	2002	"R109 (temp)"	7.9	strike slip	42.99	43
184	2114	2.40	1.79	329.40	1.9	"Denali Alaska"	2002	"TAPS Pump Station #10"	7.9	strike slip	0.18	2.74

185	2114	1.17	0.87	329.40	1.9	"Denali Alaska"	2002	"TAPS Pump Station #10"	7.9	strike slip	0.18	2.74
186	3583	1.22	0.07	309.41	0	"Taiwan SMART1(25)"	1983	"SMART1 I08"	6.5	Reverse	95.5	95.98
187	3594	1.04	0.06	300.22	0	"Taiwan SMART1(25)"	1983	"SMART1 M11"	6.5	Reverse	96.52	97
188	3744	1.06	0.40	566.42	0.6	"Cape Mendocino"	1992	"Bunker Hill FAA"	7.01	Reverse	8.49	12.24
189	3746	2.23	0.97	459.04	1.6	"Cape Mendocino"	1992	"Centerville Beach Naval Fac"	7.01	Reverse	16.44	18.31
190	3746	1.02	0.44	459.04	1.6	"Cape Mendocino"	1992	"Centerville Beach Naval Fac"	7.01	Reverse	16.44	18.31
191	3748	2.48	1.63	387.95	1.7	"Cape Mendocino"	1992	"Ferndale Fire Station"	7.01	Reverse	16.64	19.32
192	3748	1.21	0.80	387.95	1.7	"Cape Mendocino"	1992	"Ferndale Fire Station"	7.01	Reverse	16.64	19.32
193	3749	2.06	0.68	355.18	1.3	"Cape Mendocino"	1992	"Fortuna Fire Station"	7.01	Reverse	16.54	20.41
194	3749	0.98	0.32	355.18	1.3	"Cape Mendocino"	1992	"Fortuna Fire Station"	7.01	Reverse	16.54	20.41
195	3750	2.08	0.51	515.65	0.9	"Cape Mendocino"	1992	"Loleta Fire Station"	7.01	Reverse	23.46	25.91
196	3750	0.83	0.20	515.65	0.9	"Cape Mendocino"	1992	"Loleta Fire Station"	7.01	Reverse	23.46	25.91
197	3758	1.01	0.20	333.89	0.5	"Landers"	1992	"Thousand Palms Post Office"	7.28	strike slip	36.93	36.93
198	3882	1.22	0.02	571.63	0	"Tottori Japan"	2000	"HRS016"	6.61	strike slip	82.42	82.42
199	3899	1.00	0.01	617.44	0	"Tottori Japan"	2000	"HYGH02"	6.61	strike slip	88.75	88.75
200	3908	1.07	0.13	293.37	0.8	"Tottori Japan"	2000	"OKY005"	6.61	strike slip	28.81	28.82
201	3915	1.23	0.08	296.96	0.1	"Tottori Japan"	2000	"OKY012"	6.61	strike slip	66.24	66.25
202	3937	1.09	0.11	182.30	0.2	"Tottori Japan"	2000	"SMN005"	6.61	strike slip	45.73	45.73

203	3945	0.86	0.02	262.19	0	"Tottori Japan"	2000	"SMN017"	6.61	strike slip	77.85	77.85
204	3946	0.99	0.05	271.29	0.1	"Tottori Japan"	2000	"SMN018"	6.61	strike slip	85.31	85.31
205	3968	1.84	2.58	310.21	11.8	"Tottori Japan"	2000	"TTRH02"	6.61	strike slip	0.83	0.97
206	3968	1.02	1.43	310.21	11.8	"Tottori Japan"	2000	"TTRH02"	6.61	strike slip	0.83	0.97
207	3981	0.86	0.05	333.61	0	"San Simeon CA"	2003	"Coalinga - Fire Station 39"	6.52	Reverse	69.51	70.23
208	3987	0.87	0.03	280.64	0	"San Simeon CA"	2003	"Greenfield - Police Station"	6.52	Reverse	69.08	69.8
209	3994	1.05	0.10	365.15	0.2	"San Simeon CA"	2003	"San Luis Obispo - Lopez Lake Grounds"	6.52	Reverse	48.07	48.11
210	4031	2.28	0.76	410.66	1.9	"San Simeon CA"	2003	"Templeton - 1-story Hospital"	6.52	Reverse	5.07	6.22
211	4031	0.96	0.32	410.66	1.9	"San Simeon CA"	2003	"Templeton - 1-story Hospital"	6.52	Reverse	5.07	6.22
212	4040	2.28	1.74	487.40	8	"Bam Iran"	2003	"Bam"	6.6	strike slip	0.05	1.7
213	4040	0.99	0.75	487.40	8	"Bam Iran"	2003	"Bam"	6.6	strike slip	0.05	1.7
214	4054	0.83	0.04	574.88	0.2	"Bam Iran"	2003	"Mohammad Abad-e-Madkoon"	6.6	strike slip	46.2	46.22
215	4198	0.98	0.02	220.65	0	"Niigata Japan"	2004	"NIG008"	6.63	Reverse	83.83	84.28
216	4207	0.98	0.33	274.17	3.4	"Niigata Japan"	2004	"NIG017"	6.63	Reverse	4.22	12.81
217	4208	0.91	0.14	198.26	0.8	"Niigata Japan"	2004	"NIG018"	6.63	Reverse	21.55	25.84
218	4212	1.10	0.13	193.20	0.8	"Niigata Japan"	2004	"NIG022"	6.63	Reverse	17.57	18.03
219	4218	0.96	0.32	430.71	5.2	"Niigata Japan"	2004	"NIG028"	6.63	Reverse	0.46	9.79
220	4219	2.25	1.72	480.40	8.8	"Niigata Japan"	2004	"NIGH01"	6.63	Reverse	0.49	9.46
221	4219	1.10	0.84	480.40	8.8	"Niigata Japan"	2004	"NIGH01"	6.63	Reverse	0.49	9.46

222	4222	1.05	0.04	244.84	0.2	"Niigata Japan"	2004	"NIGH05"	6.63	Reverse	70.59	71.52
223	4228	2.42	0.96	375.00	2.2	"Niigata Japan"	2004	"NIGH11"	6.63	Reverse	6.27	8.93
224	4228	1.11	0.44	375.00	2.2	"Niigata Japan"	2004	"NIGH11"	6.63	Reverse	6.27	8.93
225	4451	1.97	1.71	462.23	3	"Montenegro Yugoslavia"	1979	"Bar-Skupstina Opstine"	7.1	Reverse	0	6.98
226	4451	1.23	1.07	462.23	3	"Montenegro Yugoslavia"	1979	"Bar-Skupstina Opstine"	7.1	Reverse	0	6.98
227	4456	0.93	0.42	543.26	4.6	"Montenegro Yugoslavia"	1979	"Petrovac - Hotel Olivia"	7.1	Reverse	0	8.01
228	4458	1.95	1.06	318.74	1.8	"Montenegro Yugoslavia"	1979	"Ulcinj - Hotel Olimpic"	7.1	Reverse	3.97	5.76
229	4458	1.05	0.57	318.74	1.8	"Montenegro Yugoslavia"	1979	"Ulcinj - Hotel Olimpic"	7.1	Reverse	3.97	5.76
230	4842	0.96	0.17	655.45	1.4	"Chuetsu-oki Japan"	2007	"Joetsu Uragawaraku Kamabucchi"	6.8	Reverse	18.6	22.74
231	4844	0.93	0.18	640.14	0.3	"Chuetsu-oki Japan"	2007	"Tokamachi Matsunoyama"	6.8	Reverse	23.01	28.75
232	4849	0.96	0.36	342.74	0.8	"Chuetsu-oki Japan"	2007	"Kubikiku Hyakken Joetsu City"	6.8	Reverse	20.71	22.18
233	4856	2.17	1.80	294.38	3.9	"Chuetsu-oki Japan"	2007	"Kashiwazaki City Center"	6.8	Reverse	0	11.09
234	4856	0.93	0.78	294.38	3.9	"Chuetsu-oki Japan"	2007	"Kashiwazaki City Center"	6.8	Reverse	0	11.09
235	4859	0.95	0.37	274.23	0.8	"Chuetsu-oki Japan"	2007	"Mitsuke Kazuiti Arita Town"	6.8	Reverse	11.35	20.33
236	4863	2.00	1.35	514.30	2.2	"Chuetsu-oki Japan"	2007	"Nagaoka"	6.8	Reverse	3.97	16.27
237	4863	1.17	0.79	514.30	2.2	"Chuetsu-oki Japan"	2007	"Nagaoka"	6.8	Reverse	3.97	16.27
238	4872	1.04	0.27	640.14	0.3	"Chuetsu-oki Japan"	2007	"Sawa Mizuguti Tokamachi"	6.8	Reverse	21.17	27.3
239	4874	2.42	1.28	561.59	5.3	"Chuetsu-oki Japan"	2007	"Oguni Nagaoka"	6.8	Reverse	10.31	20
240	4874	1.18	0.62	561.59	5.3	"Chuetsu-oki Japan"	2007	"Oguni Nagaoka"	6.8	Reverse	10.31	20
241	4875	1.08	0.89	282.57	6.4	"Chuetsu-oki Japan"	2007	"Kariwa"	6.8	Reverse	0	12

242	4876	2.11	1.98	655.45	8.6	"Chuetsu-oki Japan"	2007	"Kashiwazaki Nishiyamacho Ikeura"	6.8	Reverse	0	12.63
243	4876	1.03	0.96	655.45	8.6	"Chuetsu-oki Japan"	2007	"Kashiwazaki Nishiyamacho Ikeura"	6.8	Reverse	0	12.63
244	4879	1.09	0.57	265.82	0.7	"Chuetsu-oki Japan"	2007	"Yan Sakuramachi City watershed"	6.8	Reverse	12.98	18.97
245	4886	2.22	1.19	338.32	4.9	"Chuetsu-oki Japan"	2007	"Tamati Yone Izumozaki"	6.8	Reverse	0	11.48
246	4886	1.08	0.58	338.32	4.9	"Chuetsu-oki Japan"	2007	"Tamati Yone Izumozaki"	6.8	Reverse	0	11.48
247	4894	1.36	2.15	329.00	16.5	"Chuetsu-oki Japan"	2007	"Kashiwazaki NPP Unit 1: ground surface"	6.8	Reverse	0	10.97
248	4894	0.97	1.53	329.00	16.5	"Chuetsu-oki Japan"	2007	"Kashiwazaki NPP Unit 1: ground surface"	6.8	Reverse	0	10.97
249	4895	1.33	1.51	265.50	13.3	"Chuetsu-oki Japan"	2007	"Kashiwazaki NPP Unit 5: ground surface"	6.8	Reverse	0	10.97
250	4895	1.03	1.05	265.50	13.3	"Chuetsu-oki Japan"	2007	"Kashiwazaki NPP Unit 5: ground surface"	6.8	Reverse	0	10.97
251	4896	0.93	0.91	201.00	5.1	"Chuetsu-oki Japan"	2007	"Kashiwazaki NPP Service Hall Array 2.4 m depth"	6.8	Reverse	0	10.97
252	4997	1.00	0.09	305.54	0.1	"Chuetsu-oki Japan"	2007	"FKS028"	6.8	Reverse	52.63	55.38
253	5003	0.80	0.01	245.88	0	"Chuetsu-oki Japan"	2007	"FKSH04"	6.8	Reverse	93.48	95.05
254	5064	1.03	0.03	342.36	0	"Chuetsu-oki Japan"	2007	"GNM005"	6.8	Reverse	86.23	87.94
255	5254	0.96	0.02	220.65	0	"Chuetsu-oki Japan"	2007	"NIG008"	6.8	Reverse	81.51	83.31
256	5258	1.00	0.07	229.95	0.3	"Chuetsu-oki Japan"	2007	"NIG012"	6.8	Reverse	65.54	67.77
257	5264	1.77	1.66	198.26	5	"Chuetsu-oki Japan"	2007	"NIG018"	6.8	Reverse	0	10.78
258	5264	1.11	1.04	198.26	5	"Chuetsu-oki Japan"	2007	"NIG018"	6.8	Reverse	0	10.78

259	5461	0.89	0.02	279.36	0	"Iwate Japan"	2008	"AKT006"	6.9	Reverse	112.78	113.45
260	5467	0.98	0.02	449.45	0.1	"Iwate Japan"	2008	"AKT012"	6.9	Reverse	57.37	58.67
261	5471	1.08	0.09	158.16	0.3	"Iwate Japan"	2008	"AKT016"	6.9	Reverse	46.77	48.36
262	5490	1.14	0.01	232.58	0.1	"Iwate Japan"	2008	"AKTH14"	6.9	Reverse	95.32	96.11
263	5648	1.12	0.04	534.71	0.1	"Iwate Japan"	2008	"IWTH16"	6.9	Reverse	48.43	49.97
264	5656	2.34	0.78	486.41	3.5	"Iwate Japan"	2008	"IWTH24"	6.9	Reverse	3.1	5.18
265	5656	1.14	0.38	486.41	3.5	"Iwate Japan"	2008	"IWTH24"	6.9	Reverse	3.1	5.18
266	5657	1.85	1.40	506.44	26.1	"Iwate Japan"	2008	"IWTH25"	6.9	Reverse	0	4.8
267	5657	1.02	0.78	506.44	26.1	"Iwate Japan"	2008	"IWTH25"	6.9	Reverse	0	4.8
268	5658	2.37	1.06	371.06	14.1	"Iwate Japan"	2008	"IWTH26"	6.9	Reverse	5.97	6.02
269	5658	1.15	0.52	371.06	14.1	"Iwate Japan"	2008	"IWTH26"	6.9	Reverse	5.97	6.02
270	5663	2.38	0.96	479.37	9.4	"Iwate Japan"	2008	"MYG004"	6.9	Reverse	20.17	20.18
271	5663	1.03	0.41	479.37	9.4	"Iwate Japan"	2008	"MYG004"	6.9	Reverse	20.17	20.18
272	5664	2.38	1.07	361.24	4.2	"Iwate Japan"	2008	"MYG005"	6.9	Reverse	10.71	13.47
273	5664	1.16	0.52	361.24	4.2	"Iwate Japan"	2008	"MYG005"	6.9	Reverse	10.71	13.47
274	5768	0.99	0.03	291.48	0.1	"Iwate Japan"	2008	"YMTH09"	6.9	Reverse	47.01	48.59
275	5774	0.94	0.19	276.30	1	"Iwate Japan"	2008	"Nakashinden Town"	6.9	Reverse	29.37	29.38
276	5780	1.91	0.81	345.55	1.8	"Iwate Japan"	2008	"Iwadeyama"	6.9	Reverse	20.77	20.78
277	5780	0.91	0.39	345.55	1.8	"Iwate Japan"	2008	"Iwadeyama"	6.9	Reverse	20.77	20.78
278	5799	1.04	0.08	552.38	0.4	"Iwate Japan"	2008	"Misato Akita City - Tsuchizaki"	6.9	Reverse	39.86	41.72

279	5818	2.35	1.24	512.26	7.3	"Iwate Japan"	2008	"Kurihara City"	6.9	Reverse	12.83	12.85
280	5818	1.05	0.55	512.26	7.3	"Iwate Japan"	2008	"Kurihara City"	6.9	Reverse	12.83	12.85
281	5825	2.34	0.91	242.05	3.3	"El Mayor-Cucapah Mexico"	2010	"CERRO PRIETO GEOTHERMAL"	7.2	strike slip	8.88	10.92
282	5825	0.94	0.37	242.05	3.3	"El Mayor-Cucapah Mexico"	2010	"CERRO PRIETO GEOTHERMAL"	7.2	strike slip	8.88	10.92
283	5827	2.35	1.38	242.05	6.1	"El Mayor-Cucapah Mexico"	2010	"MICHOACAN DE OCAMPO"	7.2	strike slip	13.21	15.91
284	5827	1.15	0.67	242.05	6.1	"El Mayor-Cucapah Mexico"	2010	"MICHOACAN DE OCAMPO"	7.2	strike slip	13.21	15.91
285	5837	2.27	1.22	229.25	3.7	"El Mayor-Cucapah Mexico"	2010	"El Centro - Imperial and Ross"	7.2	strike slip	19.39	20.08
286	5837	0.92	0.49	229.25	3.7	"El Mayor-Cucapah Mexico"	2010	"El Centro - Imperial and Ross"	7.2	strike slip	19.39	20.08
287	5839	1.01	0.02	388.01	0	"El Mayor-Cucapah Mexico"	2010	"El Cajon - Marshall"	7.2	strike slip	115	115
288	5864	1.01	0.08	384.66	0	"El Mayor-Cucapah Mexico"	2010	"Frink"	7.2	strike slip	81.63	81.8
289	5970	0.82	0.01	619.00	0	"El Mayor-Cucapah Mexico"	2010	"Borrego Springs"	7.2	strike slip	91.9	91.9
290	5972	0.91	0.11	208.71	0.8	"El Mayor-Cucapah Mexico"	2010	"Brawley Airport"	7.2	strike slip	41.15	41.48
291	5975	1.87	0.60	231.23	2.4	"El Mayor-Cucapah Mexico"	2010	"Calexico Fire Station"	7.2	strike slip	19.12	20.46
292	5975	0.89	0.29	231.23	2.4	"El Mayor-Cucapah Mexico"	2010	"Calexico Fire Station"	7.2	strike slip	19.12	20.46
293	5985	2.19	1.22	202.26	4.3	"El Mayor-Cucapah Mexico"	2010	"El Centro Differential Array"	7.2	strike slip	22.83	23.42
294	5985	0.81	0.45	202.26	4.3	"El Mayor-Cucapah Mexico"	2010	"El Centro Differential Array"	7.2	strike slip	22.83	23.42
295	5991	1.76	1.01	202.85	3.6	"El Mayor-Cucapah Mexico"	2010	"El Centro Array #10"	7.2	strike slip	19.36	20.05
296	5991	1.10	0.63	202.85	3.6	"El Mayor-Cucapah Mexico"	2010	"El Centro Array #10"	7.2	strike slip	19.36	20.05

297	5992	2.50	1.51	196.25	5.5	"El Mayor-Cucapah Mexico"	2010	"El Centro Array #11"	7.2	strike slip	15.36	16.21
298	5992	1.08	0.65	196.25	5.5	"El Mayor-Cucapah Mexico"	2010	"El Centro Array #11"	7.2	strike slip	15.36	16.21
299	6515	0.95	0.02	279.58	0	"Niigata Japan"	2004	"FKS016"	6.63	Reverse	111.33	111.4
300	6783	1.01	0.02	265.60	0	"Niigata Japan"	2004	"TCG008"	6.63	Reverse	109.14	109.21
301	6886	1.00	0.16	280.26	0.9	"Darfield New Zealand"	2010	"Canterbury Aero Club"	7	strike slip	14.48	14.48
302	6893	2.14	0.86	344.02	2.8	"Darfield New Zealand"	2010	"DFHS"	7	strike slip	11.86	11.86
303	6893	1.11	0.44	344.02	2.8	"Darfield New Zealand"	2010	"DFHS"	7	strike slip	11.86	11.86
304	6906	1.79	1.82	344.02	4.7	"Darfield New Zealand"	2010	"GDLC"	7	strike slip	1.22	1.22
305	6906	1.12	1.14	344.02	4.7	"Darfield New Zealand"	2010	"GDLC"	7	strike slip	1.22	1.22
306	6911	2.04	1.42	326.01	3.2	"Darfield New Zealand"	2010	"HORC"	7	strike slip	7.29	7.29
307	6911	1.13	0.79	326.01	3.2	"Darfield New Zealand"	2010	"HORC"	7	strike slip	7.29	7.29
308	6927	2.26	1.28	263.20	2.7	"Darfield New Zealand"	2010	"LINC"	7	strike slip	5.07	7.11
309	6927	1.11	0.62	263.20	2.7	"Darfield New Zealand"	2010	"LINC"	7	strike slip	5.07	7.11
310	6928	0.98	0.17	649.67	0.7	"Darfield New Zealand"	2010	"LPCC"	7	strike slip	25.21	25.67
311	6933	1.09	0.05	342.70	0.1	"Darfield New Zealand"	2010	"MAYC"	7	strike slip	33.54	35.23
312	6953	2.16	0.64	206.00	1.3	"Darfield New Zealand"	2010	"Pages Road Pumping Station"	7	strike slip	24.55	24.55
313	6953	1.03	0.30	206.00	1.3	"Darfield New Zealand"	2010	"Pages Road Pumping Station"	7	strike slip	24.55	24.55
314	6962	2.23	0.85	295.74	1.6	"Darfield New Zealand"	2010	"ROLC"	7	strike slip	0	1.54

315	6962	1.09	0.42	295.74	1.6	"Darfield New Zealand"	2010	"ROLC"	7	strike slip	0	1.54
316	6965	0.95	0.12	263.20	0.7	"Darfield New Zealand"	2010	"SBRC"	7	strike slip	21.31	24.34
317	8161	2.49	1.67	196.88	3.2	"El Mayor-Cucapah Mexico"	2010	"El Centro Array #12"	7.2	strike slip	9.98	11.26
318	8161	1.22	0.81	196.88	3.2	"El Mayor-Cucapah Mexico"	2010	"El Centro Array #12"	7.2	strike slip	9.98	11.26
319	8163	1.02	0.02	483.02	0	"El Mayor-Cucapah Mexico"	2010	"SANTA ISABEL VIEJO"	7.2	strike slip	55.19	57.49
320	8166	1.01	0.19	425.00	-	"Duzce Turkey"	1999	"IRIGM 498"	7.14	strike slip	3.58	3.58

APPENDIX B. FRAGILITY CURVES IN TERMS OF PGA

Chapter 6 presented the approach and methodology for the generation of fragility curves. The median and dispersion of the fragility curves in terms of peak ground acceleration (PGA) is documented in the subsequent tables.

Table B1 – Fragility values in terms of PGA for two span continuous concrete box-girder fragilities with diaphragm abutments.

Design era	Bridge class	BSST-0		BSST-0		BSST-0		BSST-0		ζ^*
		λ	ζ	λ	ζ	λ	ζ	λ	ζ	
Era 11	S-E1-S22-C-D	0.13	0.59	0.30	0.61	0.63	0.64	0.91	0.64	0.62
	S-E1-S22-R-D	0.16	0.56	0.36	0.58	0.70	0.61	0.99	0.61	0.59
	T-E1-S22-C-D	0.07	0.79	0.18	0.83	0.42	0.93	0.66	0.94	0.87
	T-E1-S22-R-D	0.09	0.68	0.18	0.70	0.35	0.74	0.50	0.74	0.71
	M-E1-S22-C-D	0.07	0.74	0.16	0.75	0.36	1.00	0.53	1.00	0.87
	M-E1-S22-R-D	0.06	0.81	0.15	0.91	0.37	1.40	0.59	1.39	1.13
Era 22	S-E2-S22-C-D	0.15	0.61	0.53	0.60	1.12	0.66	1.45	0.66	0.63
	S-E2-S22-O-D	0.17	0.61	0.63	0.59	1.68	0.62	2.20	0.61	0.61
	T-E2-S22-C-D	0.11	0.68	0.38	0.64	0.89	0.74	1.17	0.75	0.70
	T-E2-S22-O-D	0.16	0.54	0.43	0.53	0.91	0.70	1.12	0.70	0.61
	M-E2-S22-C-D	0.09	0.70	0.30	0.68	0.60	0.86	0.77	0.86	0.78
	M-E2-S22-O-D	0.09	0.70	0.30	0.68	0.60	0.86	0.77	0.86	0.78
Era 33	S-E3-S22-C-D	0.15	0.62	0.53	0.60	1.44	0.66	2.04	0.66	0.63
	S-E3-S22-O-D	0.17	0.60	0.63	0.58	2.20	0.62	3.20	0.63	0.61
	T-E3-S22-C-D	0.11	0.68	0.38	0.64	1.16	0.75	1.66	0.76	0.71
	T-E3-S22-O-D	0.17	0.53	0.43	0.54	1.12	0.69	1.49	0.69	0.61
	M-E3-S22-C-D	0.09	0.70	0.30	0.69	0.77	0.87	1.07	0.87	0.78
	M-E3-S22-O-D	0.09	0.70	0.30	0.69	0.77	0.87	1.08	0.87	0.78

Table B2 – Fragility values in terms of PGA for two span continuous concrete box-girder fragilities with seat abutments.

Design era	Bridge class	BSST-0		BSST-0		BSST-0		BSST-0		ζ^*
		λ	ζ	λ	ζ	λ	ζ	λ	ζ	
Era 11	S-E1-S22-C-S	0.08	0.58	0.15	0.58	0.27	0.59	0.36	0.57	0.58
	S-E1-S22-R-S	0.08	0.60	0.14	0.62	0.24	0.62	0.33	0.61	0.61
	T-E1-S22-C-S	0.06	0.68	0.12	0.70	0.20	0.68	0.27	0.69	0.69
	T-E1-S22-R-S	0.09	0.71	0.14	0.71	0.23	0.69	0.31	0.69	0.70
	M-E1-S22-C-S	0.05	0.64	0.09	0.64	0.19	0.62	0.27	0.60	0.62
	M-E1-S22-R-S	0.08	0.65	0.13	0.65	0.23	0.64	0.31	0.63	0.64
Era 22	S-E2-S22-C-S	0.10	0.64	0.47	0.64	0.89	0.73	1.20	0.73	0.69
	S-E2-S22-O-S	0.12	0.55	0.49	0.53	0.96	0.60	1.29	0.60	0.57
	T-E2-S22-C-S	0.08	0.63	0.33	0.60	0.64	0.67	0.87	0.68	0.64
	T-E2-S22-O-S	0.09	0.55	0.33	0.52	0.65	0.57	0.87	0.58	0.55
	M-E2-S22-C-S	0.07	0.60	0.31	0.55	0.62	0.65	0.86	0.68	0.62
	M-E2-S22-O-S	0.07	0.63	0.37	0.59	0.79	0.80	1.12	0.82	0.71
Era 33	S-E3-S22-C-S	0.10	0.66	0.46	0.63	1.10	0.71	1.63	0.72	0.68
	S-E3-S22-O-S	0.12	0.55	0.49	0.53	1.11	0.57	1.61	0.57	0.56
	T-E3-S22-C-S	0.08	0.62	0.33	0.60	0.77	0.65	1.13	0.64	0.63
	T-E3-S22-O-S	0.09	0.54	0.33	0.52	0.72	0.56	1.01	0.56	0.54
	M-E3-S22-C-S	0.07	0.58	0.32	0.57	0.75	0.63	1.12	0.63	0.60
	M-E3-S22-O-S	0.07	0.65	0.37	0.60	0.94	0.76	1.46	0.75	0.69

Table B3 – Fragility values in terms of PGA for multi-span (S34) continuous concrete box-girder fragilities with diaphragm abutments.

Design era	Bridge class	BSST-0		BSST-0		BSST-0		BSST-0		ζ^*
		λ	ζ	λ	ζ	λ	ζ	λ	ζ	
Era 11	S-E1-S34-C-D	0.13	0.51	0.30	0.55	0.68	0.61	1.03	0.61	0.57
	S-E1-S34-R-D	0.07	0.78	0.23	0.89	0.82	1.24	1.59	1.24	1.03
	T-E1-S34-C-D	0.08	0.64	0.16	0.67	0.32	0.71	0.46	0.71	0.68
	T-E1-S34-R-D	0.07	0.68	0.17	0.73	0.39	0.83	0.59	0.83	0.77
	M-E1-S34-C-D	0.01	1.09	0.04	0.98	0.17	1.05	0.35	1.05	1.04
	M-E1-S34-R-D	0.01	1.09	0.04	0.98	0.17	1.05	0.35	1.05	1.04
Era 22	S-E2-S34-C-D	0.15	0.55	0.54	0.51	1.17	0.69	1.55	0.69	0.61
	S-E2-S34-O-D	0.19	0.49	0.69	0.47	1.71	0.64	2.29	0.64	0.56
	T-E2-S34-C-D	0.08	0.68	0.35	0.63	0.72	0.96	0.98	0.96	0.81
	T-E2-S34-O-D	0.12	0.62	0.45	0.58	0.95	0.87	1.27	0.88	0.74
	M-E2-S34-C-D	0.08	0.64	0.32	0.60	0.59	0.86	0.80	0.86	0.74
	M-E2-S34-O-D	0.02	0.79	0.42	0.61	2.00	1.82	4.13	1.81	1.26
Era 33	S-E3-S34-C-D	0.15	0.54	0.54	0.51	1.54	0.70	2.28	0.69	0.61
	S-E3-S34-O-D	0.19	0.50	0.69	0.47	2.29	0.65	3.44	0.67	0.57
	T-E3-S34-C-D	0.09	0.69	0.35	0.63	0.98	0.95	1.50	0.95	0.81
	T-E3-S34-O-D	0.12	0.61	0.45	0.58	1.27	0.88	1.91	0.87	0.73
	M-E3-S34-C-D	0.08	0.65	0.32	0.61	0.80	0.88	1.21	0.86	0.75
	M-E3-S34-O-D	0.02	0.78	0.42	0.61	4.07	1.79	9.10	1.97	1.29

Table B4 – Fragility values in terms of PGA for multi-span (S34) continuous concrete box-girder fragilities with seat abutments.

Design era	Bridge class	BSST-0		BSST-0		BSST-0		BSST-0		ζ^*
		λ	ζ	λ	ζ	λ	ζ	λ	ζ	
Era 11	S-E1-S34-C-S	0.10	0.53	0.19	0.52	0.34	0.52	0.47	0.51	0.52
	S-E1-S34-R-S	0.04	0.73	0.11	0.68	0.25	0.63	0.38	0.62	0.66
	T-E1-S34-C-S	0.05	0.74	0.10	0.70	0.19	0.69	0.27	0.67	0.70
	T-E1-S34-R-S	0.01	1.00	0.04	0.82	0.14	0.73	0.25	0.69	0.81
	M-E1-S34-C-S	0.01	0.93	0.04	0.84	0.12	0.77	0.19	0.75	0.82
	M-E1-S34-R-S	0.01	0.93	0.04	0.84	0.12	0.77	0.19	0.75	0.82
Era 22	S-E2-S34-C-S	0.08	0.73	0.42	0.75	0.80	0.97	1.15	0.98	0.86
	S-E2-S34-O-S	0.11	0.63	0.53	0.63	1.11	0.80	1.61	0.82	0.72
	T-E2-S34-C-S	0.03	0.79	0.29	0.68	0.63	1.02	1.01	1.09	0.89
	T-E2-S34-O-S	0.07	0.68	0.42	0.64	0.90	0.82	1.31	0.79	0.73
	M-E2-S34-C-S	0.06	0.75	0.26	0.70	0.46	0.87	0.64	0.89	0.80
	M-E2-S34-O-S	0.01	1.56	0.13	0.90	0.48	1.19	1.01	1.18	1.21
Era 33	S-E3-S34-C-S	0.08	0.72	0.43	0.74	1.10	0.91	1.76	0.95	0.83
	S-E3-S34-O-S	0.10	0.62	0.53	0.63	1.34	0.73	2.04	0.71	0.67
	T-E3-S34-C-S	0.03	0.78	0.29	0.68	0.85	0.93	1.44	0.89	0.82
	T-E3-S34-O-S	0.07	0.69	0.41	0.64	1.06	0.69	1.58	0.67	0.67
	M-E3-S34-C-S	0.06	0.74	0.26	0.70	0.61	0.85	0.93	0.85	0.78
	M-E3-S34-O-S	0.01	1.50	0.13	0.90	0.80	1.03	1.42	0.83	1.06

APPENDIX C. COMPONENT FRAGILITY CURVES FOR BRIDGE CLASSES

This appendix presents the component level fragility relationships for bridge classes mentioned in Chapter 6. Table C1 and C2 documents the median and deviation (logarithmic standard deviation) for the components for four damage states, for diaphragam and seat abutment bridges, respectively. When the component median value is more than 100, the corresponding median and dispersion values are reported as 99.00 and 0.00, respectively, to indicate that the contribution of the component to the system vulnerability is negligible. Note the IM of ground motion is $S_{a1.0s}$.

Table C1 – Component level fragility relationships for diaphragm abutment bridges.

	CDT-0		CDT-1		CDT-2		CDT-3	
Bridge class	λ	ζ	λ	ζ	λ	ζ	λ	ζ
S-E1-S22-C-D								
Column	0.13	0.62	0.31	0.62	0.69	0.62	1.05	0.62
Deck-max	0.65	0.59	1.94	0.59	16.26	0.59	24.42	0.59
Fnd-tran	1.61	0.96	11.04	0.96				
Fnd-rot	99.00	0.00	99.00	0.00				
Ab-Pass	1.04	0.73	3.47	0.73				
Ab-Act	0.50	0.73	1.38	0.73				
Ab-tran	0.18	0.62	0.71	0.62				
S-E1-S22-R-D								
Column	0.21	0.66	0.41	0.66	0.82	0.66	1.17	0.66
Deck-max	0.73	0.59	2.02	0.59	14.49	0.59	21.12	0.59
Fnd-tran	1.05	0.98	7.59	0.98				
Fnd-rot	99.00	0.00	99.00	0.00				
Ab-Pass	0.91	0.71	2.65	0.71				
Ab-Act	0.47	0.70	1.13	0.70				

Ab-tran	0.22	0.63	0.82	0.63				
T-E1-S22-C-D								
Column	0.08	0.71	0.20	0.71	0.46	0.71	0.72	0.71
Deck-max	0.41	0.54	1.17	0.54	9.13	0.54	13.52	0.54
Fnd-tran	2.23	0.90	11.25	0.90				
Fnd-rot	99.00	0.00	99.00	0.00				
Ab-Pass	0.75	0.72	2.55	0.72				
Ab-Act	0.35	0.73	0.98	0.73				
Ab-tran	0.11	0.58	0.43	0.58				
T-E1-S22-R-D								
Column	0.11	0.75	0.21	0.75	0.43	0.75	0.62	0.75
Deck-max	0.52	0.62	1.40	0.62	9.56	0.62	13.80	0.62
Fnd-tran	2.98	1.09	23.60	1.09				
Fnd-rot	99.00	0.00	99.00	0.00				
Ab-Pass	0.83	0.65	2.27	0.65				
Ab-Act	0.45	0.66	1.05	0.66				
Ab-tran	0.15	0.63	0.52	0.63				
M-E1-S22-C-D								
Column	0.07	1.11	0.18	1.11	0.44	1.11	0.69	1.11
Deck-max	0.41	0.70	1.10	0.70	7.20	0.70	10.32	0.70
Fnd-tran	2.05	0.82	10.22	0.82				
Fnd-rot	99.00	0.00	99.00	0.00				
Ab-Pass	0.77	0.65	1.91	0.65				
Ab-Act	0.43	0.65	0.93	0.65				
Ab-tran	0.12	0.69	0.42	0.69				
M-E1-S22-R-D								
Column	0.06	1.36	0.15	1.36	0.41	1.36	0.69	1.36
Deck-max	0.55	0.60	1.54	0.60	11.35	0.60	16.63	0.60
Fnd-tran	1.75	1.08	10.24	1.08				
Fnd-rot	99.00	0.00	99.00	0.00				
Ab-Pass	0.99	0.90	3.31	0.90				
Ab-Act	0.47	0.90	1.28	0.90				
Ab-tran	0.15	0.65	0.58	0.65				
S-E2-S22-C-D								
Column	0.23	0.69	0.95	0.69	1.44	0.69	1.92	0.69
Deck-max	0.65	0.68	1.96	0.68	16.53	0.68	24.84	0.68
Fnd-tran	1.72	1.14	12.95	1.14				
Fnd-rot	99.00	0.00	99.00	0.00				
Ab-Pass	1.05	0.73	3.30	0.73				

Ab-Act	0.50	0.74	1.36	0.74				
Ab-tran	0.17	0.71	0.69	0.71				
S-E2-S22-O-D								
Column	0.30	0.73	1.48	0.73	2.36	0.73	3.24	0.73
Deck-max	0.73	0.63	2.52	0.63				
Fnd-tran	1.03	1.00	7.89	1.00				
Fnd-rot	99.00	0.00	99.00	0.00				
Ab-Pass	0.94	0.78	3.35	0.78				
Ab-Act	0.42	0.78	1.23	0.78				
Ab-tran	0.17	0.64	0.79	0.64				
T-E2-S22-C-D								
Column	0.16	0.66	0.64	0.66	0.97	0.66	1.27	0.66
Deck-max	0.43	0.63	1.18	0.63				
Fnd-tran	1.36	0.97	8.66	0.97				
Fnd-rot	99.00	0.00	99.00	0.00				
Ab-Pass	0.80	0.66	2.36	0.66				
Ab-Act	0.40	0.65	1.00	0.65				
Ab-tran	0.12	0.64	0.44	0.64				
T-E2-S22-O-D								
Column	0.25	0.57	0.83	0.57	1.17	0.57	1.49	0.57
Deck-max	0.56	0.58	1.62	0.58				
Fnd-tran	1.12	1.05	10.61	1.05				
Fnd-rot	99.00	0.00	99.00	0.00				
Ab-Pass	1.52	0.96	8.03	0.96				
Ab-Act	0.53	0.93	2.10	0.93				
Ab-tran	0.16	0.59	0.59	0.59				
M-E2-S22-C-D								
Column	0.13	0.74	0.47	0.74	0.67	0.74	0.86	0.74
Deck-max	0.36	0.58	0.97	0.58				
Fnd-tran	1.21	1.10	8.04	1.10				
Fnd-rot	99.00	0.00	99.00	0.00				
Ab-Pass	0.58	0.69	1.64	0.69				
Ab-Act	0.31	0.69	0.73	0.69				
Ab-tran	0.11	0.60	0.37	0.60				
M-E2-S22-O-D								
Column	0.01	13.40	0.02	13.40	0.01	13.40	0.38	13.40
Deck-max	0.61	0.50	1.78	0.50				
Fnd-tran	0.59	0.74	3.18	0.74				
Fnd-rot	99.00	0.00	99.00	0.00				
Ab-Pass	0.79	0.58	2.35	0.58				

Ab-Act	0.41	0.59	1.02	0.59				
Ab-tran	0.16	0.50	0.63	0.50				
S-E3-S22-C-D								
Column	0.23	0.69	0.95	0.69	1.92	0.69	2.82	0.69
Deck-max	0.65	0.68	1.96	0.68				
Fnd-tran	1.72	1.14	12.95	1.14				
Fnd-rot	99.00	0.00	99.00	0.00				
Ab-Pass	1.05	0.73	3.30	0.73				
Ab-Act	0.50	0.74	1.36	0.74				
Ab-tran	0.17	0.71	0.69	0.71				
S-E3-S22-O-D								
Column	0.30	0.73	1.48	0.73	3.24	0.73	4.99	0.73
Deck-max	0.73	0.63	2.52	0.63				
Fnd-tran	1.03	1.00	7.89	1.00				
Fnd-rot	99.00	0.00	99.00	0.00				
Ab-Pass	0.94	0.78	3.35	0.78				
Ab-Act	0.42	0.78	1.23	0.78				
Ab-tran	0.17	0.64	0.79	0.64				
T-E3-S22-C-D								
Column	0.16	0.66	0.64	0.66	1.27	0.66	1.85	0.66
Deck-max	0.43	0.63	1.18	0.63				
Fnd-tran	1.36	0.97	8.66	0.97				
Fnd-rot	99.00	0.00	99.00	0.00				
Ab-Pass	0.80	0.66	2.36	0.66				
Ab-Act	0.40	0.65	1.00	0.65				
Ab-tran	0.12	0.64	0.44	0.64				
T-E3-S22-O-D								
Column	0.25	0.57	0.83	0.57	1.49	0.57	2.06	0.57
Deck-max	0.56	0.58	1.62	0.58				
Fnd-tran	1.12	1.05	10.61	1.05				
Fnd-rot	99.00	0.00	99.00	0.00				
Ab-Pass	1.52	0.96	8.03	0.96				
Ab-Act	0.53	0.93	2.10	0.93				
Ab-tran	0.16	0.59	0.59	0.59				
M-E3-S22-C-D								
Column	0.13	0.74	0.47	0.74	0.86	0.74	1.20	0.74
Deck-max	0.36	0.58	0.97	0.58				
Fnd-tran	1.21	1.10	8.04	1.10				
Fnd-rot	99.00	0.00	99.00	0.00				

Ab-Pass	0.58	0.69	1.64	0.69				
Ab-Act	0.31	0.69	0.73	0.69				
Ab-tran	0.11	0.60	0.37	0.60				
M-E3-S22-O-D								
Column	0.01	13.40	0.02	13.40	0.01	13.40	0.38	13.40
Deck-max	0.61	0.50	1.78	0.50				
Fnd-tran	0.59	0.74	3.18	0.74				
Fnd-rot	99.00	0.00	99.00	0.00				
Ab-Pass	0.79	0.58	2.35	0.58				
Ab-Act	0.41	0.59	1.02	0.59				
Ab-tran	0.16	0.50	0.63	0.50				
S-E1-S34-C-D								
Column	0.14	0.70	0.34	0.70	0.84	0.70	1.34	0.70
Deck-max	0.76	0.57	2.37	0.57				
Fnd-tran	1.36	0.86	8.49	0.86				
Fnd-rot	99.00	0.00	99.00	0.00				
Ab-Pass	1.05	0.73	3.66	0.73				
Ab-Act	0.46	0.68	1.29	0.68				
Ab-tran	0.20	0.57	0.80	0.57				
S-E1-S34-R-D								
Column	0.06	1.32	0.24	1.32	0.99	1.32	2.03	1.32
Deck-max	1.06	0.58	3.47	0.58				
Fnd-tran	1.09	0.80	6.96	0.80				
Fnd-rot	99.00	0.00	99.00	0.00				
Ab-Pass	1.09	0.62	3.71	0.62				
Ab-Act	0.51	0.63	1.45	0.63				
Ab-tran	0.29	0.60	1.30	0.60				
T-E1-S34-C-D								
Column	0.06	0.89	0.15	0.89	0.36	0.89	0.56	0.89
Deck-max	0.44	0.57	1.31	0.57				
Fnd-tran	1.72	0.90	8.84	0.90				
Fnd-rot	99.00	0.00	99.00	0.00				
Ab-Pass	0.71	0.56	2.15	0.56				
Ab-Act	0.35	0.57	0.90	0.57				
Ab-tran	0.11	0.59	0.46	0.59				
T-E1-S34-R-D								
Column	0.07	0.91	0.17	0.91	0.41	0.91	0.66	0.91
Deck-max	0.54	0.53	1.57	0.53				
Fnd-tran	3.86	0.93	37.46	0.93				

Fnd-rot	99.00	0.00	99.00	0.00				
Ab-Pass	0.86	0.63	2.58	0.63				
Ab-Act	0.43	0.63	1.08	0.63				
Ab-tran	0.15	0.55	0.58	0.55				
M-E1-S34-C-D								
Column	0.01	1.13	0.04	1.13	0.19	1.13	0.40	1.13
Deck-max	0.54	0.46	1.42	0.46				
Fnd-tran	3.68	1.05	34.68	1.05				
Fnd-rot	99.00	0.00	99.00	0.00				
Ab-Pass	0.81	0.60	2.52	0.60				
Ab-Act	0.41	0.62	1.08	0.62				
Ab-tran	0.17	0.46	0.60	0.46				
M-E1-S34-R-D								
Column	0.01	1.13	0.04	1.13	0.19	1.13	0.40	1.13
Deck-max	0.54	0.46	1.42	0.46				
Fnd-tran	3.68	1.05	34.68	1.05				
Fnd-rot	99.00	0.00	99.00	0.00				
Ab-Pass	0.81	0.60	2.52	0.60				
Ab-Act	0.41	0.62	1.08	0.62				
Ab-tran	0.17	0.46	0.60	0.46				
S-E2-S34-C-D								
Column	0.23	0.69	0.95	0.69	1.44	0.69	1.92	0.69
Deck-max	0.65	0.68	1.96	0.68				
Fnd-tran	1.72	1.14	12.95	1.14				
Fnd-rot	99.00	0.00	99.00	0.00				
Ab-Pass	1.05	0.73	3.30	0.73				
Ab-Act	0.50	0.74	1.36	0.74				
Ab-tran	0.17	0.71	0.69	0.71				
S-E2-S34-O-D								
Column	0.30	0.73	1.48	0.73	2.36	0.73	3.24	0.73
Deck-max	0.73	0.63	2.52	0.63				
Fnd-tran	1.03	1.00	7.89	1.00				
Fnd-rot	99.00	0.00	99.00	0.00				
Ab-Pass	0.94	0.78	3.35	0.78				
Ab-Act	0.42	0.78	1.23	0.78				
Ab-tran	0.17	0.64	0.79	0.64				
T-E2-S34-C-D								
Column	0.16	0.66	0.64	0.66	0.97	0.66	1.27	0.66
Deck-max	0.43	0.63	1.18	0.63				

Fnd-tran	1.36	0.97	8.66	0.97				
Fnd-rot	99.00	0.00	99.00	0.00				
Ab-Pass	0.80	0.66	2.36	0.66				
Ab-Act	0.40	0.65	1.00	0.65				
Ab-tran	0.12	0.64	0.44	0.64				
T-E2-S34-O-D								
Column	0.25	0.57	0.83	0.57	1.17	0.57	1.49	0.57
Deck-max	0.56	0.58	1.62	0.58				
Fnd-tran	1.12	1.05	10.61	1.05				
Fnd-rot	99.00	0.00	99.00	0.00				
Ab-Pass	1.52	0.96	8.03	0.96				
Ab-Act	0.53	0.93	2.10	0.93				
Ab-tran	0.16	0.59	0.59	0.59				
M-E2-S34-C-D								
Column	0.13	0.74	0.47	0.74	0.67	0.74	0.86	0.74
Deck-max	0.36	0.58	0.97	0.58				
Fnd-tran	1.21	1.10	8.04	1.10				
Fnd-rot	99.00	0.00	99.00	0.00				
Ab-Pass	0.58	0.69	1.64	0.69				
Ab-Act	0.31	0.69	0.73	0.69				
Ab-tran	0.11	0.60	0.37	0.60				
M-E2-S34-O-D								
Column	0.13	0.74	0.47	0.74	0.67	0.74	0.86	0.74
Deck-max	0.36	0.58	0.97	0.58				
Fnd-tran	1.21	1.10	8.04	1.10				
Fnd-rot	99.00	0.00	99.00	0.00				
Ab-Pass	0.58	0.69	1.64	0.69				
Ab-Act	0.31	0.69	0.73	0.69				
Ab-tran	0.11	0.60	0.37	0.60				
S-E3-S34-C-D								
Column	0.23	0.69	0.95	0.69	1.92	0.69	2.82	0.69
Deck-max	0.65	0.68	1.96	0.68				
Fnd-tran	1.72	1.14	12.95	1.14				
Fnd-rot	99.00	0.00	99.00	0.00				
Ab-Pass	1.05	0.73	3.30	0.73				
Ab-Act	0.50	0.74	1.36	0.74				
Ab-tran	0.17	0.71	0.69	0.71				
S-E3-S34-O-D								
Column	0.30	0.73	1.48	0.73	3.24	0.73	4.99	0.73

Deck-max	0.73	0.63	2.52	0.63				
Fnd-tran	1.03	1.00	7.89	1.00				
Fnd-rot	99.00	0.00	99.00	0.00				
Ab-Pass	0.94	0.78	3.35	0.78				
Ab-Act	0.42	0.78	1.23	0.78				
Ab-tran	0.17	0.64	0.79	0.64				
T-E3-S34-C-D								
Column	0.16	0.66	0.64	0.66	1.27	0.66	1.85	0.66
Deck-max	0.43	0.63	1.18	0.63				
Fnd-tran	1.36	0.97	8.66	0.97				
Fnd-rot	99.00	0.00	99.00	0.00				
Ab-Pass	0.80	0.66	2.36	0.66				
Ab-Act	0.40	0.65	1.00	0.65				
Ab-tran	0.12	0.64	0.44	0.64				
T-E3-S34-O-D								
Column	0.25	0.57	0.83	0.57	1.49	0.57	2.06	0.57
Deck-max	0.56	0.58	1.62	0.58				
Fnd-tran	1.12	1.05	10.61	1.05				
Fnd-rot	99.00	0.00	99.00	0.00				
Ab-Pass	1.52	0.96	8.03	0.96				
Ab-Act	0.53	0.93	2.10	0.93				
Ab-tran	0.16	0.59	0.59	0.59				
M-E3-S34-C-D								
Column	0.13	0.74	0.47	0.74	0.86	0.74	1.20	0.74
Deck-max	0.36	0.58	0.97	0.58				
Fnd-tran	1.21	1.10	8.04	1.10				
Fnd-rot	99.00	0.00	99.00	0.00				
Ab-Pass	0.58	0.69	1.64	0.69				
Ab-Act	0.31	0.69	0.73	0.69				
Ab-tran	0.11	0.60	0.37	0.60				
M-E3-S34-O-D								
Column	0.13	0.74	0.47	0.74	0.86	0.74	1.20	0.74
Deck-max	0.36	0.58	0.97	0.58				
Fnd-tran	1.21	1.10	8.04	1.10				
Fnd-rot	99.00	0.00	99.00	0.00				
Ab-Pass	0.58	0.69	1.64	0.69				
Ab-Act	0.31	0.69	0.73	0.69				
Ab-tran	0.11	0.60	0.37	0.60				

Table C2 – Component level fragility relationships for seat abutment bridges.

Bridge class	CDT-0		CDT-1		CDT-2		CDT-3	
	λ	ζ	λ	ζ	λ	ζ	λ	ζ
S-E1-S22-C-S								
Column	0.10	0.67	0.23	0.67	0.54	0.67	0.83	0.67
Hinge	0.09	0.59	0.16	0.59	0.30	0.59	0.43	0.59
Deck-max	0.53	0.57	1.58	0.57				
Fnd-tran	1.53	1.07	12.21	1.07				
Fnd-rot	99.00	0.00	99.00	0.00				
Ab-Pass	1.39	0.64	4.31	0.64				
Ab-Act	0.68	0.69	1.69	0.69				
Ab-tran	0.31	0.74	1.38	0.74				
Bearing	0.16	0.59	0.55	0.59				
Seal	0.30	0.59	7.36	0.59				
Key	7.75	1.32	59.34	1.32				
S-E1-S22-R-S								
Column	0.12	0.61	0.24	0.61	0.51	0.61	0.74	0.61
Hinge	0.09	0.53	0.15	0.53	0.28	0.53	0.39	0.53
Deck-max	0.49	0.51	1.33	0.51				
Fnd-tran	0.97	1.02	7.44	1.02				
Fnd-rot	99.00	0.00	99.00	0.00				
Ab-Pass	1.35	0.73	3.94	0.73				
Ab-Act	0.69	0.74	1.62	0.74				
Ab-tran	0.38	0.68	1.50	0.68				
Bearing	0.15	0.53	0.49	0.53				
Seal	0.28	0.53	5.79	0.53				
Key	5.41	1.19	32.43	1.19				
T-E1-S22-C-S								
Column	0.09	0.65	0.19	0.65	0.41	0.65	0.61	0.65
Hinge	0.07	0.60	0.12	0.60	0.21	0.60	0.30	0.60
Deck-max	0.33	0.55	0.87	0.55				
Fnd-tran	3.40	1.08	33.47	1.08				
Fnd-rot	99.00	0.00	99.00	0.00				
Ab-Pass	1.32	0.68	4.57	0.68				
Ab-Act	0.62	0.70	1.64	0.70				
Ab-tran	0.26	0.64	0.97	0.64				
Bearing	0.11	0.58	0.35	0.58				
Seal	0.21	0.60	4.49	0.60				

Key	7.24	1.04	55.39	1.04				
T-E1-S22-R-S								
Column	0.12	0.69	0.23	0.69	0.45	0.69	0.63	0.69
Hinge	0.09	0.56	0.15	0.56	0.26	0.56	0.36	0.56
Deck-max	0.41	0.55	1.10	0.55				
Fnd-tran	0.95	1.02	7.62	1.02				
Fnd-rot	99.00	0.00	99.00	0.00				
Ab-Pass	1.25	0.74	3.96	0.74				
Ab-Act	0.57	0.80	1.38	0.80				
Ab-tran	0.29	0.68	1.12	0.68				
Bearing	0.14	0.56	0.43	0.56				
Seal	0.26	0.56	4.50	0.56				
Key	5.67	1.41	27.83	1.41				
M-E1-S22-C-S								
Column	0.04	1.19	0.11	1.19	0.29	1.19	0.48	1.19
Hinge	0.07	0.50	0.12	0.50	0.22	0.50	0.31	0.50
Deck-max	0.35	0.51	0.97	0.51				
Fnd-tran	3.30	1.13	28.69	1.13				
Fnd-rot	99.00	0.00	99.00	0.00				
Ab-Pass	1.17	0.72	3.54	0.72				
Ab-Act	0.60	0.71	1.48	0.71				
Ab-tran	0.25	0.80	1.12	0.80				
Bearing	0.11	0.48	0.36	0.48				
Seal	0.22	0.50	4.83	0.50				
Key	6.99	1.38	52.84	1.38				
M-E1-S22-R-S								
Column	0.13	0.71	0.25	0.71	0.49	0.71	0.70	0.71
Hinge	0.09	0.58	0.16	0.58	0.28	0.58	0.39	0.58
Deck-max	0.46	0.55	1.25	0.55				
Fnd-tran	0.90	0.99	7.25	0.99				
Fnd-rot	53.72	0.49	99.00	0.00				
Ab-Pass	1.18	0.71	3.33	0.71				
Ab-Act	0.62	0.77	1.41	0.77				
Ab-tran	0.34	0.70	1.20	0.70				
Bearing	0.16	0.58	0.47	0.58				
Seal	0.28	0.58	4.89	0.58				
Key	6.36	1.29	35.05	1.29				
S-E2-S22-C-S								
Column	0.16	0.66	0.66	0.66	1.01	0.66	1.34	0.66

Hinge	0.16	0.63	0.82	0.63	1.97	0.63	3.06	0.63
Deck-max	0.52	0.56	1.69	0.56				
Fnd-tran	1.16	1.12	10.55	1.12				
Fnd-rot	99.00	0.00	99.00	0.00				
Ab-Pass	1.31	0.62	3.19	0.62				
Ab-Act	0.73	0.64	1.48	0.64				
Ab-tran	0.38	0.52	0.98	0.52				
Bearing	0.13	0.59	0.76	0.59				
Seal	0.34	0.63	17.71	0.63				
Key	99.00	0.00	99.00	0.00				
S-E2-S22-O-S								
Column	0.20	0.60	0.86	0.60	1.32	0.60	1.77	0.60
Hinge	0.15	0.54	0.66	0.54	1.44	0.54	2.14	0.54
Deck-max	0.50	0.52	1.54	0.52				
Fnd-tran	0.75	0.98	5.06	0.98				
Fnd-rot	99.00	0.00	99.00	0.00				
Ab-Pass	1.24	0.59	3.17	0.59				
Ab-Act	0.66	0.60	1.35	0.60				
Ab-tran	0.39	0.53	1.09	0.53				
Bearing	0.14	0.54	0.70	0.54				
Seal	0.30	0.54	10.35	0.54				
Key	99.00	0.00	99.00	0.00				
T-E2-S22-C-S								
Column	0.11	0.59	0.53	0.59	0.84	0.59	1.14	0.59
Hinge	0.12	0.56	0.52	0.56	1.14	0.56	1.70	0.56
Deck-max	0.36	0.54	1.11	0.54				
Fnd-tran	1.32	0.94	9.35	0.94				
Fnd-rot	99.00	0.00	99.00	0.00				
Ab-Pass	1.02	0.53	2.65	0.53				
Ab-Act	0.55	0.60	1.15	0.60				
Ab-tran	0.25	0.49	0.71	0.49				
Bearing	0.10	0.54	0.50	0.54				
Seal	0.23	0.56	8.27	0.56				
Key	99.00	0.00	99.00	0.00				
T-E2-S22-O-S								
Column	0.14	0.65	0.61	0.65	0.92	0.65	1.23	0.65
Hinge	0.12	0.46	0.48	0.46	1.02	0.46	1.50	0.46
Deck-max	0.35	0.44	1.02	0.44				
Fnd-tran	0.47	0.89	2.69	0.89				
Fnd-rot	99.00	0.00	99.00	0.00				

Ab-Pass	1.00	0.51	2.46	0.51				
Ab-Act	0.46	0.42	0.90	0.42				
Ab-tran	0.29	0.46	0.80	0.46				
Bearing	0.10	0.46	0.47	0.46				
Seal	0.22	0.46	6.89	0.46				
Key	99.00	0.00	99.00	0.00				
M-E2-S22-C-S								
Column	0.11	0.67	0.50	0.67	0.79	0.67	1.07	0.67
Hinge	0.11	0.53	0.50	0.53	1.16	0.53	1.76	0.53
Deck-max	0.35	0.47	1.07	0.47				
Fnd-tran	0.97	0.90	6.15	0.90				
Fnd-rot	99.00	0.00	99.00	0.00				
Ab-Pass	0.94	0.42	2.20	0.42				
Ab-Act	0.54	0.42	1.06	0.42				
Ab-tran	0.27	0.41	0.67	0.41				
Bearing	0.09	0.52	0.49	0.52				
Seal	0.22	0.53	9.46	0.53				
Key	99.00	0.00	99.00	0.00				
M-E2-S22-O-S								
Column	0.14	0.75	0.66	0.75	1.04	0.75	1.41	0.75
Hinge	0.12	0.54	0.58	0.54	1.35	0.54	2.07	0.54
Deck-max	0.40	0.50	1.27	0.50				
Fnd-tran	0.49	0.87	3.89	0.87				
Fnd-rot	99.00	0.00	99.00	0.00				
Ab-Pass	1.10	0.52	2.74	0.52				
Ab-Act	0.63	0.52	1.28	0.52				
Ab-tran	0.32	0.42	0.81	0.42				
Bearing	0.10	0.58	0.58	0.58				
Seal	0.25	0.54	11.29	0.54				
Key	99.00	0.00	99.00	0.00				
S-E3-S22-C-S								
Column	0.16	0.66	0.66	0.66	1.34	0.66	1.99	0.66
Hinge	0.16	0.63	0.82	0.63	1.97	0.63	3.06	0.63
Deck-max	0.52	0.56	1.69	0.56				
Fnd-tran	1.16	1.12	10.55	1.12				
Fnd-rot	99.00	1.15	99.00	1.15				
Ab-Pass	1.31	0.62	3.19	0.62				
Ab-Act	0.73	0.64	1.48	0.64				
Ab-tran	0.38	0.52	0.98	0.52				

Bearing	0.13	0.59	0.76	0.59				
Seal	0.34	0.63	17.71	0.63				
Key	99.00	0.00	99.00	0.00				
S-E3-S22-O-S								
Column	0.20	0.60	0.86	0.60	1.77	0.60	2.64	0.60
Hinge	0.15	0.54	0.66	0.54	1.44	0.54	2.14	0.54
Deck-max	0.50	0.52	1.54	0.52				
Fnd-tran	0.75	0.98	5.06	0.98				
Fnd-rot	99.00	0.00	99.00	0.00				
Ab-Pass	1.24	0.59	3.17	0.59				
Ab-Act	0.66	0.60	1.35	0.60				
Ab-tran	0.39	0.53	1.09	0.53				
Bearing	0.14	0.54	0.70	0.54				
Seal	0.30	0.54	10.35	0.54				
Key	99.00	0.00	99.00	0.00				
T-E3-S22-C-S								
Column	0.11	0.59	0.53	0.59	1.14	0.59	1.75	0.59
Hinge	0.12	0.56	0.52	0.56	1.14	0.56	1.70	0.56
Deck-max	0.36	0.54	1.11	0.54				
Fnd-tran	1.32	0.94	9.35	0.94				
Fnd-rot	99.00	0.00	99.00	0.00				
Ab-Pass	1.02	0.53	2.65	0.53				
Ab-Act	0.55	0.60	1.15	0.60				
Ab-tran	0.25	0.49	0.71	0.49				
Bearing	0.10	0.54	0.50	0.54				
Seal	0.23	0.56	8.27	0.56				
Key	99.00	0.00	99.00	0.00				
T-E3-S22-O-S								
Column	0.14	0.65	0.61	0.65	1.23	0.65	1.82	0.65
Hinge	0.12	0.46	0.48	0.46	1.02	0.46	1.50	0.46
Deck-max	0.35	0.44	1.02	0.44				
Fnd-tran	0.47	0.89	2.69	0.89				
Fnd-rot	99.00	0.00	99.00	0.00				
Ab-Pass	1.00	0.51	2.46	0.51				
Ab-Act	0.46	0.42	0.90	0.42				
Ab-tran	0.29	0.46	0.80	0.46				
Bearing	0.10	0.46	0.47	0.46				
Seal	0.22	0.46	6.89	0.46				
Key	99.00	0.00	99.00	0.00				

M-E3-S22-C-S								
Column	0.11	0.67	0.50	0.67	1.07	0.67	1.63	0.67
Hinge	0.11	0.53	0.50	0.53	1.16	0.53	1.76	0.53
Deck-max	0.35	0.47	1.07	0.47				
Fnd-tran	0.97	0.90	6.15	0.90				
Fnd-rot	99.00	0.00	99.00	0.00				
Ab-Pass	0.94	0.42	2.20	0.42				
Ab-Act	0.54	0.42	1.06	0.42				
Ab-tran	0.27	0.41	0.67	0.41				
Bearing	0.09	0.52	0.49	0.52				
Seal	0.22	0.53	9.46	0.53				
Key	99.00	0.00	99.00	0.00				
M-E3-S22-O-S								
Column	0.14	0.75	0.66	0.75	1.41	0.75	2.15	0.75
Hinge	0.12	0.54	0.58	0.54	1.35	0.54	2.07	0.54
Deck-max	0.40	0.50	1.27	0.50				
Fnd-tran	0.49	0.87	3.89	0.87				
Fnd-rot	99.00	0.00	99.00	0.00				
Ab-Pass	1.10	0.52	2.74	0.52				
Ab-Act	0.63	0.52	1.28	0.52				
Ab-tran	0.32	0.42	0.81	0.42				
Bearing	0.10	0.58	0.58	0.58				
Seal	0.25	0.54	11.29	0.54				
Key	99.00	0.00	99.00	0.00				
S-E1-S34-C-S								
Column	0.12	0.58	0.28	0.58	0.63	0.58	0.96	0.58
Hinge	0.13	0.50	0.22	0.50	0.40	0.50	0.56	0.50
Deck-max	0.68	0.48	1.99	0.48				
Fnd-tran	1.24	0.81	7.07	0.81				
Fnd-rot	99.00	0.00	99.00	0.00				
Ab-Pass	1.47	0.72	4.39	0.72				
Ab-Act	0.74	0.73	1.78	0.73				
Ab-tran	0.34	0.67	1.38	0.67				
Bearing	0.22	0.50	0.71	0.50				
Seal	0.40	0.50	8.12	0.50				
Key	3.98	1.04	18.68	1.04				
S-E1-S34-R-S								
Column	0.06	1.07	0.17	1.07	0.50	1.07	0.88	1.07
Hinge	0.10	0.49	0.18	0.49	0.33	0.49	0.47	0.49

Deck-max	0.61	0.51	1.82	0.51				
Fnd-tran	1.59	0.95	12.69	0.95				
Fnd-rot	99.00	0.00	99.00	0.00				
Ab-Pass	1.37	0.67	3.86	0.67				
Ab-Act	0.71	0.67	1.62	0.67				
Ab-tran	0.54	0.88	2.80	0.88				
Bearing	0.18	0.49	0.61	0.49				
Seal	0.33	0.49	8.00	0.49				
Key	5.70	1.14	32.67	1.14				
T-E1-S34-C-S								
Column	0.06	0.90	0.13	0.90	0.29	0.90	0.44	0.90
Hinge	0.09	0.51	0.16	0.51	0.27	0.51	0.37	0.51
Deck-max	0.39	0.58	1.01	0.58				
Fnd-tran	2.93	0.87	18.56	0.87				
Fnd-rot	99.00	0.00	99.00	0.00				
Ab-Pass	1.06	0.64	3.31	0.64				
Ab-Act	0.54	0.78	1.28	0.78				
Ab-tran	0.24	0.78	0.95	0.78				
Bearing	0.15	0.52	0.44	0.52				
Seal	0.27	0.51	4.34	0.51				
Key	3.12	0.99	12.03	0.99				
T-E1-S34-R-S								
Column	0.02	1.10	0.08	1.10	0.26	1.10	0.49	1.10
Hinge	0.08	0.56	0.14	0.56	0.27	0.56	0.39	0.56
Deck-max	0.45	0.54	1.33	0.54				
Fnd-tran	5.04	1.29	86.51	1.29				
Fnd-rot	99.00	0.00	99.00	0.00				
Ab-Pass	1.09	0.60	3.18	0.60				
Ab-Act	0.54	0.65	1.29	0.65				
Ab-tran	0.29	0.70	1.14	0.70				
Bearing	0.13	0.56	0.47	0.56				
Seal	0.27	0.56	7.18	0.56				
Key	24.57	1.96	99.00	1.96				
M-E1-S34-C-S								
Column	0.01	1.36	0.02	1.36	0.11	1.36	0.24	1.36
Hinge	0.11	0.58	0.18	0.58	0.32	0.58	0.44	0.58
Deck-max	0.45	0.45	1.23	0.45				
Fnd-tran	3.54	1.30	28.44	1.30				
Fnd-rot	99.00	0.00	99.00	0.00				

Ab-Pass	1.55	1.01	4.35	1.01				
Ab-Act	0.75	0.99	1.67	0.99				
Ab-tran	0.22	0.60	0.71	0.60				
Bearing	0.16	0.54	0.50	0.54				
Seal	0.32	0.58	5.58	0.58				
Key	15.07	1.94	99.00	1.94				
M-E1-S34-R-S								
Column	0.01	1.36	0.02	1.36	0.11	1.36	0.24	1.36
Hinge	0.11	0.58	0.18	0.58	0.32	0.58	0.44	0.58
Deck-max	0.45	0.45	1.23	0.45				
Fnd-tran	3.54	1.30	28.44	1.30				
Fnd-rot	99.00	0.00	99.00	0.00				
Ab-Pass	1.55	1.01	4.35	1.01				
Ab-Act	0.75	0.99	1.67	0.99				
Ab-tran	0.22	0.60	0.71	0.60				
Bearing	0.16	0.54	0.50	0.54				
Seal	0.32	0.58	5.58	0.58				
Key	15.07	1.94	99.00	1.94				
S-E2-S34-C-S								
Column	0.11	0.82	0.59	0.82	0.97	0.82	1.36	0.82
Hinge	0.22	0.64	1.12	0.64	2.67	0.64	4.16	0.64
Deck-max	0.65	0.57	2.11	0.57				
Fnd-tran	1.46	1.02	12.66	1.02				
Fnd-rot	99.00	0.00	99.00	0.00				
Ab-Pass	1.75	0.61	4.55	0.61				
Ab-Act	0.99	0.63	2.11	0.63				
Ab-tran	0.39	0.48	1.05	0.48				
Bearing	0.17	0.61	0.96	0.61				
Seal	0.46	0.64	23.96	0.64				
Key	99.00	2.32	99.00	2.32				
S-E2-S34-O-S								
Column	0.15	1.05	1.05	1.05	1.85	1.05	2.70	1.05
Hinge	0.21	0.56	1.00	0.56	2.29	0.56	3.50	0.56
Deck-max	0.65	0.55	2.22	0.55				
Fnd-tran	0.87	0.90	5.98	0.90				
Fnd-rot	99.00	0.00	99.00	0.00				
Ab-Pass	1.43	0.53	3.47	0.53				
Ab-Act	0.81	0.54	1.64	0.54				
Ab-tran	0.50	0.60	1.43	0.60				

Bearing	0.17	0.59	1.01	0.59				
Seal	0.43	0.56	18.68	0.56				
Key	99.00	0.00	99.00	0.00				
T-E2-S34-C-S								
Column	0.03	1.38	0.32	1.38	0.66	1.38	1.09	1.38
Hinge	0.14	0.54	0.63	0.54	1.42	0.54	2.14	0.54
Deck-max	0.40	0.49	1.24	0.49				
Fnd-tran	1.55	0.92	11.68	0.92				
Fnd-rot	99.00	0.67	99.00	0.67				
Ab-Pass	1.08	0.55	2.71	0.55				
Ab-Act	0.58	0.56	1.20	0.56				
Ab-tran	0.29	0.48	0.83	0.48				
Bearing	0.11	0.49	0.57	0.49				
Seal	0.28	0.54	11.00	0.54				
Key	99.00	0.00	99.00	0.00				
T-E2-S34-O-S								
Column	0.05	1.22	0.65	1.22	1.35	1.22	2.22	1.22
Hinge	0.14	0.54	0.69	0.54	1.59	0.54	2.43	0.54
Deck-max	0.45	0.55	1.48	0.55				
Fnd-tran	0.65	0.77	3.91	0.77				
Fnd-rot	99.00	0.00	99.00	0.00				
Ab-Pass	1.32	0.69	3.29	0.69				
Ab-Act	0.68	0.69	1.35	0.69				
Ab-tran	0.34	0.50	0.87	0.50				
Bearing	0.11	0.58	0.67	0.58				
Seal	0.29	0.54	13.16	0.54				
Key	99.00	0.00	99.00	0.00				
M-E2-S34-C-S								
Column	0.07	0.96	0.36	0.96	0.58	0.96	0.80	0.96
Hinge	0.15	0.55	0.69	0.55	1.53	0.55	2.31	0.55
Deck-max	0.44	0.52	1.40	0.52				
Fnd-tran	1.11	0.81	7.42	0.81				
Fnd-rot	99.00	0.70	99.00	0.70				
Ab-Pass	1.12	0.55	2.87	0.55				
Ab-Act	0.62	0.60	1.28	0.60				
Ab-tran	0.30	0.50	0.82	0.50				
Bearing	0.12	0.58	0.66	0.58				
Seal	0.30	0.55	11.72	0.55				
Key	99.00	0.00	99.00	0.00				

M-E2-S34-O-S								
Column	0.01	1.17	0.31	1.17	0.89	1.17	1.82	1.17
Hinge	0.15	0.55	0.66	0.55	1.44	0.55	2.14	0.55
Deck-max	0.52	0.56	1.63	0.56				
Fnd-tran	0.89	0.95	8.41	0.95				
Fnd-rot	99.00	0.00	99.00	0.00				
Ab-Pass	1.08	0.54	2.59	0.54				
Ab-Act	0.61	0.55	1.22	0.55				
Ab-tran	0.40	0.50	1.11	0.50				
Bearing	0.14	0.56	0.69	0.56				
Seal	0.30	0.55	10.25	0.55				
Key	99.00	0.00	99.00	0.00				
S-E3-S34-C-S								
Column	0.11	0.82	0.59	0.82	1.36	0.82	2.16	0.82
Hinge	0.22	0.64	1.12	0.64	2.67	0.64	4.16	0.64
Deck-max	0.65	0.57	2.11	0.57				
Fnd-tran	1.46	1.02	12.66	1.02				
Fnd-rot	99.00	0.00	99.00	0.00				
Ab-Pass	1.75	0.61	4.55	0.61				
Ab-Act	0.99	0.63	2.11	0.63				
Ab-tran	0.39	0.48	1.05	0.48				
Bearing	0.17	0.61	0.96	0.61				
Seal	0.46	0.64	23.96	0.64				
Key	99.00	0.00	99.00	0.00				
S-E3-S34-O-S								
Column	0.15	1.05	1.05	1.05	2.70	1.05	4.55	1.05
Hinge	0.21	0.56	1.00	0.56	2.29	0.56	3.50	0.56
Deck-max	0.65	0.55	2.22	0.55				
Fnd-tran	0.87	0.90	5.98	0.90				
Fnd-rot	99.00	0.00	99.00	0.00				
Ab-Pass	1.43	0.53	3.47	0.53				
Ab-Act	0.81	0.54	1.64	0.54				
Ab-tran	0.50	0.60	1.43	0.60				
Bearing	0.17	0.59	1.01	0.59				
Seal	0.43	0.56	18.68	0.56				
Key	99.00	0.00	99.00	0.00				
T-E3-S34-C-S								
Column	0.03	1.38	0.32	1.38	1.09	1.38	2.15	1.38

Hinge	0.14	0.54	0.63	0.54	1.42	0.54	2.14	0.54
Deck-max	0.40	0.49	1.24	0.49				
Fnd-tran	1.55	0.92	11.68	0.92				
Fnd-rot	99.00	0.00	99.00	0.00				
Ab-Pass	1.08	0.55	2.71	0.55				
Ab-Act	0.58	0.56	1.20	0.56				
Ab-tran	0.29	0.48	0.83	0.48				
Bearing	0.11	0.49	0.57	0.49				
Seal	0.28	0.54	11.00	0.54				
Key	99.00	0.00	99.00	0.00				
T-E3-S34-O-S								
Column	0.05	1.22	0.65	1.22	2.22	1.22	4.35	1.22
Hinge	0.14	0.54	0.69	0.54	1.59	0.54	2.43	0.54
Deck-max	0.45	0.55	1.48	0.55				
Fnd-tran	0.65	0.77	3.91	0.77				
Fnd-rot	99.00	0.00	99.00	0.00				
Ab-Pass	1.32	0.69	3.29	0.69				
Ab-Act	0.68	0.69	1.35	0.69				
Ab-tran	0.34	0.50	0.87	0.50				
Bearing	0.11	0.58	0.67	0.58				
Seal	0.29	0.54	13.16	0.54				
Key	99.00	0.00	99.00	0.00				
M-E3-S34-C-S								
Column	0.07	0.96	0.36	0.96	0.80	0.96	1.24	0.96
Hinge	0.15	0.55	0.69	0.55	1.53	0.55	2.31	0.55
Deck-max	0.44	0.52	1.40	0.52				
Fnd-tran	1.11	0.81	7.42	0.81				
Fnd-rot	99.00	0.00	99.00	0.00				
Ab-Pass	1.12	0.55	2.87	0.55				
Ab-Act	0.62	0.60	1.28	0.60				
Ab-tran	0.30	0.50	0.82	0.50				
Bearing	0.12	0.58	0.66	0.58				
Seal	0.30	0.55	11.72	0.55				
Key	99.00	0.00	99.00	0.00				
M-E3-S34-O-S								
Column	0.01	1.17	0.31	1.17	1.82	1.17	4.85	1.17
Hinge	0.15	0.55	0.66	0.55	1.44	0.55	2.14	0.55
Deck-max	0.52	0.56	1.63	0.56				
Fnd-tran	0.89	0.95	8.41	0.95				

Fnd-rot	99.00	0.51	99.00	0.51				
Ab-Pass	1.08	0.54	2.59	0.54				
Ab-Act	0.61	0.55	1.22	0.55				
Ab-tran	0.40	0.50	1.11	0.50				
Bearing	0.14	0.56	0.69	0.56				
Seal	0.30	0.55	10.25	0.55				
Key	99.00	1.79	99.00	1.79				

REFERENCES

Ala Saadeghvaziri, M., and Rashidi, S. (1998). *Effect of steel bearings on seismic response of bridges in Eastern United States.* Proceedings of 6th US National Conf. on Earthquake Engineering. Oakland, California

ATC. (1985). *Earthquake damage evaluation data for California, Report No. ATC-6*. Retrieved from Applied Technology Council, Redwood City, California.

Avsar, O., Yakut A and Caner, A. (2001). *Analytical Fragility Curves for Ordinary Highway Bridges in Turkey*. Earthquake Spectra, 27(4), pp: 971-996.

Baker, J. W., Lin, T., Shahi, S. K., and Jayaram, N. (2011). *New ground motion selection procedures and selected motions for the PEER transportation research program*. Pacific Earthquake Engineering Research Center.

Banerjee, S., and Shinozuka, M. (2007). *Nonlinear static procedure for seismic vulnerability assessment of bridges*. Computer-Aided Civil and Infrastructure Engineering, 22(4), pp:293-305.

Banerjee, S., and Shinozuka, M. (2008). *Mechanistic quantification of RC bridge damage states under earthquake through fragility analysis*. Probabilistic Engineering Mechanics, 23, pp:12-22.

Basöz, N., and Mander, J. (1999). *Enhancement of the highway transportation lifeline module in HAZUS*. National Institute of Building Sciences, 16(1), pp:31-40.

Basoz, N., and Kiremidjian, A. S. (1998). *Evaluation of bridge damage data from the Loma Prieta and Northridge, California earthquakes*. California earthquakes (No. MCEER-98-0004).

BDS (1990). Bridge design details, Caifornia Department of Trnasportations, Sacramento. CA.

BDA (2012). Bridge design aids, Caifornia Department of Trnasportations, Sacramento. CA.

Başöz, N., and Kiremidjian, A. S. (1996). *Risk assessment for highway transportation systems*: John A. Blume Earthquake Engineering Center.

Bavirisetty, R., Vinayagamoorthy, M., and Duan, L. (2003). *Dynamic Analysis, Bridge Engineering – Seismic Design*, Edited by Wai-Fah Chen and Lian Duan, CRC Press LLC, Boca Raton, FL, ISBN: 0-8493-1683-9/02.

Bradley, B. A. (2010). *Epistemic Uncertainties in Component Fragility Functions*. Earthquake Spectra 26(1), pp: 41-62.

Calderone, A., Lehman, D. E., and Moehle J. P. (2001). *Behavior of reinforced concrete bridge columns having varying aspect ratios and varying lengths of confinement*, Pacific Earthquake Engineering Research Center.

Caltrans (2017). *Personal communication with the P266, Task 1780 Fragility project panel members including Roblee C, Shantz T, Turner L*. California Department of Transportation. Sacramento.

Caltrans, S. (2010). *Caltrans Seismic Design Criteria version 1.6.* California Department of Transportation, Sacramento, California.

Celik, O. C., and B. R. Ellingwood (2010). *Seismic fragilities for non-ductile reinforced concrete frames - Role of aleatoric and epistemic uncertainties*. Structural Safety 32(1), pp: 1-12.

Chai, Y. H., Priestley, M. N., and Seible, F. (1991). *Seismic retrofit of circular bridge columns for enhanced flexural performance*. ACI Structural Journal, 88.

Chang, G. A. and Mander, J. B. (1994). *Seismic energy based fatigue damage analysis of bridge columns: Part 1: Evaluation of seismic capacity*. In Technical Report, US National Center for Earthquake Engineering Research.

Cheok, G. S. and Stone, W. C. (1990). *Behavior of 1/6-scale model bridge columns subjected to inelastic cyclic loading*. ACI Structural Journal 87(6).

Choi, E. (2002). *Seismic analysis and retrofit of mid-America bridges.* Ph.D Thesis, Georgia Institute of Technology, Atlanta, USA.

Coffman, H. L., Marsh, M. L., and Brown, C. B. (1993). *Seismic durability of retrofitted reinforced-concrete columns. Journal of Structural Engineering*, 119(5), 1643-1661.

Cornell, C., Jalayer, F., Hamburger, R., and Foutch, D. (2002). *Probabilistic Basis for 2000 SAC Federal Emergency Management Agency Steel Moment Frame Guidelines*. Journal of Structural Engineering, 128(4), pp:526-533.

Cornell, C. A., and Krawinkler, H. (2000). *Progress and challenges in seismic performance assessment.* PEER Center News, 3(2), 1-3.

Correal, J. F., Saiidi, M. S., Sanders, D., and El-Azazy, S. (2007). *Analytical evaluation of bridge columns with double interlocking spirals*. ACI structural journal, 104(3), 314.

Dicleli, M., and Bruneau, M. (1995*). Seismic performance of single-span simply supported and continuous slab-on-girder steel highway bridges*. Journal of structural engineering, 121(10), pp:1497-1506.

Dukes, J. D. (2013). *Application of bridge specific fragility analysis in the seismic design process of bridges in california*. Ph.D Thesis, Georgia Institute of Technology, Atlanta, USA.

Dukes, J., Mangalathu, S., Padgett, J. E., and DesRoches, R. (2017). *Development of bridge-specific fragility methedology to improve the seismic resilience of bridges*, Earthquakes and Structures (in review).

Esmaeily, A., and Xiao, Y. (2005). *Behavior of reinforced concrete columns under variable axial loads: analysis*. ACI Structural Journal, 102(5), 736.

Fang, J. Q., Li, Q. S., Jeary, A. P., and Liu, D. K. (1999). *Damping of tall buildings: its evaluation and probabilistic characteristics*. The Structural Design of Tall Buildings, 8(2), 145-153.

Friedman, J., Hastie, T., and Tibshirani, R. (2001) *The elements of statistical learning*. Springer series in statistics Springer, Berlin.

Filippou, F. C., Popov, E. P., and Bertero, B. V. (1983). *Effects of bond deterioration on hysteretic behavior of reinforced concrete joint*s, Report No. FEMA-351. Washington DC: SAC Joint Venture.

Fajfar, P. (2000). *A nonlinear analysis method for performance-based seismic design*. Earthquake Spectra, 16(3), 573-592.

Gardoni, P., Mosalam, K. M., and der Kiureghian, A. (2003). *Probabilistic seismic demand models and fragility estimates for RC bridges*. Journal of Earthquake Engineering, 7, pp:79-106.

Ghosh, J., Padgett, J. E., and Dueñas-Osorio, L. (2013). *Surrogate modeling and failure surface visualization for efficient seismic vulnerability assessment of highway bridges.* Probabilistic Engineering Mechanics, *34*, pp:189-199.

Haselton, C., A. Whittaker, A. Hortacsu, J. Baker, J. Bray and Grant, D. (2012). *Selecting and scaling earthquake ground motions for performing response-history analyses*. Proceedings of the 15th World Conference on Earthquake Engineering.

HAZUS-MH. (2003). *Multi-Hazard Loss Estimation Methodology: Earthquake Model*. Department of Homeland Security, FEMA, Washington, DC.

Hesterberg, T., Choi, N. H., Meier, L., Fraley, C., (2008). *Least angle and ℓ1 penalized regression: A review*. Statistics Surveys, 2,pp:61-93.

Hoerl, A. E., and Kennar., R. W. (1970). *Ridge regression: Biased estimation for nonorthogonal problems*, Technometrics, 12,pp:55-67.

Hose, Y. D., Priestley, M. and Seible, F. (1997). *Strategic relocation of plastic hinges in bridge columns*. Structural Systems Research Project, 97/05, University of California, San Diego.

Huitema, B. E. (1990). *Analysis of Covariance, in Encyclopedia of Statistics in Behavioral Science*. John Wiley and Sons, Ltd: Hoboken, New Jersey.

Hwang, H., Jernigan, J. B., and Lin, Y.-W. (2000). *Evaluation of seismic damage to Memphis bridges and highway systems*. Journal of Bridge Engineering, *5*(4), pp:322-330.

Jangid, R. S. (2004). Seismic response of isolated bridges. *Journal of Bridge Engineering*, 9(2), pp:156–166.

Jaradat, O. A., McLean, D. I. and Marsh, M. L. (1998). *Performance of Existing Bridge Columns under Cyclic Loading Part 1: Experimental Results and Observed Behavior*. ACI Structural Journal 95(6).

Jeon, J. S. (2013). *Aftershock vulnerability assessment of damaged reinforced concrete buildings in California*, PhD. Thesis, Georgia Tech, Atlanta.

Jeon, J. S., Shafieezadeh, A., Lee, D. H., Choi, E., and DesRoches, R. (2015). *Damage assessment of older highway bridges subjected to three-dimensional ground motions: characterization of shear–axial force interaction on seismic fragilities*. Engineering Structures, 87, pp: 47-57.

Jeon, J.-S., Mangalathu, S., Song, J., and DesRoches, R. (2017). *Parameterized seismic fragility curves for curved multi-frame concrete box-girder bridges using Bayesian parameter estimation.* Journal of Earthquake Engineering (In press).

Jeong, S.-H., and Elnashai, A. S. (2007). *Probabilistic fragility analysis parameterized by fundamental response quantities.* Engineering Structures, 29(6), pp:1238-1251.

Ji, J., Elnashai, A. S., and Kuchma, D. A. (2007). *An analytical framework for seismic fragility analysis of RC high-rise buildings*. Engineering structures, 29(12), pp:3197-3209.

Kameshwar, S. and Padgett, J. E. (2014) *Multi-hazard risk assessment of highway bridges subjected to earthquake and hurricane hazards*. Engineering Structures, 78, pp:154-166.

Keselman, H., Huberty, C. J., Lix, L. M., Olejnik, S., Cribbie, R. A., Donahue, B., Kowalchuk, R. K., Lowman, L. L., Petoskey, M. D., and Keselman, J. C. (1998). *Statistical practices of educational researchers: An analysis of their ANOVA, MANOVA, and ANCOVA analyses*. Review of Educational Research, 68, pp:350-386.

Kim, S.-H., and Shinozuka, M. (2004). *Development of fragility curves of bridges retrofitted by column jacketing*. Probabilistic Engineering Mechanics, 19(1), pp:105-112.

Kircher, C. A., Whitman, R. V., and Holmes, W. T. (2006). HAZUS earthquake loss estimation methods. Natural Hazards Review, 7(2), pp:45-59.

Kowalsky, M. J. and Priestley, M. N. (2000). *Improved analytical model for shear strength of circular reinforced concrete columns in seismic regions*. ACI Structural Journal 97(3).

Kolmogorov, A. N. (1933). Sulla determinazione empirica di una legge di distribuzione.

Kruskal, W. H., and Wallis, W. A. (1952). *Use of ranks in one-criterion variance analysis*. Journal of the American statistical Association, 47(260),pp:583-621.

Kunnath, S. K., El-Bahy, A.,Taylor, A. W. and Stone, W. C. (1997). *Cumulative seismic damage of reinforced concrete bridge piers*. Technical Report NCEER, US National Center for Earthquake Engineering Research.

Kunnath, S. K., Larson, L., and Miranda, E. (2006) *Modelling considerations in probabilistic performance-based seismic evaluation: case study of the I-880 viaduct*. Earthquake Engineering and Structural Dynamics, 35, pp:57-75.

Kvam, P. H., and Vidakovic, B. (2007). *Nonparametric statistics with applications to science and engineering*. John Wiley and Sons..

Lehman, D., Moehle, J., Mahin, S., Calderone, A. and Henry. L. (2004). *Experimental evaluation of the seismic performance of reinforced concrete bridge columns*. Journal of Structural Engineering, 130, pp:869-879.

Lehman, D. E. and Moehle, J. P. (2000). *Seismic performance of well-confined concrete bridge columns*, Pacific Earthquake Engineering Research Center.

Mackie, K., and Stojadinovic, B. (2001). *Probabilistic seismic demand model for California highway bridges.* Journal of Bridge Engineering, 6(6), 468-481.

Mackie, K. R., and Stojadinović, B. (2005). *Fragility basis for California highway overpass bridge seismic decision making*. Pacific Earthquake Engineering Research Center, College of Engineering, University of California, Berkeley.

Mackie, K. R., Cronin, K. J., Nielson, B. G. (2011). *Response Sensitivity of Highway Bridges to Randomly Oriented Multi-Component Earthquake Excitation*, Journal of Earthquake Engineering, 15(6), pp: 850-876.

Mander, J., Priestley, M., and Park, R. (1988). *Theoretical Stress-Strain Model for Confined Concrete*. Journal of Structural Engineering, 114(8), pp:1804-1826.

Mander, J. B., and Basöz, N. (1999). *Seismic fragility curve theory for highway bridges*. Paper presented at the Optimizing post-earthquake lifeline system reliability.

Mangalathu, S., Jeon, J.-S., Soleimani, F., DesRoches, R., Padgett, J., and Jiang, J. (2015a). *Seismic vulnerability of multi-span bridges: An analytical perspective*. Proceedings of the 10th Pacific Conference on Earthquake Engineering, Sydney, Australia.

Mangalathu, S., Jeon, J.-S., DesRoches, R., and Padgett, J. (2015b). *Analysis of Covariance to Capture the Importance of Bridge Attributes on the Probabilistic Seismic Demand Model*. Proceedings of the 10th Pacific Conference on Earthquake Engineering, Sydney, Australia.

Mangalathu, S., Jeon, J.-S., DesRoches, R., and Padgett, J. (2016a). ANCOVA-based grouping of bridge classes for seismic fragility assessment. *Engineering Structures, 123*, 379-394.

Mangalathu, S., Jeon J-S., DesRoches, R., and Padgett, J. E. (2016b). *Application of Bayesian Methods to Probabilistic Demand Analyses of Concrete Box-Girder Bridges*. Proceedings of the Geotechnical and Structural Engineering Congress, Phoenix, Arizona.

Mangalathu, S., Jeon, J.-S., DesRoches, R., and Padgett, J. (2017a). *Performance-based grouping methods of bridge classes for regional seismic risk assessment: Application of ANOVA, ANCOVA, and non-parameteric approach*. Earthquake Engineering and Structural Dynamics (In review).

Mangalathu, S., Soleimani, F., DesRoches, R., and Padgett, J. E. (2017b). *ANOVA based grouping of bridge classes*. Proceedings of the 16th World Conference on Earthquake Engineering, Santiago, Chile.

Mangalathu, S., Jeon J-S., Soleimani, F., DesRoches, R., Padgett, J. E., and Jiang, J. (2017c). *Sensitivity of Fragility Curves to Parameter Uncertainty using Lasso*. Proceedings of the 16th World Conference on Earthquake Engineering, Santiago, Chile.

Mangalathu, S., Soleimani, F., DesRoches, R., and Padgett, J. E. (2017d). *Bridge Classes for Regional Risk assessment of Box-Girder Bridges in California: Improving HAZUS Model*. Proceedings of the Structures Congress, Denver, Colorado.

Mangalathu, S., Jeon J-S., DesRoches, R., (2017e) *Identification of critical parameters on the seismic performance of concrete bridges using Lasso regression*, Earthquake Engineering and Structural Dynamics (In review).

Mazzoni, S, McKenna. F., Scott, M. H., Fenves, G. L. (2006) *OpenSees command language manual*. Pacific Earthquake Engineering Research (PEER) Center.

Megally, S. H., Silva, F. P., and Seible, F. (2002). *Seismic Response of Sacrificial Shear Keys in Bridge Abutments.* Department of Structural Engineering, University of California, San Diego.

Mehr, M. and Zaghi, A. E. (2016). *Seismic response of multi-frame bridges*. Bulletin of Earthquake Engineering. 14, pp:1219-43.

Moehle, J., and Deierlein, G. G. (2004). *A framework methodology for performance-based earthquake engineering*. Proceedings of the 13th World Conference on Earthquake Engineering.

Moschonas, I. F., Kappos, A. J., Panetsos, P., Papadopoulos, V., Makarios, T. and Thanopoulos, P. (2008). *Seismic fragility curves for greek bridges: methodology and case studies*. Bulletin of Earthquake Engineering. 7(2), pp:439-468.

Melek, M. and Wallace, J. W. (2004). *Cyclic behavior of columns with short lap splices*. ACI Structural Journal, 101.

Menegotto, M. and Pinto, P. (1973). *Method of Analysis for Cyclically Loaded RC Frames Including Changes in Geometry and Non-elastic Behaviour of Elements Under Combined Normal Force and Bending*. IABSE Congress Reports of the Working Commission.

Miller Jr, R. G. (1997). *Beyond ANOVA: basics of applied statistics*. CRC Press.

Moschonas, I. F., Kappos, A. J., Panetsos, P., Papadopoulos, V., Makarios, T., and P. Thanopoulos (2008*). Seismic fragility curves for greek bridges: methodology and case studies*. Bulletin of Earthquake Engineering 7(2), pp:439-468.

MTD (2008). *Bridge Memo to Designers (10-20*), California Department of Transportation, Sacramento, CA.

Muthukumar, S. and DesRoches, R. (2006). *A Hertz contact model with non-linear damping for pounding simulation*. Earthquake Engineering and Structural Dynamics, 35, pp:811-828.

Ni, P., Mangalathu, S., Mei, G., Zhao, Y. (2017) *Permeable Piles: An Alternative to Improve the Performance of Driven Piles*, Computers and Geotechnics, Vol. 84, 2017.

Nielson, B. G. (2005). *Analytical fragility curves for higway bridges in moderate seismic zones*. PhD. Thesis, Georgia Tech, Atlanta.

Nielson, B. G, and DesRoches, R. (2006). *Influence of modeling assumptions on the seismic response of multi-span simply supported steel girder bridges in moderate seismic zones*. Engineering Structures, 28, pp:1083-1092.

Ohtaki, T., Benzoni, G., Priestley, M., and Seible, F. (1997). *Seismic performance of a full scale bridge column-as built and as repaire*d. Second National Seismic Conference on Bridges and Highways.

Orozco, G. L. (2001). *The effects of a large velocity pulse on reinforced concrete bridge columns*. Dept. of Structural Engineering, University of California, San Diego.

Owen, S. V. and Froman, R. D. (1998*). Focus on qualitative methods uses and abuses of the analysis of covariance*. Research in Nursing and Health, 21(6), pp:557–562.

Park, J. and Towashiraporn, P. (2014). *Rapid seismic damage assessment of railway bridges using the response-surface statistical model*. Structural Safety, 47, pp:1-12.

Padgett, J. E. (2007). *Seismic vulnerability assessment of retrofitted bridges using probabilistic methods,* Ph.D Thesis, Georgia Tech, Atlanta, Georgia.

Padgett, J. E., and DesRoches, R. (2007*). Sensitivity of seismic response and fragility to parameter uncertainty*. Journal of Structural Engineering, 133, pp:1710-1718.

Porter, K. (2010). *Cracking an open safe: uncertainty in HAZUS-based seismic vulnerability functions*, Earthquake Spectra, 26(3), pp:893-900.

Porter, K. A. (2003). *An overview of PEER's performance-based earthquake engineering methodology*. Proceedings of Ninth International Conference on Applications of Statistics and Probability in Civil Engineering.

Potyondy, J. G. (1961). *Skin friction between various soils and construction materials*. Geotechnique, 11(4), pp: 339-353.

Priestley, M. N., Seible, F., and Calvi, G. (1996). *Seismic design and retrofit of bridges*. John Wiley and Sons, New York.

Priestley, M. N. and Benzoni, G. (1996). Seismic performance of circular columns with low longitudinal reinforcement ratios. ACI Structural Journal 93(4).

Ramanathan, K. N. (2012*). Next generation seismic fragility curves for California bridges incorporating the evolution in seismic design philosophy*. Ph.D Thesis, Georgia Tech, Atlanta, Georgia.

Ramanathan, K., Jeon, J.-S., Zakeri, B., DesRoches, R., and Padgett, J. E. (2015). *Seismic response prediction and modeling considerations for curved and skewed concrete box-girder bridges.* Earthquakes and Structures, 9(6), pp:1153-1179.

Ramanathan, K., Padgett, J. E., and DesRoches, R. (2015). *Temporal evolution of seismic fragility curves for concrete box-girder bridges in California*, Engineering Structures, 97, pp:29-46.

Ranf, R. T., Eberhard, M. O., and Malone, S. (2007). *Post-earthquake Prioritization of Bridge Inspections*. Earthquake Spectra 23(1), pp:131-146.

Ranf, R. T., Nelson, J. M., Price, Z., Eberhard, M. O., and Stanton, J. F. (2006). *Damage accumulation in lightly confined reinforced concrete bridge colum*ns, Pacific Earthquake Engineering Research Center.

Roblee, C. J. (2016a). *Memorandum: Box Girder bridges – span length models. P266-T1780 Technical Archives File Bridge Component Models*, California Department of Transportation, Sacramento, California.

Roblee, C. J. (2016b). *Memorandum: Box Girder bridges – transverse profile models. P266-T1780 Technical Archives File Bridge Component Models*, California Department of Transportation, Sacramento, California.

Saiidi, M., Maragakis, E., and Feng, S. (1996). *Parameters in bridge restrainer design for seismic retrofi*t. Journal of Structural Engineering, 122(1), pp:61-68.

Saini, A. and Saiidi, M. S. (2014). *Probabilistic Damage Control Approach for Seismic Design of Bridges*. University of Nevada, Reno.

Sanchez, A. V., Priestley, M., and Seible, F. (1997). *Seismic performance of flared bridge columns*. UC San Diago test report.

Schoettler, M., Restrepo, J., Guerrini, G., Duck, D., and Carrea, F. (2012). *A full-scale, single-column bridge bent tested by shake-table excitation*. Las Vegas, NV: Center for Civil Engineering Earthquake Research, Department of Civil Engineering, University of Nevada.

Seo, J., and Linzell, D. G. (2012) *Use of response surface metamodels to generate system level fragilities for existing curved steel bridges*. Engineering Strutures, 52, pp:642-653.

Shamsabadi, A. and Yan, L. (2008). *Closed-form force-displacement backbone curves for bridge abutment-backfill systems*. Geotechnical Earthquake Engineering and Soil Dynamics IV. 2008. 1-10.

Shanmugam, S. P. (2009). *Seismic behavior of circular reinforced concrete bridge columns under combined loading including torsion*, Ph.D thesis, Missouri University of Science and Technology.

Shinozuka, M., Feng, M. Q., Lee, J., and Naganuma, T. (2000). *Statistical analysis of fragility curves*. Journal of engineering mechanics, 126(12), pp:1224-1231.

Soleimani (2017). Fragility of California bridges – development of modification factors. Ph.D Thesis, Georgia Tech, Atlanta, Georgia.

Soleimani, F., Mangalathu, S., and DesRoches, R. (2017) *A comparative analytical study on the fragility assessment of bridges with various column shapes*, in Review.

Stefanidou, S. P., and Kappos, A. J. (2017). Methodology for the development of bridge-specific fragility curves. Earthquake Engineering and Structural Dynamics, 46(1), 73-93.

Stone, W. C. and Cheok, G. S. (1989). *Inelastic behavior of full-scale bridge columns subjected to cyclic loading*. Gaithersburg, MD, National Institute of Science and Technology.

Sun, Z., Priestley, M., and Seible, F. (1993*). Diagnostics and retrofit of rectangular bridge columns for seismic load*s, Department of Applied Mechanics and Engineering Sciences, University of California, San Diego.

Tibshirani, R, (1996). *Regression shrinkage and selection via the lasso*. Journal of Royal Statistical Society 58(1), pp:267-288.

Vickers, A. J. (2005). *Parametric versus non-parametric statistics in the analysis of randomized trials with non-normally distributed data*. BMC medical research methodology, 5(1), pp: 35.

Vidakovic, B. (2011). *Statistics for bioengineering sciences: with MATLAB and WinBUGS Support*, Springer Science and Business Media.

Wald, D., Lin, K.-W., Porter, K. and Turner, L. (2008). *ShakeCast: Automating and Improving the Use of ShakeMap for Post-Earthquake Decision-Making and Response*. Earthquake Spectra 24(2), pp:533-553.

Yu, O., Allen, D. L., and Drnevich, V. P. (1991). *Seismic vulnerability assessment of bridges on earthquake priority routes in Western Kentucky*. Lifeline Earthquake Engineering, pp. 817-826.

Zou, H. and Hastie, T. (2005). *Regularization and variable selection via the elastic net*. Journal of Royal Statistical Socirty B 67, pp:301-320.

Zhang, J. and Huo, Y. L. (2009) *Evaluating effectiveness and optimum design of isolation devices for highway bridges using the fragility function method*. Engineering Structures, 31, pp:1648-60.

Zhong, J., Gardoni, P., Rosowsky, D., and Haukaas, T. (2008). *Probabilistic seismic demand models and fragility estimates for reinforced concrete bridges with two-column bents*. Journal of engineering mechanics, 134(6), pp:495-504.

Zelaschi, C., Monteiro, R. and Pinho, R. (2016). *Parametric Characterization of RC Bridges for Seismic Assessment Purposes*. Structures, 7, pp: 14-24.

VITA

SUJITH MANGALATHU

Ph. D (Jan 2013 - Mar 2017) (GPA 3.92/4.0)	**Georgia Institute of Technology, USA** **Minor:** Probability and statistics Dissertation: Performance based grouping and fragility analysis of box-girder bridges in California
M.Sc. (GPA 9.0/10.0) May 2012	**Istituto Universitario di Studi Superiori (IUSS)** in Pavia, Italy, and **University of Patras**, Greece Specialization: Masters in Earthquake Engineering and Engineering Seismology (MEEES) Dissertation (**EPFL, Switzerland**): Force-deformation characteristics of masonry spandrels
M.Tech. (GPA 8.78/10.0) May 2009	**Indian Institute of Technology Madras (IITM)**, India Specialization: Structural Engineering Dissertation: Reliability analysis of cantilever retaining walls

PUBLICATIONS

Refereed Journal Articles

1. Ni, P., **Mangalathu, S.,** Mei, G., Zhao, Y., "Permeable Piles: An alternative to improve the performance of driven Piles", *Computers and Geotechnics*, Vol. 84, 2017.

2. **Mangalathu, S.,** Jeon J-S., DesRoches, R., Padgett, J. E., "ANCOVA-based grouping of bridge classes for seismic fragility assessment", *Engineering Structures*, Vol. 123, 2016.

3. Beyer, K., **Mangalathu, S**., "Numerical study on the peak strength of masonry spandrels with arches", *Journal of Earthquake Engineering*, Vol. 18, No. 2, 2014.

4. Beyer, K., **Mangalathu, S**., "Review of strength models for masonry spandrels", *Bulletin of Earthquake Engineering*, Vol. 11, No. 2, 2013.

5. **Sujith, M. S**., Menon, D., Dodagowdar, G. R., "Reliability analysis and design of cantilever RC retaining walls against sliding Failure", *International Journal of Geotechnical Engineering*, vol. 5, No. 2, 2011.

6. Mandali, A. K. **Sujith, M. S**., Rao, B. N., Janardhana Maganti., "Reliability analysis of counterfort retaining Walls", *Electronic Journal of Structural Engineerin*g, vol. 11, No. 1, 2011.

Journal Articles (In review)

7. **Mangalathu, S.,** Jeon J-S., DesRoches, R., Padgett, J. E., "Performance-based grouping methods of bridge classes for regional seismic risk assessment: application of ANOVA, ANCOVA, and non-parametric approach", *Earthquake Engineering and Structural Dynamics*.

8. Dukes, J., **Mangalathu, S.,** Padgett, J. E., DesRoches, R., " Development of bridge specific fragility methodology to improve the seismic resilience of bridges", *Earthquakes and Structures*.

9. Jeon J-S., **Mangalathu, S**., Song, J., DesRoches, R., "Parameterized seismic fragility curves for curved multi-frame concrete box-girder bridges using Bayesian parameter estimation", *Journal of Earthquake Engineering*.

10. **Mangalathu, S.,** Jeon J-S., DesRoches, R., "Identification of Critical Parameters on the Seismic Performance of Concrete Bridges using Lasso Regression", *Earthquake Engineering and Structural Dynamics*.

11. Ni, P.**, Mangalathu, S.,** Mei, G., Zhao, Y., "Compressive and flexural behavior of Reinforced Concrete Permeable Piles", *Engineering Structures.*

12. Nishanth, M., Dhir, P., Davis, R. Mangalathu, S., "Stochastic response of RC buildings under high dimensional model representation", *Earthquake Engineering and Structural Dynamics*.

Conference Proceedings and Oral presentations

1. **Mangalathu, S.,** Soleimani, F., DesRoches, R., Padgett, J. E., "ANOVA based grouping of bridge classes", *16th World Conference on Earthquake Engineering,* Santiago, Chile, 2017**.**

2. **Mangalathu, S.,** Jeon J-S., Soleimani, F., DesRoches, R., Padgett, J. E., Jiang, J., "Sensitivity of fragility curves to parameter uncertainty using Lasso regression", *16th World Conference on Earthquake Engineering,* Santiago, Chile, 2017.

3. **Mangalathu, S.,** Jeon J-S., DesRoches, R., Padgett, J. E., "Application of Bayesian methods to probabilistic demand analyses of concrete box-girder bridges", *Geotechnical and Structural Engineering Congress*, Phoenix, Arizona, 2016.

4. **Mangalathu, S.,** Jeon J-S., DesRoches, R., Padgett, J. E., "Analysis of covariance to capture the importance of bridge attributes on the probabilistic seismic demand model", *10th Pacific Conference on Earthquake Engineering*, Sydney, Australia, 2015.

5. **Mangalathu, S.,** Jeon J-S., Soleimani, F., DesRoches, R., Padgett, J. E., Jiang, J., "Seismic vulnerability of multi-Span bridges: an analytical perspective", *10th Pacific Conference on Earthquake Engineering*, Sydney, Australia, 2015.

6. **Mangalathu, S.,** Jeon J-S., Soleimani, F., DesRoches, R., Padgett, J. E., "Fragility analysis of box-girder bridges with lap-splice mode of failure", *EERI Annual meeting*, Boston, 2015.

7. **Mangalathu, S.,** Beyer, K., "Force-deformation characteristics of masonry spandrels with shallow arches", *Twelfth Rose School Seminar*, Italy 2012.

8. **Mangalathu, S.,** Beyer, K., "Numerical analysis of masonry spandrels with shallow arches", *15th World Conference on Earthquake Engineering*, Portugal, Lisbon 2012.

HONORS AND AWARDS

2015	EERI travel grant for 2015 EERI Annual meeting, Boston.
2010-2012	Erasmus Mundus Scholarship, European Union
2007	All India **Rank 17 (99.98 percentile)** in the national engineering examination "Graduate Aptitude Test in Engineering (GATE)" for admissions to graduate program

MEMBERSHIPS

American Concrete Institute (ACI), American Society of Civil Engineers (ASCE), Earthquake Engineering Research Institute (EERI), Structural Engineering Institute (SEI)

PROFESSIONAL ACTIVITIES

Technical Committee Member, SEI-ASCE's Task Group 3 (TG3) on the risk assessment of structural and infrastructural systems

- Machine learning technique for the reliability analysis of networks

President, EERI chapter Georgia Tech (2015 – 2017)

- Visited various schools in Atlanta to present activities and demos for the children.
- Associated with a team in developing the website for EERI (http://eeri.ce.gatech.edu/)

Chair, SEI chapter Georgia Tech (2016 – 2017)

- Involved in a team to organize workshops and seminars in Georgia Tech